ORGANISATION EUROPÉENNE POUR LA RECHERCHE NUCLÉAIRE
EUROPEAN ORGANIZATION FOR NUCLEAR RESEARCH
Laboratoire Européen pour la Physique des Particules
European Laboratory for Particle Physics

Simulations of Liquid Argon Spills in the ATLAS Cavern

Technical Inspection and Safety Division ▪ CERN - TIS/2001 - 03/GS

Blanca Perea Solano

Supervisors : **Marc Vadon**, CERN TIS / GS ▪ **Lluis Mañosa**, UB Facultat de Fisica

ABSTRACT

ATLAS is a high energy physics detector for the Large Hadron Collider (LHC) at CERN. It is located in a cavern 100m underground and uses Liquid Argon in one of its sub-detectors. We simulated accidental spillage scenarios with a Finite-Volume Element code, Star-CD, in order to evaluate the consequences. We used a 2D model using 100% of flash-evaporation to carry out a sensitivity analysis on the main parameters, which revealed the most critical factors regarding temperature and argon distributions. A series of Liquid Argon tests were performed in a 250 m^3 enclosed space. Experimental and simulation results corroborated each other with regards to Argon concentration but not for temperature. The latent heat of liquid evaporation had to be taken into account. After carrying out a computing time consuming droplet simulation, we implemented a model with energy sinks extracting the latent heat of evaporation, which gave good results with a flash-evaporation of 82%. We eventually renormalized the full ATLAS model and could confidently evaluate the critical leak rates vs. evacuation time.

EDMS : 337749 Geneva, August 2001

Acknowledgements

First of all I would like to thank my supervisors at CERN, Wolfgang Weingarten and Marc Vadon and at Universitat de Barcelona, Lluis Manosa Carrera, to have made this project possible.

Of course, thanks to Fabrizio Balda, whose excellent work opened the path for this one.

Thanks to Richard Clayton, Fred Mendonca, Radenko Drakulic and Jean-Yves Tillier of Computational Dynamics, Ldt. London for their help in meshing modelling, droplet understanding, humidity implementing, convergence, control and coding.

Thanks a lot to Manuel Guijarro, Christian Boissat, Jerome Fournier and Tony Osborne for their collaboration when solving StarCD implementation problems; Harry Renshall for the space in AFS and HSM.

Many thanks to Guillermo Peon, for his patience and his always ready offer to share knowledge and resources. Thanks to Jean Roche, Daniel Gasser and Emma Vigo, from the Cooling and Ventilation group. Thanks to Dr. P. Watkins, from UMIST, Manchester, for his help in understanding depressurisation of highly pressurised liquids.

Thanks to Jean Claude Carlier, Johan Bremer, Joseph Nebout, Olivier Goudard, Gianpaolo Benincasa, Andre Castel, Claude Millerin, Nicole Wauquier, Pierre Baehler, Christophe Mugnier, Fabio Follin and all the Transport team, for their collaboration in the experiment set up and manipulation of cryogenics.

Thanks to all the TIS-GS group, who have made my day-to-day fun: Ana-Paula Bernardes, Paul Beynel, Raymond Cambarrat, Alain Chauvelon, Mario Danesin, Roland Dessens, Christine Negri, Daniel Palvadeau, Bruno Pichler, Carine Pividori, Guy Salomon, Fritz Szoncso; and the Medical Service, Joanne Madden, Florence Rabier, Veronique Fassnacht and Etienne-Paul Maquet; and to the TIS Division Leader, Helmut Schonbacher.

I would also like to express my thanks to Josep Llosa, Arturo Lousa and J.M.Parra for their time and help in my studies during this last year.

... La verdad, como siempre,

sera mucho mas extraordinaria.

Arthur C.Clarke

Abstract

Liquid Argon spills in the ATLAS cavern were simulated using a Finite-Volume Element code, Star-CD, in order to evaluate the consequences of this kind of accident. A first series of analysis were carried out with a model proposing 100% of flash-evaporation of the liquid argon. A sensitivity analysis on the main parameters of the model let us study whether these elements were critical for the temperature and argon distribution or not. A series of Liquid Argon tests were performed at a hall at CERN. Experimental and simulation results agreed well for Argon concentration but not for temperature. The latent heat of evaporation of the liquid had to be included in the model. A first model implementing a mixed inlet of droplets of LAr and argon gas was studied but resulted to be too computing time consuming. We then implemented a model with sinks of energy extracting directly from the enthalpy equation the latent heat of evaporation of the liquid. This model, with a flash-evaporation of 82% gave good results. This renormalized model was implemented for ATLAS and allowed us to perform with confidence an evaluation of the critical leak rates in relationship with an evacuation time.

Contents

Chapter 1

Introduction

In this chapter we describe the ATLAS experiment and the underground cavern UX15, where all the study takes place. An emphasis is put on the ventilation system, cryogenics and the heat loads.

1.1 The ATLAS experiment

ATLAS will be one of the four detectors of the new LHC (Large Hadron Collider). It will be located at Point 1 of the new accelerator complex and 100 m underground. The overall detector layout is shown on the picture below.

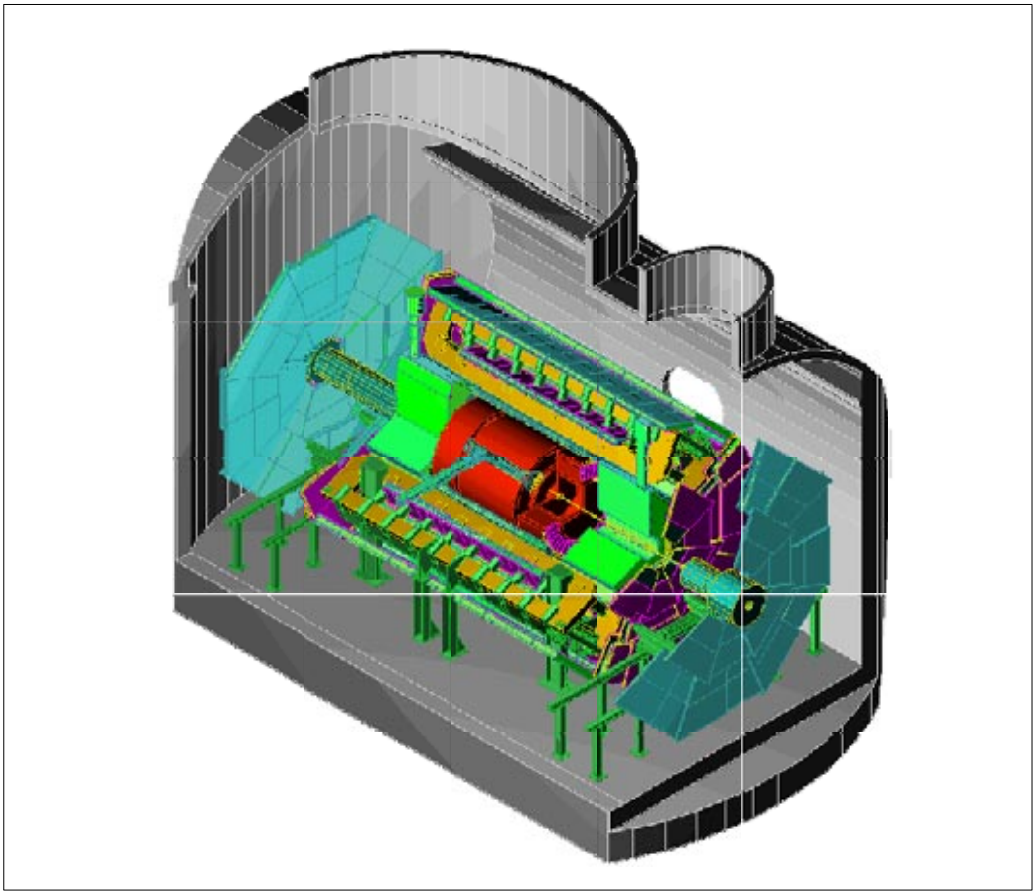

Figure 1.1 3D view of the ATLAS detector installed in the underground hall

The magnet configuration is based on an inner superconducting solenoid around the inner detector cavity and a large superconducting air-core toroid consisting of independent coils arranged with an eight-fold symmetry outside the calorimetry.

A combination of discrete high-resolution pixel and strip detectors in the inner part and continuous straw-tube tracking detectors with transition radiation capability in the outer part of the tracking volume, grant pattern recognition, momentum and vertex measurement, and enhanced electron identification. All the calorimetry is contained in a cylinder with an outer radius of 2.25 m and extends 6.65 m in both directions along the beam axis. The calorimetry is surrounded by the muon spectrometer, which defines the overall dimensions of the ATLAS detector.

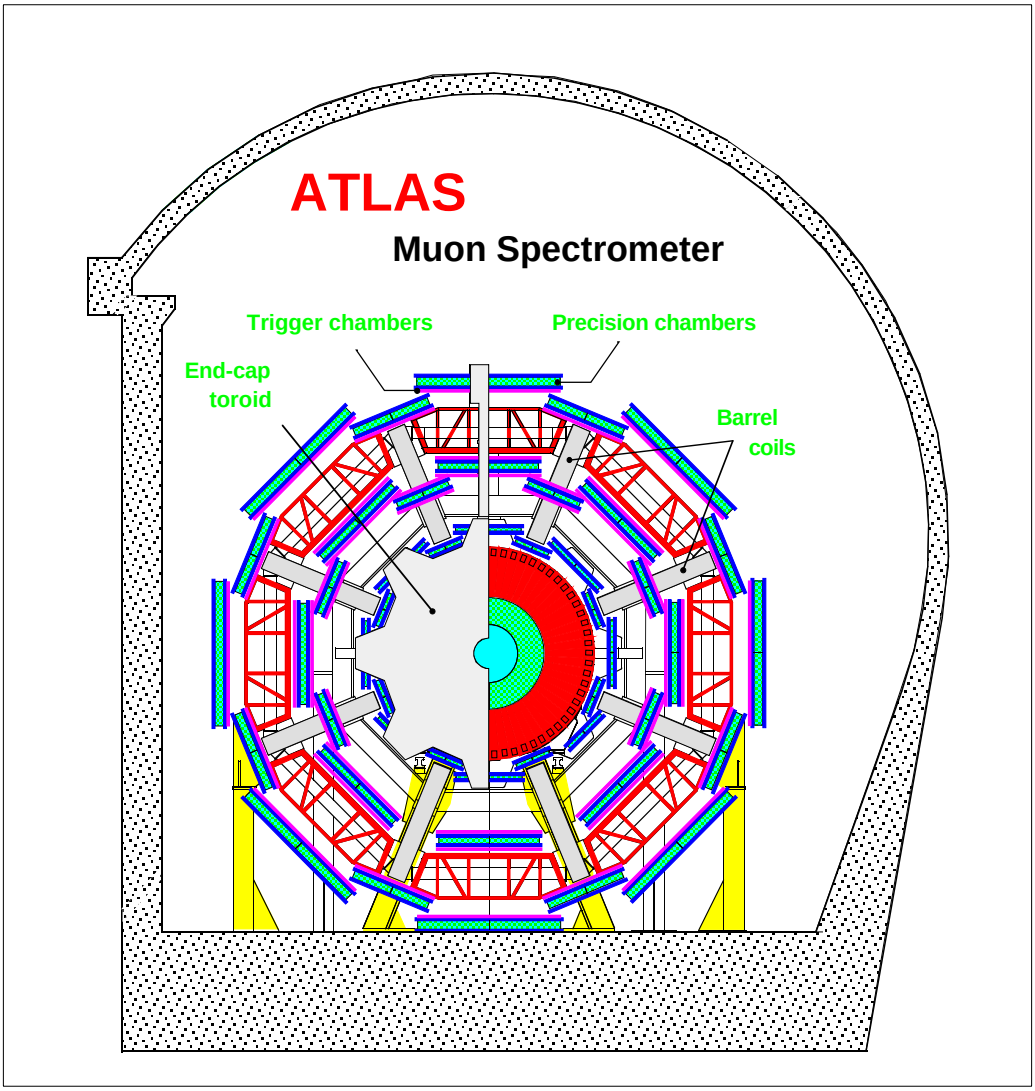

Figure 1.2 Transverse view of the ATLAS muon spectrometer

UX15 is the experimental cavern, containing the detector, while USA 15 will contain the readout electronics. Cavern UH15 will contain the cryogenics services of the experiment (liquid Argon, stored in dewars); it will be connected to the surface by pit PH14. The two access shafts, PX15 and PX16, reach down to the roof of the cavern, while PX15 will be the principal access for personnel to the experimental area. Some general characteristics of the cavern are listed below:

Table 1.1 Some characteristic parameters of the cavern

Surface	970 m^2
Height	25 m
Floor width	26 m
Length	~ 45 m
Volume	~ 25.000 m^3
Detector volume	~ 10.000 m^3
Free volume	~ 15.000 m^3

1.2 Calorimetry

The ATLAS calorimeter has been designed to meet the demands of the LHC physics program while operating in a very high luminosity environment. Figure 2.3 shows the calorimeter layout. A barrel cryostat around the inner detector cavity, supported by the iron-scintillator Tile calorimeter, contains the barrel electromagnetic calorimeter and the solenoidal coil which supplies a uniform field to the inner tracking volume. This coil is placed in front of the electromagnetic calorimeter. Two end-cap cryostats enclose the electromagnetic and hadronic end-cap calorimeters as well as the integrated forward calorimeter. The barrel and the extended barrel hadronic calorimeters are contained in an outer support cylinder, acting also as main solenoid flux return, and consists of scintillating tiles and iron absorber plates. The electromagnetic calorimeter must be able to identify and accurately reconstruct electrons and photons (coming from Higgs Boson decays, for instance: H-->γγ ; H-–>ZZ-–>4 e) over a wide energy range, while the major goals of the hadronic calorimeter are to identify hadronic jets and measure their energy and direction, as well as to measure the total missing transverse energy and to enhance the particle identification capability of the electromagnetic calorimeter by measuring quantities as leakage and isolation.

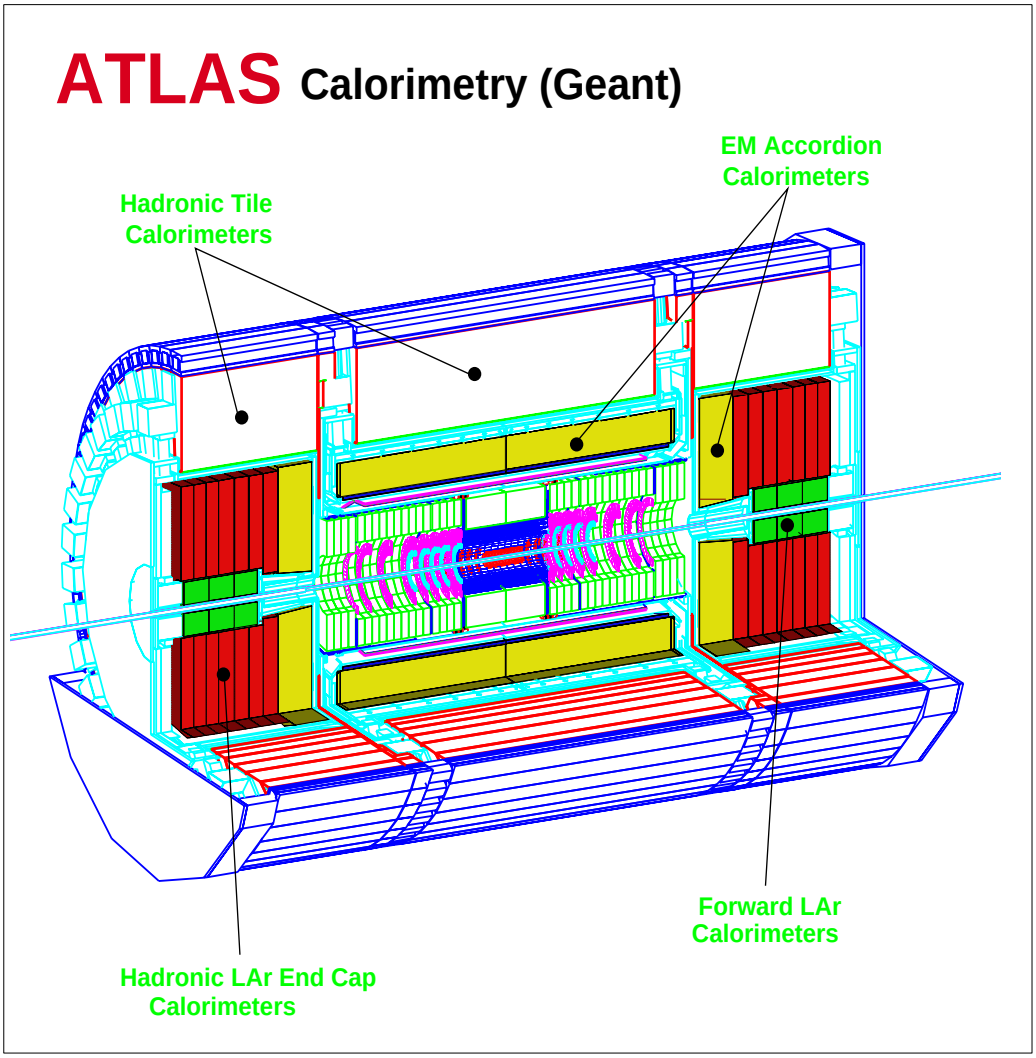

Figure 1.3 3D view of the ATLAS calorimetry

The barrel **electromagnetic calorimeter** , contained into the central cryostat, consists of two identical half-barrels, each independent since its connections to the outside are made at its respective end of the cryostat, and each composed by accordion-shaped absorbers and read-out electrodes. The end-cap calorimeters consist of accordion-shaped lead absorbers interleaved with electrodes, the gap being filled with liquid Argon.

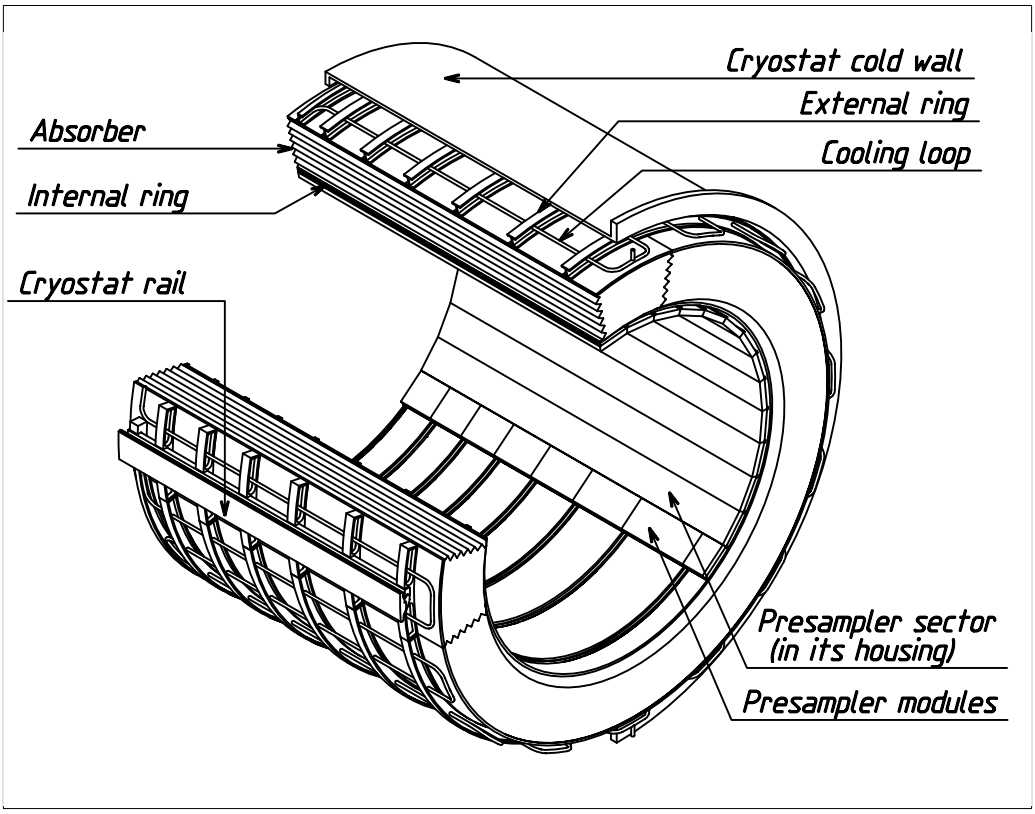

Figure 1.4 Layout of the electromagnetic barrel calorimeter

The **forward calorimeter** is a particular challenging detector owing to the high level or radiation it has to cope with. It is integrated into the end-cap cryostat.The calorimeter consists of a metal matrix with regularly spaced longitudinal channels filled with concentric rods and tubes. The rods are at positive high voltage while the matrix is grounded. The liquid argon gap in between is the sensitive medium.

The ATLAS detector includes a large scintillating cylindrical **hadronic barrel calorimeter** . The technology for this calorimeter is based on a sampling technique using steel absorber material and scintillating plates read out by wavelength shifting (WLS) fibres. The scintillating tiles are placed perpendicular to the colliding beams and staggered in depth. The steel structure of each sector module consists of a stack of repeating elements (periods) and each period is a stack of four layers of different trapezoidal steel plates.

Each **hadronic end-cap calorimeter** consists of two independent wheels. The gap between consecutive copper plates is equipped with three parallel electrodes, forming an electrostatic transformer. This LAr sampling calorimeter is designed to provide coverage for hadronic showers, and is equipped with GaAs preamplifiers and summing networks located at the outer radius of the modules.

In our study, we will refer to the barrel cryostat, neglecting the end-caps. This cryostat serves as housing for the electromagnetic barrel calorimeter. In addition it

supports and provides the vacuum for the superconducting solenoid coil which serves the inner tracker.

Figure 2.3. shows a view of half of the barrel cryostat.

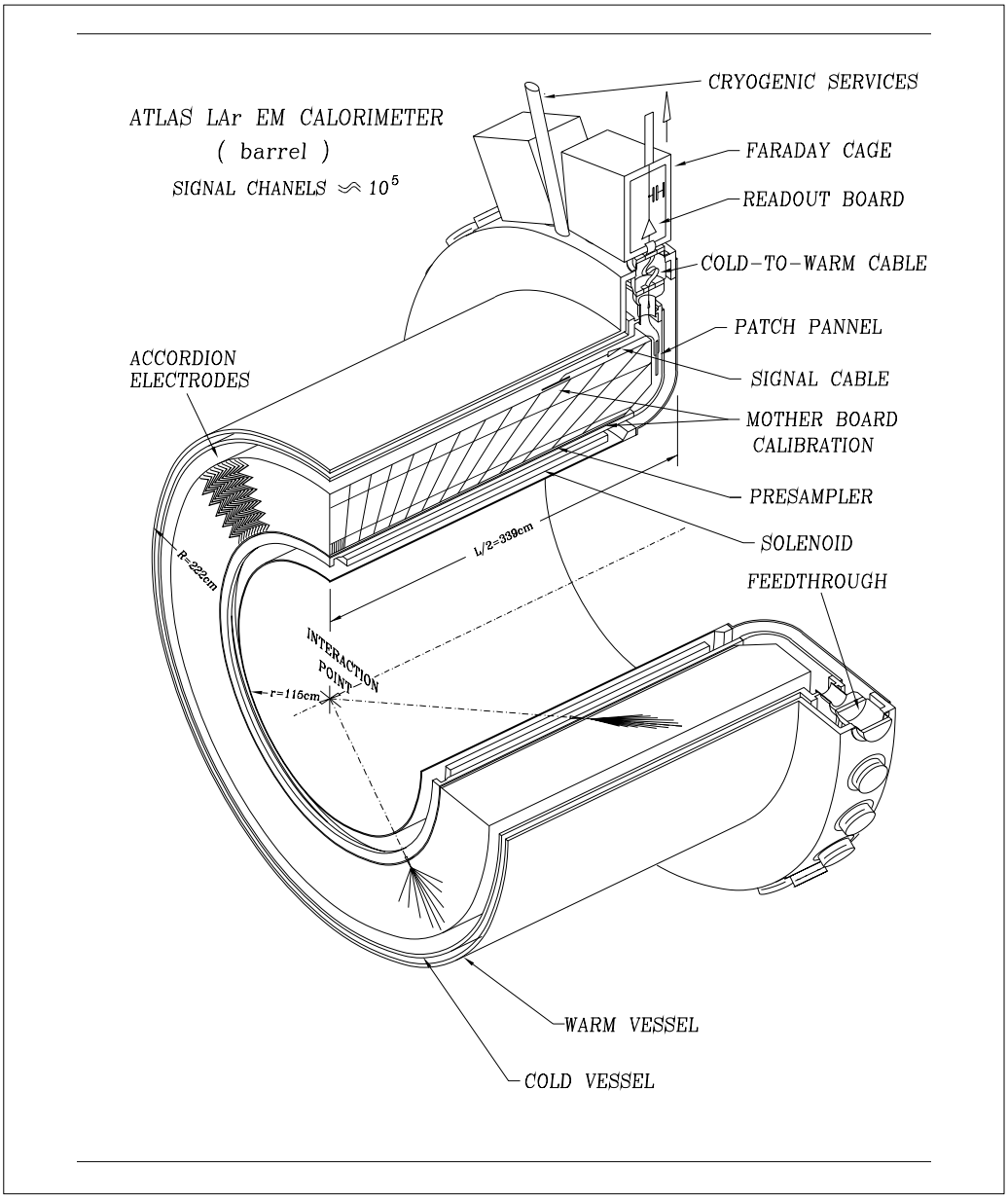

Figure 1.5 3D view of one half of the barrel cryostat

1.3 The cryogenic system

The cryogenic system is an integrated installation for the barrel and end-caps argon cryostats, including the system for their cooling down and warming up. In routine operation, the cooling of the cryostats is achieved using liquid nitrogen produced in a closed loop by a liquefier located in the cryogenics cavern.

Some of the main parameters related to cryogenic systems are listed in the following table:

Table 1.2 Main parameters of the cryogenics system

Cryostat	Barrel	End-cap
Volumes [m^3]		
Cold vessel	58	43
Expansion vessel	5	2
Liquid argon	45	19
Insulating vacuum	26	6
Weight [t]		
Cold vessel	12	14
Detector	110	219
Vacuum vessel	13	9,5
Solenoid	5,5	
Full-cryostat	203	269
Surface Areas [m^2]		
Cold vessel	160	80
Solenoid	85	

The system is based on the use of subcooled liquid argon. The gas pressure above the liquid surface will be regulated to typically 1,25 bar using a liquid nitrogen heat exchanger. The liquid argon close to the surface is at about 89,3K. Liquid nitrogen cooling loops, installed in each cryostat will be used to compensate the heat leaks, and to maintain the baths at the same temperature being between 3 and 7 K below the saturation temperature at the top or bottom of the cryostat. The temperature of the subcooled volume can be lowered down to 87,3 K, which is the minimum to avoid the freezing of liquid argon in the region of the heat exchangers.

The following figure and table summarize the normal and maximum pressure at different levels in the barrel cryostat.

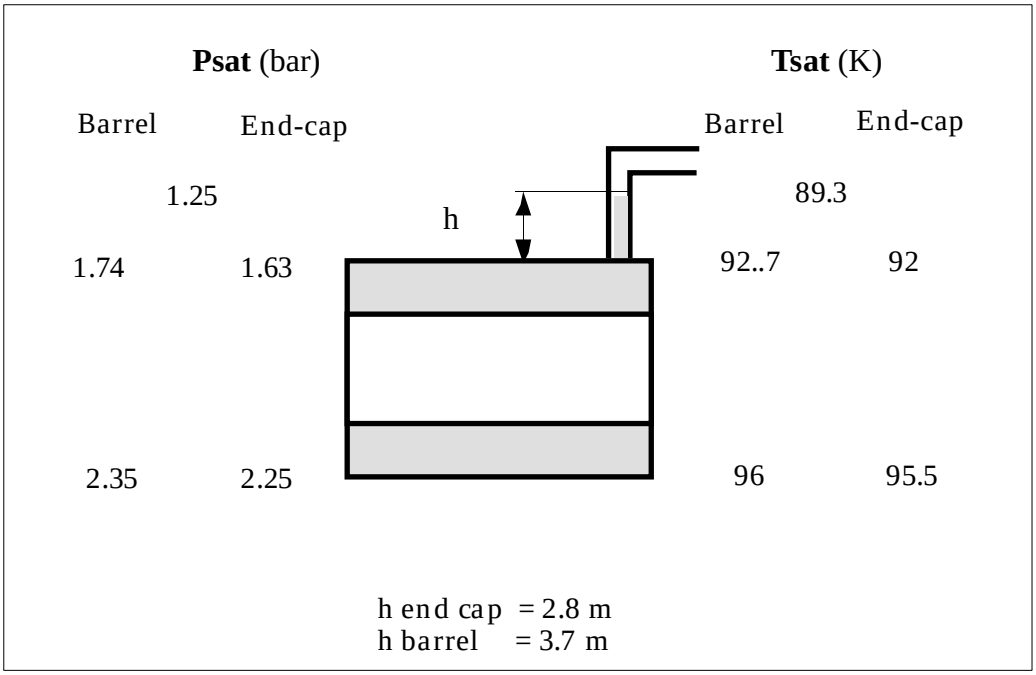

Figure 1.6 Diagram of saturated pressure and temperature on the cryostats

Table 1.3 Normal and maximum pressure values during normal operation

	Barrel, norm.	End-cap, norm
P_0	1,25 bar	1,25 bar
P_h	1,74 bar	1,63 bar
P_b	2,35 bar	2,25 bar
	Barrel, max.	End-cap, max.
P_o	1,7 bar	1,7 bar
P_h	2,2 bar	2,1 bar
P_b	2,8 bar	2,7 bar

P_b is estimated to be able to rise up to 3,2 bar (barrel cryostat) in exceptional situations such as the breakdown of the isolation vacuum.

1.4 Ventilation in UX15

The ventilation system consists of ten air diffusers placed in several points of the cavern, and of a system of ducts connected with the outside. Figure 1.7. shows the overall view of ventilation of UX15.

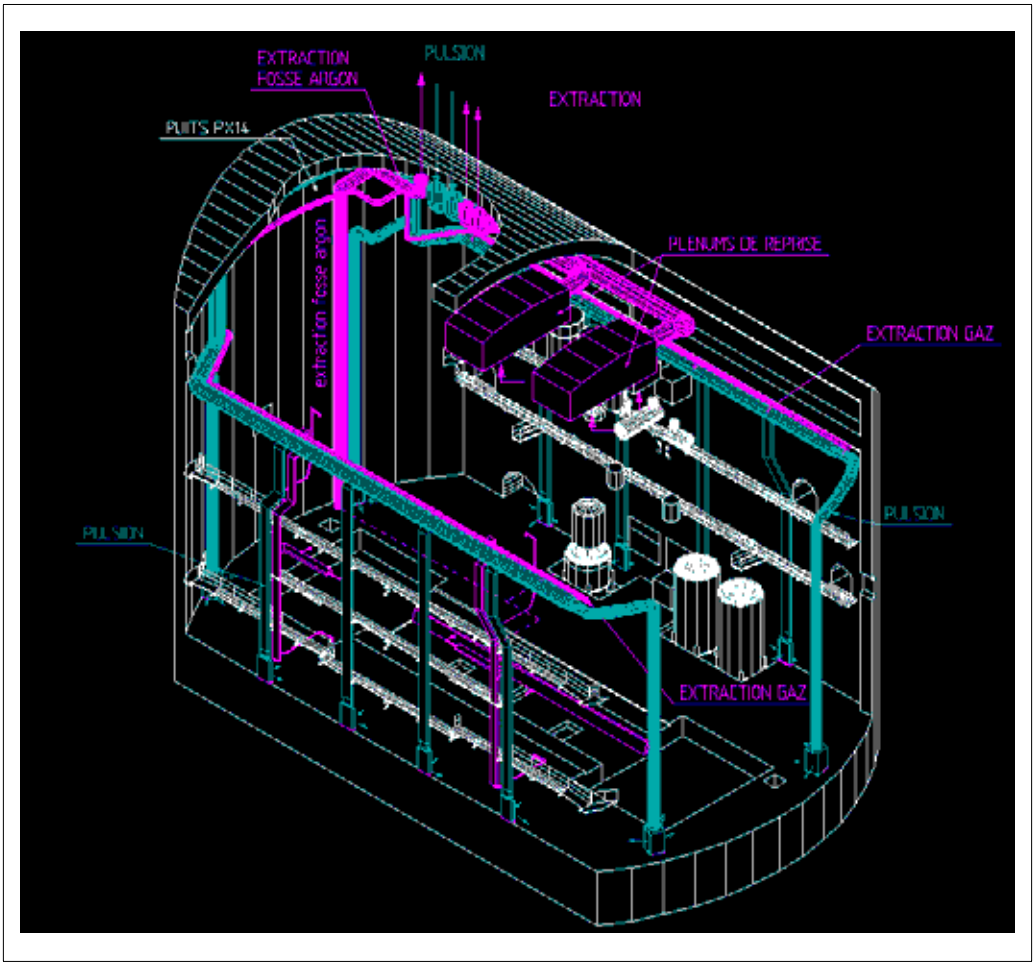

Figure 1.7 Ventilation in UX15

Fresh air is taken into UX15 by means of a series of five diffusers placed at floor level on each side of the room. There is also air coming into the cavern from USA 15, only from one side of the cavern. The foreseen dimensions of these diffusers are 2,0 x 1,2 x 1,2 m. On the other hand, air or gas mixtures are extracted from UX15 by two big exhaust plenums on top of the hall (2,0 x 1,2 x 1,2 m) and by extraction fans placed on the retention pit (2,0 x 1,2 x 0,3 m).

Some characteristic parameters of the ventilation system of UX15 are given in the following table.

Table 1.4 Ventilation system parameters (normal running)

	m^3/h
Supply	60.000
Supply (from USA 15)	16.000
Extraction (ceiling)	60.000
Extraction (Ar retention pit)	16.000

In exceptional situations, such as in an accident, air flows are doubled. We should stress that these values have changed during the years. These are the latest data provided by J.Roche, from the Cooling and Ventilation division. Nevertheless, we obtained this information after the study had began, and consequently part of it is still done with the ancient data for ventilation. The study carried out by F.Balda was considering the old specifications: 45.000 m^3/h for the supply air and the extraction, instead of the actual 60.000 m^3/h.

1.5 Heat Load

The heat load specifications have also changed lately. The old estimation was about 100 kW, while the present estimation of heat dissipated into the UX15 cavern can be summarized in the following table:

Table 1.5 Estimate of the heat dissipation into the air in the UX15 cavern

System	Sub-system	Heat Source	Q (kW) into coolant	Q (kW) into US air
Inner Detector	Pixels	Modules	21	
		Cables	10,8	1,5
		Pipes	42	
	SCT	Modules	61,5	
		Cables	48	3
		Pipes	67,5	
		Thermal enc.	15	
	TRT	Cables	52	3
		Racks	9	3
LAr Calorimeter		Crates	235	26
		Power Supply	35	4
		Racks		0
		Cables	?	?
Tile Calorimeter		Drawers	46	5
		Power Supply	12	1
		Cables	0	1
Muon	Total (racks+cables)			70
Magnets	Solenoid	Bus-bars		5
		Equipment		2
	Barrel Toroid	Bus-bars		10
		Equipment		2
	End-cap Tor-oid	Bus-bars		10
		Equipment		2
Other	Lights			30
TOTAL	**178,5 kW**			

Therefore the new estimation of total heat load into the cavern is nearly twice the old one.

Chapter 2

Previous simulations

In this chapter we show the results of the simulations of liquid argon spills in the ATLAS cavern carried out at TIS by Fabrizio Balda and Marc Vadon during 1999.

2.1 Introduction

During 1999, simulations of spills of liquid argon in the ATLAS cavern were carried out at TIS by Marc Vadon and Fabrizio Balda. This work was intended to recommend safety measures to be taken in case an accident of this kind takes place.

This work was the starting point for the present study. Therefore, it is important to present, even if briefly, the results achieved by this previous work.

The main points treated in this work are:

- Air flow in UX15 distribution during normal running
- Argon accidents
  - Catastrophic failure of a feedthrough
  - Argon leak from a weld / seal
  - Argon leak with internal overpressure
- Experiment simulation

We describe each of these points in the following paragraphs.

2.2 Air Flow field in UX15

Before performing the simulations of liquid argon accidents, it was necessary to get an idea of the normal running of the detector or maintenance periods. It was necessary to find out whether a steady flow was stabilizing in the room after a period of time, if the flow was turbulent, laminar or transition and how much the ventilation system was influencing it. It was also important to determine which of natural and forced convection was dominating the flow. The main parameters considered were density, turbulent viscosity and pressure fields.

This study was carried out with two different geometries of the cavern: both models were two dimensional (cells with volume and symmetry planes), the second one being far more precise than the other, including the external layer of muon chambers and the racks, as we see in figure 2.1. The boundary conditions for both geometries are the following:

Table 2.1 Inlets' geometric dimensions and calculated speeds (coarse grid)

Inlet	*Cross-length [m]*	*Air speed [m/s]*
Exhaust plenum	9.29	0.029901
Left diffuser	2.0	0.069444
Right top diffuser	2.4	0.041152
Right bottom diffuser	2.0	0.069444
Left pit extractor	1.414	0.049383
Right pit extractor	1.414	0.049383

Table 2.2 Inlets' geometric dimensions and calculated speeds (fine grid)

Inlet	*Cross-length [m]*	*Air speed [m/s]*
Exhaust plenum	9.29	0.029901
Left diffusor	2.0	0.069444
Right top diffusor	2.4	0.041152
Right bottom diffusor	2.0	0.069444
Central pit extractor	0.937	0.083808
Right pit extractor	0.9	0.023045

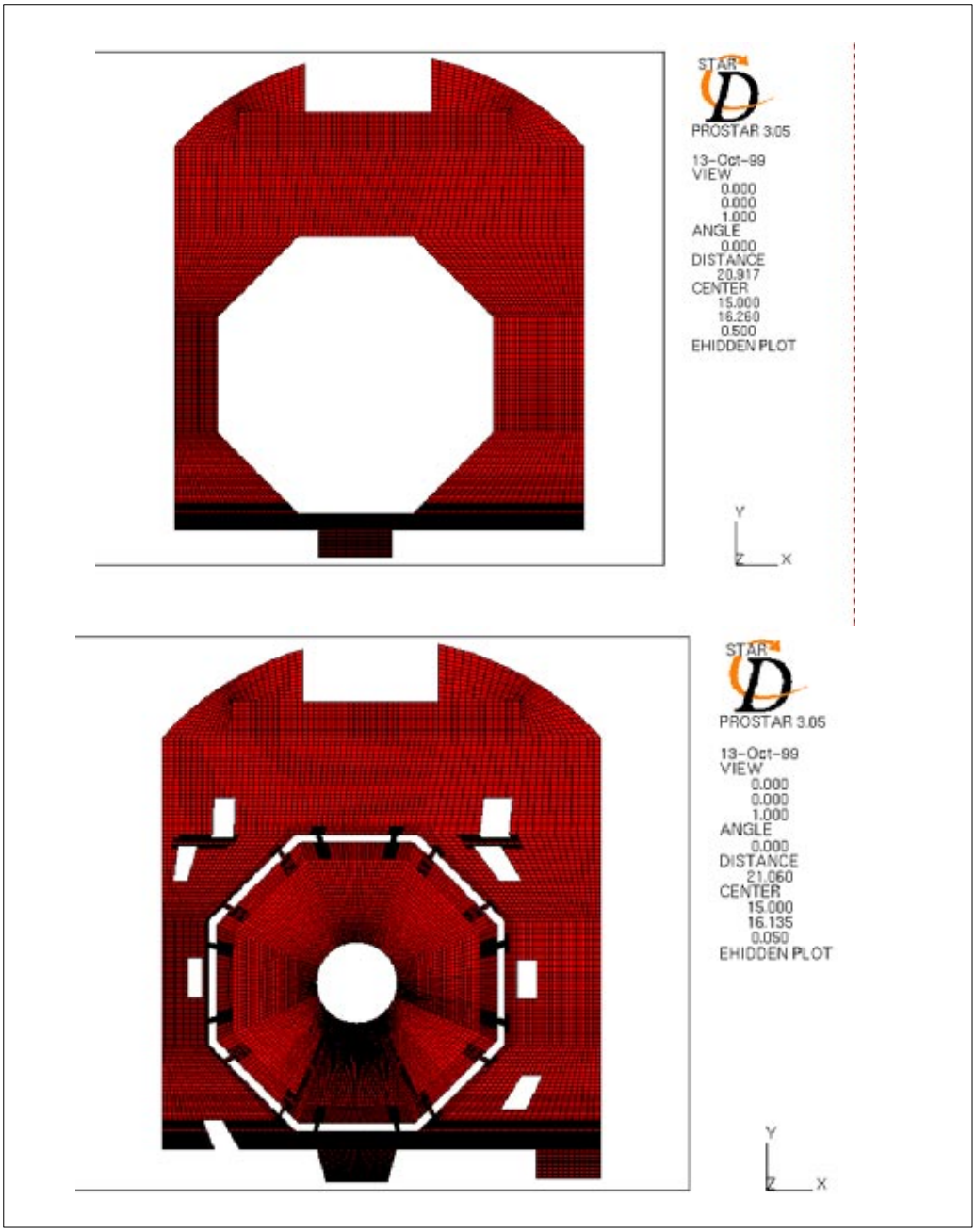

Figure 2.1 Coarse, simple mesh and finer, more complex model

One of the main conclusions of the study was that the coarse and fine-mesh simulations gave similar results, showing a clear tendency of the system to reach a steady state. Secondly, buoyancy plays a dominant role: air velocity induced by the temperature gradient is an order of magnitude higher than the one due to the ventilation.

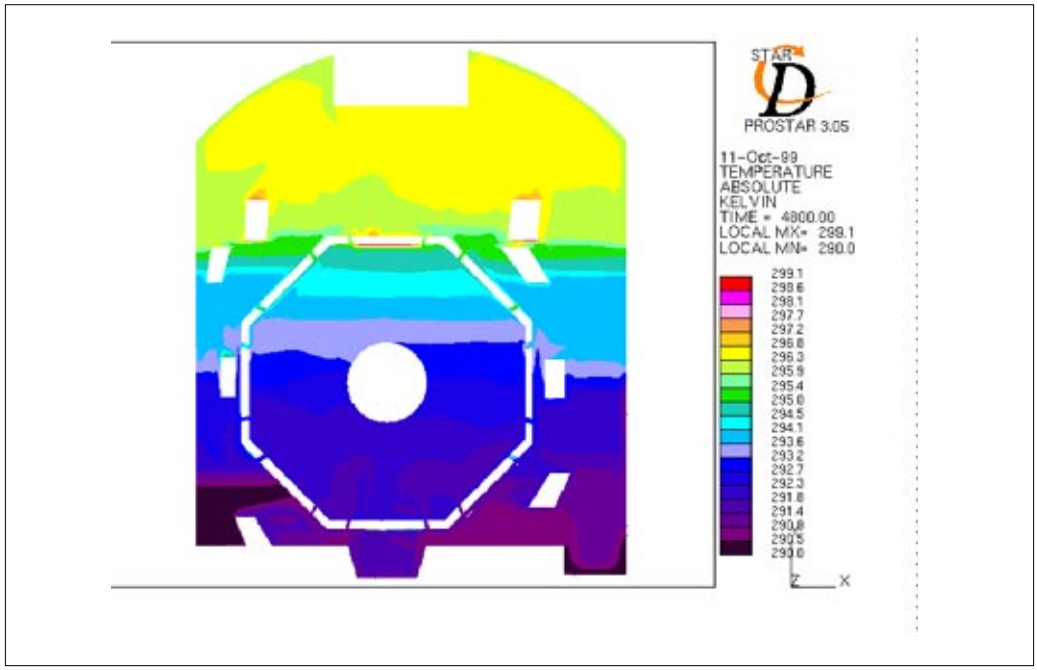

Figure 2.2 Temperature distribution

Density follows the temperature behavior, and shows how colder air stratifies at the bottom of the cavern while warmer air flows towards the top. During normal running ventilation is not negligible, and acts as a stabilizing factor for air flow field, significantly cooling the atmosphere.

At this point of the study it was already pointed out that in an event such as liquid argon accident getting into the domain, buoyancy forces would be much increased and would dominate the flow field. This has been demonstrated in the following steps.

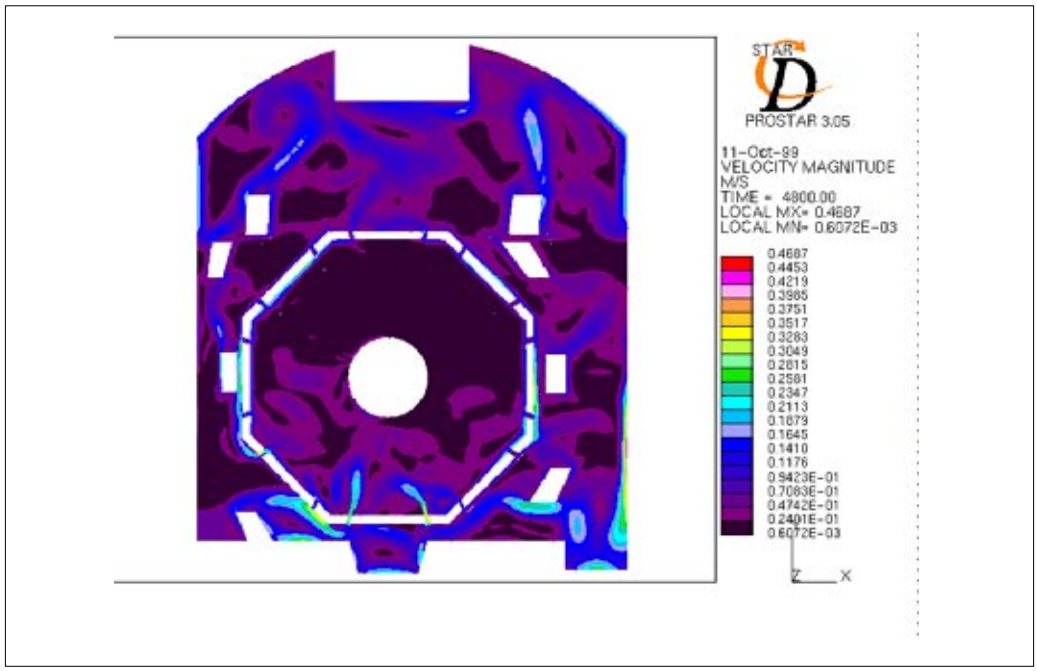

Figure 2.3 Velocity magnitude

2.3 Argon accidents

The main part of the study was the simulation of liquid argon accidents inside the experimental cavern of ATLAS. Three different spills were simulated, a catastrophic one and two small ones, in different geometries (describing close detector geometries with one and three layer muon chambers).

Common Boundaries

We should describe the boundary conditions common to the three different scenarios taken into consideration, that is to say, ventilation, heat load and wall temperature. The gas argon inlet is different for each flow.

For these simulations some refinement was done in the meshing, but the geometry was basically the same as had been proposed for the previous simulation (figure 2.1, finer mesh).

The ventilation conditions where adjusted to the accidental situation (double flow). The following tables sum up the speeds and the turbulent parameters of each air inlet:

Table 2.3 Inlets' geometric dimensions and calculated speeds

Inlet	*Cross-length [m]*	*Air speed [m/s]*
Exhaust plenum	9.29	0.059802
Left diffuser	2.0	0.138888
Right top diffuser	2.4	0.082304
Right bottom diffuser	2.0	0.138888
Left pit extractor	0,937	0.167616
Right pit extractor	0,9	0.046090

Table 2.4 Calculated values for k and ε

Inlet	*k* $[m^2/s^2]$	*ε* $[m^2/s^3]$
Exhaust plenum	$5{,}364\ 10^{-5}$	$6{,}949\ 10^{-8}$
Left diffuser	$2{,}893\ 10^{-4}$	$4{,}044\ 10^{-6}$
Right top diffuser	$1{,}016\ 10^{-4}$	$7{,}012\ 10^{-7}$
Right bottom diffuser	$2{,}893\ 10^{-4}$	$4{,}044\ 10^{-6}$
Central pit extractor	$4{,}214\ 10^{-4}$	$1{,}5727\ 10^{-5}$
Right pit extractor	$3{,}186\ 10^{-5}$	$3{,}284\ 10^{-7}$

The cavern walls were kept at a constant temperature of 292,5 K, and the heat load considered was of 100 kW.

2.3.1 Catastrophic failure of a feedthrough

This accident was simulating an extremely unlikely event, but could happen as a consequence of mechanical failure or, for instance, if a crane hit the cryostat cutting a feedthrough.

The argon inlet was equivalent to a 13 cm diameter hole, which corresponds -if we consider a pressure of 1,25 bar at the top of the dewar- to a mass flow of 254,7 kg / s. With this mass flow the barrel calorimeter would empty at about 244 s, but we saw that the consequences of this accident became catastrophic much before the complete emptying. The flow is assumed to be constant.

Therefore, the argon inlet is characterized by:

Table 2.5 Argon inlet for a catastrophic failure of a feedthrough scenario

Q gas [m^3/s]	47,72
v [m/s]	8,15
k [m^2/s^2]	0,998
ε [m^2/s^3]	12,60
ρ [kg/m^3]	5,3375
T [K]	90

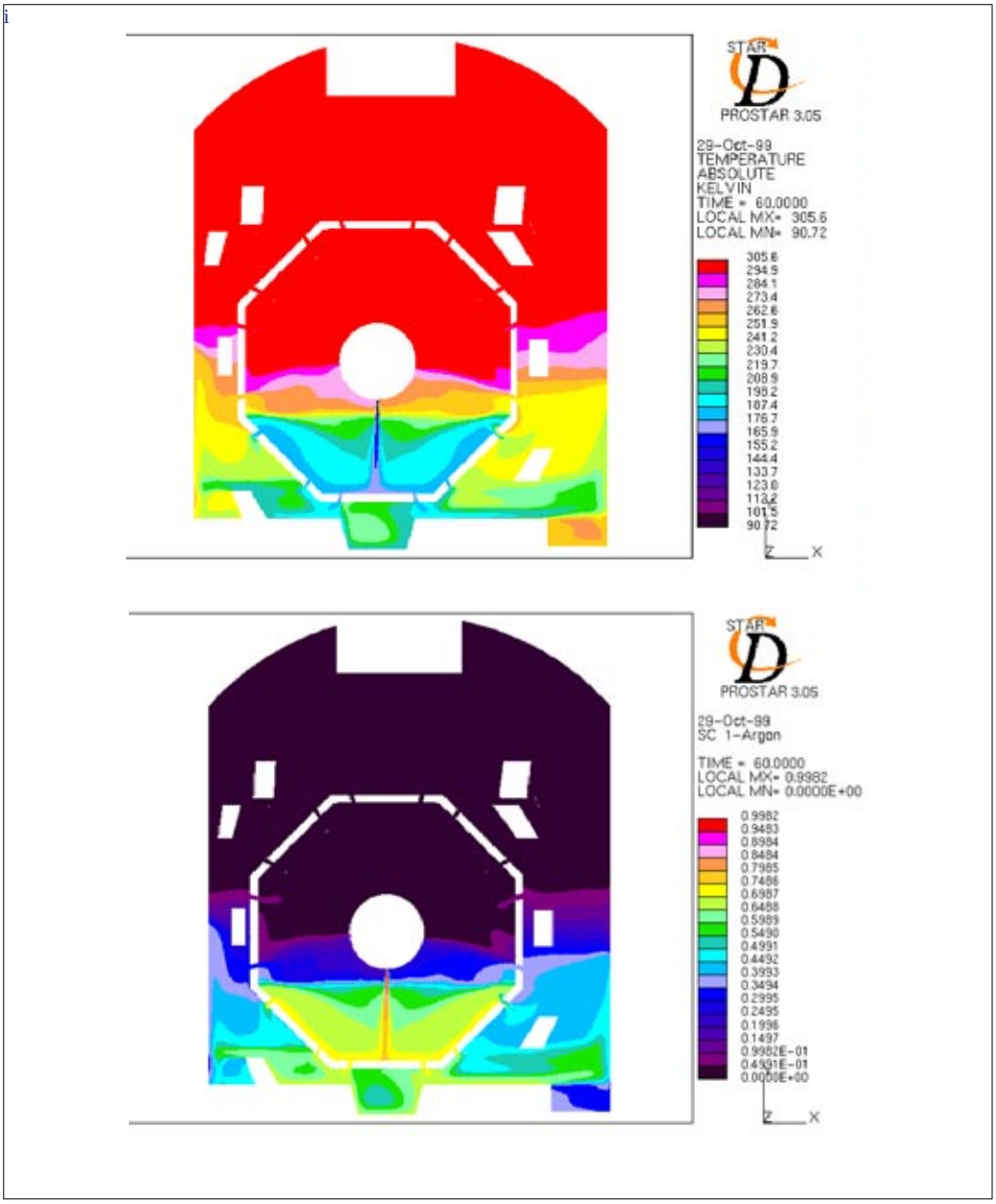

Figure 2.4 Temperature and Argon concentration distributions 60 seconds after the spill. Catastrophic failure of a feedthrough

The simulation pointed out that both temperature and argon concentration fields were rapidly becoming dangerous or deadly for human beings inside the experimental chamber. Already after 30 seconds, the situation is catastrophic, argon concentration reaching the limit of 25 % (weight percentage). Thus, any person located at lower and medium heights of the cavern are in critical danger. The consequences of this kind of accident would be death or serious health damage for anybody close to the detector.

2.3.2 Argon leak from a weld/seal

This is a more probable accident, involving a smaller argon release than the previous one. Here we suppose that a leak takes place in a sealed or welded point at the bottom of the vessel. In reality this kind of leak is more likely to occur at a penetration point or in a cryoline.

The main hypothesis was again that all the argon instantly vaporizes just after exiting the rupture point. The geometry that was used was the same as for the catastrophic leak, but the region next to the argon inlet was refined in order to capture the gradients of the magnitudes in this area.

The inlet of argon, if we consider a hole equivalent to 17,3 mm of diameter and the pressures we had assumed before:

Table 2.6 Argon inlet for a weld/seal scenario

Q gas $[m^3/s]$	0,849
v $[m/s]$	1,088
k $[m^2/s^2]$	0,01776
ε $[m^2/s^3]$	0,22421
ρ $[kg/m^3]$	5,3375
T [K]	90

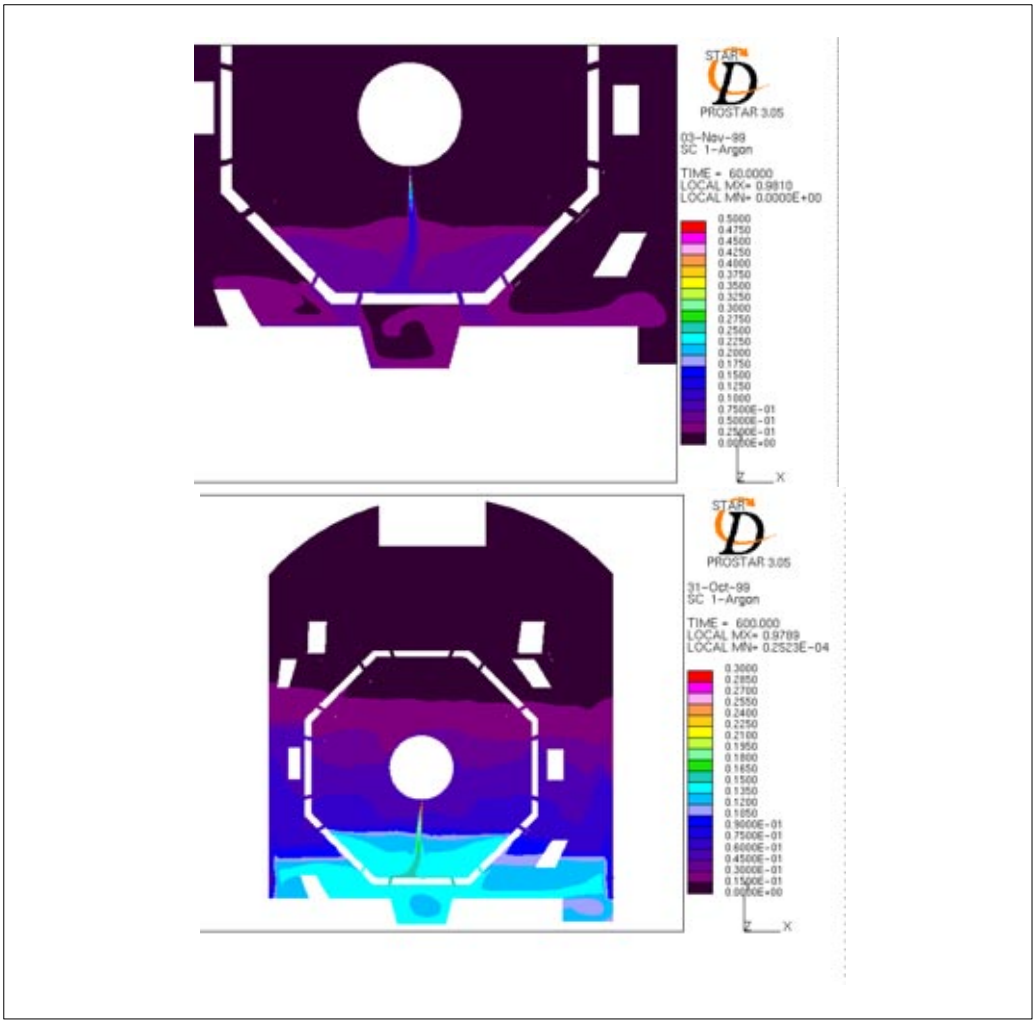

Figure 2.5 Argon concentration 60 s and 10 minutes after the spill. Argon leak from a weld/seal

The argon distribution shows that there is a fast spreading of the argon into the cavern, even though it does not reach dangerous levels except very close to the spill point. After 10 minutes the oxygen concentration is still close to normal in most zones. This time should be enough to allow people escape from the dangerous points close to the cryostat spill point.

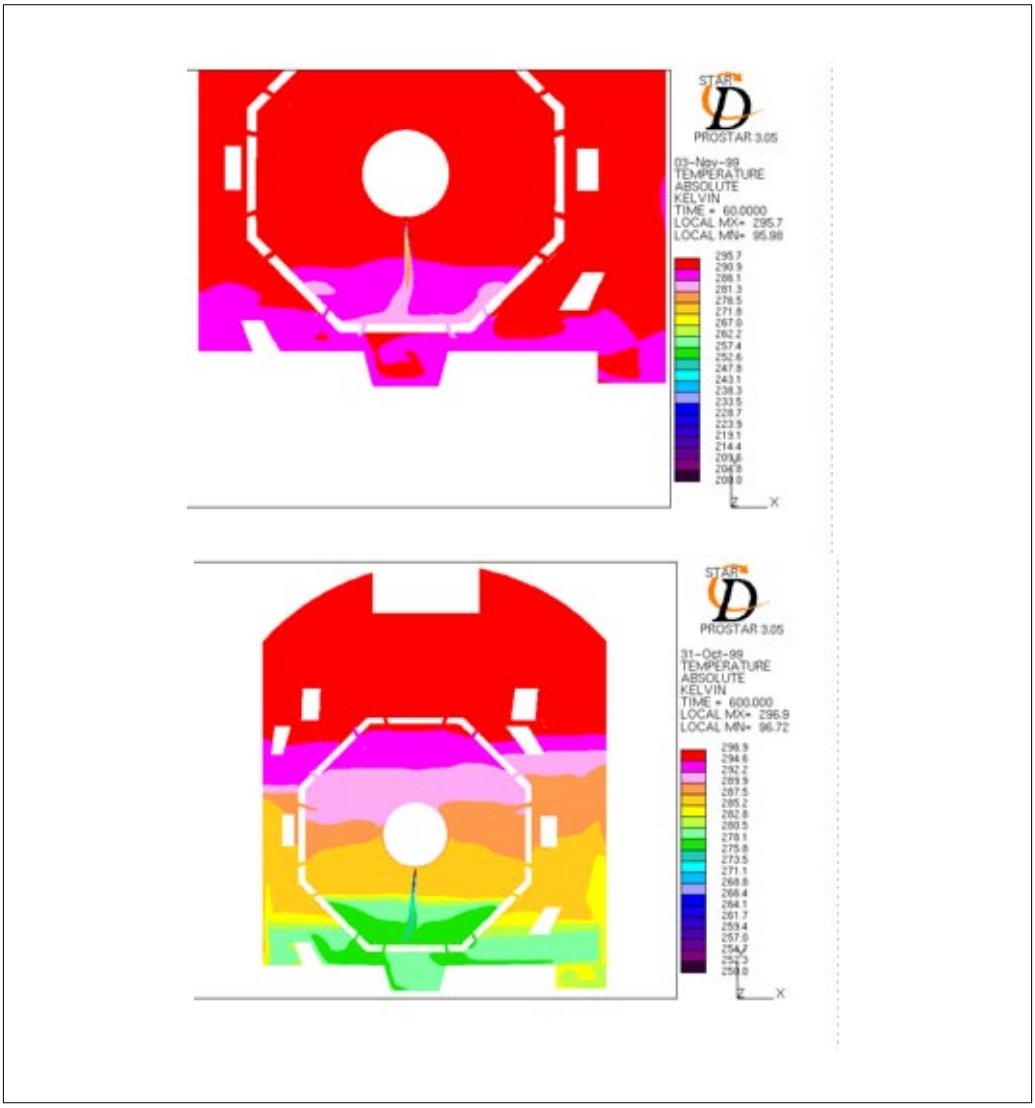

Figure 2.6 Temperature distribution 60 s and 10 minutes after the spill. Argon leak from a weld/seal

In this kind of accident the danger might come from the low temperatures reached in some areas, which would lead to freezing and frostbite or other damages caused by the contact with a cold liquid or gas. Also, the formation of a cloud should not be neglected, because it can slow down the people's way out and cause panic.

2.3.3 Argon leak with internal overpressure

There is also the possibility that the leak occurs because of an internal overpressure of a mechanical failure at the same time. Pressure can rise up to 1,7 bar in the overflow vessel in an exceptional situation. If this happens, a safety valve opens, preventing further pressure increasing. We will suppose that the pressure remains constant at this value.

This scenario was simulated within a more refined geometry with three layers of muon chambers, as we can appreciate in the figures.

Assuming the same hole diameter as before (17,3 mm) but now the new pressures that we have specified, we have the following inlet properties:

Table 2.7 Argon inlet for a leak with internal overpressure scenario

Q gas $[m^3/s]$	0,9517
v $[m/s]$	1,22
k $[m^2/s^2]$	0,02233
ε $[m^2/s^3]$	0,3028
ρ $[kg/m^3]$	5,5075
T [K]	90

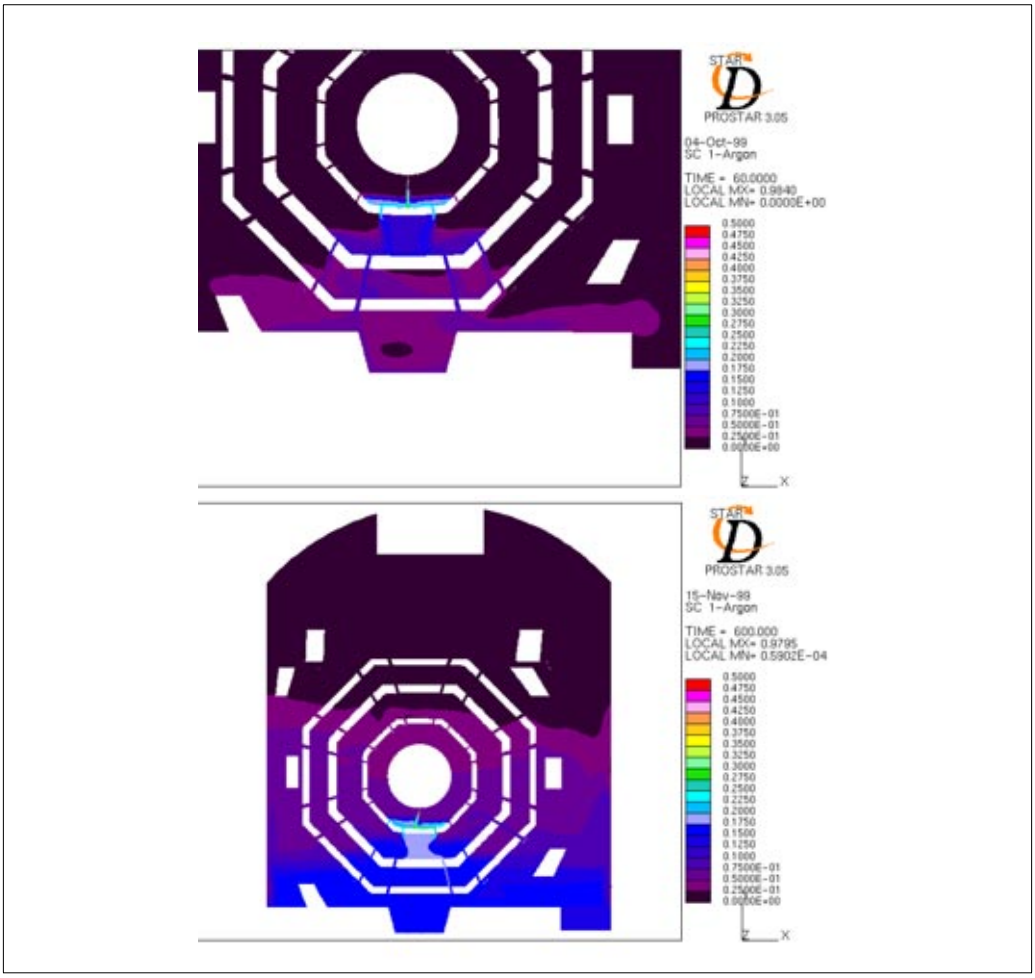

Figure 2.7 Argon concentration 60 s and 10 minutes after the spill. Argon leak with internal overpressure

The conclusions are very similar to those obtained in the previous model. The small differences in the mass flow coming from the higher pressure, resulting in a higher argon velocity and other small changes, do not give rise to significant changes in the flow fields, even if the geometry is quite different.

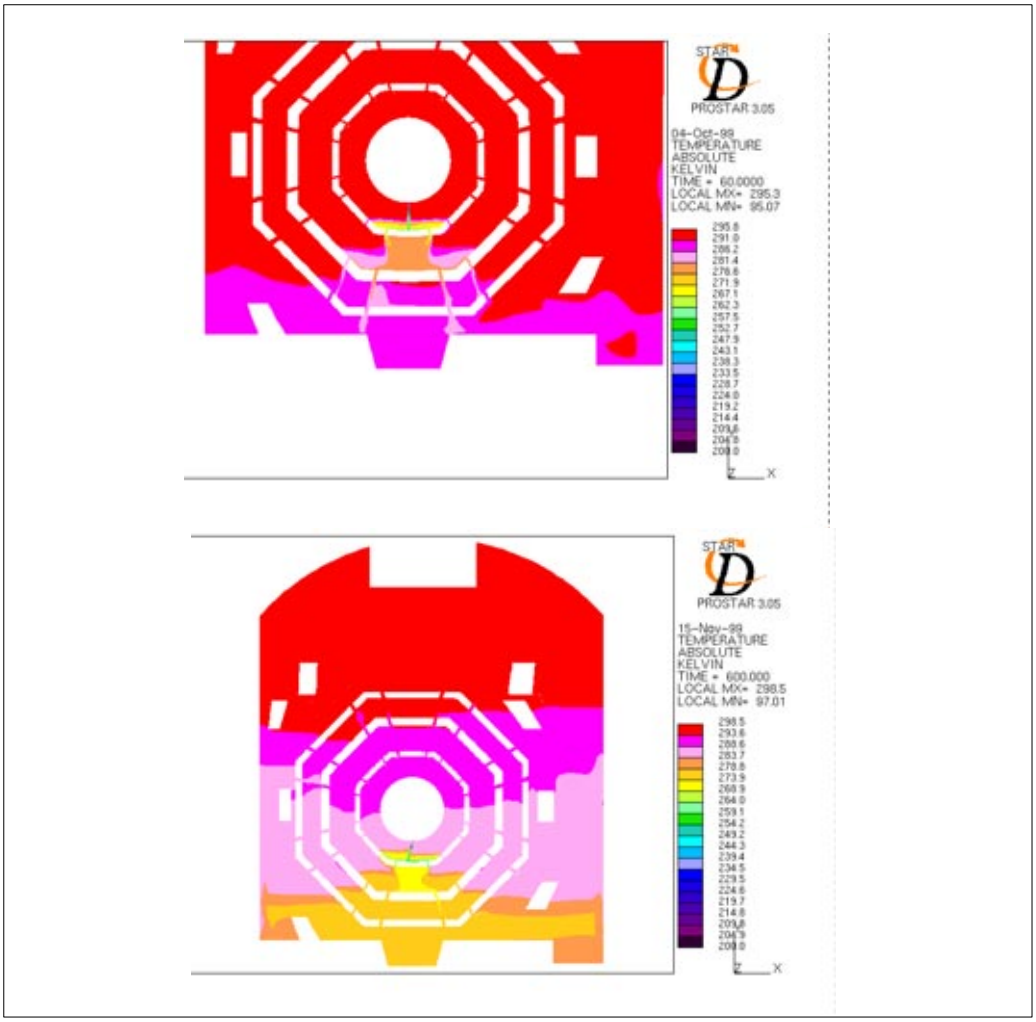

Figure 2.8 Temperature distribution 60 s and 10 minutes after the spill. Argon leak with internal overpressure

Any worker located inside the inner layer of the muon chamber is in danger, argon concentration reaching levels higher than the prescribed limit. In every other zone of UX15 it seems that argon is not reaching dangerous concentrations. Again, the main risk comes from the temperature, which should be sustainable by personnel if there is no direct contact with cold liquid or just vaporized gas. As in the other accidents, the formation of a cloud must not be forgotten as it could seriously complicate any escape attempt.

2.4 Experiment simulation

In this study, a simulation of a real experiment with liquid Argon (CERN, J.Nebout and C.R.Gregory) was carried out in order to validate the model that had been proposed for the ATLAS cavern. The comparison was done just in terms of Oxygen concentration.

The experiment consisted in spilling liquid argon from a vessel, which was pressurized with an argon gas bottle. The spill was taking place at 0,15 m from the floor, and therefore a pool of liquid argon was forming on the floor. The acquisition of the oxygen concentrations was done with five para-magnetic Oxygen detectors.

The simulation was done in two different ways, using the same assumptions and models except for the Argon inlet and time step definition. The goal was to simulate the pool evaporation, even if StarCD is not able to cope with free surface evaporation.

The first model was implementing instantaneous evaporation: the liquid was instantaneously evaporated, and no accumulation of liquid was taking place. This meant that the floor would provide enough heat for the cryogenic liquid evaporation from the beginning until the end of the spill. This model resulted to be conservative, the simulated oxygen concentrations being below the experimental values. The results were very similar to the experimental ones, despite the large number of assumptions made.

The second model was based on The Netherlands Organization model (TNO) for pool evaporation. This model is taking into account that the floor is getting colder with time. Despite the very different boundaries for each model, the results were not far from the ones obtained with the previous model.

Therefore one of the conclusions was that the most critical factor is liquid pool modelling, final results depending rather strongly on its dimensions.

Another experiment was recommended, in which the conditions of ATLAS would be better reproduced and some other important parameters measured.

Chapter 3

Methodology

All the study is based on computational fluid dynamics (CFD) simulations. In this chapter we are going to describe the StarCD code, which uses the Finite-Volume method. We will also describe the boundary conditions used for the ATLAS models, which are presented in chapter 4.

3.1 Basis of the simulation in StarCD

The analysis of systems involving fluid flow, heat transfer and associated phenomena such as chemical reactions by means of computer-based simulation is called 'computational fluid dynamics' (CFD). This technique can be applied to a wide range of industrial and non-industrial areas, such as aerodynamics, environment, chemical processes, biomedicine and many others. CFD codes are structured around the numerical algorithms that can tackle fluid flow problems. All this kind of codes contain three main elements: a pre-processor, a solver and a post-processor.

The *Pre-processor* essentially consists of inputting the problem to the code: this includes definition of geometric domain, grid generation, selection of the physical and chemical phenomena that need to be modelled, definition of fluid(s) properties and specification of appropriate boundary and initial conditions.

The numerical methods that form the basis of the *solver* perform the following steps: approximation of the unknown flow variables by means of simple functions, discretisation by substitution of the approximations into the governing flow equations and subsequent mathematical manipulations, and solution of the algebraic equations.

Finally, the *post-processor* helps us to display results, plot the interesting physical or chemical fields and eventually manipulate them for our purposes.

StarCD uses the *Finite-Volume method* to model fluid flow problems. This is a well-established, thoroughly validated general purpose CFD technique. The numerical algorithm consists of the following steps:

- formal integration of the governing equations of fluid flow over all the (finite) control volumes of the solution domain.
- discretisation of these equations by substituting of a variety of finite-difference-type approximations for the terms in the integrated equation representing flow process as convection, diffusion and sources. This converts the integral equations into a system of algebraic equations.
- solution of the algebraic equations by an iterative method.

We are describing the Finite-Volume method with more details in the next paragraphs. Here we only say that the first step is the one which distinguishes this method from all other CFD techniques (finite differences, finite elements, spectral methods): the resulting statements express the (exact) *conservation of relevant properties for each finite size cell.* This relationship between the algorithm and the underlying physical conservation principle forms one of the main attractions of the finite volume method. Moreover, one of the most important features of this method is that we are enabled to use *embedded refinement* while meshing. This technique is not available in other CFD methods and provides great flexibility to our modelling. An arbitrary number of further refinements is allowed.

3.1.1 Governing equations of fluid flow and heat transfer

The general physical method to approach the fluid flow problem consists in manipulating and solving the conservation equations, which represent mathematical statements of the conservation laws of physics:

- the mass of a fluid is conserved.
- the rate of change of momentum equals the sum of forces on a fluid's particle (Newton's second law). These forces can be "surface forces" (pressure, viscous forces) or "body forces" (gravity, centrifugal, Coriolis, electromagnetic forces).
- the rate of change of energy is equal to the sum of the rate of heat addition to and the rate of work done on a fluid particle (First Law of Thermodynamics).

Without showing all the physical-mathematical process which leads to the conservation equations, we give here their general expressions. Some further considerations will explain which will be the most convenient form of these equations for our purposes.

Mass conservation (turbulence not taken into account):

$$\frac{\partial \rho}{\partial t} + \nabla \bullet (\rho \vec{u}) = 0$$

Momentum conservation (Navier-Stokes equations):

$$\frac{\partial}{\partial t}(\rho u) + \nabla \bullet (\rho u \vec{u}) = -\frac{\partial p}{\partial x} + \nabla \bullet (\mu \nabla u) + S_{Mx} \quad \text{(x-momentum)}$$

$$\frac{\partial}{\partial t}(\rho v) + \nabla \bullet (\rho v \vec{u}) = -\frac{\partial p}{\partial y} + \nabla \bullet (\mu \nabla v) + S_{My} \quad \text{(y-momentum)}$$

$$\frac{\partial}{\partial t}(\rho w) + \nabla \bullet (\rho w \vec{u}) = -\frac{\partial p}{\partial z} + \nabla \bullet (\mu \nabla w) + S_{Mz} \quad \text{(z-momentum)}$$

Energy conservation:

$$\rho\frac{dE}{dt} = ——\sum(p\vec{u}) + \left[\frac{\partial}{\partial x}(u\tau_{xx}) + \frac{\partial}{\partial y}(u\tau_{yx}) + \frac{\partial}{\partial z}(u\tau_{zx}) + \right.$$
$$+ \frac{\partial}{\partial x}(v\tau_{xy}) + \frac{\partial}{\partial y}(v\tau_{yy}) + \frac{\partial}{\partial z}(v\tau_{zy}) + \frac{\partial}{\partial x}(w\tau_{xz}) + \frac{\partial}{\partial y}(w\tau_{yz}) +$$
$$\left. + \frac{\partial}{\partial z}(w\tau_{zz})\right] + \nabla\bullet(k\nabla T) + S_E$$

where:

- $\vec{u} = u\vec{i} + v\vec{j} + w\vec{k}$ (velocity vector);
- S_{Mi} = source of momentum in the *i*-direction per unit volume per unit time;
- for Newtonian fluids (in which the viscous stresses are proportional to the rates of deformation), we have:
  1. $\tau_{xx} = -p + 2\mu\frac{\partial u}{\partial x} - \frac{2}{3}\mu\nabla\bullet\vec{u}$
  2. $\tau_{yy} = -p + 2\mu\frac{\partial v}{\partial y} - \frac{2}{3}\mu\nabla\bullet\vec{u}$
  3. $\tau_{zz} = -p + 2\mu\frac{\partial w}{\partial z} - \frac{2}{3}\mu\nabla\bullet\vec{u}$
  4. $\tau_{xy} = \tau_{yx} = \mu\left(\frac{\partial u}{\partial y} + \frac{\partial v}{\partial x}\right)$
  5. $\tau_{xz} = \tau_{zx} = \mu\left(\frac{\partial u}{\partial z} + \frac{\partial w}{\partial x}\right)$
  6. $\tau_{yz} = \tau_{zy} = \mu\left(\frac{\partial v}{\partial z} + \frac{\partial w}{\partial y}\right)$, and μ = dynamic viscosity;
- S_E = source of energy per unit volume per unit time;
- $E = i + \frac{1}{2}(u^2 + v^2 + w^2)$, with *i* = specific internal energy.

We must underline the fact that in our simulations we will *always* work with gases (air, Argon and / or a mixture of the two), so the flow will be considered *compressible* and the following equations of state are valid:

$$p = \rho RT \text{ and } i = C_v T;$$

these equations of state provide the linkage between the energy equation on the one hand and mass conservation and momentum equations on the other. This linkage arises through the possibility of density variations as a result of pressure and temperature variations in the flow field.

For compressible flows this equation is often re-arranged to give an equation for the *enthalpy*. The specific enthalpy *h* and the specific total enthalpy h_0 of a fluid are defined as:

$$h = i + \frac{p}{\rho} \text{ and } h_0 = h + \frac{1}{2}(u^2 + v^2 + w^2),$$

and, recombining these two definitions with the one for specific energy E we get

$$h_0 = E + \frac{p}{\rho}.$$

Substituting this expression into the energy conservation equation and after some re-arrangement, we get

$$\frac{\partial}{\partial t}(\rho h_0) + \nabla\cdot(\rho h_0 \vec{u}) = \nabla\bullet(k\nabla T) + \frac{\partial p}{\partial t} + \left[\frac{\partial}{\partial x}(u\tau_{xx}) + \frac{\partial}{\partial y}(u\tau_{yx}) + \right.$$

$$+ \frac{\partial}{\partial z}(u\tau_{zx}) + \frac{\partial}{\partial x}(v\tau_{xy}) + \frac{\partial}{\partial y}(v\tau_{yy}) + \frac{\partial}{\partial z}(v\tau_{zy}) + \frac{\partial}{\partial x}(w\tau_{xz}) + \frac{\partial}{\partial y}(w\tau_{yz}) +$$

$$\left. + \frac{\partial}{\partial z}(w\tau_{zz})\right] + S_h$$

where turbulence is not taken into account.

We have to notice that this last equation is *not* a new extra conservation law, but merely an alternative form of the energy equation. We can find many forms of the conservation equations in literature. In particular, StarCD offers a wide range of implementing possibilities, depending on the physical conditions of the problem and including the possibility of having more than one chemical species at the same time. Without going in the deepest details, we report here the three main conservation equations and the most important secondary equations for our work in the form used by Star-CD:

Mass conservation:

$$\frac{1}{\sqrt{g}}\frac{\partial}{\partial t}(\rho\sqrt{g}) + \frac{\partial}{\partial x_j}(\rho\tilde{u}_j) = s_m$$

Momentum conservation (considering turbulence):

$$\frac{1}{\sqrt{g}}\frac{\partial}{\partial t}(\rho\sqrt{g}u_i) + \frac{\partial}{\partial x_j}(\rho\tilde{u}_j u_i - \tau_{ij}) = -\frac{\partial p}{\partial x_i} + s_i$$

Thermal enthalpy conservation:

$$\frac{1}{\sqrt{g}}\frac{\partial}{\partial t}(\rho\sqrt{g}h_t) + \frac{\partial}{\partial x_j}\left(\rho\tilde{u}_j h_t - F_{h_t,\,j}\right) = \frac{1}{\sqrt{g}}\frac{\partial}{\partial t}(\sqrt{g}p) + \tilde{u}_j\frac{\partial p}{\partial x_j} +$$

$$+ \tau_{ij}\frac{\partial u_i}{\partial x_j} + s_h - \sum_m m_m H_m s_{c,\,m}$$

Mass transfer in fluid mixtures (species conservation equation):

$$\frac{1}{\sqrt{g}}\frac{\partial}{\partial t}(\rho\sqrt{g}m_m) + \frac{\partial}{\partial x_j}(\rho\tilde{u}_j m_m - F_{m,\,j}) = s_m$$

Ideal gas law for gas mixtures:

$$\rho = \frac{p}{RT\left(\sum_m \frac{m_m}{M_m}\right)}$$

Mixture properties (viscosity, mean specific heat and thermal conductivity):

$$\phi = \sum_{m \neq bg} m_m \phi_m + \left(1 - \sum_{m \neq bg} m_m\right)\phi_{bg}$$

where:

- t = time;
- x_i = Cartesian coordinate (i = 1, 2, 3);
- u_i = absolute fluid velocity component in direction x_i;
- $\tilde{u}_i = u_j - u_{cj}$, relative velocity between fluid and local (moving) coordinate frame that moves with velocity u_{cj};
- p = piezometric pressure = $p_s - \rho_0 g_m x_m$, where p_s is static pressure, ρ_0 is reference density, the g_m are gravitational field components and the x_m are coordinates from a datum, where ρ_0 is defined;
- ρ = density;
- $\tau_{ij} = 2\mu s_{ij} - \frac{2}{3}\mu\frac{\partial u_k}{\partial x_k}\delta_{ij} - \bar{\rho}\overline{u'_i u'_j}$ = stress tensor components for Newtonian fluids in turbulent flows, where all the dependent variables assume their ensemble averaged values; the u' are fluctuations about the ensemble average velocity and the overbar denotes the ensemble averaging process; δ_{ij} is the so-called “Kronecker delta”, equal to unity when i = j and zero otherwise. The rightmost term represent the additional Reynolds stresses due to turbulent motion (see also next paragraph);
- $s_{ij} = \frac{1}{2}\left(\frac{\partial u_i}{\partial x_j} + \frac{\partial u_j}{\partial x_i}\right)$ = rate of strain tensor;
- s_m = mass source;
- $s_i = g_i(\rho - \rho_0)$ = buoyant forces, essentially the only contribution to momentum source components; here g_i is the gravitational acceleration in direction x_i;
- $\sqrt{g}$ = determinant of metric tensor;
- m_m = mass fraction of mixture component m;
- H_m = heat of formation of constituent m;
- $h_t = \tilde{c}_p T - c_p^0 T_0$ = thermal enthalpy, with $\tilde{c}_p$ = mean constant-pressure specific heat at temperature T, and c_p^0 = reference specific heat at temperature T_0;

- s_h = energy source;
- $s_{c,m} = s_m$ = rate of production or consumption of species m due to chemical reaction (always =0 for us, as Argon does not react with anything);
- $F_{h_t,\,j} = k\frac{\partial T}{\partial x_j} - \bar{\rho}\overline{u'_j h'} + \sum_m h_{m,\,t}\rho D_m \frac{\partial m_m}{\partial x_j}$ = diffusional energy flux
- in direction x_j in turbulent flow, where the middle term containing static enthalpy ($h_{m,t}$) or thermal enthalpy fluctuations (h'_t) represents the turbulent diffusional flux of energy, k is the thermal conductivity and D_m is the molecular diffusivity of constituent m;
- $F_{m,\,j} = \rho D_m \frac{\partial m_m}{\partial x_j} - \bar{\rho}\overline{u'_j m'_m}$ = diffusional flux component; the rightmost term, containing the concentration fluctuation m'_m, represents the turbulent mass flux;

- ϕ is a mixture value of one between viscosity, thermal conductivity and mean specific heat, ϕ_m is the property value of constituent m and ϕ_{bg} is the property value of the background ("bg") fluid.
- Note: $\frac{\partial}{\partial x_j}(\rho u_j) = \frac{\partial}{\partial x}(\rho u) + \frac{\partial}{\partial y}(\rho v) + \frac{\partial}{\partial yz}(\rho w) = \nabla\bullet(\rho\vec{u}) = div(\rho\vec{u})$

3.1.2 Turbulence modelling

In experiments on fluid systems it is observed that at values below the so-called critical Reynolds number the flow is smooth and adjacent layers of fluid slide past each other in an orderly fashion *(laminar flow)*. Above this critical value of the Reynolds number a complicated series of events takes place, eventually leading to a radical change of the flow character, and in the final state the flow behavior is random and chaotic: the motion becomes intrinsically unsteady even with constant imposed boundary conditions, and velocity and all other fluid properties vary in a chaotic way *(turbulent flow)*.

The random nature of a turbulent flow precludes computations based on a complete description of the motion of all the fluid particles. We must re-define the velocity in this way:

$$\vec{u}(t) \rightarrow \vec{U}(t) = \vec{u} + \vec{u}'(t)$$

where the velocity is decomposed into a steady mean value u with a fluctuating component u' superimposed on it.

Particles of fluid which are initially separated by a long distance can be brought close together by the eddying motions in turbulent flows. As a consequence, heat, mass and momentum are very effectively exchanged, and diffusion coefficients for mass, momentum and heat reach high values. The point where instability first occurs is always upstream of the point of transition to fully turbulent flow. The distance between the point of instability where the Reynolds number assumes its

critical value and the point of transition depends on the degree of amplification of the unstable disturbances and on the type of flow (jet, flow over a flat plate, pipe flow), but there is no comprehensive theory regarding the path leading from initial instability to fully turbulent flows. Transition to turbulence is strongly affected by factors as pressure gradient, disturbance levels, wall roughness and heat transfer.

The most important dimensionless groups in turbulence mathematical modelling are the following:

- Reynolds = $Re = \frac{\rho UL}{\mu}$ ----> (inertia force) / (viscous force);
- Prandtl = $Pr = \frac{\mu c_p}{k}$ ----> (diffusion of momentum) / (diffusion of heat);
- Peclet = $Pe = Re\ Pr$ ----> (heat transfer by convection) / (heat transfer by conduction);
- Grashof = $Gr = \frac{g\beta\rho^2\Delta T L^3}{\mu^2}$ ----> (buoyancy force)(inertia forces) / (viscous force)^2;
- Raleigh = $Ra = Pr\ Gr$,

where ρ is the density, μ is the viscosity, k is the thermal conductivity, c_p is the specific heat, g is the gravitational acceleration (= 9.81 m / s^2), β is the thermal expansion coefficient, and U, L and ΔT are characteristic velocity, length and temperature difference of the considered domain.

In jet flows all wavelength disturbances are amplified (by one or more point of inflexion) at all Reynolds numbers typically above about 10: after the flow emerges from the orifice the laminar exit flow produces the rolling up of a vortex fairly close to the orifice. Subsequent amplification results in the generation of a large number of small scale eddies and in rapid transition to the fully developed turbulent regime.

In the case of flow over a flat plate, if the incoming flow is laminar numerous experiments confirm the predictions of the theory that initial linear instability occurs around $Re_{crit} \sim 91.000$. Transition involves the formation of turbulent spots at active sites and the subsequent merging of different turbulent spots convected downstream by the flow. This takes place at $Re_{tran} \sim 10^6$.

Transition to turbulence in a pipe flow - an example of a category of flows without an inflexion point - takes place for values of Re between 2000 and 10^5.

In natural convection problems the strength of buoyancy-induced flow can be measured by the Raleigh number, Ra. Raleigh numbers less than 10^8 usually indicate laminar flow, with onset of turbulence occurring over the range $10^8 < Ra < 10^{10}$. Generally if $Ra >> 10^9$ we are allowed to say that flow is fully turbulent.

As it will be shown in the next chapters, in our conditions the flow is always turbulent, then a complete, conservation equation-like mathematical model is necessary.

There are essentially two main type of models for turbulence modelling: *mixing length models*, attempting to describe the Reynolds stresses $\tau'_{ij} = -\bar{\rho}\overline{u'_i u'_j}$ by means of simple algebraic formulae for μ_t (turbulent viscosity) as a function of

position, and the more sophisticated and costly *K*-ε *models*, which allow for the effects of transport of turbulence properties by the mean flow and diffusion and for the production and destruction of turbulence. In the latter, two transport, partial differential equations, one for the turbulent kinetic energy *K* and a further one for the rate of dissipation of turbulent kinetic energy ε, are solved.

The underlying assumption of both these types of models is that μ_t is isotropic, in other words the ratio between Reynolds stress and mean rate of deformation is the same in all directions. The *K*-ε model is the most widely used and validated turbulence model. It is the simplest model for which only initial and / or boundary conditions need to be supplied, and provides excellent performances for many industrially relevant flows. On the other hand, it is rather more expensive to implement than mixing length models.

StarCD provides a wide choice of turbulence models. We will always choose a recent variant of the *K*-ε model, the so-called *Renormalization Group (RNG) K*-ε *model*. This model is based on the work of Yakhot and Orszag of Princeton University, and the formulation employed by StarCD is one of the most recently published. The RNG procedure systematically removes the small scales of motion from the governing equations by expressing their effects in terms of larger scales motions and a modified viscosity.

The main constitutive relations are:

$$-\bar{\rho}\overline{u'_i u'_j} = 2\mu_t s_{ij} - \frac{2}{3}\left(\mu_t \frac{\partial u_k}{\partial x_k} + \rho K\right)\delta_{ij}, \quad \bar{\rho}\overline{u'_j h'} = -\frac{\mu_t}{\sigma_{h,t}}\frac{\partial h}{\partial x_j},$$

$$\bar{\rho}\overline{u'_j m'_m} = -\frac{\mu_t}{\sigma_{m,t}}\frac{\partial m}{\partial x_j}, K = \frac{1}{2}(u'^2 + v'^2 + w'^2) \text{ and } \mu_t = f_\mu \frac{C_\mu \rho K^2}{\varepsilon},$$

where $\sigma_{h,t}$ and $\sigma_{m,t}$ are the turbulent Prandtl and Schmidt numbers, respectively. Both these two numbers and C_μ and f_μ are empirical coefficients usually assigned constant.

The two new differential equations to be solved are:

Turbulent kinetic energy:

$$\frac{1}{\sqrt{g}}\frac{\partial}{\partial t}(\rho\sqrt{g}K) + \frac{\partial}{\partial x_j}\left(\rho\tilde{u}_j K - \frac{\mu_{eff}}{\sigma_k}\frac{\partial K}{\partial x_j}\right) =$$

$$= \mu_t(P + P_B) - \rho\varepsilon - \frac{2}{3}\left(\mu_t \frac{\partial u_i}{\partial x_i} + \rho K\right)\frac{\partial u_i}{\partial x_i}$$

Turbulence dissipation rate:

$$\frac{1}{\sqrt{g}}\frac{\partial}{\partial t}(\rho\sqrt{g}\varepsilon) + \frac{\partial}{\partial x_j}\left(\rho\tilde{u}_j\varepsilon - \frac{\mu_{eff}}{\sigma_\varepsilon}\frac{\partial\varepsilon}{\partial x_j}\right) = \frac{\varepsilon}{K}[\mu_t(C_{\varepsilon 1}P + C_{\varepsilon 3}P_B) +$$

$$-\frac{2}{3}\left(\mu_t\frac{\partial u_i}{\partial x_i} + \rho K\right)\frac{\partial u_i}{\partial x_i}] - C_{\varepsilon 2}\rho\frac{\varepsilon^2}{K} + C_{\varepsilon 4}\rho\varepsilon\frac{\partial u_i}{\partial x_i} - \frac{C_\mu\eta^3\left(1-\frac{\eta}{\eta_0}\right)}{1+\beta'\eta^3}\frac{\rho\varepsilon^2}{K}$$

where:

- $\mu_{eff} = \mu + \mu_t$;
- $P = 2s_{ij}\frac{\partial u_i}{\partial x_j}$ and $P_B = -\frac{g_i}{\sigma_{h,t}}\frac{1}{\rho}\frac{\partial\rho}{\partial x_i}$;
- $\eta = S\frac{K}{\varepsilon}$ and $S = \sqrt{2s_{ij}s_{ij}}$.

The other empirical, constant coefficient are listed in table 2.11:

Table 3.1 Values assigned to RNG K-ε turbulence model coefficients

C_μ	σ_k	σ_ε	$C_{\varepsilon 1}$	$C_{\varepsilon 2}$	$C_{\varepsilon 3}$[a]	$C_{\varepsilon 4}$	κ	η_0	β’
0.085	0.719	0.719	1.42	1.68	0 or 1.42	-0.387	0.4	4.38	0.012

a. $C_{\varepsilon 1} = 1.42$ for $P_B > 0$ and zero otherwise.

The RNG model, as originally proposed, takes no explicit account of compressibility or buoyancy effects. However, in StarCD these effects are modelled as in the standard *K*-ε models (options are available to omit or select them).

3.1.3 Convergence in transient models

Since our flow is turbulent, we will carry on a transient analysis type, basing ourselves on the PISO algorithm. This choice is expensive in computational time, because StarCD has to solve the closed equations’ system at each cell and time step, thus needing internal iterations for the solution variables, but in the mean time will allow us to follow the whole history of flow.

There are several parameters we have to periodically monitor in order to check if the computed solution is numerically stable and satisfies our needs. We have to stress that all these parameters are all related with convergence, consistency and stability, but their weight is not well defined, so we cannot say that there exists a precise limit not to be exceeded to ensure the respect of such constraints. However, experience in Computational Fluid Dynamics can give useful advice about the best way to get a reliable solution and to judge convergence. Respecting the prescribed

parameter constraints or building models which stand inside the suggested limits can most times lead to the construction of a reliable flow field.

Under-Relaxation

In order to reduce the risk of numerical instability, we use under-relaxation technique for pressure (when running transient simulations it is not allowed to use under-relaxation in all variables but only for Pressure). Thus if *k* is the internal iteration counter inside a certain time step, the solution for pressure at each cell p^k is taken as a weighted mean of the previous iterate p^{k-1} and the (provisional) current one, denoted by p^{kk}, as follows:

$$p^k = \alpha_p p^{kk} + (1 - \alpha_p) p^{k-1}$$

where α_p, the under-relaxation factor, is a number between 0 and 1. The default value is 1, we chose $\alpha_p = 0.8$.

Precision

Also, we will run our simulations in *double precision* (always adviced for turbulent models). This is because in buoyancy driven flows the body force terms in the momentum equation are often so small compared to the other terms that they can be masked by the round-off error of the calculation. The consequences of working in single precision might be non-convergence of the solution.

Courant Number

Maximum and mean Courant number give us an idea of the velocity of diffusion of the magnitudes. Both numbers are important since they are somehow related to the time step. The maximum courant number should be not higher than 100, while a good mean courant number should not exceed 1.

The Courant number is calculated the following way:

$$Cou = \frac{|\vec{v}|\Delta t}{l}$$

where $|\vec{v}|$ and l are characteristic velocity and dimension, respectively. The Courant number has to be calculated in two ways:

- Cell-wise: $|\vec{v}|$ must be set to an estimated local velocity and l to the corresponding local mesh dimension (generally, cell diagonal). As we said, the time step should be chosen such that the maximum Courant number *does not exceed* 100.
- Globally: $|\vec{v}|$ must be set to the estimated average velocity and l to a characteristic overall dimension of the problem. This one should not exceed 500 in any case, being recommended that this number remains under 100.

Star-CD calculates the maximum and mean Courant number above the whole domain at each step, thus enabling us to keep it under control and, if necessary, reduce it.

Piso Correctors

During loop execution, the algorithm corrects the computed value of a variable in subsequent stages, each time approaching to the final converged value for the current cell and timestep. The maximum default number for the PISO correctors is 20. A high number of correctors could mean that the chosen timestep is too large to get acceptable temporal detail on flow. When the piso correctors are exceeded, one of the first actions to take is to reduce the time step.

Sweeps

Inside each time step, StarCD performs internal iterations to get the values for all the solution variables in the whole domain. Then we have to set a residual error tolerance to be respected for these 'internal sweeps'. Normally it is sufficient to set it to a value of the order of 10-2 or 10-3.

HDIFF

We are also able to check in the *.info file the residual of the energy conservation equation, HDIFF. This value should be kept as small as possible, otherwise this means that some non-physical energy source or sink has been created in the domain.

Time Differential Scheme and Time Step

We choose the Fully-Implicit method for temporal discretisation, in order to have an unconditionally stable scheme. The only remaining thing is to choose the temporal increment Δt. This choice should be -in theory- independent from the problem or the mesh, but practically it isn't.

In order to reach an acceptable accuracy, Δt should ideally be of same order of magnitude as the smallest characteristic time δt_c for convection and diffusion, i.e.

$$\delta t_c = min(\frac{\delta l}{U}, \frac{\rho \delta l^2}{\Gamma})$$

where U and Γ are a characteristic velocity and diffusivity, respectively, and δl is a mean mesh dimension. Typically, it is possible to operate with $\Delta t \approx 50 \delta t_c$ and still obtain reasonable temporal accuracy. Values significantly above this may lead to errors and numerical instability, whereas smaller values will lead to increased computing times. It is not easy to estimate δl and Γ, so it is hard to find a reasonable value for δt_c.

Buoyancy-driven flows with a high Grashof number are naturally unstable and the time step could also be calculated from

$$\Delta t = \frac{1}{N} = \frac{1}{\sqrt{\beta g \frac{\Delta T}{d}}}$$

where N is called the Brunt Vaissala frequency, ΔT is the temperature range within the solution domain, d is a characteristic length based the distance between the maximum- and minimum-temperature boundaries and β is the volumetric thermal expansion coefficient.

By means of this formula, and setting $\beta_{max} = 1/T_{min} = 1/90K = 0.0111\ K^{-1}$ and $\Delta T \sim$ 200 K, it comes out that we only have to estimate d (distance between the points at maximum and minimum temperature). It is immediately clear that d varies with time, and that these points are close to Argon inlet, where we have the steepest temperature gradients. At the very beginning the distance of the point at 90 K from those at 293 K will be of the order of half the inlet section (~ cm), then it will increase as Argon mixes with air, reaching ~ m after several seconds. Thus we'll probably be allowed to increase the value of Δt after some time from the beginning of the accident.

Spatial Differential Scheme and Blending factors

The manner in which the convective and diffusive fluxes are treated from the spatial differential point of view is one of the key factors determining accuracy and stability, both for steady and transient calculations. There are basically two approaches:

Low-order schemes, which characteristically generate discretised equation forms that are easy to solve, produce solutions which obey the expected physical bounds, but sometimes give rise to smearing of gradients. This effect is known as numerical diffusion. This is a form of truncation error that diminishes as the grid is refined, but at an increased cost of calculation.

Among low-order schemes, we have Upwind differencing (UD), which we will use for all the variables except for density, for which we preferred Central Differencing (CD), a higher order scheme.

Higher-order schemes, which better preserve steep gradients, but may result in equations that are more difficult to solve (and, in extreme cases, may provoke numerical instabilities) and / or have solutions exhibiting non-physical spatial oscillations ('wiggles'). These oscillations may, in some cases, lead to spurious values, e.g. negative species concentration or turbulent kinetic energy. This phenomenon is called numerical dispersion. It too can be diminished by grid refinement or by using monotone schemes (e.g. a blending methodology).

Among these high order schemes, we can find:

- Linear upwind differencing (LUD), a second-order accurate scheme formulated for non-structured meshes;
- Central Differencing (CD), also second-order, which simply interpolates linearly on nearest neighbour values, irrespective of flow direction;
- Quadratic upstream interpolation of convective kinematics (QUICK);
- Monotone advection and reconstruction scheme (MARS), which is a multidimensional second-order accurate differencing scheme that operates in two separate steps: reconstruction and advection. The user can control the ability of the advection scheme to accurately capture sharp discontinuities in the flow by setting the scheme's compression level to a value between 0 and 1. The default value for this parameter is 0,5, which is the best compromise between accuracy and convergence rate.
- Self-filtered central differencing (SFCD). This scheme, as the name implies, is effectively central differencing with a built-in adaptive filter to remove non-physical extrema whenever they would arise.

- Gamma differencing scheme
- Blended differencing. The method here is similar to SFCD scheme, in that a higher order, non-monotone scheme like CD (or LUD or QUICK) is blended with the lower-order UD scheme to suppress dispersion.

As we said before, we use Central Differencing scheme for density, with a blending factor of 0,8 to avoid dispersion. We experienced that keeping a blending factor of 1 was leading to negative densities in a huge part of the domain, and therefore to non convergence.

3.2 Common boundaries for the ATLAS model

In this section we will describe the boundaries common to all the models. They basically share the same air inlets-outlets, the heat load, the isothermal walls, symmetry planes.The detailed description of all the boundaries for each model can be found at Appendix A.

3.2.1 Ventilation

The ventilation parameters have changed while doing this study. Therefore, some models are still considering the old parameters (which have been explicitly described in chapter 1.4 and 1.5), while others consider the new specifications provided by the Cooling and Ventilation group.

The air speed value at each inlet is given by:

$$\upsilon = \frac{Q \cdot f_k}{3.600 \cdot l_k \cdot L}$$

where Q is the prescribed volumetric flow in m^3/h, f_k is the foreseen fraction of total volumetric flow at inlet k, l_k is the cross-length of the inlet and L is the depth of the room (L=45 m). Then the speed value is given in m/s.

The volumetric flow for the inlets is the one given in the description above.

Apart from the averaged speed, values still to be specified at inlets are temperature, density, turbulent kinetic energy (*k*) and turbulent energy dissipation (ε).

In order to calculate the turbulent kinetic energy and its rate of dissipation, we define the turbulence intensity and the turbulent mixing length for the inlet in the following way:

$$I \equiv \frac{u'}{u} = \text{turbulence intensity}$$

where *u* is the magnitude of the local velocity on the boundary. The turbulence intensity is usually much less than unity so we will assume:

$$I = 0,1(10\%)$$

and as suggested in StarCD literature, then the turbulent mixing length is defined as follows:

$$\tilde{l_k} = 0,1 \cdot l_k = \text{turbulent mixing length}$$

Once we have defined these parameters, then we calculate the turbulent kinetic energy (*k*) and turbulent energy dissipation (ε) in the following way:

$$K = 1,5 \cdot (u_k \cdot I)^2$$

$$\varepsilon = \frac{(C_{\mu}^{0,75} \cdot K^{1,5})}{\tilde{l}_k}$$

As for the temperature of the outlets, we will consider that the ventilation system is designed to be able to absorb all the thermal power (equal to 180 kW for the new specifications). Then the heat balance will let us know the temperature the air goes out in normal conditions (we use the flow in normal running, so half of the volumetric flow that has been described until now). Therefore we can calculate this temperature from the balance:

$$180.000 W = \omega \cdot c_p \cdot (T_{out} - T_{in})$$

where ω is the mass of air ($\omega=\rho\ Q_{tot}$), ρ =1,19 kg / m^3, considered constant in our range of temperatures, Q_{tot}(m^3 / h) is the total quantity of air, C_p = 1006 J / kg K and T_{in} is set to 290 K. Substituting these values, we reach a temperature:

$$T_{out} = 297,2K$$

The boundary properties that correspond to the new specifications are shown in the following tables:

Table 3.2 Inlets' geometric dimensions and calculated speeds

Inlet	*Cross-length [m]*	*Air speed [m/s]*
Exhaust plenum	9,29	0,079735
Left diffuser	2,0	0,85185
Right top diffuser	2,4	0,082304
Right bottom diffuser	2,0	0,185185
Central pit extractor	0,937	0,167616
Right pit extractor	0,9	0,04609

Table 3.3 Inlet's turbulence parameters k and ε

Inlet	*K [m^2/s^2]*	*ε [m^2/s^3]*
Exhaust plenum	9,536 e-05	1,578 e-07
Left diffuser	0,0005145	9,183 e-06
Right top diffuser	1,016 e-04	7,012 e-07
Right bottom diffuser	0,0005145	9,183 e-06
Central pit extractor	4,214 e-04	1,527 e-05
Right pit extractor	3,186 e-05	3,284 e-07

3.2.2 Heat Load

The heat load specifications have changed from a heat load of about 100 kW to 180 kW. This is reflected in the boundary conditions in the following way.

The heat load is inserted through boundaries of wall with constant heat flux. This way we do not insert conductivity into the model -which would need conjugate heat transfer options- but we remain in the convection domain.

The heat load is considered to be 50% due to the racks and 50% due to the muon chambers. This heat is introduced via walls of no-slip type -the velocity components always set to zero, as well as the swirl term - with constant heat flux. An option of roughness is available, and we choose the 'standard' model via specification of the parameter Elog, which we keep to the default value of 9,0, which stands for a smooth wall. The thermal boundary conditions are set by the description of a constant heat flux. StarCD needs a value of the specific heat flux in W / m^2, and we will calculate is as follows:

$$q_{r,\,m} = \frac{\frac{180.000}{2}[W]}{p \cdot L}$$

where p is the cross section perimeter of the racks or of the muon chambers, in meters and L is again the depth of the cavern (45 m). According to our geometry, for the racks, p_r = 67,14 m, which leads us to a heat flux value of q_r = 29,78 W / m^2. For the muon chambers we have: p_{muon} = 315,8 m, which leads us to a heat flux value of q_{racks}= 6,33 W / m^2.

3.2.3 Isothermal walls

One of the hypothesis of the model is to set walls as isothermal. We define them as constant temperature no-slip walls, again setting all the velocity components to zero and using the 'standard' model of roughness with the default value for the Elog parameter, equal to 9,0. The temperature of the walls has been defined as an average between inlet and outlet temperature, that is to say:

$$T_{wall} = \frac{T_{in} + T_{out}}{2} = 293,6K$$

3.2.4 Symmetry plane

We define the z=0 planes as symmetry planes. This allows us to transform a 3D one-cell thick model in a 2D domain. The symmetry plane condition involves normal component of velocity and normal gradient of all other variables to be equal to zero.

3.2.5 Air and Argon. properties

The most important assumption we are forced to make is that Argon becomes *immediately* gaseous after entering UX atmosphere. This assumption is due to the fact that StarCD *does not provide an evaporation model for free surfaces.* We could think to model the evaporation just considering the formation of a liquid pool on the ground, calculating the evaporation flux and starting simulation from this point. It is not possible to get reliable results if we do not know the pool dimension, which is a critical factor. Not enough data to calculate the spreading of a pool are available, nor any theoretical evaluation previous to test is feasible.

As we just did for air, we will average on the whole length of the room, which somehow could seem strange and unrealistic for a localized rupture, but is done so as to be coherent with other velocities- and heat transfer-related calculations. We must remember that the simulation uses a bidimensional domain, and this technique is quite common is such cases. There seems to be a good experimental evidence that this choice is appropriate.

Air Properties

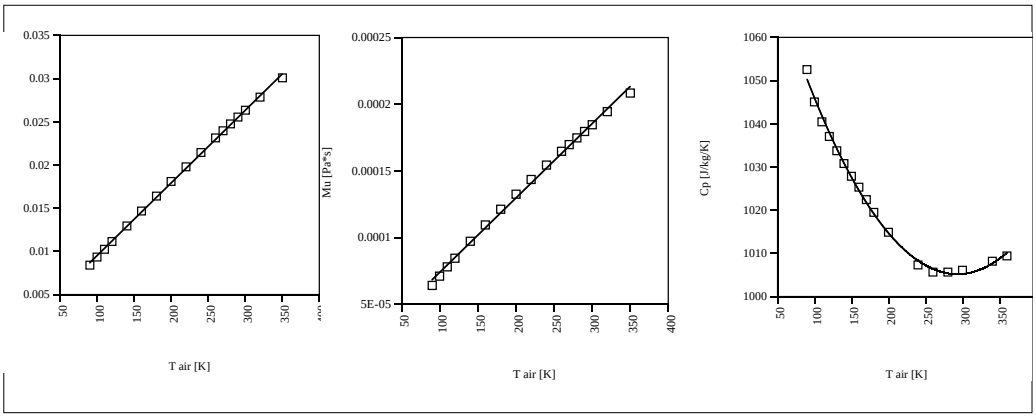

Figure 3.1 Air properties

Therefore, the Air properties that we will implement are:

- c_p = 1006 J / kg / K;
- k = 0.02637 W / m / K;
- $\mu = 1.81*10^{-5}$ Pa*s;
- Molecular weight = 28.96 g / mol.
- Density is implemented in function of T and P. Compressible flow

Argon Properties:

Argon is a gas in normal atmospheric conditions. It is a colorless, odorless and tasteless gas, and has a perfect physical and chemical stability. It is a nontoxic, nonflammable, noncorrosive gas. At atmospheric pressure and temperatures below -183 C, Argon is liquid. Some general characteristics are listed in the following table:

Table 3.4 Argon characteristics

Characteristic	*Value*
T at triple point	83.78 K
Pressure at triple point	0.687 bar
Boiling point (1 atm)	87.3 K
Liquid density at b. p.	1392.8 kg / m^3
Gas density at b. p.	5.8530 kg / m^3
Heat of vaporization	160.78 kJ / kg
T at critical point	150.86 K
Pressure at critical point	48.98 bar
Atomic weight	39.94
Natural isotopes	Ar^{36} (0.337%) Ar^{38} (0.063%) Ar^{40} (99.6%)

The following figure is representing the argon's properties:

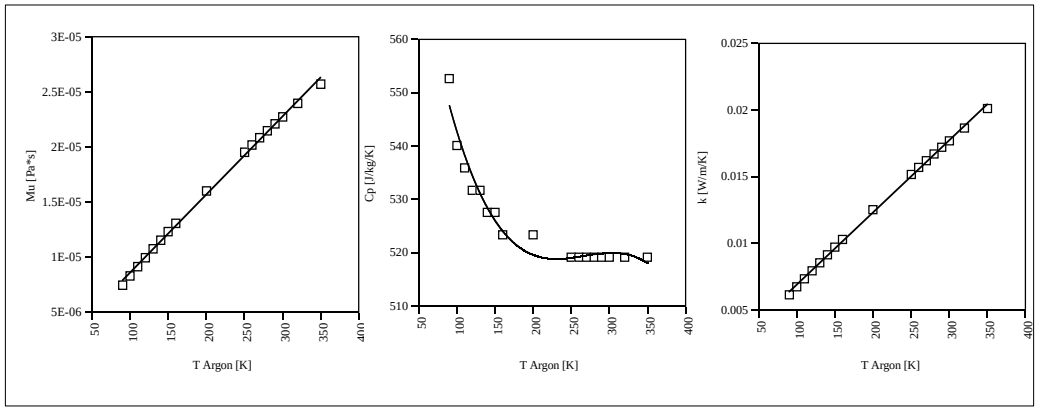

Figure 3.2 Argon properties

We implemented a polynomial expression for specific heat for Argon, since it is varying a lot and is quite an important parameter. The other variables will remain constant (values for 1bar, 90K for the Argon).

Argon is defined inside Star-CD by means of the introduction of a *scalar variable* (up to 50 scalar variables can be defined). The modelled Argon is associated to the background fluid (air), and the two gases are then effectively treated as a mixture. To make this possible, we must define the specific heat, thermal conductivity and molecular viscosity as *Multicomponent* in the Property Module. The required data about Argon in the Scalar Module is listed in the following table.

Table 3.5 Implemented Argon properties and parameters

Property / Parameter	Value / Setting
Influence	Active
Molecular weight	39.94 g / mol
Density (1 bar, 90 K)	5.3375 kg / m^3 [a]
Thermal exp. coefficient	0.0111 K^{-1} [b]
Specific heat (1 bar, 90 K)	552.658 J / kg / K
Thermal conductivity (1 bar, 90 K)	0.006142 W / m / K
Molecular viscosity (1 bar, 90 K)	7.45*10^{-6} Pa*s
Initial concentration	0
Molecular diffusivity	3.004*10^{-5} [c]
Schmidt number	0.9 [d]

a. Just a reference value.
b. Calculated by means of the well-known formula for ideal gases $\beta = 1/T$, with $T = 90$ K.
c. Default value from Star-CD's database.
d. Default value from Star-CD's database.

Finally, in the following picture we see the cavern meshing and all the boundaries.

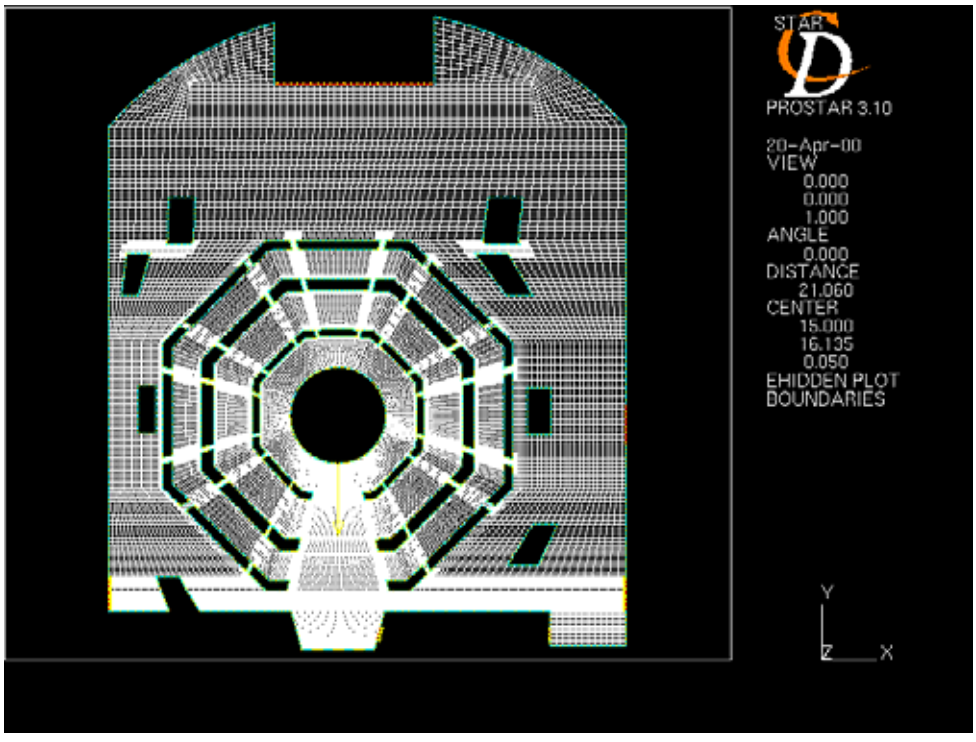

Figure 3.3 Boundary conditions and meshing of the ATLAS model

3.3 Argon & Safety

Argon does not give rise to any oxidation reaction and is physiologically inert and nontoxic. By displacing the Oxygen in air, it may have harmful effects on the organism, by reducing the partial pressure of Oxygen and acting as an asphyxiant.

Contrary to widespread belief, an Oxygen-poor atmosphere does *not* cause respiratory difficulty or a feeling of suffocation in a healthy person, but is only manifested by minor effects, substantially corresponding to periods of incipient anesthesia. The most easily detectable symptoms could be: gradual loss of balance, dizziness; feeling of tightness or compression in the head, located near the forehead; tingling sensation in the tongue, fingertips and toes; difficulty and weakening of speech, leading to the inability to utter a sound; unnoticeable and then rapid reduction of the ability to exert physical effort and to coordinate movements, leading to total immobility; reduced awareness of the outside world and dampening of sensory characteristics, particularly the touch; frequently heightened mental activity.

It should not be presumed, however, that any of the symptoms enumerated above will necessary be felt or detected, thus providing a guarantee of sufficient warning. In practice, unsuspecting persons could breathe Oxygen, air, Nitrogen or Argon with equal ease, without being promptly aware of the fact. Difficulties caused by Oxygen-poor atmospheres can only be effectively detected by persons who are familiar with conditions prevailing in incipient anesthesia. Persons who are unaware of these factors generally reach the stage of immobility and effective voicelessness by the time they notice any peculiarity. This is one of the reasons why personnel working in experimental areas should be carefully trained and equipped with air-supply or independent respiratory devices. Referring to other studies, we can show a more precise assessment of symptoms of Oxygen deficiency:

Table 3.6 Symptoms of Oxygen deficiency

% in volume of Oxygen in the atmosphere	*Symptoms*
21 - 19	No symptoms
19 - 15	Markedly slower reaction times
15 - 12	Heavy breathing, rapid pulse, lack of co-ordination
12 - 10	Dizziness, unclear thinking, lips slightly bluish
10 - 8	Nausea, vomiting, loss of consciousness
8 - 6	Death within 8 minutes, brain damage within 4 - 8 minutes
4	Coma after 40 seconds, respiratory failure, death

We will consider an Oxygen volume concentration of **17%** as the critical value at which people begin to have problems due to Argon breathing.

The volumetric and weight concentrations of Argon that correspond to this Oxygen limit-concentration can be calculated as follows:

Gas volume percentuals of dry air are approximatively: N_2 --> 78%, O_2 --> 21%, Ar --> 1%.

Then in 10 mass units of air we have 28.01*7.8 = 218.478 g of Nitrogen, 32*2.1 = 67.2 g of Oxygen and 39.94*0.1 = 3.994 g of Argon, for 289.672 g total.

The mass concentration are then: N_2 --> 75.42%, O_2 --> 23.20%, Ar --> 1.38%.

Let us suppose of adding Argon until the volume concentration of Oxygen reaches 17%. This means that Oxygen relative abundance has been reduced by 17 / 21 = 0.81. If we suppose homogeneous distribution of gases, also Nitrogen's abundance will be reduced by the same factor, then its new volume concentration is 78*0.81 = 63.18%.

Thus the "limit atmosphere" for a human being could be assumed to be (volume %): N_2 --> 63.18%, O_2 --> 17%, Ar --> 19.82%.

Following the same procedure as before, we obtain the corresponding *mass* concentration: N_2 --> 56.99%, O_2 --> 17.52%, **Ar --> 25.49%** . The last percentual is very important because Star-CD can plot chemical species' concentration in terms of mass percentual, then this will be our referring value.

Prolonged inhalation of cold vapor can produce effects on the lungs which may lead to serious illness. Danger of hypothermia may be present at temperatures up to 10° C. Besides, even brief contact with the cryogenic fluids can cause cryo-burns. Continuous exposure of naked flesh to a cold atmosphere can result in frostbite. The cornea of the eye is particularly sensitive to splashes of cryogenic liquids. Naked or insufficiently protected parts of the body or clothing may stick to cold surfaces by virtue of the freezing and skin may be torn off on removal of the clothing. Finally, it must not be forgotten that if a thick gaseous Argon cloud is created, opacity could prevent people from finding the escape ways. Panic or unexpected psychological reactions should be taken into account when discussing evacuation plans or safety exits.

Obviously, not only personnel could be subjected to danger due to cold Argon release, but also installations. First of all, the volume occupied by the gas in normal conditions (1 atm, 15° C) increases by a factor 835 respect to liquid. This could cause increased pressure within a tank and create the risk of an explosion and generation of projectiles. Moreover, when materials are subjected to the extreme temperatures of cryogenic liquids, their properties can change radically and sometimes unespectedly (thermal stress and embrittlement). Care must be taken to avoid such events affect vital mechanical and / or safety equipment.

Chapter 4

New Simulations

In this chapter we describe the new simulations carried out for the ATLAS cavern. New geometries are presented, as well as a sensitivity study on the flow, and on the main elements of the model.

4.1 Goal of the study

The previous study had proposed a model for spills of liquid argon in the ATLAS cavern. Two leaks (a catastrophic and a very small one) had been analyzed for a one layer of muon chambers geometry.

Therefore, there was still plenty of work to be done. We oriented our work in three aspects:

1. Sensitivity study on the flow, in order to analyze the consequences of intermediate flows. We wanted to determine which would be a *critical* flow, defining it as the biggest leak which would allow people to escape following a safety evacuation plan. We also wanted to study more in depth the effect of ventilation in small leaks, and determine which flow would be totally absorbed by it.

2. Sensitivity study on the main elements of the model. We wanted to define which were the elements really influencing the argon concentration and temperature distributions. We studied the isothermal vs. adiabatic walls, different turbulence models, old vs. new specifications and different spatial differential schemes.

3. Open detector vs. Closed detector scenario. All the previous simulations had been carried out for a closed detector geometry, but we know that the regular maintenance of the detector, as well as shorter accesses, will be done with the detector opened (long and short opening scenario respectively). The regular maintenance will be made during shutdown periods of the LHC machine, which will take place every year between November and April. Shorter accesses for minor maintenance will happen throughout run periods, possibly up to 2 or 3 times a year. Therefore, it is important to recreate liquid argon spill accidents within this geometry, which implies the removal of the bottom muon chambers.

After this analysis is done, we need to validate the model by comparing simulation and experimental results. The test which was carried out for this purpose and the results of the comparison of experimental and simulation data, are presented in chapter 5.

4.2 Sensitivity study on the flow

Since the previous studies simulated only two flows, and the simulation time was a few minutes, we wanted to study the consequences, in terms of temperature and argon concentration distributions, for intermediate leaks. One of our goals was to determine the maximum flow that would allow people to escape following a safety evacuation plan. It was also important to analyze in detail the effect of ventilation for small leaks.

We show the results of this sensitivity study beginning with huge flows and we go down in the flux magnitude.

69,34 l LAr/min. in an open detector scenario

The temperature and argon concentration distributions for a flow of 69,34 l LAr / min. are the following:

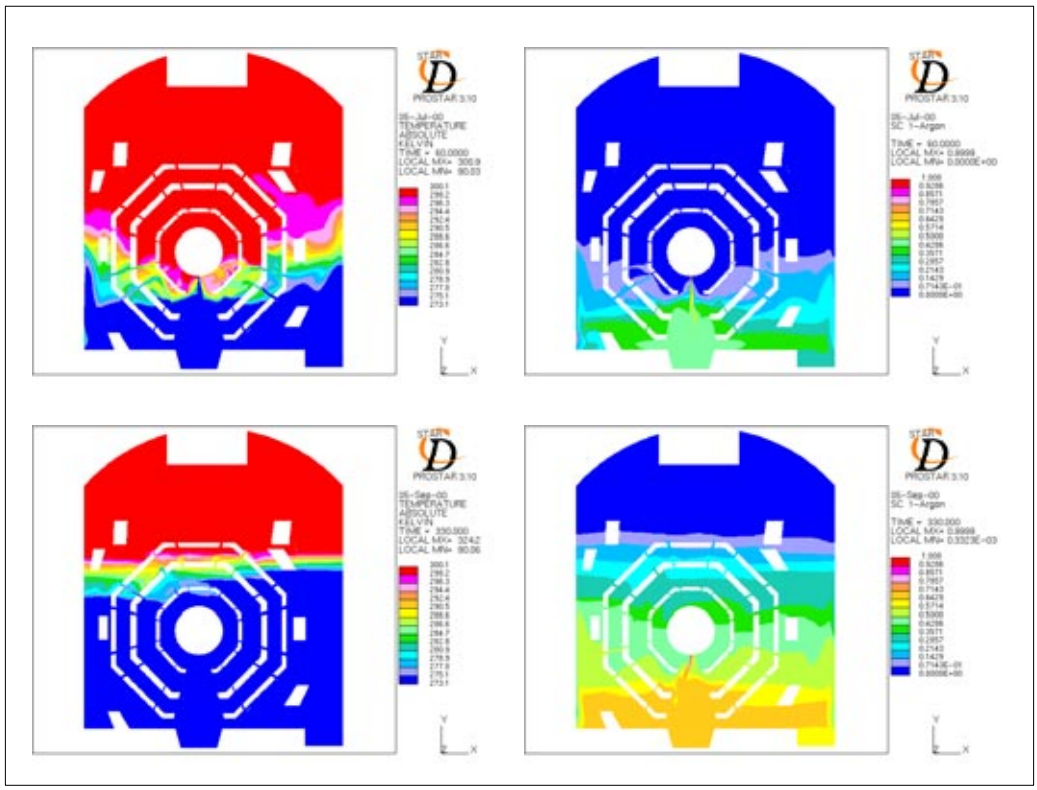

Figure 4.1 Temperature and Argon concentration distributions 60 s and 5,5 min. after the spill. 69,34 l LAr/s.

As we see in these pictures, this flow, like the one of 184 l LAr / s presented in the previous study, has catastrophic consequences. One minute after the spill, the lowest part of the cavern is below 0 ° C; this means not only that it is cold, but also full of mist, which prevents people from finding their way our.

Five minutes after the spill, nearly all the cavern has reached temperatures below 0 ° C and the argon concentration is largely above the safety limits (25% weight) in nearly all the cavern.

26,08 l LAr/min. in an open detector scenario

Our search for a critical flow, which would give people enough time to escape from the cavern in a reasonable time, lead us to simulate a flow of 26,08 l LAr / min. The results are shown in the following figure.

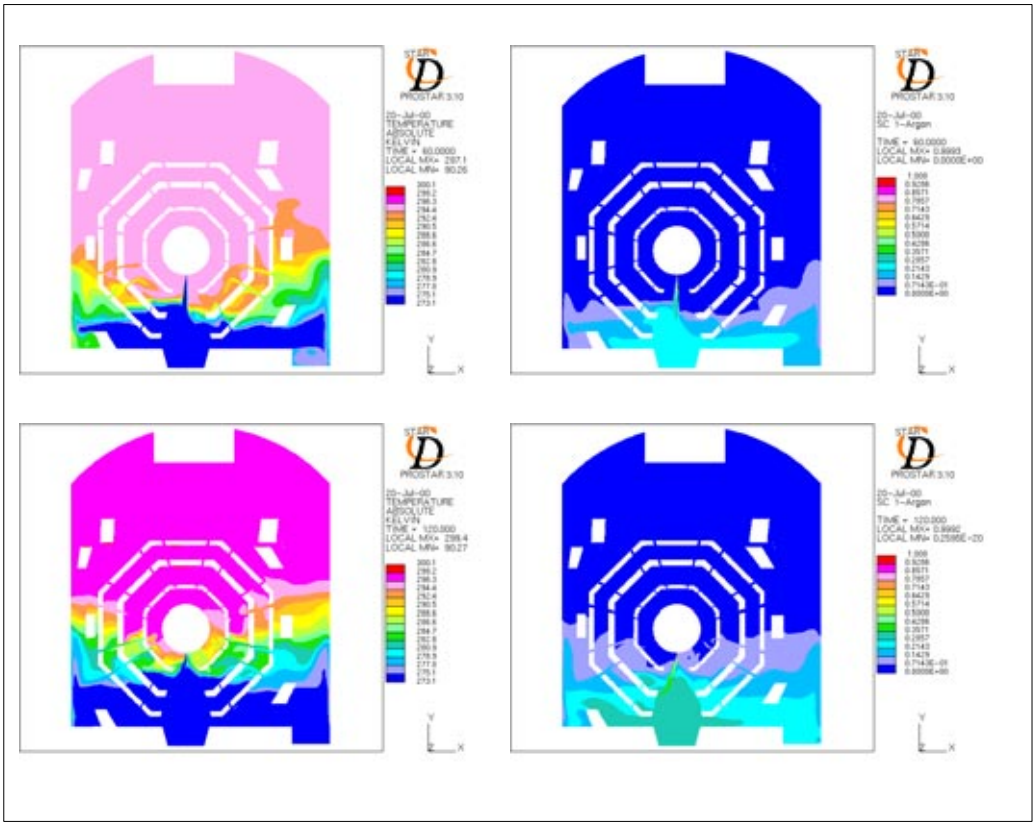

Figure 4.2 Temperature and Argon concentration distributions 1 and 2 min. after the spill

One minute after the spill both argon concentration and temperature are becoming dangerous in the low part of the cavern. We calculated the model until 2 minutes for completeness, knowing that we had to search for lower flows to reach the critical flux we were looking for.

17,46 l LAr/min. in an open detector scenario

We simulated a flow of 17,46 l LAr / min. obtaining the following results:

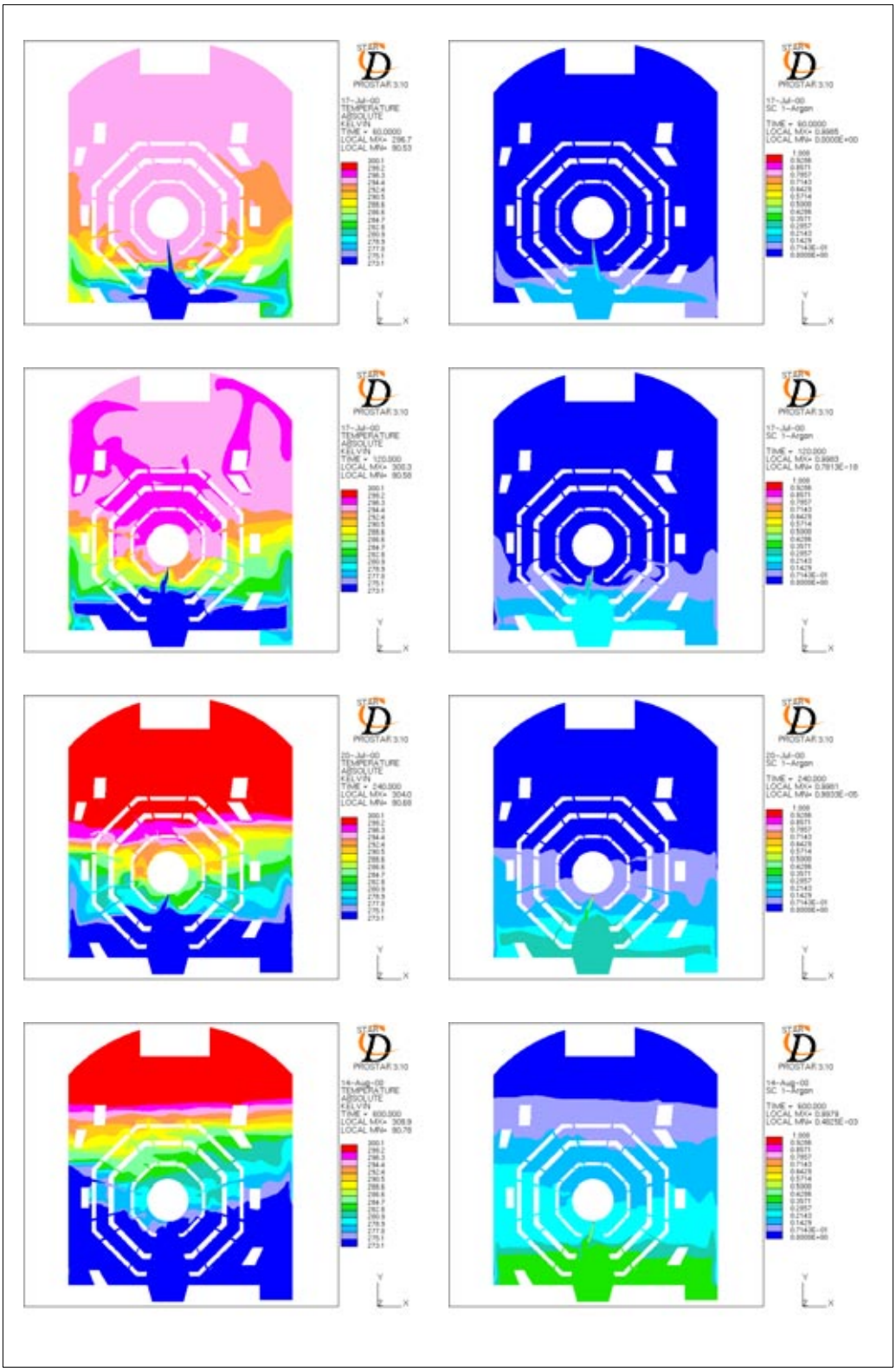

Figure 4.3 Temperature and Argon concentration distributions 1,2,4,10 min. after the spill. 17,46 lLAr/min.

If a spill of this flow occurs, people would have about two minutes to leave the area really close to the spill point and the area close to the pit. If after four minutes

people have succeeded in reaching five metres high of the cavern, then they will be able to find their way out.

This flow could be defined as critical, in the sense that a good evacuation strategy could help people escape from this accident.

9,3 l LAr/min. in an open detector scenario

Another important aspect of this sensitivity study was the ventilation effects on small flows. In our aim to search for a flow that could be totally absorbed by the ventilation, we analyzed a smaller flow of 9,3 l LAr / min.

The temperature and argon concentration distributions for this flow is the one shown in the following figure:

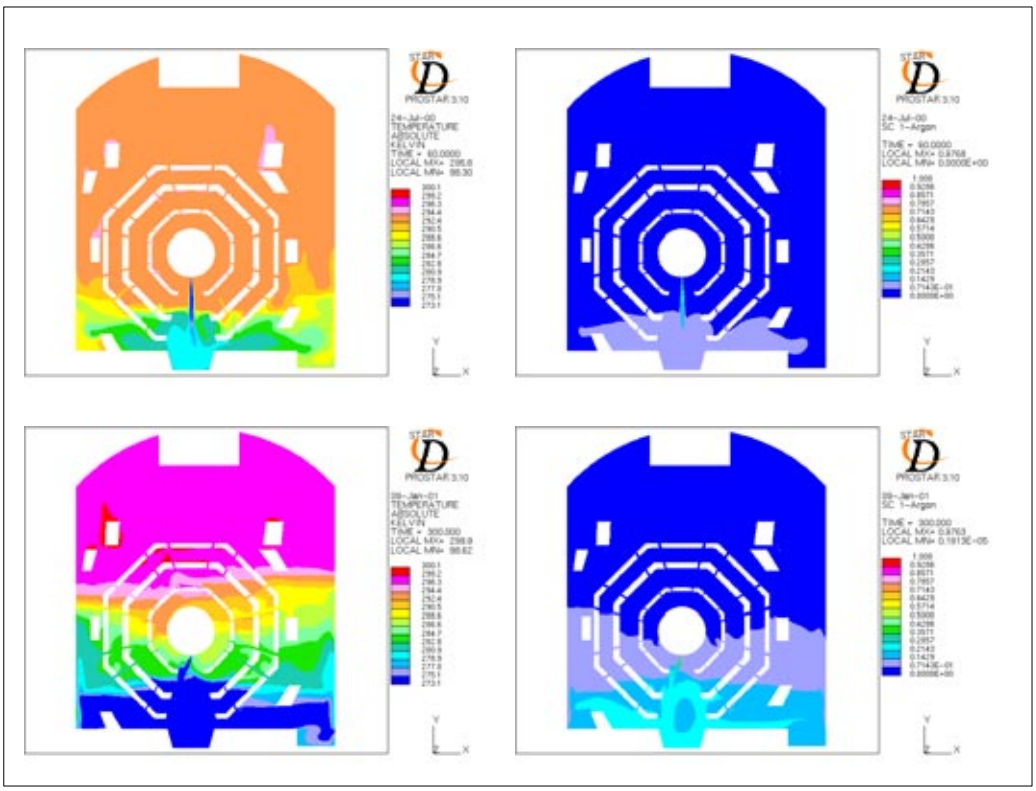

Figure 4.4 Temperature and Argon concentration distributions for a 9,3 l LAr/min. flow 1 and 5 minutes after the spill

The argon concentration figure five minutes after the spill takes place shows that this flow is not completely absorbed by ventilation. Therefore, we should go ahead analyzing a smaller leak.

3,79 l LAr/min. in an open detector scenario

If we plot the temperature and argon concentration distributions for a flow of 3,79 l LAr / min., the outcome is the following.

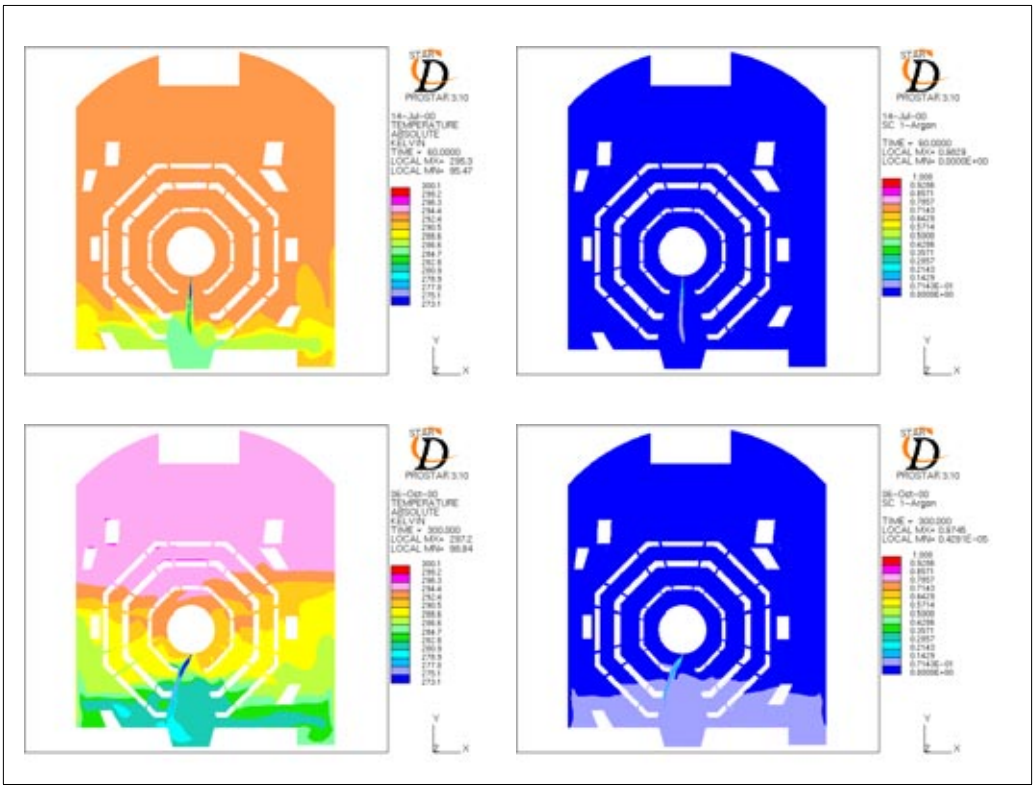

Figure 4.5 Temperature and Argon concentration distribution 1 and 5 min. after the spill. 3,79 l LAr/min.

Five minutes after the spill, the concentration of argon in the pit is nearly zero. We could conclude that this is a leak that is totally absorbed by the pit extraction.

4.3 Open detector vs. Closed detector scenario

All the previous simulation had been carried out for a closed detector scenario (one and three layers of muon chambers). We wanted to compare the results for a catastrophic, an intermediate and a small flow, for both open and closed detector configuration.

Catastrophic failure of a feedthrough

This flow was already studied by F.Balda; the purpose now is to represent the three muon chamber layers in open detector configuration, instead of the one-layer model proposed before. The geometry is the one shown in the figures. The main characteristics of the mesh are summed up in the following table:

Table 4.1 Characteristic parameters of the open detector scenario geometry

Cells	37313
Vertices	87139
Boundaries	76494
Couples	210
Boundary regions	16

As we can see in figure 4.7, no major changes in the catastrophic consequences of such a huge spill due to the geometry is observed. One minute after the spill the one-layer geometry accumulates very high concentrations between the muon layer and the cryostat, while in the open scenario these quantities are kept in the pit.

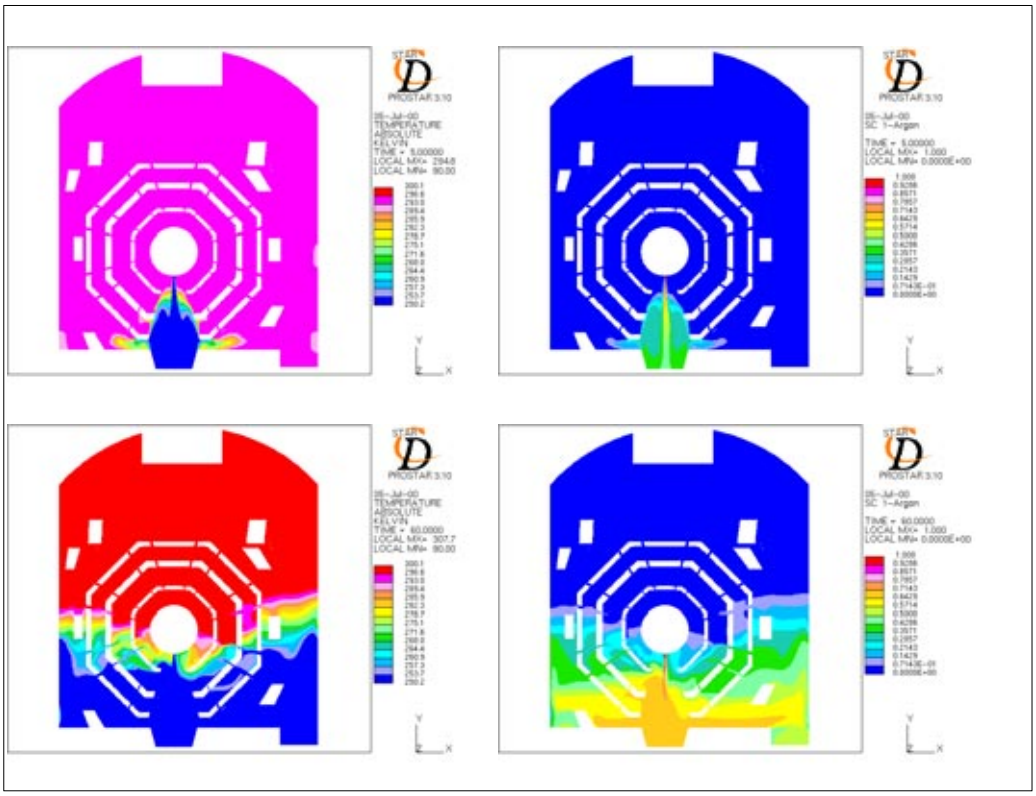

Figure 4.6 Temperature and Argon concentration distributions 5 and 60 s after the spill. Catastrophic failure of a feedthrough in an open detector scenario

Comparing the argon concentration for both geometries:

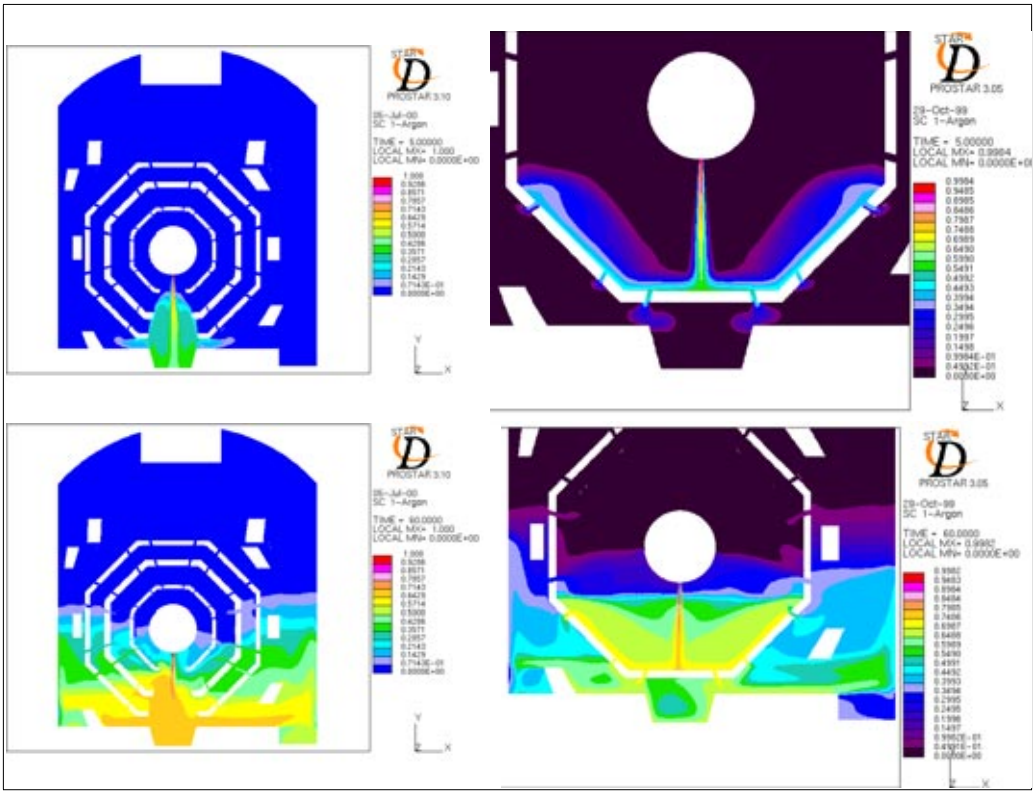

Figure 4.7 Argon concentration comparison for a Catastrophic failure of a feedthrough in an open detector scenario and a One layer model, 5 and 60 seconds after the spill release

However, for such a catastrophic flow it is difficult to reach conclusions. We need to compare the geometries for lower spills.

Intermediate Leak 12,39 l LAr/min.

In our open vs. closed detector comparison it was important to test an intermediate flow. Therefore, we studied this 12,39 l LAr / min. The temperature and oxygen concentration for a closed detector scenario are shown in the following figure:

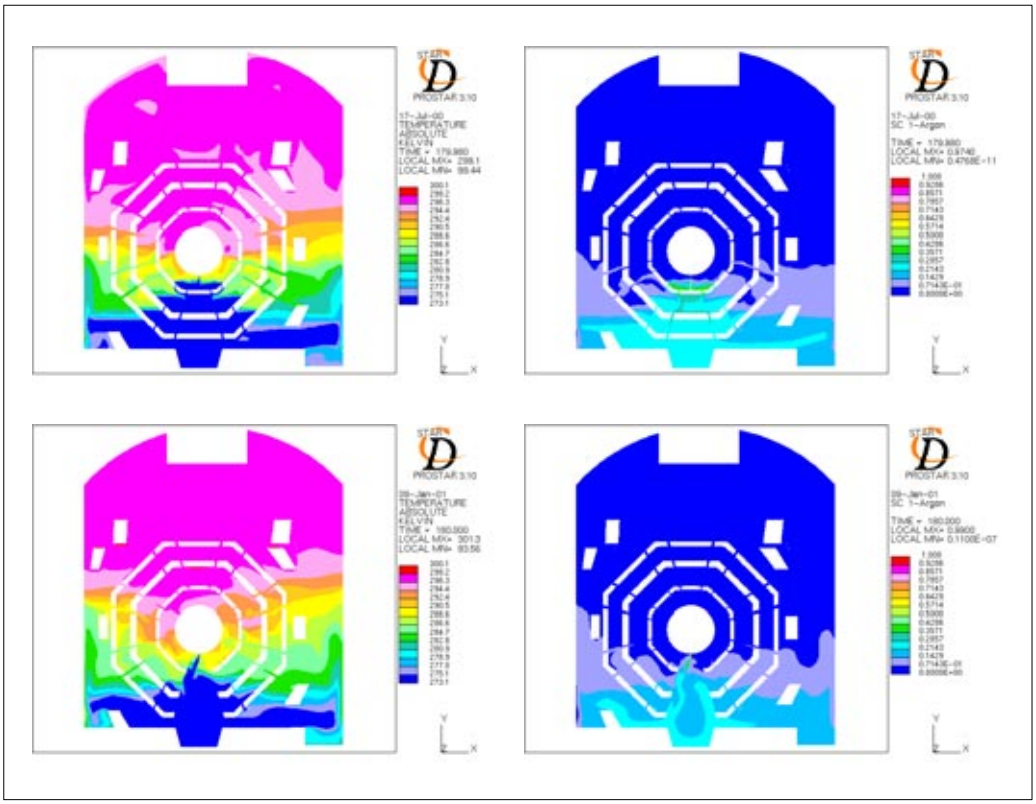

Figure 4.8 Comparison between Temperature and Argon concentration distributions 3 minutes after a 12,39 l LAr/s. in a closed or open detector scenario.

If we compare both open and closed detector geometries for this flow three minutes after the spill, we see how the open detector scenario is helping the evacuation of the argon through the pit extraction. This results in lower argon concentrations and higher temperatures for the open detector scenario.

Small Leak 3,79 l LAr/min.

We also did the comparison analysis for a small leak such as 3,79 l LAr / min.

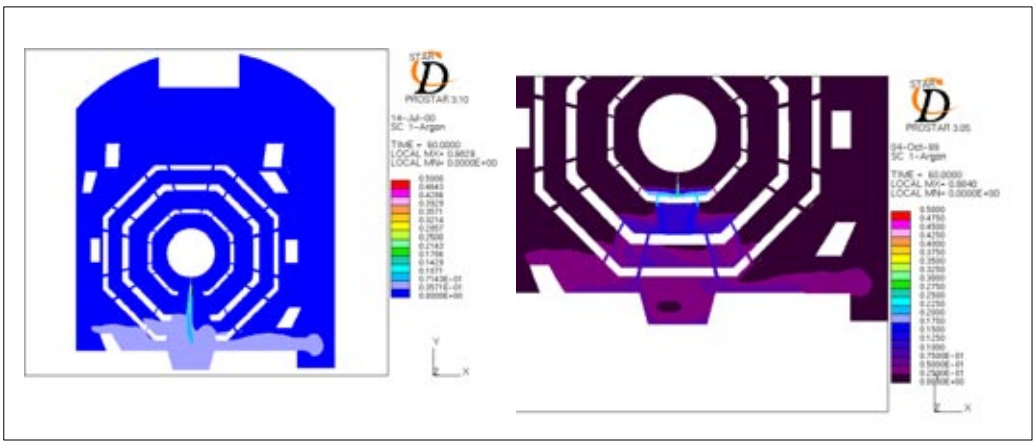

Figure 4.9 Argon concentration distribution 1 min. after the spill. 3,79 l LAr/min.

We could conclude that the open detector scenario with removal of the bottom muon chambers is favouring the evacuation of argon, while the closed detector scenario is accumulating the argon between the layers.

The argon pit plays a key role in avoiding the spreading of argon, specially during shutdown periods (open detector scenario), when people is present.

4.4 Critical elements of the model

It was important, for a better understanding of the model and the physical phenomena, to have an idea of the elements that were playing a determinant role on the model. This is the reason why we wanted to simulate a constant intermediate flow (12,39 l LAr / min.) in a geometry where the boundary conditions, turbulence models, differencing scheme were changing.

Old vs. New specifications

As we have mentioned earlier, the specifications on heat load and ventilation have changed. We summarize in this table both the old and new specifications:

Table 4.2 Old and New specifications

	Old Specifications	New Specifications
Heat Load	100 kW	180 kW
Two-side / One-side Lateral Supply	45.000 m^3/h 16.000 m^3/h	60.000 m^3/h 16.000 m^3/h
Top and Ar Pit Extraction	45.000 m^3/h 16.000 m^3/h	60.000 m^3/h 16.000 m^3/h

We wanted to see the influences of this change on the temperature and argon concentration distributions.

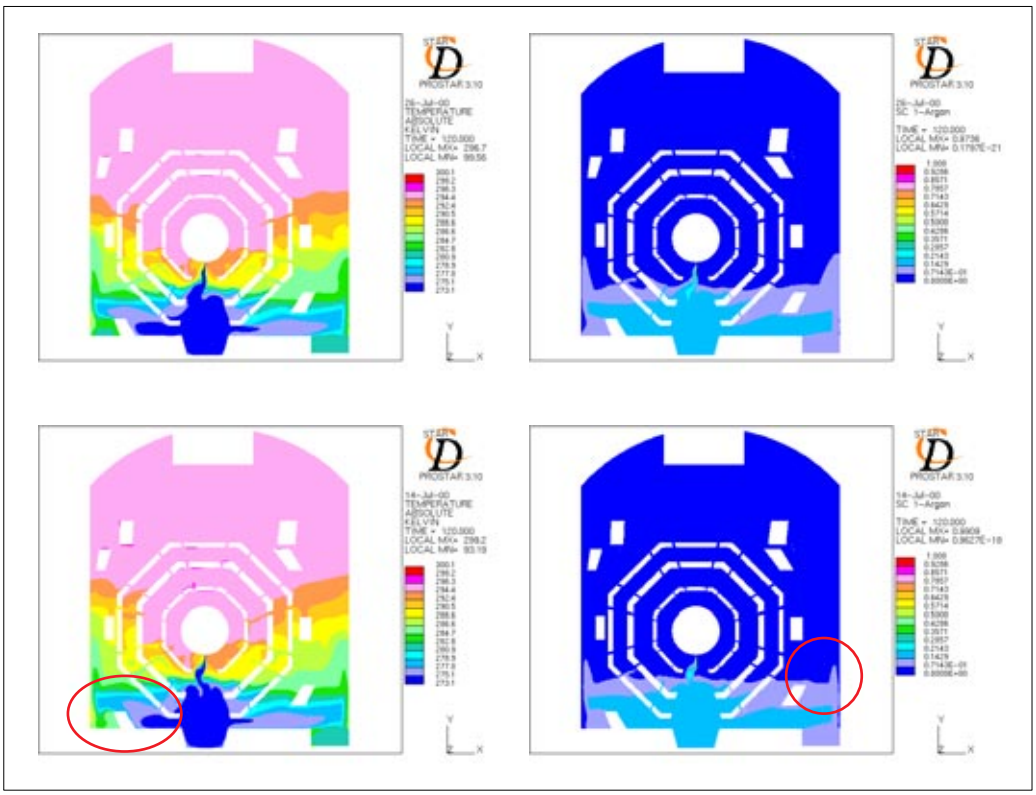

Figure 4.10 Old (top) vs. New specifications (bottom)

As we can see in these figures, the change from one specification to the other is not leading to significantly different temperature or argon distributions.

Therefore we can conclude that neither ventilation nor heat load are critical elements for this kind of accident, where buoyancy effects are clearly dominating.

Isothermal vs. Adiabatic pit

One of our hypothesis was to consider isothermal walls. In this case we wanted to investigate what happened when the pit was implemented as an adiabatic wall.

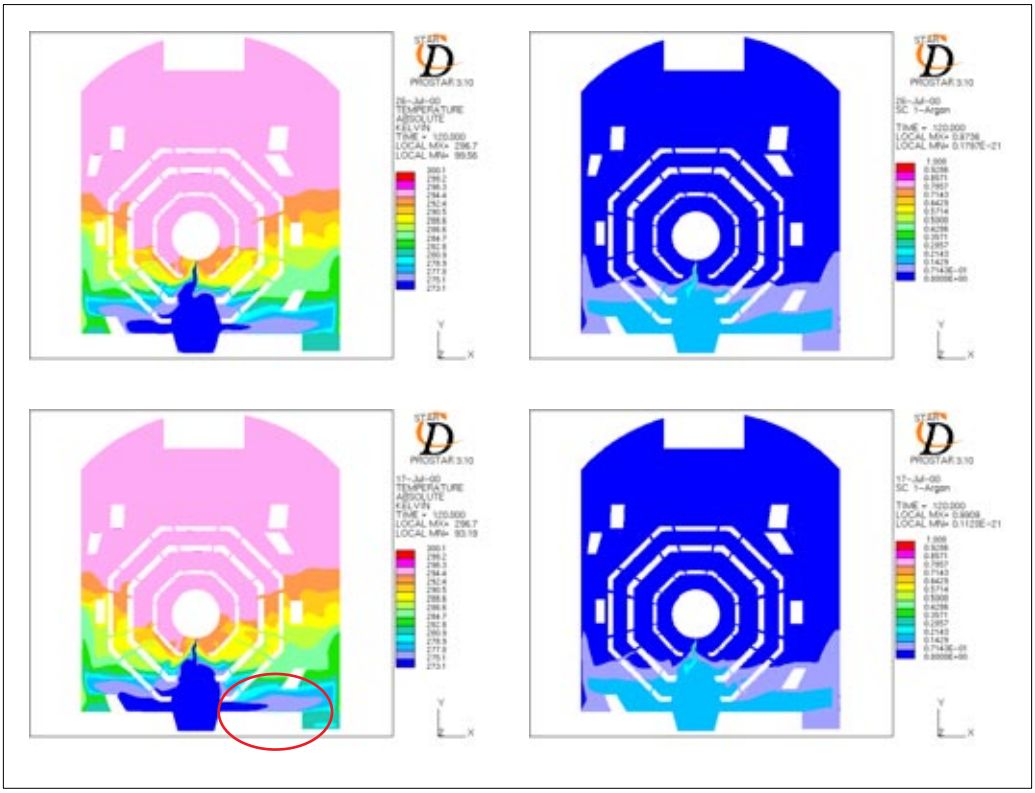

Figure 4.11 Isothermal (top) vs. Adiabatic pit (bottom).

Comparing both temperature and argon concentration distributions for both models, we can conclude that this boundary condition is not critical for the model.

Heat Flux vs. No Heat Flux

In this case we explored the effect of stopping the heat flux coming from the racks and from the muon chambers. The results are shown in this picture:

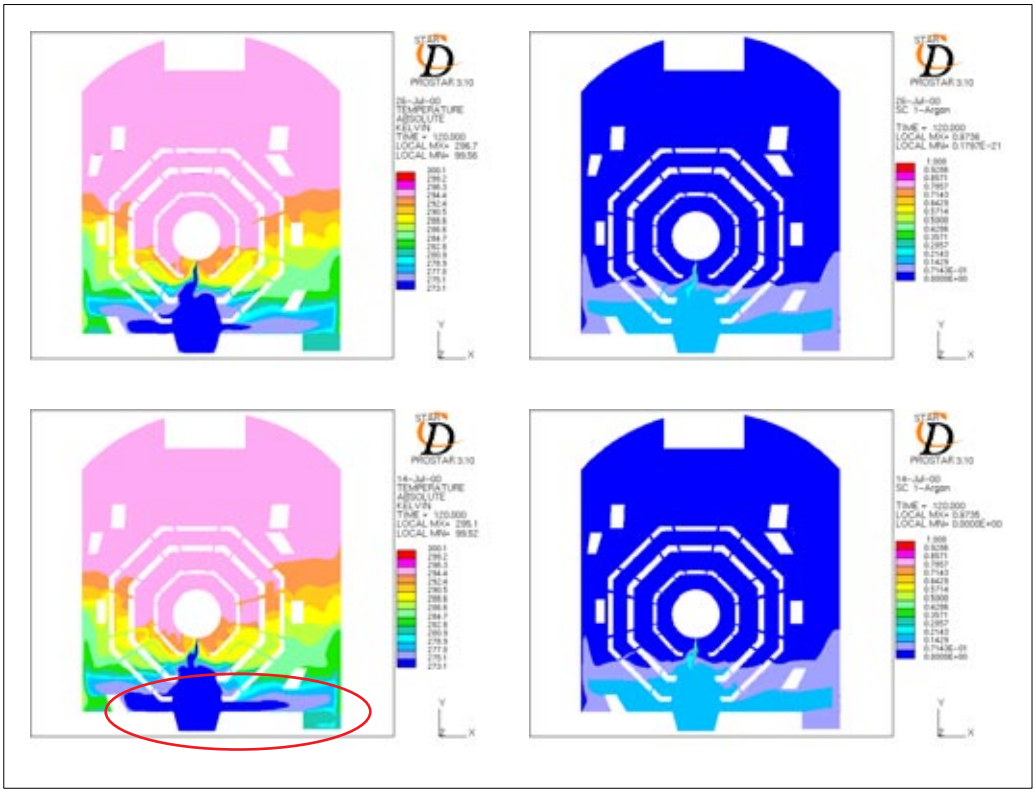

Figure 4.12 Heat load of 100 kW (top) vs. no heat load (bottom)

Comparing the temperature and argon concentration distributions, we reach the conclusion that heat load is not a key element of the model.

Spatial differencing schemes

In this model we used the MARS with 0,5 of blending factor for the u,v,T,k,e variables, instead of the UD spatial differencing scheme. In both models the spatial differencing scheme used for density was CD with a blending factor of 0,8.

Two minutes after the spill the distributions of temperature and argon concentration are the following:

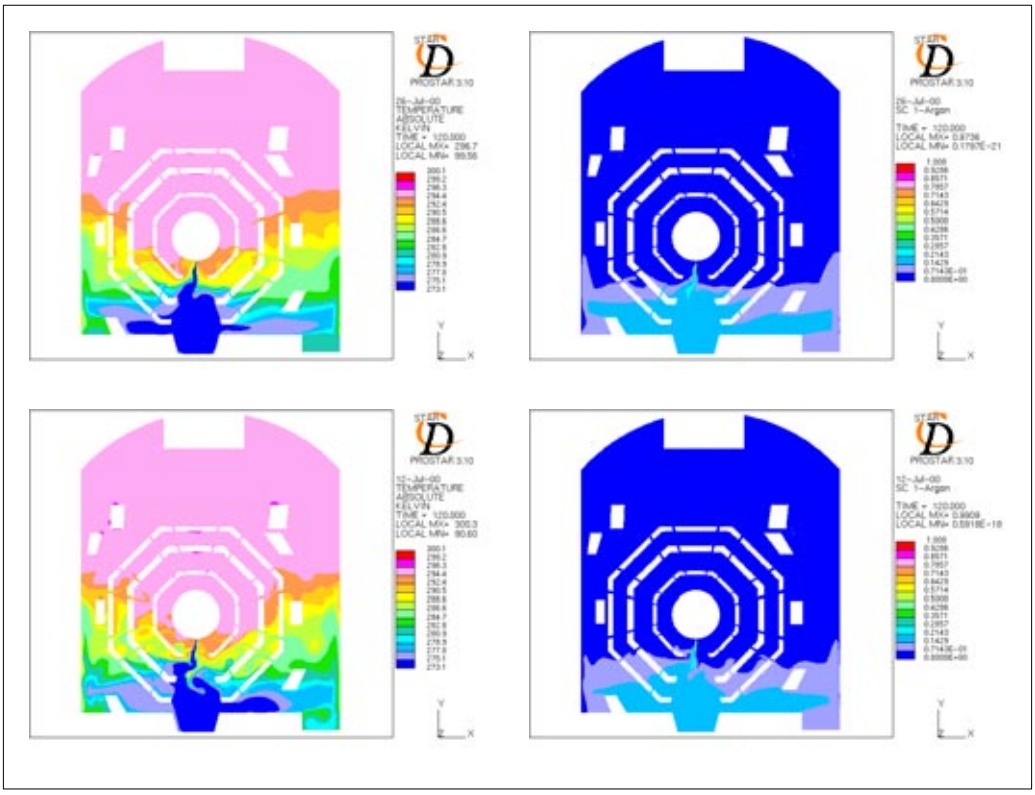

Figure 4.13 UD (top) vs. MARS (bottom) differentiating spatial schemes

In this case, the temperature and argon concentration distributions look different but are very close in magnitude. The flow pattern seems somehow unrealistic for the calculation with the MARS spatial differencing scheme.

Low Reynolds vs. High Reynolds

When it comes to analyzing the flow characteristics near the walls, the Reynolds number might be small enough close to them to consider the flux laminar.

StarCD allows the implementation of a turbulence model that treats the flow close to the walls as laminar, using a Low Reynolds approach in this area. To know whether we are going to a low Re number, StarCD is calculating a parameter y+ that should be no less than 1 if we treat the flow with High-Reynolds models. However, when we look at this parameter for the ATLAS model, some parts of the walls were too refined, driving this parameter under 1. This is why we wanted to check if a Low Reynolds model applied close to the walls would lead to substantial different results.

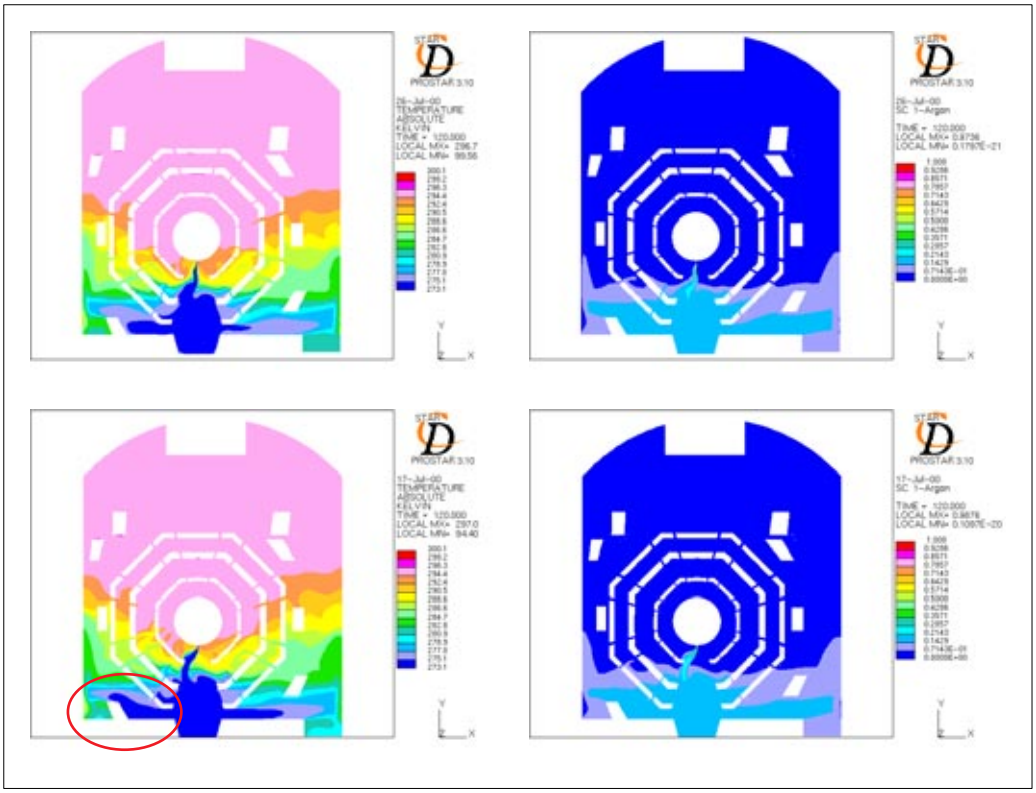

Figure 4.14 High Reynolds (top) vs. Low Reynolds (bottom) turbulence models

If the differences in the temperature distribution are more evident than for other parameters, again, the argon concentration distribution is nearly identical. Therefore, we can assume the turbulence model is not a critical factor for this model, and a High-Reynolds approach is correct.

4.5 Conclusions

The simulation of liquid argon spills in the ATLAS cavern allowed us to evaluate how much time people can take to escape before the concentration of argon or room temperature create a real risk of asphyxia or hypothermia. This is a crucial factor for the design of a good evacuation plan.

The sensitivity study on the flow showed how a flow of 18 l LAr / s. is a critical flow: people could escape from this accident following a good evacuation plan, which would last no more than two minutes. Bigger spills than this critical one would quickly create dangerous conditions, preventing people from escaping without being dangerously injured. Flows below 4 l LAr / s., on the other hand, are completely absorbed by the pit extraction.

The open detector scenario where the bottom muon chambers are removed, is not disturbing the flow motion towards the pit, and therefore the absorption by the pit extraction is favoured in comparison to the closed detector scenario. This is specially clear for small leaks. In an open detector scenario the argon pit plays an important role in avoiding the argon to spread.

The sensitivity study on the main parameters of the model showed that neither the variation of the ventilation flow rate nor the heat load were influencing significantly the temperature or argon concentration distribution. Secondly, the hypothesis of isothermal wall is not critical. This study also demonstrated how a High-Reynolds model is good, even though the mesh is too refined near some walls, where we could eventually implement a Low-Reynolds model. As for the spatial differencing schemes, the UD spatial differencing for speed, temperature and turbulence parameters is an appropriate and stable scheme.

However, all these results depend on the reliability of the model. In order to validate these results, we carried out an experiment with various liquid argon spills. The test description, as well as the comparison between experimental and simulation data can be found in the following chapter.

Chapter 5

Liquid Argon Spill Tests

In order to validate the model of liquid argon spills in the ATLAS cavern, we have carried out an experiment where a spill of liquid argon takes place. In this chapter we will describe this test,- where we try to reproduce the main conditions of ATLAS, that is to say, argon and air turbulent fluids, forced and natural convection, heat loads, a geometry with a pit, etc. - and will analyze if the experimental results differ significantly from the ones predicted by Star CD.

5.1 Goal

The main goal of this experiment is to know whether or not we can validate the argon spill model that we have implemented for ATLAS, which was presented in the previous chapter. In case of non-validation, this test will help us to renormalize the model.

In May 1994, a series of test had been carried out at CERN by C.R. Gregory and J.Nebout in order to establish time constants for the depletion of ambient oxygen levels resulting from the spillage of various quantities of liquid argon. Little literature exists concerning the spillage of liquid argon, in semi-enclosed spaces such as experimental caverns. For this reason it was decided to perform a series of spills, in order to monitor the effect on ambient air with respect to oxygen concentration*.

Why another test? In the test that had been carried out, there is not only a lack of important data, which makes it difficult to match experimental conditions and modelling hypothesis, but also the conditions of the experiment were not reproducing all the main elements in ATLAS (constant pressure spill, forced convection, heat load). For all these reasons, a new test, which tries to solve both problems, has been carried out. By comparing the temperature and oxygen concentration fields for different spill flows of liquid argon -obtained on the one side in an experimental way and on the other side through the Computed Fluid Dynamics (CFD) code StarCD- we will be able to evaluate how close to reality is our prediction.

* For the results of this test, please refer to AT-XA/01NCG/JN.

5.2 Experiment setup, main elements and DAQ

5.2.1 General description of the layout

The tests have been carried out in a zone specially set up for the purpose at CERN, building 180. The spill of argon takes place in an area delimited by concrete blocks of 9,6 x 4,8 x 4,8 m. (see general layout in figure).

The test is trying to reproduce the main elements of the ATLAS cavern. One of them is forced convection, which is introduced in the experiment via three fans: two lateral fans to insert air into the room, and a third fan to extract the air from the pit. In order to achieve the good order of magnitude for the speed of the air, we used diffusers. Another important element is the heat load, created by the electronic racks and muon chambers; To reproduce this heat load we inserted two oil heatings (avoiding extra forced convection). The technical description of these elements can be found in the next paragraph.

A cylindrical dewar was placed out of the room space, an isolated cryogenic pipe allowing the spill to take place from the ceiling. The measurement of the flow was made with the help of a scale, so that the difference of weight before and after the experience allowed us to calculate the flow of liquid argon. So as to avoid damaging the concrete of the hall, the pit was covered with a 5 cm isolation.

For the DAQ, we used twelve zirconia oxygen sensors, and sixteen thermocouples type J, distributed in the whole volume.

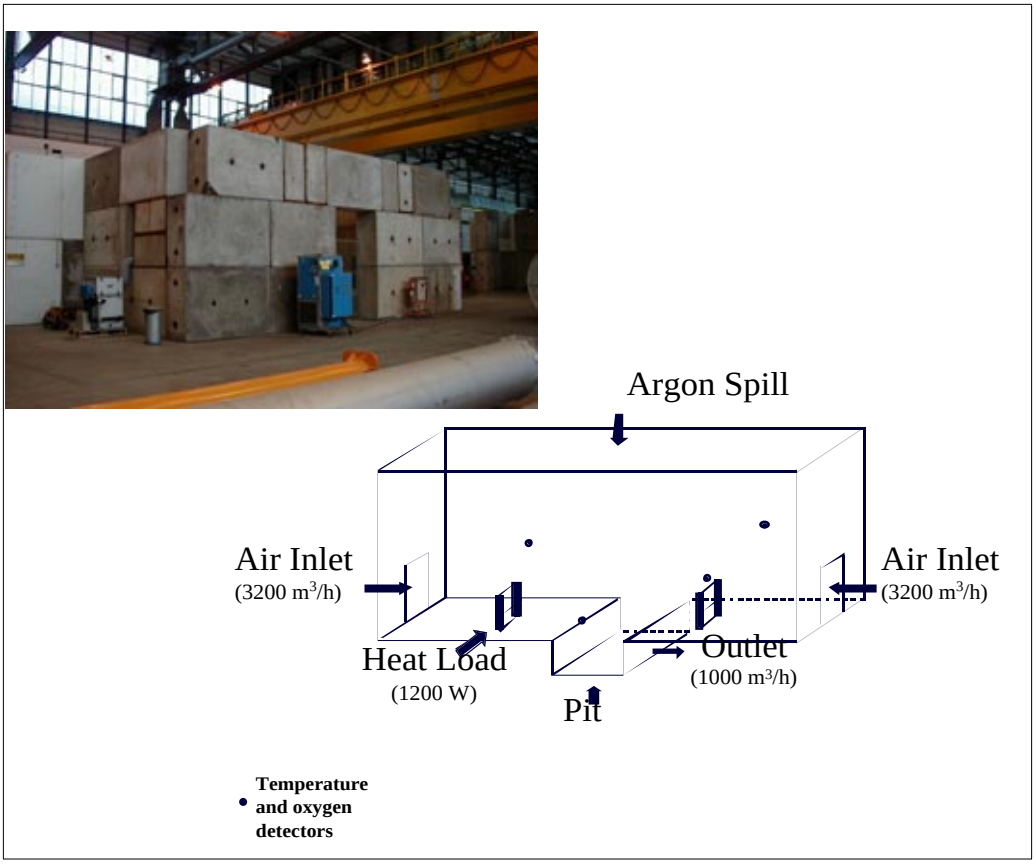

Figure 5.1 General layout of the test space

Figure 5.2 Weighting the dewar, Johan Bremer (left) and Thermocouples and Oxygen detectors (right)

The main geometric and physical features of the test are summarized in the following table:

Table 5.1 Test geometric parameters

Floor Area	9,8 x 4,8 m^2
Pit dimensions	1,6 x 4,8 m^2
Distance of spill point from floor	4,8 m
Dewar volume	500 l
Internal absolute dewar pressure	12 bar
Isolated cryogenic line diameter	23 mm
Argon Temperature	90 K
Performed spills	From 4 l LAr / min. to 50 l LAr / min.

We carried out the tests from the 8th to the 17th August 2000. The basic description of each test can be found in the table of the following page. The first test was intended to check the detectors. The third test was not valid, due to the fact that the extraction fan slowed down because of the freezing of the heat exchanger, which was removed immediately afterwards. We spilled a total amount of approximately 1.300 l of liquid Ar, approximately equivalent to three full dewars.

In order to get an idea of the flows we should test, before carrying the real experiment, we did a sensitivity study by simulating flows from 5 l LAr / min. to nearly 70 l LAr / min. See appendix B, Previous simulations, to see the results.

We came out to the conclusion that it was worth testing both small and huge leaks. Huge flows allow us to see a large and quick variation of the magnitudes (temperature and argon concentration), and therefore it is easier to establish

comparisons. On the other hand, small flows allow us to better evaluate the effect of ventilation on the argon flow.

Finally, the tests performed were the following ones:

Table 5.2 Performed tests

Test 1. 8th August, 14:00	Checking of detectors		
Test 2. 10th August 10:30	3,8 l LAr / min.	V[a]	17’
Test 3. 10th August 11:30	Not valid test (battery of extraction fan frozen)		
Test 4. 10th August 15:00	4,9 l LAr / min.	V	11’
Test 5. 10th August 15:40	8,7 l LAr / min.	NV[b]	15’
Test 6. 10th August 16:40	3,7 l LAr / min.	V	21’
Test 7. 14th August 14:30	17,7 l LAr / min.	V	12’
Test 8. 14th August 16:30	50,0 l LAr / min.	V	4’
Test 9. 16th August 15:30	14,4 l LAr / min.	NV	10’
Test 10. 16th August 16:00	27,3 l LAr / min.	V	5’
Test 11. 17th August 11:30	40,8 l LAr / min.	V	4’

a. V: Test performed with ventilation
b. NV: Test performed without ventilation

Figure 5.3 Spill of liquid argon and sensor disposition

From the point of view of safety, several portable oxygen detectors were located around the experiment and close to the people working in the hall while the tests were taking place. Altogether, the underground galleries were temporary closed during the tests, after which it was checked that no substantial quantity of argon could have remained.

5.2.2 Main Elements

We will describe in more detail the main elements that were used in the tests: fans, diffusers, detectors and heating.

Inlet and Extraction Fans

The two inlet fans, located at opposite walls, provided, each of them, an air flow of about 3.200 m^3/h, while the exhaust fan, located in the pit, extracted a flow of about 1.000 m^3/h. Since the inlet flow is larger than the extraction one, the ceiling was covered by a plastic tissue leaving a hole in order to avoid overpressure in the room.

The diffusers where 1,12 m high and 0,6 m radius, its shape being a quarter of a cylinder. The area of the diffuser was therefore 1,06 m^2.

Figure 5.4 Supply fan and diffuser

We measured the real flow of the fans with a flowmeter, in 162 points of the diffusers for the inlet fans and in 42 for the extraction fan, obtaining 3.264 m^3/h and 1.070 m^3/h respectively.

The inlet fans are double inlet centrifugal fans with galvanized scroll casing, halogen-free plastic-rotor with rearwardly-inclined blades. They have a three-phase fan motor of 400 V. The main characteristics are shown down in the following table:

Table 5.3 Inlet fan specification

FAN		
Air Flow	3.000	m^3/h
External Pressure Drop	530	Pa
Total Increase Pressure	780	Pa
Fan Efficiency	79	%
Fan Rotating Speed	3.288	rpm
Power Demand	0,82	kW
AIR FILTER		
Air flow	3.000	m^3/h
Initial Pressure Drop	62	Pa
Design Pressure Drop	130	Pa
Maximum Pressure Drop	200	Pa
Dimension	595 x 595 x 595	mm
MOTOR		
Voltage	400	V
Rating	1,1	kW
Rotating Speed	2.835	rpm
Max. Current Consumption	2,45	A

Figure 5.5 Extraction diffuser in the pit

We do not have such technical data for the extraction fan, which had a variable speed motor adjusted for the flow of 1.070 m^3/h.

Heat Load

As we said, we have two oil heatings of 1.200 W each. We measured both Intensity and Voltage and we checked this was a good value. The dimensions of these heatings are 55 x 10 x 91 cm. The diameter of the pipes is 5 cm and the spaces between the pipelines are 3 cm.

Figure 5.6 Heating

Temperature detectors: thermocouples

Thermocouples are based in the Seebeck effect, which affirms that an electrical flow is created in a circuit formed by two different metals whose union points (hot and cold one) are maintained at different temperature. This circulation obeys to two effects: Peltier and Thomson.

Depending on the materials they are built of, thermocouples show different curves temperature / voltage. Thermocouples E, J, T and K are having most sensibility to temperature changes. We used thermocouples type J (positive branch made out of Fe and a negative branch made out of Constantan).

We had 16 thermocouples, 15 of which were distributed within the domain and the last one was measuring the $0^{o}C$ in a bath of melting ice (see photograph below).

Figure 5.7 Thermocouples and Cold Junction

The distribution of the Thermocouples within the domain is the following:

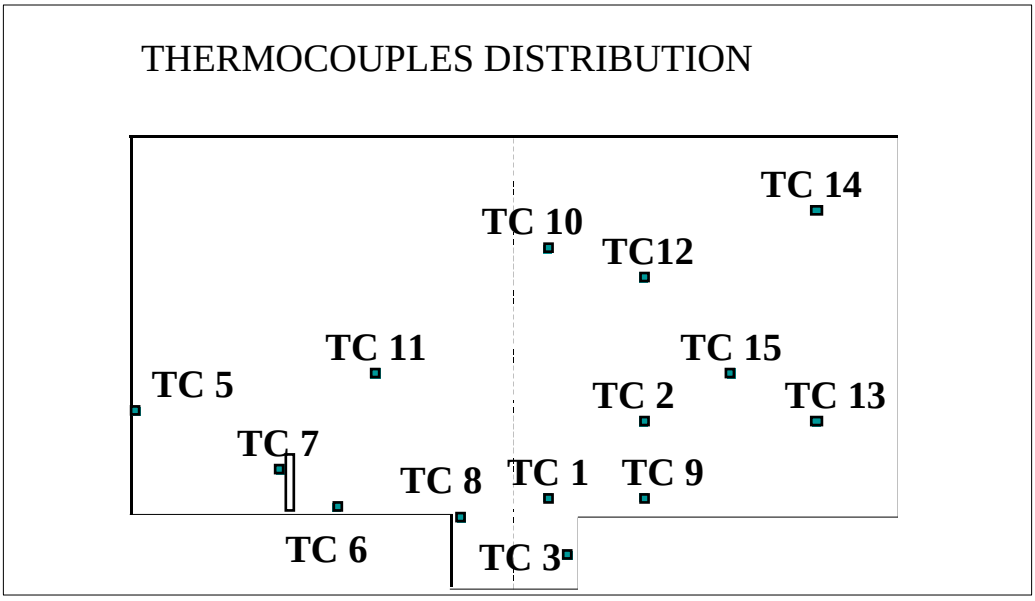

Figure 5.8 Thermocouple's notation and distribution in the test room

Zirconium oxygen detector

We will use zirconia oxygen sensors based on limiting current method using Zirconia Solid Electrolyte. The technical specifications of the sensors are shown in the following table:

Table 5.4 Technical Specification for Oxygen Sensor

Measuring gas	Oxygen
Measurement method	Limiting current method using Zirconia Solid Electrolyte
Measurement range	0.1 .... 25% O_2
Sampling method	pump aspiration
Accuracy	within 1% FS
Warm Up time	about 5 minutes
Output	I (mA) = - 57,0 x ln (1 -[O_2] / 100) + 4 [O_2]= Oxygen concentration %
Supply	9 ... 15 VDC
Flow Rate	100 ... 1.000 cm^3 / min.
Power consumption	about 3 Watt
Operation temperature	-10 ... +50 ^{o}C
Humidity	0 ... 85% r.H. (without vapour condensing)
Dimensions	160 x 125 x 25 mm

We had twelve oxygen detectors spread into the domain, in the same points as the thermocouples. We display them anyway, since the numbering is different.

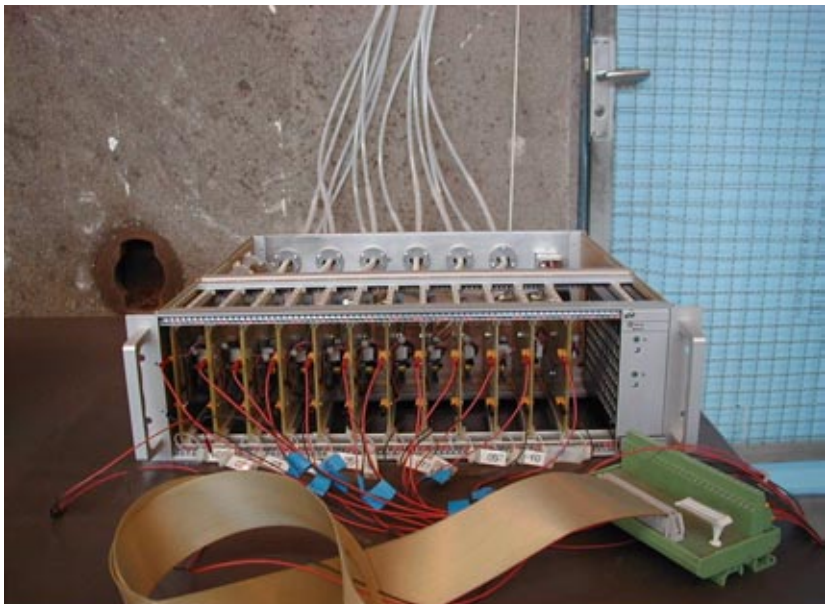

Figure 5.9 Oxygen sensors

The location of the sensors is the following:

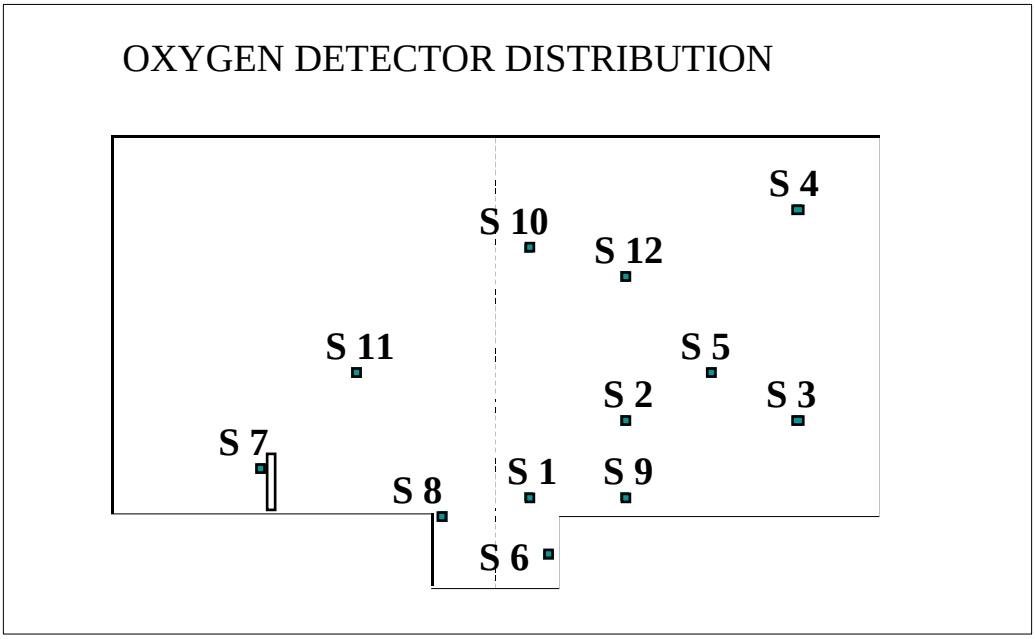

Figure 5.10 Oxygen detectors' notation and distribution in the test room

5.2.3 Data Acquisition

The data acquisition was done with LabView. We programmed some modules and combined them with some others already available at LabView's library so as to be able to register the voltages measured in the sixteen thermocouples and twelve oxygen detector. The connection with the oxygen detector Data Logger was done via a GPIB interface. The acquisition of the thermocouple data was done through the DAQCard-AI-16XE-50.

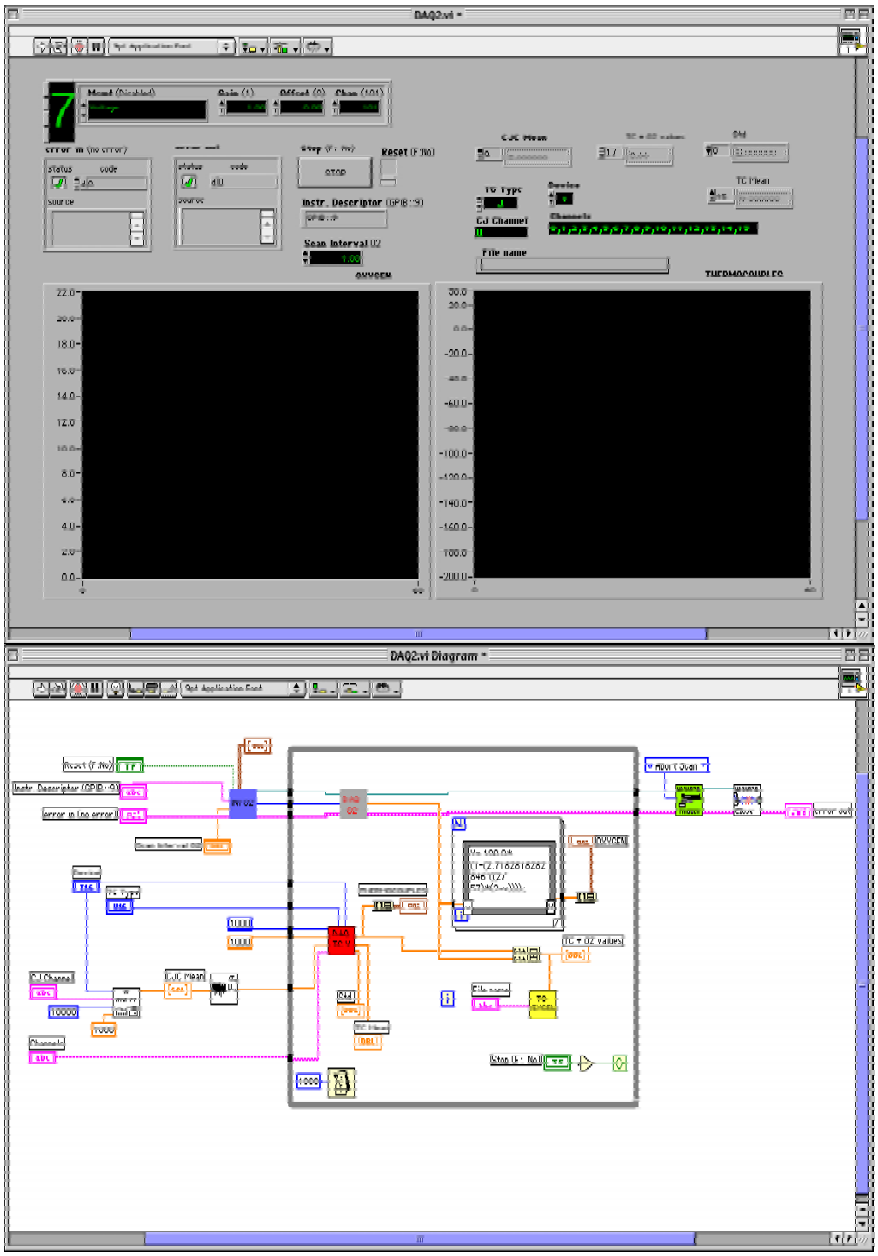

Figure 5.11 LabView block diagram and main panel used for the data acquisition in the test

5.3 Learnings from the experience

This series of 11 tests, provided us with a lot of valuable data as well as allowed us to gain intuition on the behavior of liquid argon when it is released from a pressurized dewar to ambient conditions. Since we tested a wide range of flows, we had the physical appreciation for both catastrophic and really small leaks.

We observed how quickly the mist was spreading into the room -even though the temperatures or the oxygen concentrations were not still so low- and we noticed -as far as it was possible- how the surroundings of the supply air diffusers were free from this mist and were pushing the argon cloud to the center, confining it to the pit. This has also been observed, afterwards, in the simulations. This means that in case of accident, approaching the diffusers could prevent people from asphyxiation.

Also related to the ventilation, we could appreciate how effective it was in evacuating the argon once the spill was over. Even though the quantity of argon was not reaching the normal levels so fast, the cloud of mist was disappearing quite fast (even for huge flows).

We could hear the liquid argon rain falling, and after the cloud of mist had disappeared, we observed white traces on the isolation, prove of the formation of a small pool of liquid argon that was not evaporating instantaneously. This was pointing out the existence of a two-phase flow, even though there was certainly a big quantity of liquid that had evaporated in the dewar valve and the pipeline (flash-evaporation).

We filmed several of these experiences.

5.4 Simulation vs. experimental data

Our target was to validate the model that had been implemented for the ATLAS cavern. In this section we present the results of the comparison between experimental and simulation data for several flows. All the experimental and simulation data for all the tests performed, can be found in the Appendix B.

5.4.1 One-Phase Flow

This model is equivalent to the one implemented for the ATLAS cavern.

Model Description

We used a two-dimensional model, which is the typical cross section of the experiment. The geometry is the same for all the simulations, the mesh being refined in the regions which are expected to show the steepest gradients of all the variables (regions close to the boundaries). The following figure shows the meshing and boundary regions. In this figure -where symmetry planes are not shown- we can see the heat load (heating), the two lateral air inlets and air outlets (one in the pit and another on the roof) and the Argon inlet on the ceiling.

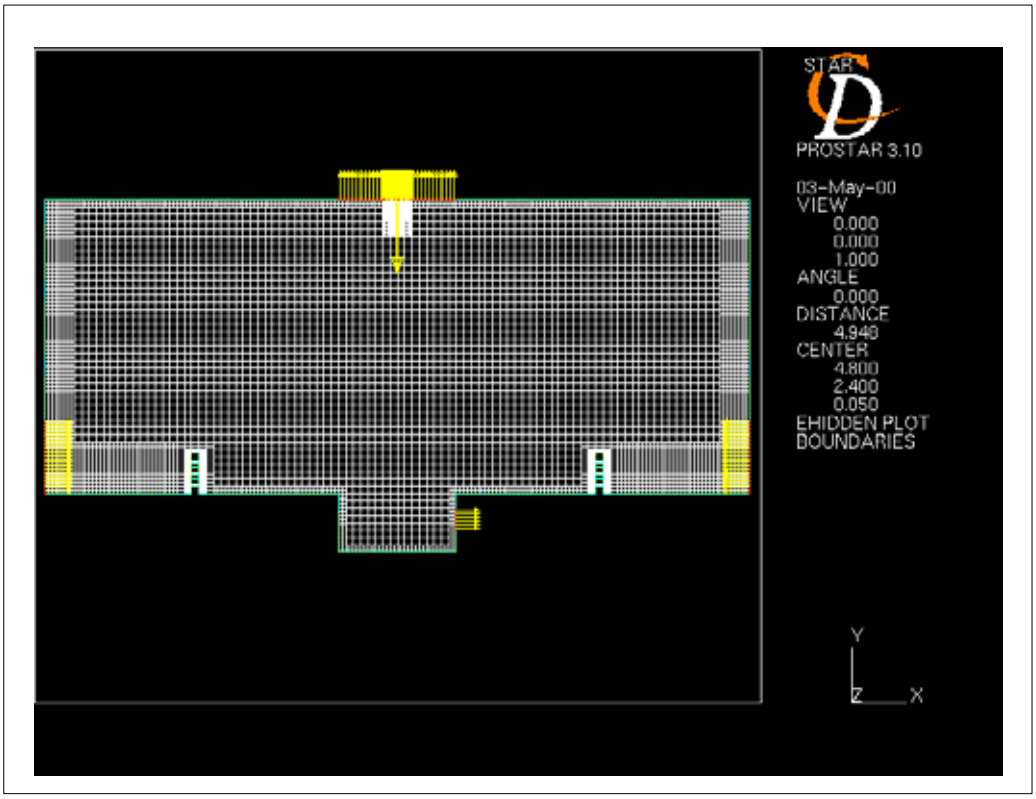

Figure 5.12 Meshing and boundary regions of the one-phase flow 2D model

Some characteristic parameters of the used mesh are listed in the table on the following page.

Cells	8.092
Vertices	25.318
Boundaries	15.727
Couples	458
Boundary regions	8

The smallest cells are located close to the Argon spill and to the radiators, their dimensions being 0,01 m x 0,05 m and 0,01 m x 0,1 m respectively. The refinement close to the boundaries is done with cells of 0,05 m x 0,05 m.

Boundary conditions

Following the same methodology as in chapter 3, and knowing that the volumes of supply air are 3.265 m^3/h and the extraction volume is 1.070 m^3/h (from the mass balance then the top extraction should be of 5.460 m^3/h), we get the following flow parameters:

Table 5.5 Air Inlets properties

Air Inlets	**Pit Extraction**	**Ceiling Extraction**
Q=3.265 m^3/h	Q=1.070 m^3/h	Q=5.460 m^3/h
v=0,16149 m/s	v=0,41281 m/s	v=0,19748 m/s
k=3,912 e-04 m^2/s^2	k=0,002566 m^2/s^2	k=0,000585 m^2/s^2
ε=1,0 e-05 m^2/s^3	ε=0,001356 m^2/s^3	ε=0,000014 m^2/s^3

The initial room temperature corresponds to the average of the values of all the thermocouples (except those close to the radiator, walls and spill point) before the experiment. The wall temperature is an average of the measurements of the thermocouples before the test. The temperature of the exhaust fan in the pit is measured by thermocouple 3 (located in the extraction grid). The temperature of the outlet located in the ceiling is equal to the room temperature.

Table 5.6 Boundary conditions for the simulation of the real tests

TEST	Argon Flow (lLAr/min.)	v (m/s), k(m^2/s^2), ε (m^2/s^3)	Initial T room (K)	Wall T (K)
4	4,9	v=0,224 m / s k=7,52 10^{-4} m^2/s^2 ε=1,62 10^{-3} m^2/s^3	300,0 K	295,7 K
5	8,7	v=0,392 m / s k=2,306 10^{-3} m^2/s^2 ε=8,714 10^{-3} m^2/s^3	299,0 K	294,1 K
6	3,7	v=0,167 m / s k=4,19 10^{-4} m^2/s^2 ε=6,79 10^{-3} m^2/s^3	300,3 K	293,7 K
7	17,7	v=0,798 m / s k=9,56 10^{-3} m^2/s^2 ε=0,073 m^2/s^3	301,8 K	297,9 K
8	50,0	v=2,2459 m / s k=0,07566 m^2/s^2 ε=1,63808 m^2/s^3	300,6 K	296,7 K
9	10,4	v=0,46812 m / s k=0,003287 m^2/s^2 ε=0,014834 m^2/s^3	300,9 K	298,5 K
10	27,3	v=1,2274 m / s k=0,022598 m^2/s^2 ε=0,267394 m^2/s^3	301,8 K	296,6 K
11	40,8	v=1,8345 m / s k=0,050481 m^2/s^2 ε=0,892745 m^2/s^3	299,7 K	295,3 K

Results *Huge Leak.* If we compare the experimental and simulation results for a huge leak, such as that of Test 8, 50 l LAr / min., we find out the curves shown in the following figures. The results are for a sensor close to the pit (TC 3 / S6 located at the extraction diffuser) and for TC14 / S4, far from the pit.

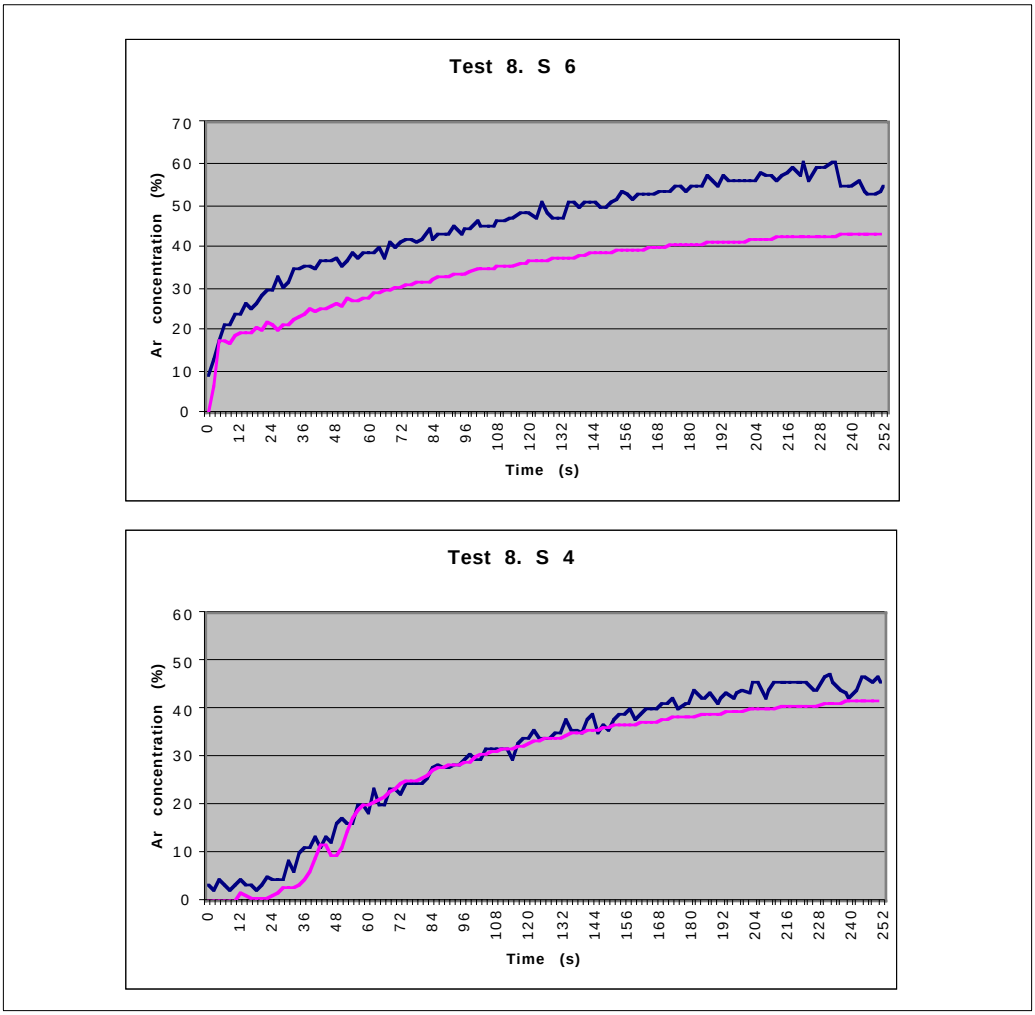

Figure 5.13 Evolution of Argon Concentration.TC 3/S6, close to the pit, and TC4/S14, far from the pit. Blue: experimental data; Pink: simulation data

As we can see in these figures, the argon concentration predicted by the simulation is reaching close results both for sensors, close to the pit, where we found the maximum differences - 2,3 % O_2 (volume)- and sensors far from it, where we have quasi identical results.

The temperature evolution for the same sensors are the following curves:

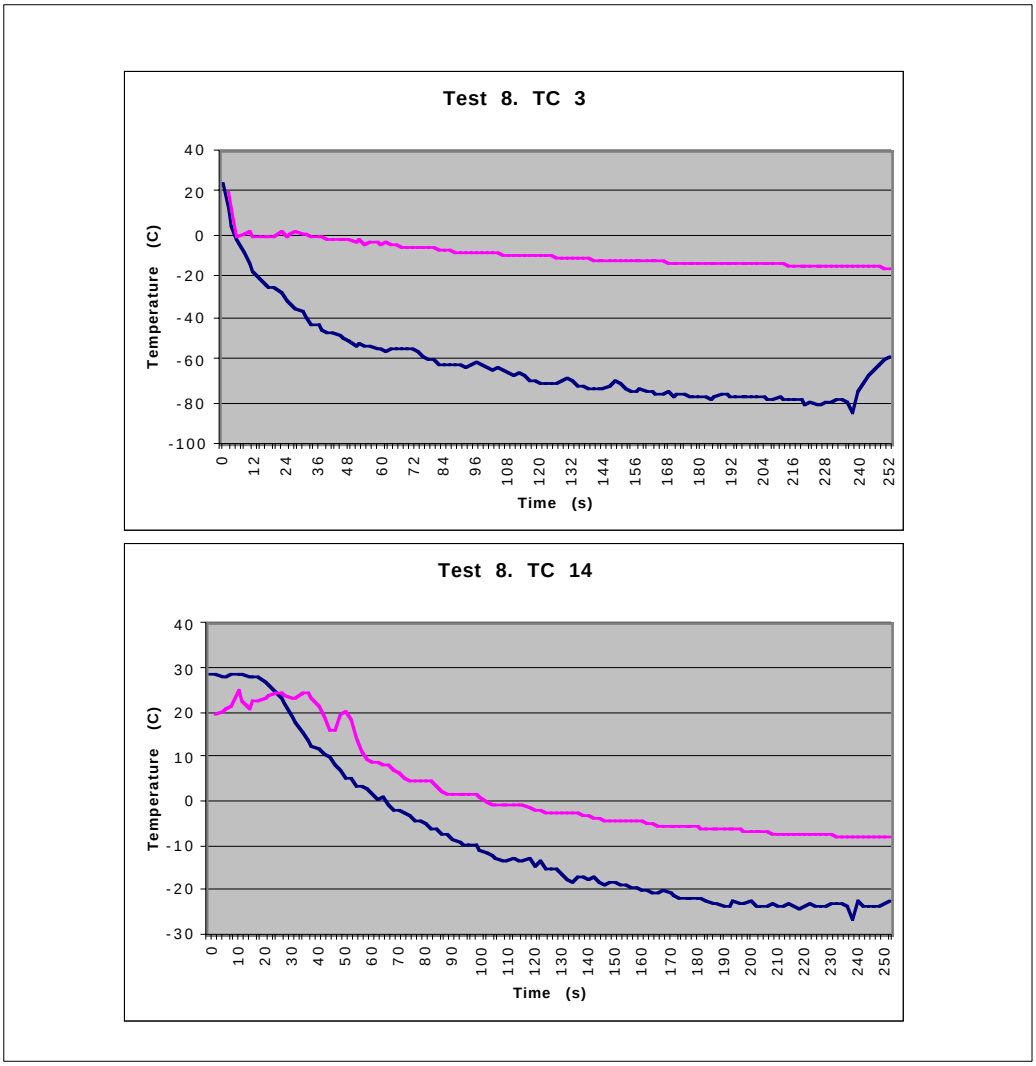

Figure 5.14 Evolution of Temperature.TC 3/S6, close to the pit, and TC4/S14, far from the pit. Blue: experimental data; Pink: simulation data

The StarCD predictions for Temperature are not good, nor close to the pit, where we reach differences of sixty degrees, neither far from it, where we reach differences of ten degrees. This sensors would represent the extremes, meaning we present the worst prediction and the best prediction points.

To have a global idea of the difference between the experimental and the simulation data, we have plotted all the thermocouples and oxygen sensors, with these differences: ΔT and ΔO_2 (% in volume) respectively.

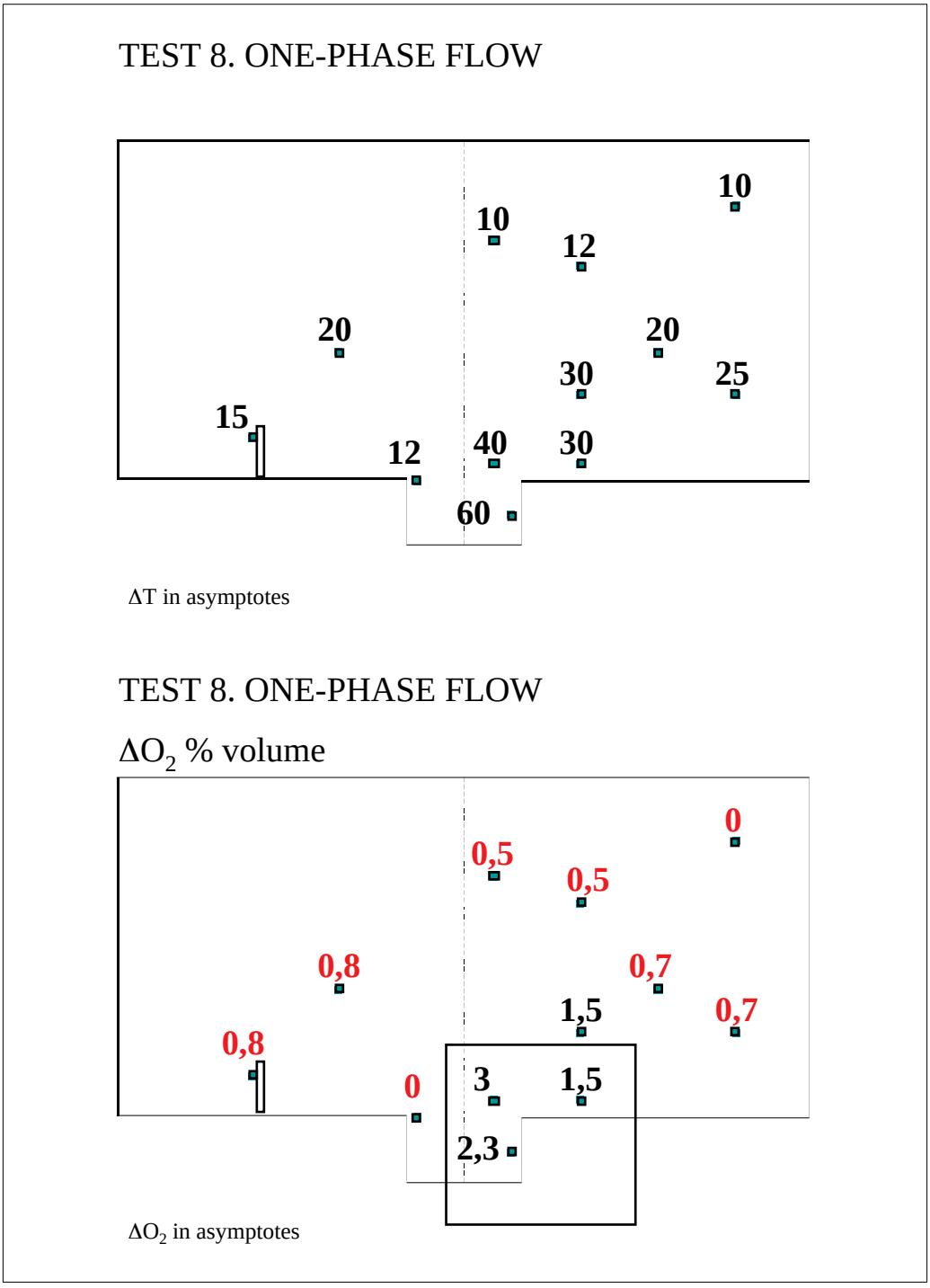

Figure 5.15 Test 8. One-Phase Flow. Temperature and Oxygen concentration comparison

It is important to see whether this divergence is comparable for all magnitudes of flow. Therefore, we will plot the same curves for an intermediate flow, like the one tested at Test 10, 27,33 l LAr / min.

Intermediate leak. For such a leak, we find out the following curves for the argon concentration:

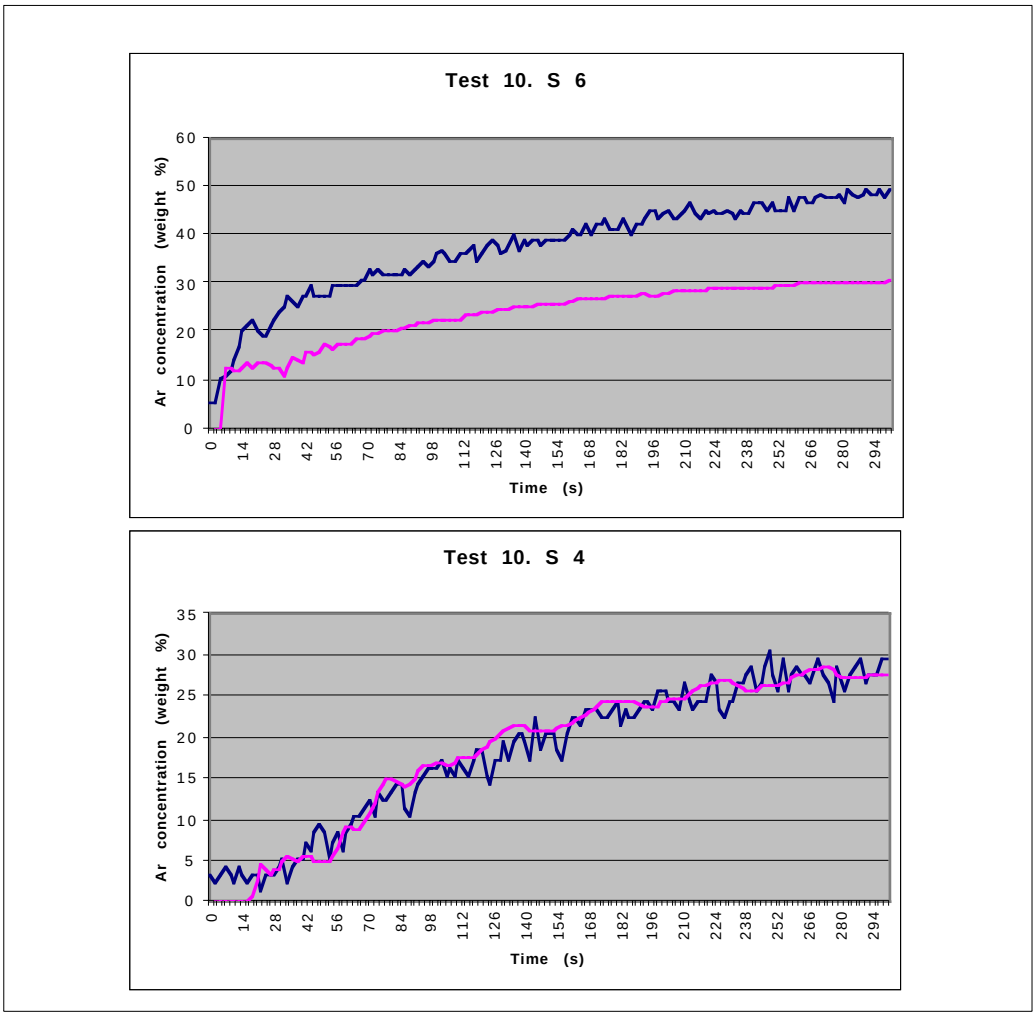

Figure 5.16 Evolution of Argon Concentration.TC 3/S6, close to the pit, and TC4/S14, far from the pit. Blue: experimental data; Pink: simulation data

For this intermediate leak, we observe the same effect as for the huge leak: close to the pit the results are less accurate - 2,7 % O_2 volume - than for sensors far from the pit, where we the prediction is exact to the simulation.

The temperature curves are shown in the following page.

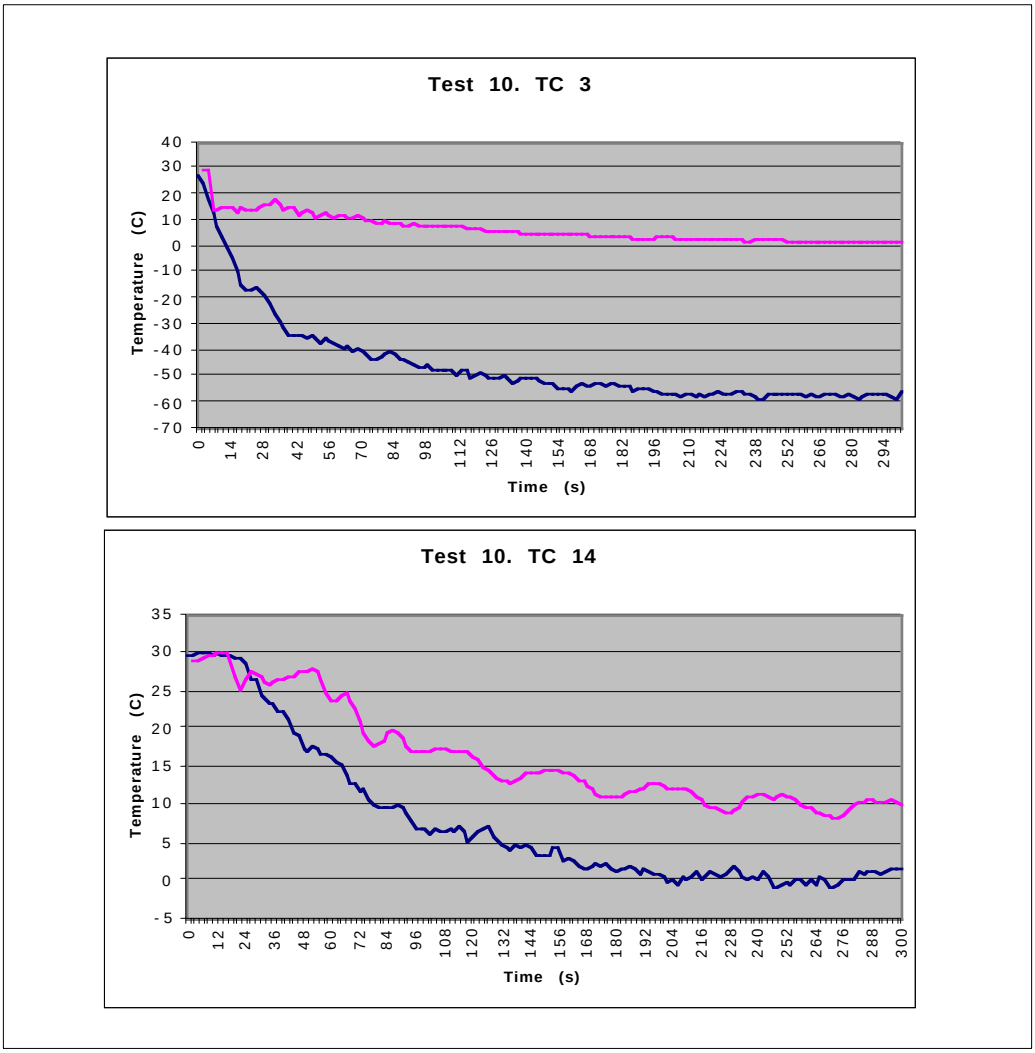

Figure 5.17 Evolution of Temperature.TC 3/S6, close to the pit, and TC4/S14, far from the pit. Blue: experimental data; Pink: simulation data

As for the temperatures, again we reach the same results: close to the pit we observe differences of about sixty degrees, and for points far from the pit, we reach differences of about ten degrees.

If we plot all the thermocouples and oxygen sensors together, we obtain:

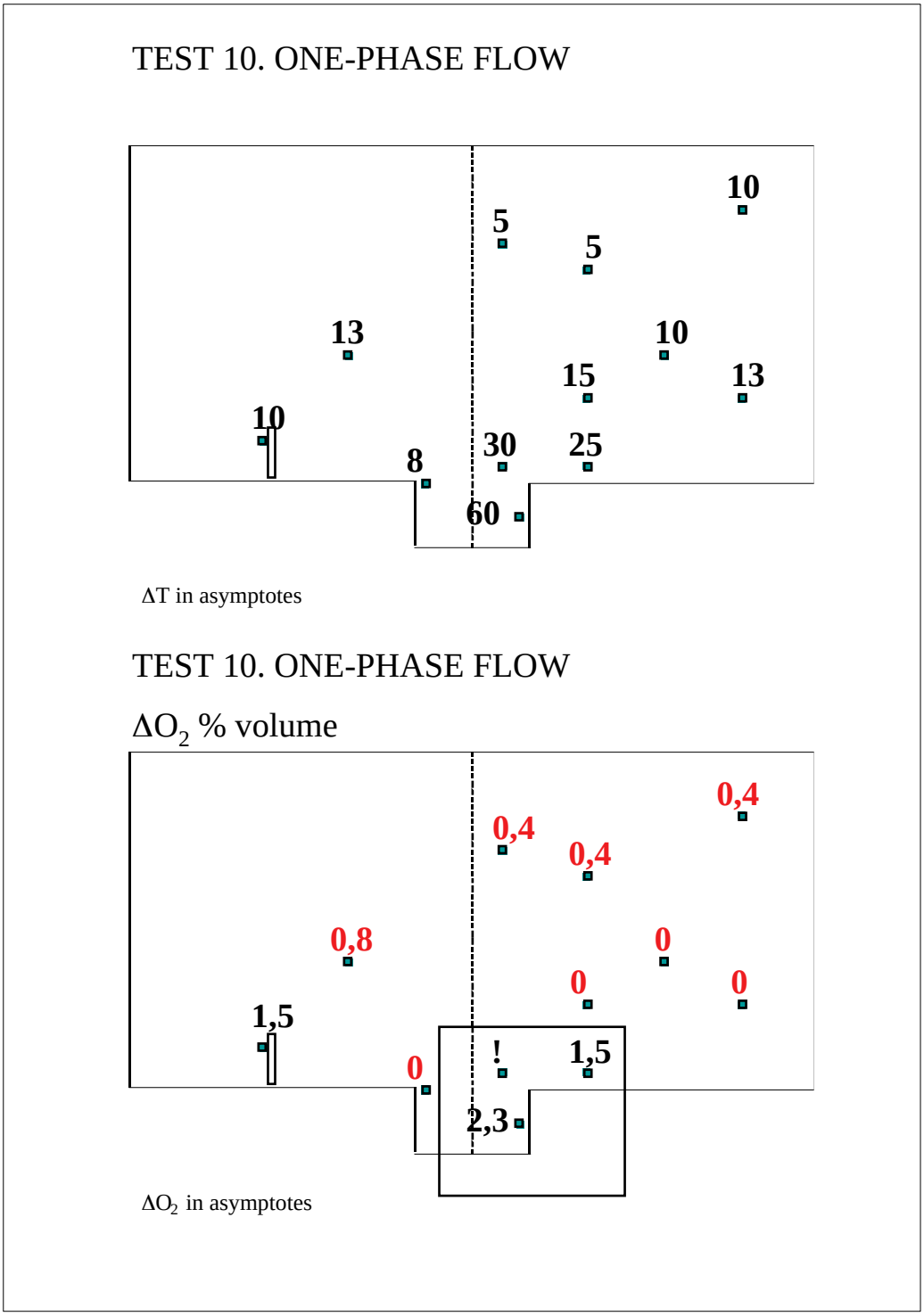

Figure 5.18 Test 10. One-Phase Flow. Temperature and Oxygen concentration comparison

For completeness, we will study what happens for a small flow, such as Test 4 of 4,9 l LAr / min.

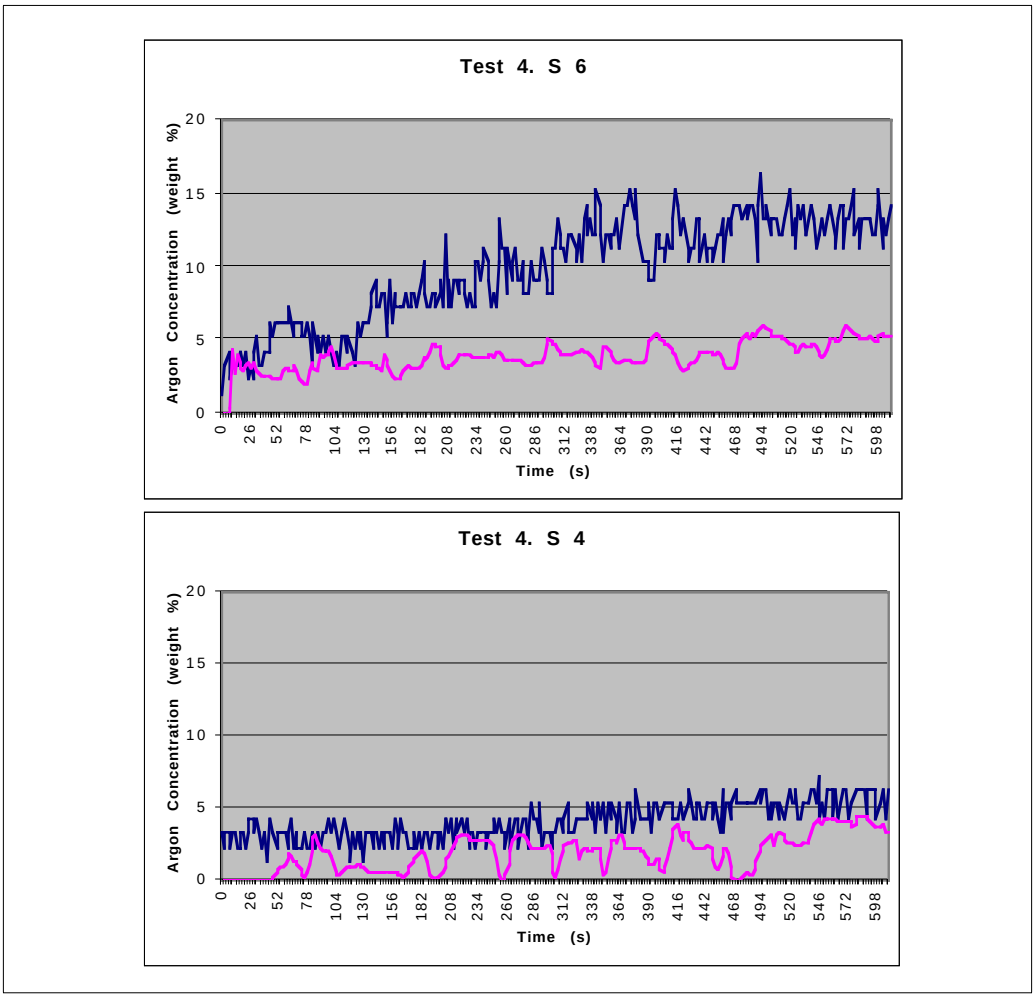

Figure 5.19 Evolution of Argon Concentration.TC 3/S6, close to the pit, and TC4/S14, far from the pit. Blue: experimental data; Pink: simulation data

For the oxygen detector located in the pit, there is a difference between the experimental and the simulation of 5 % Ar (weight). This is equivalent to a difference of approximately 1 % O_2 in volume, which is reasonable, and within the error of the zirconia detector. Once more, the experimental and simulation results are very close for sondes far from the pit, such as S4.

The temperature curves are shown in the following page.

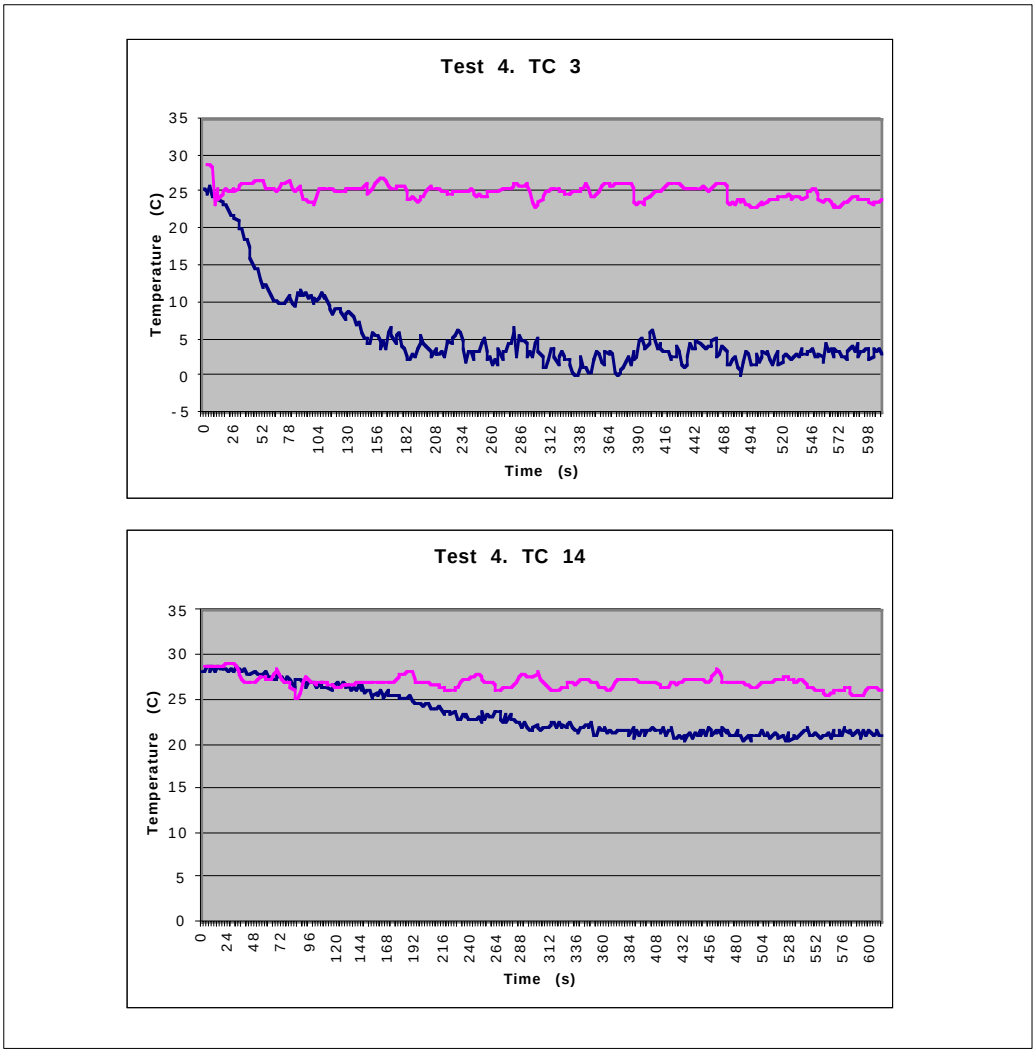

Figure 5.20 Evolution of Temperature.TC 3/S6, close to the pit, and TC4/S14, far from the pit. Blue: experimental data; Pink: simulation data

The temperature difference for the TC 3 located at the extraction fan is again very big, of about twenty degrees. However, this is far less than for the previous flows, for which we found a difference of sixty degrees.

As for the TC 14, the delta T is of about five degrees, also less than for the previous flows, where we found a difference of ten degrees.

If we plot all the thermocouples and oxygen detectors together, the outcome is the following:

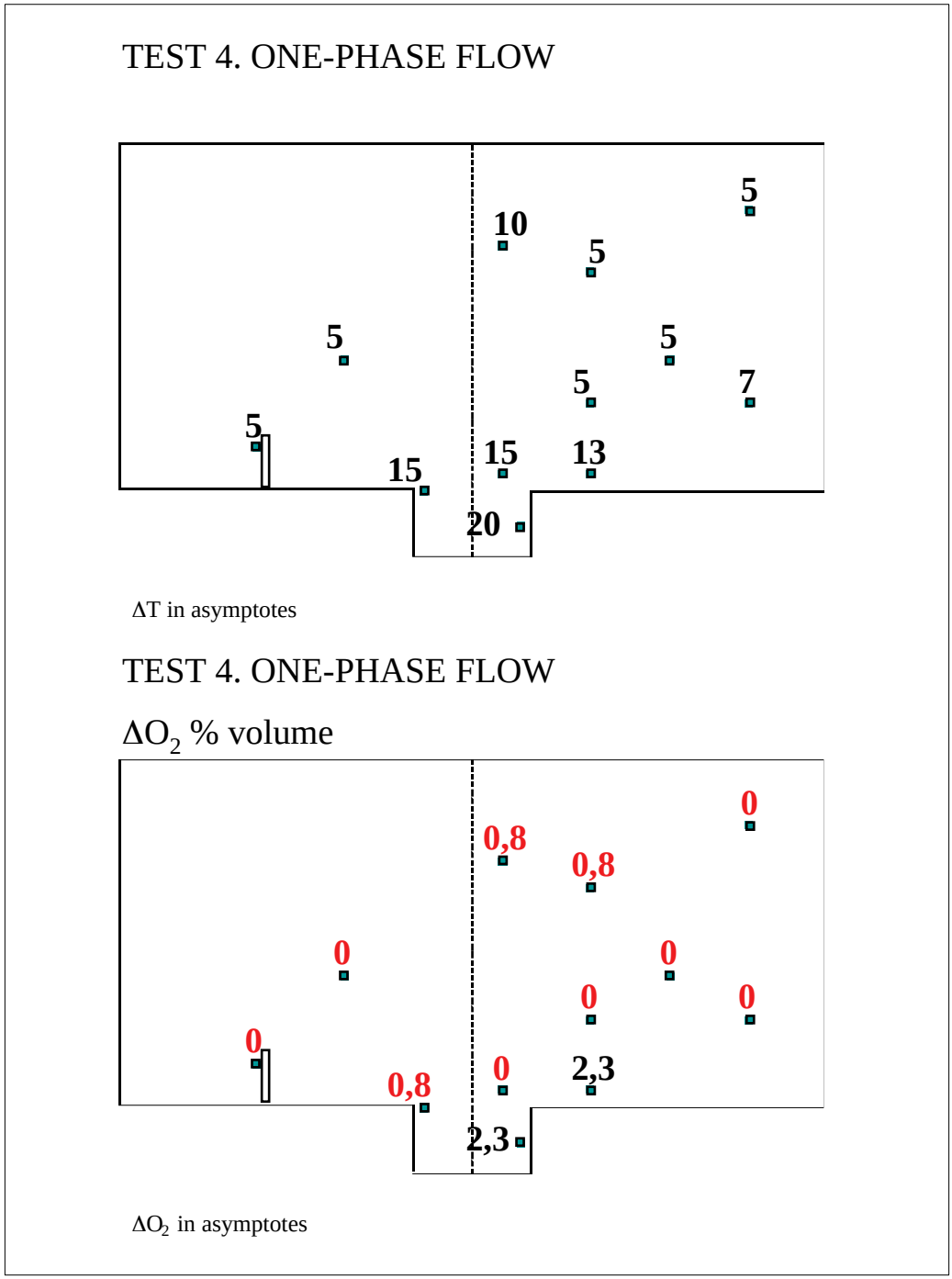

Figure 5.21 Test 4. One-Phase Flow. Temperature and Oxygen concentration comparison

Conclusions

For the Argon concentration distribution, we can conclude that the model is doing correct predictions. The sensors located close to the pit are the worst ones, with a maximum deviation from experimental results of 2,7 % O_2 (volume) -this is the worst value obtained in one pit sonde-, which is acceptable if we think that the error for the zirconia detectors is of 1% O_2 (volume).

The comparison between the experimental temperature and the results obtained with StarCD for the One-Phase 2D model for this magnitude, show that there is some important element missing in the modelisation. Differences of sixty degrees are detected close to the pit (worst predictions) and of about ten degrees far from the pit, for huge spills of 50 lLAr / min. For small leaks of about 5 l LAr / min., we

found out differences of twenty degrees in the pit and five degrees for thermocouples far from the pit.

We are going to analyze some aspects of the model in order to renormalize it in such a way that the temperature predictions are closer to reality.

5.4.2 One-Phase flow with Adiabatic walls

One of the hypothesis that was made, was that walls were isothermal. To check if this fact was influencing the results, we decided to implement a somehow opposite boundary condition: Adiabatic walls, where no exchange of heat takes place.

Model Description

The meshing and boundary conditions of this model are the same as the one we have proposed in the One-Phase flow model, but for the definition of the walls, which are adiabatic instead of isothermal.

Results

This model was studied for Test 8, therefore, a huge flow. The curves for temperature, are the following:

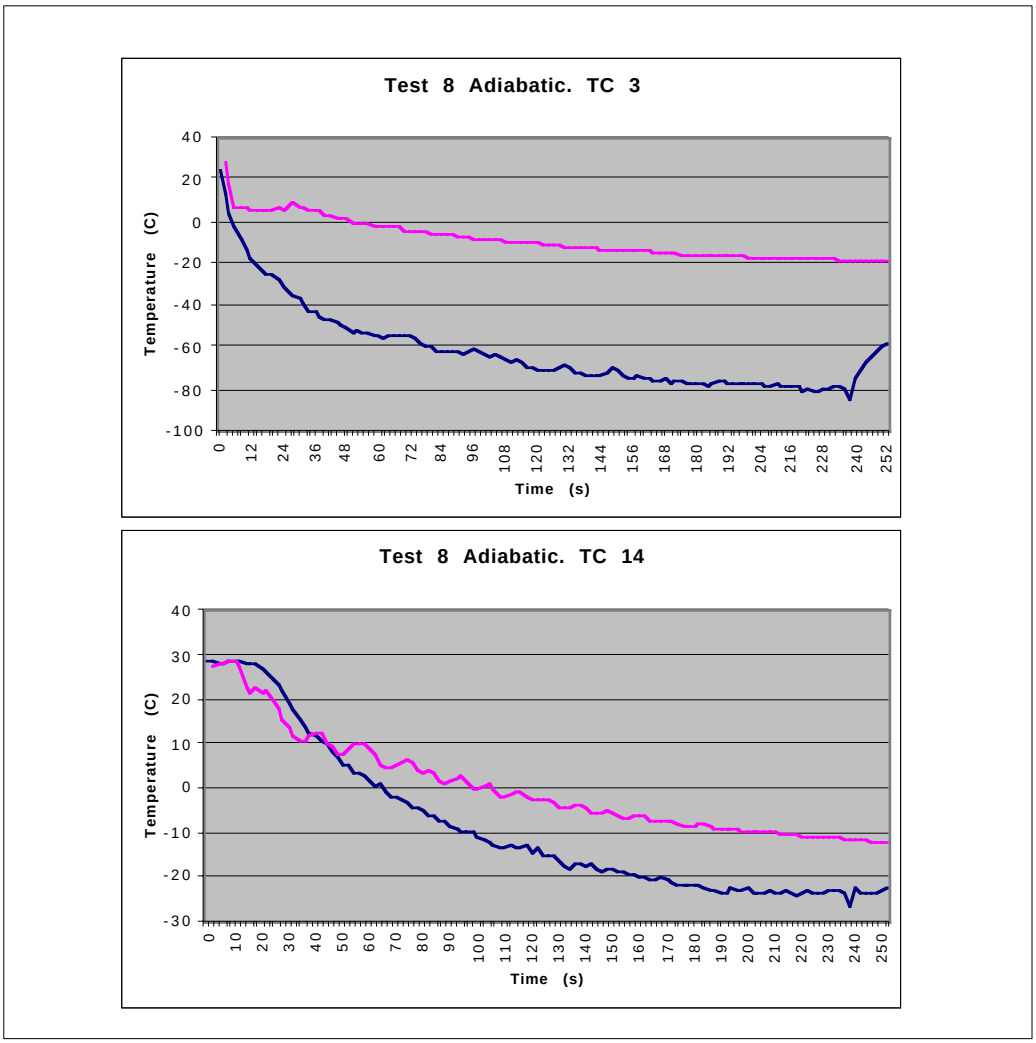

Figure 5.22 Evolution of Temperature.TC 3/S6, close to the pit, and TC4/S14, far from the pit. Blue: experimental data; Pink: simulation data

We see nearly no difference between the adiabatic or isothermal choice. There are still important differences between temperature prediction and experimental data.

If we plot again all the thermocouples together, the differences between experimental and simulated data are the following:

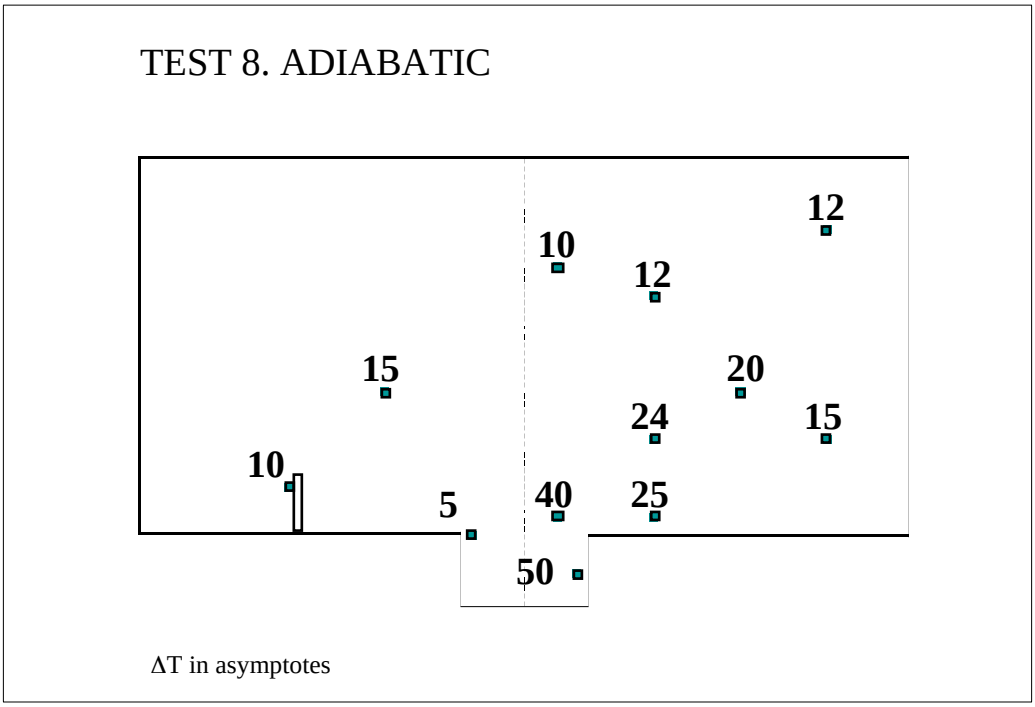

Figure 5.23 Test 8 Adiabatic. Temperature comparison

Conclusions Adiabatic walls implementation does not change significantly the results. This is consistent with the study of the critical parameters of the model carried out in chapter 4.

5.4.3 One-Phase flow with a 3D geometry

2D geometries with symmetry planes are implying a zero gradient in the transversal direction. We know that the pit shape is introducing a 3D effect in the motion of the fluid. We wanted to know whether this effect was significant. This is the reason why we implemented this model for several tests, namely Test 8 (50 l LAr / min.) and Test 10 (27,3 l LAr / min.).

Model Description

The meshing has been refined at the boundary proximities, that is to say, at the air inlets, outlets and argon inlet.

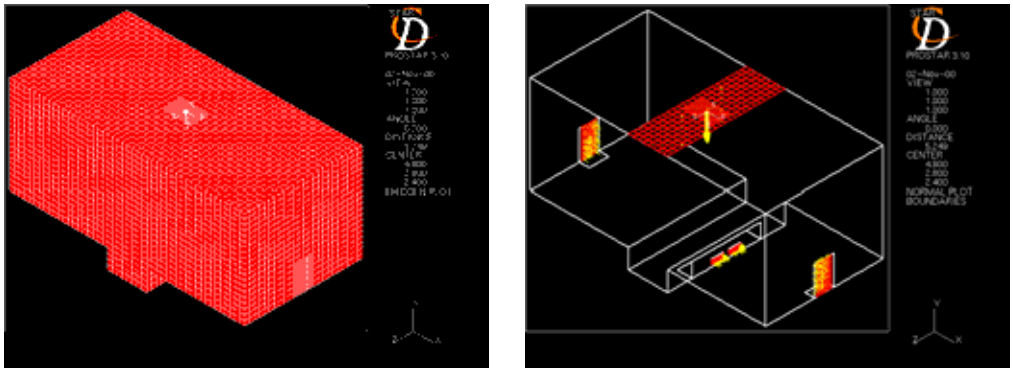

Figure 5.24 3D meshing and boundary conditions

The main characteristics of the model are summarized in the following table:

Table 5.7 Meshing parameters of the 3D model

Cells	26.398
Vertices	30.983
Boundaries	6.040
Couples	410
Boundary regions	10

As for the boundaries, they have not been averaged with the length of the room. The dimensions of the boundary regions try to maintain the dimensions of the real elements as far as the refinement of the mesh allows. The new implemented boundaries could be summed up the following way:

Table 5.8 Boundary properties

	v (m / s)	k (m^2 / s^2)	ε (m^2 / s^3)
Air Inlet	1,2569	2,38 e-02	4,817e-03
Air Pit Extraction	1,9814	5,889 e-02	0,149996
Air Top Extraction	0,1975	0,00585	0,000014
Heating	Area=1,66 m^2	q=1.445 W / m^2	

The model was implemented with adiabatic walls. As for the Argon inlet, the area of the spill was increased to 10 x 10 cm so as to avoid supersonic flows (see details for boundaries at Appendix B).

Results So as to be able to compare with the previous results, we present the curves for the flow of 50,0 l LAr / min., Test 8.

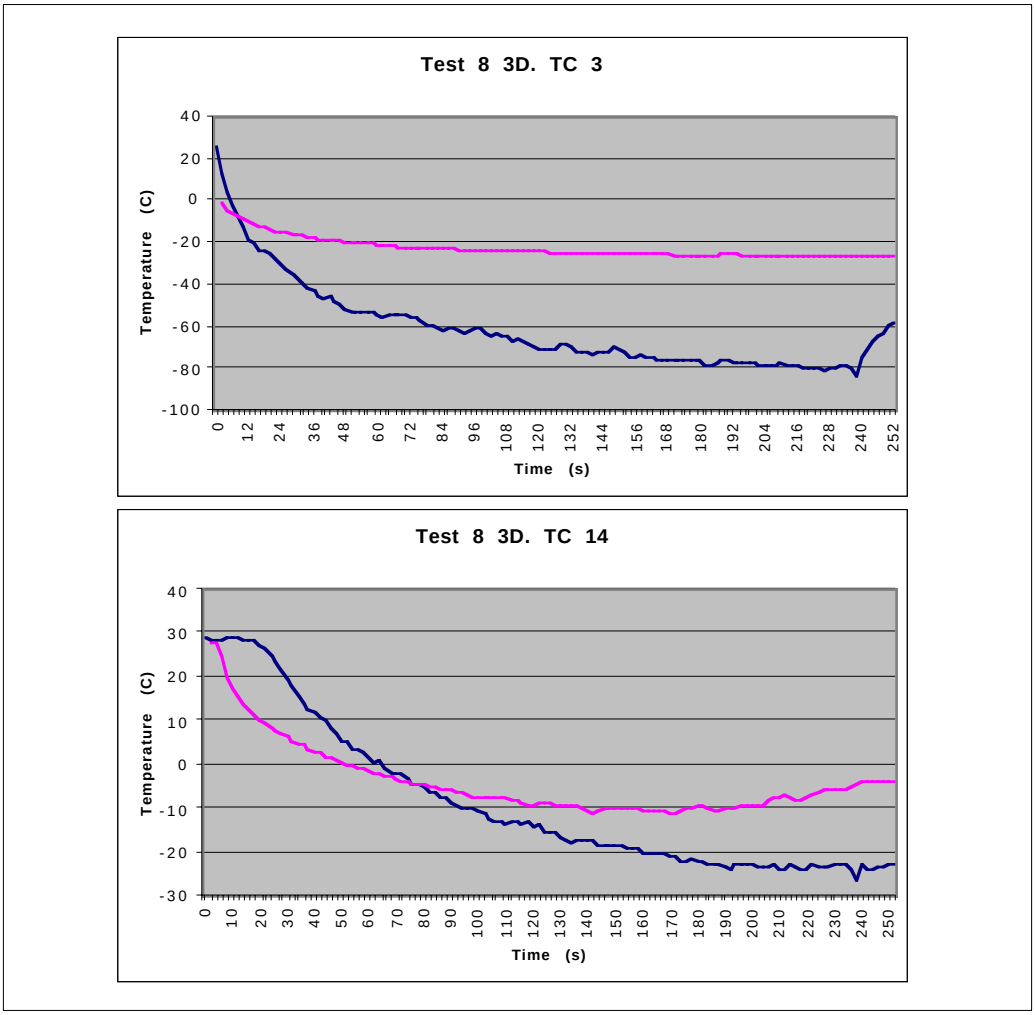

Figure 5.25 Evolution of Temperature.TC 3/S6, close to the pit, and TC4/S14, far from the pit. Blue:experimental data; Pink: simulation data

As we see in the figures, the difference between experimental and simulation data is decreasing only slightly. The ΔT for all the thermocouples is the shown in the following figure, where we should point out a coincidence between the experimental and simulation data for TC 8, located in the left side of the pit.

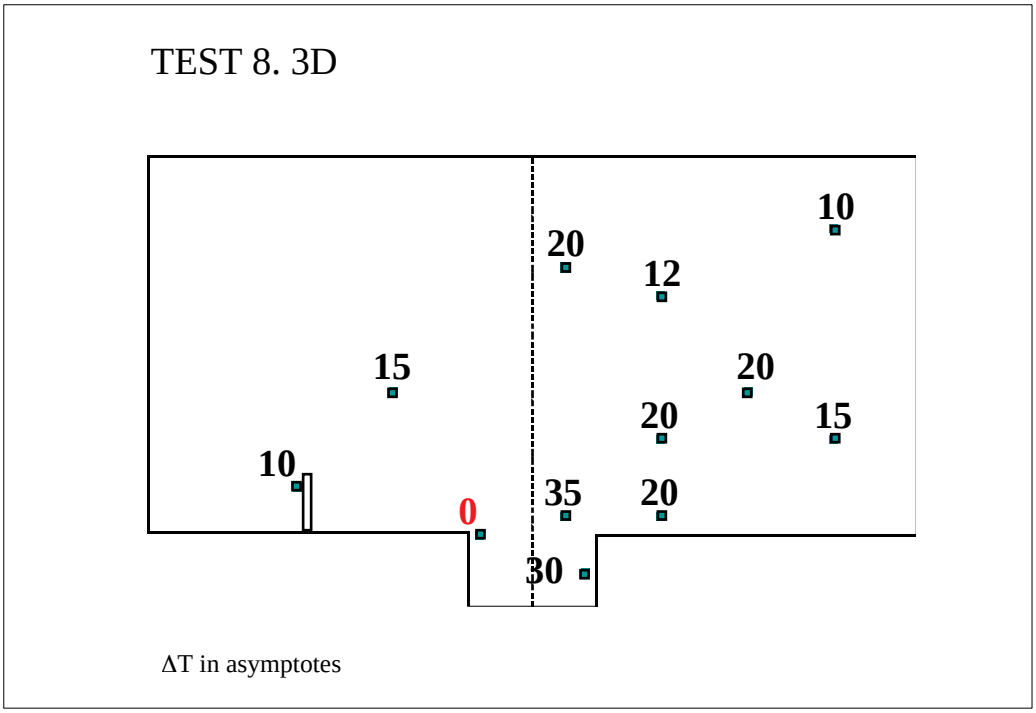

Figure 5.26 Test 8 3D. Temperature comparison

Conclusions

A 2D approach is a good one, since the results are not differing much from the 3D implementation. If we take into account that computing time is far smaller for 2D than for 3D, we chose to implement a 2D model.

We observed that the main improvements of the 3D model where in the pit area, which is allowing the flow moving through its longitudinal direction. These improvements are not enough to consider that this is the cause of the huge differences in temperature.

5.5 Two-Phase Flow model

The results shown in the previous section let us conclude that the predictions from the point of view of argon distribution are correct, but there is a problem when it comes to predicting the temperature distribution. The experimental data is always some degrees under the simulated one, so our model is too optimistic.

The fact that the experimental temperature data are always far lower than the simulation leads us to the fact that there is some absorption of energy into the solution domain that we did not take into account. This absorption source could be easily explained by the latent heat of evaporation, which is not considered in our model: we just implemented an inlet of gas argon, assuming that all the liquid had evaporated because of flash-evaporation (due to the difference of pressure between the dewar and atmospheric pressure). The experiment showed us that this was not fully true, since we could hear rain of liquid falling and once the cloud of water vapor had disappeared, we could see traces of liquid on the isolant. The latent heat for argon is of 160,8 kJ/kg, so even if a small quantity of liquid is evaporating into the air the heat balance will change significantly. Therefore we wanted to include this change of phase in a new model that should give better predictions for temperature.

5.5.1 Spray Model

StarCD cannot model evaporation with free surface; Since a direct implementation is therefore not possible, we had to search for another way of implementing the change of phase. We implemented a Spray model, that is to say, simulate that all the liquid coming out of the pipe/dewar that had not evaporated by flash-evaporation was atomizing in droplets at the exit and evaporating afterwards within the domain. This Lagrangian model is allowing coupling between the dispersed and the continuous phase, therefore establishing a dynamic thermal, mass, momentum interaction and change of phase. This is one of the only ways of implementing change of phase in StarCD.

Model description

If a breach occurs, liquid moving isothermally from a high pressure zone to a low pressure zone often crosses the bubble point curve and disintegrates into a spray by partial evolution of vapor. It has been theorized that after the initial bubbles, the vapor will be more likely to form at the bubble surface, causing rapid growth of the bubble and a corresponding physical displacement of the adjacent liquid. On passing through the nozzle, the displacement will cause the disintegration of the liquid, resulting into formation of a spray.

Here, a methodology similar to a discharge from a pressurized metered dose inhaler (pMDI) developed by Dunbar and Watkins (1997) is followed. They found that the primary atomization process was dominated by flash-evaporation of the superheated fluid within the nozzle. This was modelled by assuming that the liquid would instantaneously flash-evaporate upon entering the nozzle, the % of liquid that could flash being calculated using a simple adiabatic heat balance equation. The only problem remains whether the usage of sonic discharge of an ideal gas under adiabatic conditions, be applicable.

Flash Evaporation. Flow evaporation is assumed to occur when the fluid goes from the pressure in the dewar to ambient pressure. Therefore, we can calculate the flash evaporation that takes place at our dewar valve, making the assumption of adiabatic expansion, where the enthalpy is conserved. The enthalpy balance is therefore:

$$\dot{m} \cdot h^{IN}{}_{liquid} = \dot{m} \cdot (1 - x) \cdot h^{OUT}{}_{liquid} + \dot{m} \cdot x \cdot h^{OUT}{}_{gas}$$

From this expression we obtain the quality x:

$$x = \frac{h^{IN}{}_{liquid} - h^{OUT}{}_{liquid}}{h^{OUT}{}_{gas} - h^{OUT}{}_{liquid}}$$

If we consider that our dewar was at 12 bar sat.*, we obtain a value of the quality at the valve of 25 %, which would mean 75 % of the flow at the exit of the valve is still liquid.

For our calculations we assumed that the exit of the pipeline and the dewar valve are the same point (though we will see later that this is a very rough estimation, and we should account that there is quite a lot of evaporation in the pipeline).

Multi phase Jet. Secondly, we have to model the multi phase jet. This is based on the Lagrangian approach, based on discrete droplet model. Droplet break-up models and collision models are taken into consideration. The behavior of droplet collisions is found to be dependent on the surface tension and viscosity of the droplet fluid as well as the gas pressure, density and viscosity. The model is implying several aspects. Here we describe the main assumptions:

Speed of each phase. One of the big questions is related to the speed of the two-phases. Following M.A.Aamir and A.P.Watkins study about “Numerical analysis of depressurization of highly pressurized liquid propane”, we should determine first whether our flow is critical or sub-critical. For this, we calculate the critical coefficient first:

$$R_c = \left(\frac{2}{\gamma + 1}\right)^{\frac{\gamma}{\gamma - 1}}$$

Where γ is the ratio between the specific heats at constant pressure and volume.

The condition of critical flow is given by the ratio:

$$R_c > \frac{p_{atm}}{p_{vessel}}$$

For us R_c=0,43 and therefore we are dealing with a critical flow. Therefore, we cannot calculate the speeds of the phases by just applying Bernoulli’s law, but we will do it following the expressions below.

* Compromise reached with J.Bremer.

For the gas phase:

$$U_{gas} = \left(\frac{\gamma \cdot P \cdot R_c^{\frac{\gamma - 1}{\gamma}}}{\rho_{gas}} \right)^{0,5} \sim 163 \frac{m}{s}$$

And for the fluid phase:

$$U_{liquid} = \left(\frac{\gamma \cdot P - (P \cdot R_c)}{\rho_{liquid}} \right)^{0,5} \sim 34 \frac{m}{s}$$

Heat Transfer process. We use the formulation of El Wakil, in which heat transfer coefficient is evaluated from a correlation applicable in absence of mass transfer and then multiplied by a correction factor to account for the mass process. This coefficient is:

$$h = \frac{K_m \cdot Nu \cdot Z}{(e^Z - 1) \cdot D_d}$$

Where the magnitudes are evaluated at film-mean temperature. The Nusselt number should be calculated as follows:

$$Nu = 2 \cdot \left(1 + 0,3 \cdot Re_d^{\frac{1}{2}} \cdot Pr^{\frac{1}{3}} \right)$$

and the Z:

$$Z = \frac{-Cp \cdot \left(\frac{dm_d}{dt} \right)}{\pi \cdot D_d \cdot K_m \cdot Nu}$$

Mass Transfer Process. The calculation of the mass coefficient comes from the Ranz Correlation:

$$K_g = \frac{Sh \cdot D_m}{R_m \cdot T_m \cdot D_d}$$

where R_m is the mixture gas constant, T_m is the mean temperature, D_m is the vapor diffusivity and Sh is the Sherwood number, calculated as:

$$Sh = 2 \cdot \left(1 + 0,3 \cdot Re_d^{\frac{1}{2}} \cdot Sc^{\frac{1}{3}} \right)$$

where Sc is the Schmidt number.

Break up model. Droplets and bubbles may become unstable under the action of the interfacial forces induced by their motion relative to the continuous phase. We implemented the Reitz and Diwakar break-up model, which explains droplet break-up due to aerodynamic forces in the following two modes:

(a) Bag break-up: non-uniform pressure field around the droplet causes it to expand in the low-pressure wake region and eventually disintegrate when surface tension forces are overcome. The instability is determined by a critical value of the Weber number, which is compared to an empirical coefficient whose value is between 3,6 and 8,4). The Weber number is calculated as:

$$We = \frac{\rho \cdot \left|\vec{u} - \vec{u}_d\right|^2 \cdot D_d}{2 \cdot \sigma_d}$$

(b) Stripping break-up: process in which liquid is sheared or stripped from the droplet surface. The criteria used is:

$$\frac{We}{\sqrt{Re_d}} > 0,5$$

Wall Impingement. The impact of droplets, bubbles on rigid surfaces may produce a wide range of consequences. Droplets may adhere, bounce or shatter and the liquid deposited on the surface may retain its droplet form or merge into a liquid film.

Star-CD gives us a wide range of possibilities:

(a) Perfect Rebound

(b) Adherence in spherical form, so that heat and mass transfer will go ahead

(c) Instantaneous evaporation

(d) Bai's spray impingement model

We implemented the instantaneous evaporation since this is quite close to reality: liquid argon is evaporating very quickly when it reaches the floor.

Diameter of the droplet. This is one of the most problematic points of the model. The code allows us several ways of initializing our droplet distribution. Basically, we used two of them:

(a) Spray initialisation: this possibility enables us to specify the liquid volumetric flow rate entering the solution domain through an injection nozzle. It is necessary to introduce the cone angle where the spray takes place, the type of fluid, its initial temperature, 87,29 K (we propose that the droplets are at wet bulb temperature, which is defined as the temperature of saturated argon at atmospheric pressure),

the kind of atomization model we want (we will use the Reitz-Diwakar atomization model, linked to the use of the same author's break-up model) and the characteristics of the nozzle (discharge coefficient, nozzle hole cross-sectional area, contraction ratio and roughness). In this model of atomization, the radio of the droplet is equal to the radio of the nozzle. Then this droplet is suffering break-up so its diameter is becoming smaller while it is getting closer to the pit, and until it reaches the floor, where it will evaporate.

(b) User initialisation: this way of initializing allows us to choose the number of droplets, the quantity of mass liquid to come into the domain, also with the droplet diameter and the cone angle where there will be a distribution of velocities depending on the angle. This is done via programming a fortran subroutine such as the one we shown below:

```
C**********************************************************************
      SUBROUTINE DROICO(IDRT,RNDP,XD,YD,ZD,UD,VD,WD,DRD,DENDR,TD,
     &                  ICSRGP,OMEGRP)
C     Droplet initial conditions
C**********************************************************************
C     STAR RELEASE 3.100                                    *
      INCLUDE'comdb.inc'
      COMMON / USR001 / INTFLG(100)
      INCLUDE'usrdat.inc'
      EQUIVALENCE(UDAT05(001), IDR)
C     This subroutine enables the user to specify droplet initial
C     conditions.
C     ** Parameters to be returned to STAR: IDRT, RNDP, XD,YD,ZD,
C                                 UD,VD,WD, DRD, DENDR, TD
C                                 ICSRGP,OMEGRP
C     Droplet type IDRT is passed to this subroutine as a negative
C     number.
C     If its value is not changed to positive value (between 1 and 10)
C     this subroutine will not be called and injection of particles will
C     be held until the next time step.
C----------------------------------------------------------------------
      INTEGER*4 NN,ISEED,TWO14
      SAVE NN
      data NN / 0 /
C----------------------------------------------------------------------
      IF(.NOT.TIME.LT.20) RETURN
C-----NUMBER OF PARCELS INJECTED PER TIME STEP
      NPAPTS=1
      IF(IDN.GT.NPAPTS) RETURN
      PI=3.1415927
      DEGRAD=PI / 180
C-----DROPLET MASS INJECTION RATE (kg / s)
      FLOWDR=0.3172102
C-----DROPLET TYPE
      IDRT=1
C-----DROPLET DIAMETER
      DRD=1.0E-03
C-----DROPLET DENSITY (KG / M3)
```

```
      DENDR=1392.8
C-----DROPLET TEMPERATURE (K)
      TD=87.29
C-----MASS OF A SINGLE DROPLET
      DRMAS=DENDR*PI/6.*DRD**3
C-----NUMBER OF DROPLETS REPERESENTED BY DROPLET IDR
      RNDP=FLOWDR/(NPAPTS*DRMAS)*DT
C-----INITIAL POSITION OF THE DROPLET(m)
      XD=4.8
      YD=4.75
      ZD=0.0
C-----GET RANDOM NUMBERS RN1 AND RN2
      ISEED=150623
      TWO14=16384
      IF(NN.LT.1500.AND.NN.GT.-1500) NN=ISEED
      NN=NN*ISEED
      RN1=MOD(NN,16384)/16384.
      NN=NN*ISEED
      RN2=MOD(NN,16384)/16384.
C-----INITIAL VELOCITY OF DROPLET (m/s)
      CONANG=11.31
      FI=(90.+CONANG*RN1)*DEGRAD
      TH=180.*CONCNG*RN2*DEGRAD
      UMAG=0.016283
      UD=UMAG*COS(FI)*SIN(TH)
      VD=UMAG*SIN(FI)
      WD=O
C---------------------------------------------------------------
      RETURN
      END
```

Droplet properties. Of course we have to describe the droplets properties. We can sum-up them in the following table:

Table 5.9 Argon Droplets properties

Viscosity	10,4 e-04 poises
Density	1392,8 kg / m^3
Superficial tension	0,1053 N / m
Critical Point	150,86 K / 122,29 ^{o}C at 48,98 bar
Latent heat of evaporation	160,81 kJ / kg / 38,409 kcal / kg
Saturation pressure	P(bar)=5,19 / 1000*exp(6,26 / 100*T(K))

As we see, we had to implement in another subroutine the saturation pressure curve, since pressure is varying a lot with temperature.

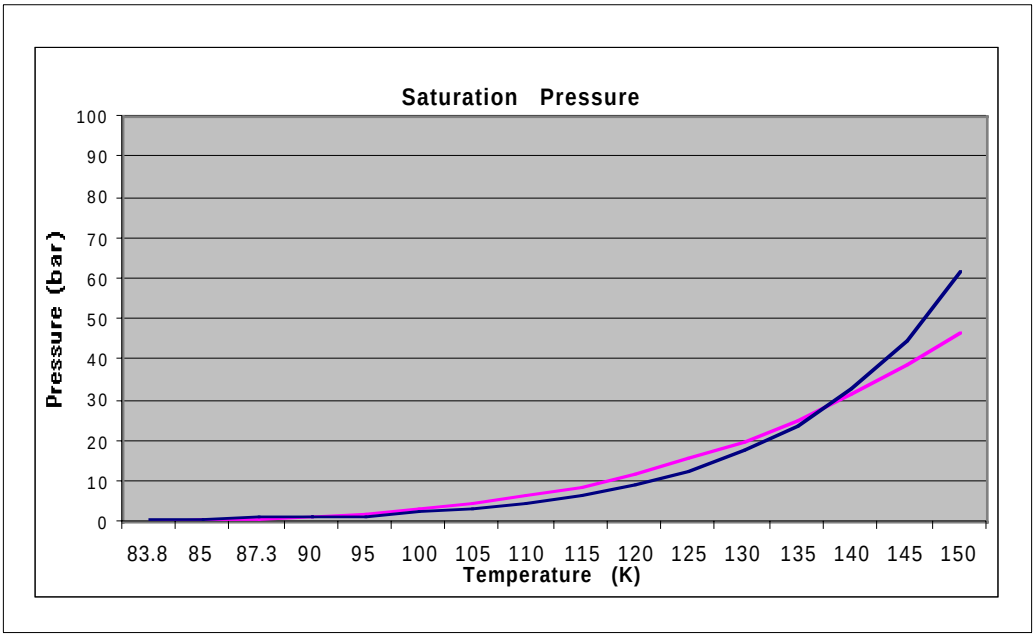

Figure 5.27 Saturation Pressure curve and the representation of the correlation curve

Results It is difficult to write about real results in this case, since the simulation time was so long that after several weeks of calculation, we just obtained several seconds in real time. Therefore, we just want to show a little how the simulation looked like.

The model that was implemented was the Test 10, 27,33 l LAr / min. Here we have the first second of one of the models, which was using spray initialization:

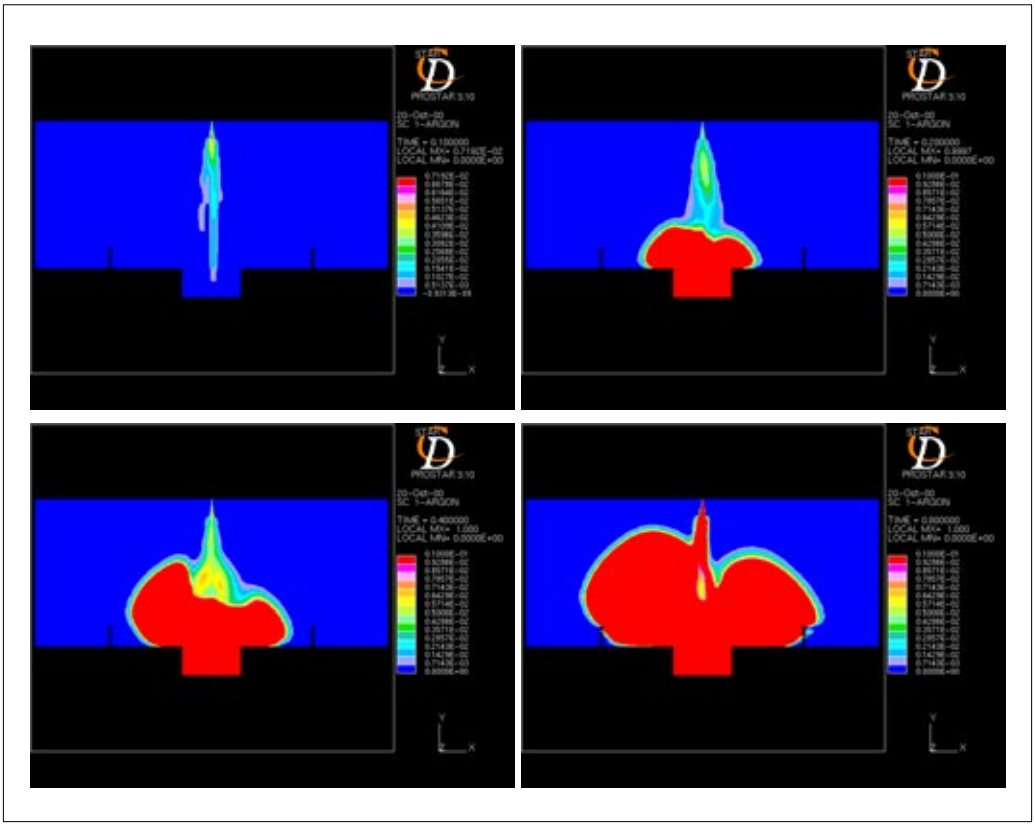

Figure 5.28 Spray initialisation. Test 10. Less than one second of calculation.

The manual initialisation was more attractive, since we could control directly the diameter of the droplet. We did some tries for diameters of 1 and 0,5 mm. Here we are the results:

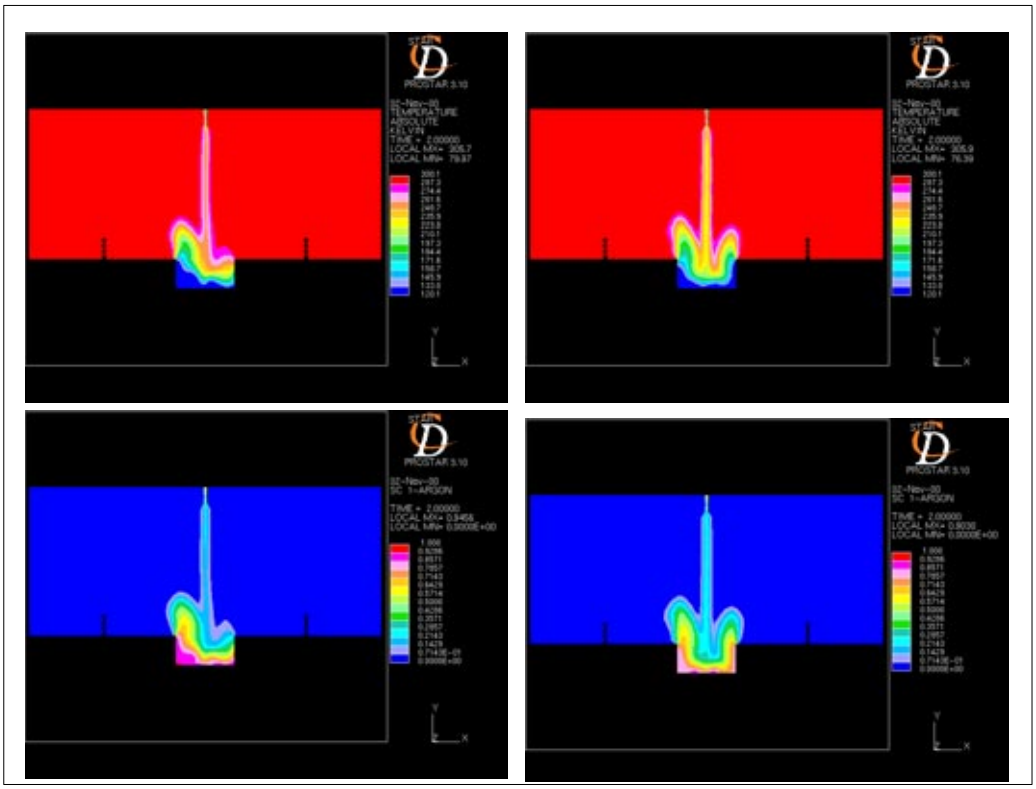

Figure 5.29 Manual Initialisation. Sensibility on the Droplet Diameter: 1mm (left) and 0,5 mm (right)

From the figures, we see that temperatures are too low in the pit. This means too much evaporation is taking place there, and little in the jet cone. Therefore, we should look for smaller diameters.

This study could not go ahead due to the lack of computing resources so as to do it in a reasonable way.

Conclusions

This kind of model was perfect from the point of view that it was allowing coupling between the dispersed and the continuous phase: heat transfer, momentum transfer, mass transfer. Therefore we just had to insert the liquid phase (droplets) and leave the changing conditions decide when the evaporation should take place. Unfortunately, this became a quite complex model, both from the point of view of implementation and from the point of view of control (really low time steps -0.005s- are needed to make this model converge).

From the little results on the sensibility study of the droplet, we could conclude that we should go on searching for diameters smaller than 0,5 mm. To go on with this study we should ensure more computing power.

Finally, we should also point out that even if the model had been successful, an extrapolation to the ATLAS cavern would have been nearly impossible.

Even if this model did not work, from a physical point of view it remains very interesting as well as a challenge from a CFD implementation point of view. Therefore we wanted to describe it in depth, so as to leave this way open for a

future, where faster and more powerful machines will be able to cope with this kind of problems.

5.5.2 Negative Heat Flux Wall Model

Since the Spray model was not suitable, for all the reasons we just pointed out, we decided to search for a much more simple model that could still simulate the evaporation of liquid argon.

We decided to keep an argon gas inlet, while extracting as heat flux all the latent heat of evaporation of the liquid that was coming into the domain. Since the liquid is evaporating all along the jet axis, it was easy to think we could extract this heat flux through a wall located at this axis. Since this wall represents a physical obstacle against the fluid motion, an intrinsic assumption is symmetry. We know this is not exact, due to the extraction fan in the pit, but this is nevertheless a good approximation to begin with.

Model Description

The difficult point of modeling this two-phase flow is determining the quantity of liquid argon that is flash-evaporating and the quantity of liquid that remains and therefore enters the domain in this state. It is not easy to reach a figure from the theory, since there is flash-evaporation taking place in the dewar valve and also plenty of evaporation in the pipeline. We can easily calculate the flash-evaporation in the dewar valve, as we did before. We reach an evaporation rate of 25%. To this rate we should add the evaporation taking place into the pipeline, which is not easily determined theoretically.

From the observation of the jet during the experiments, we can account that this evaporation was far larger than 25 %. A sensibility study of the percentage of evaporated argon and comparison with the experimental results is needed to achieve a good approximation of this parameter.

This model was giving us the opportunity to test quickly different ratios of flash evaporation. In the following picture we can see the boundary conditions and meshing of this model.

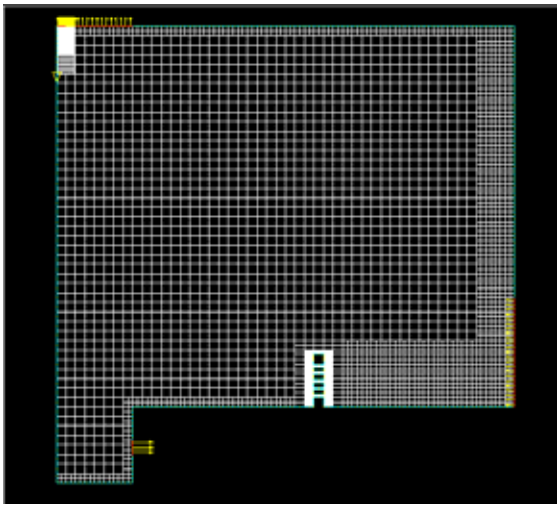

Figure 5.30 Negative Flux Model. Boundary conditions

Results We made a sensibility study on the flash-evaporation rate, for Test 10. First we tried a proportion 50%-50%, to see how the temperatures were changing:

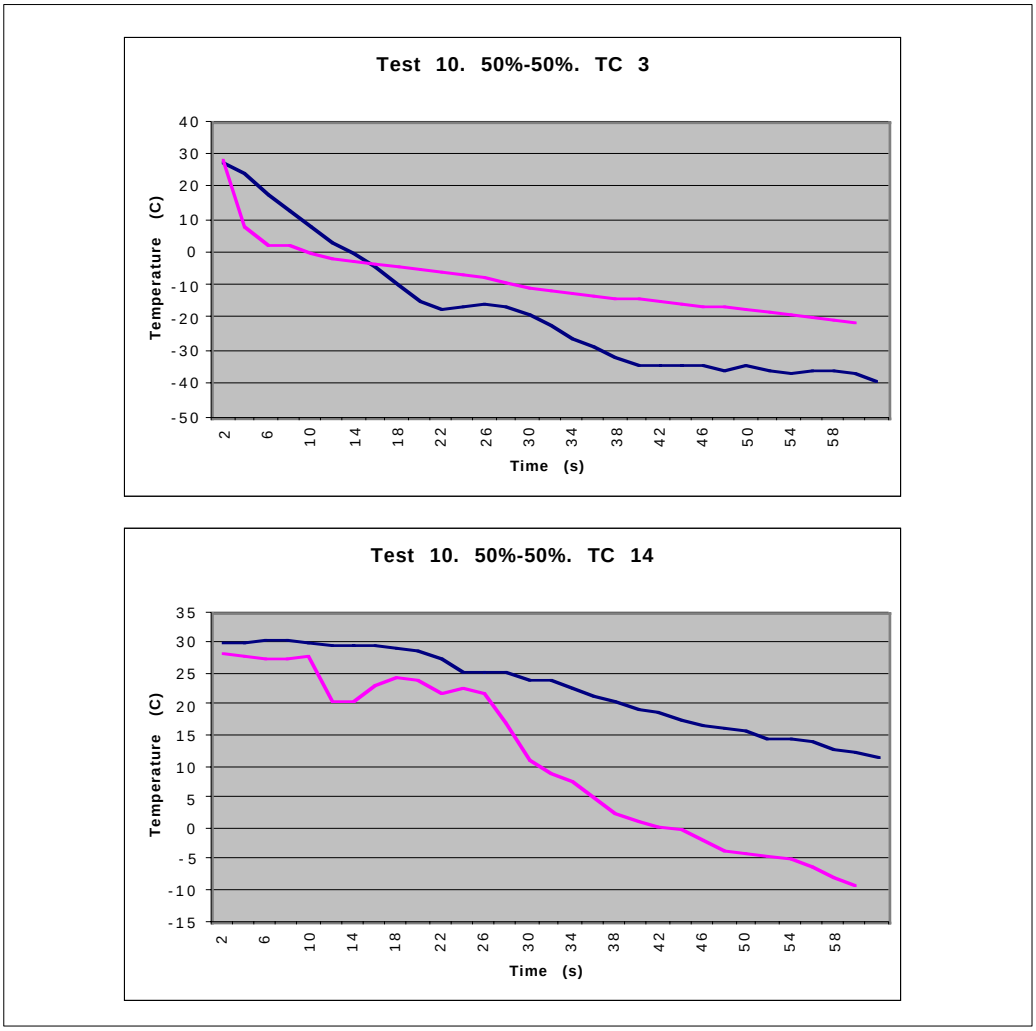

Figure 5.31 Evolution of Temperature.TC 3/S6, close to the pit, and TC4/S14, far from the pit. Blue:experimental data; Pink: simulation data

We observe that while for detectors close to the pit, temperatures are getting closer (from sixty degrees difference we go to twenty degrees difference), for thermocouples far from it, such as TC 14, the simulation temperatures are too low.

On the one side, we should say that to renormalize all the thermocouples at the same time, the heat flux distribution along the wall cannot be constant. This is logical, due to the fact that more evaporation is taking place in the pit than in the jet. Besides, the colder the air is getting, the more evaporation is taking place in the pit.

On the other hand, we should insert less liquid into the domain to find a good renormalization for the thermocouples far from the pit.

We decided to keep the heat flux constant and search for a good ratio of flash-evaporation to renormalize the thermocouples located far from the pit. Therefore, we tried the proportion 75 % flash-evaporation -25 % liquid into the domain. The results are shown down:

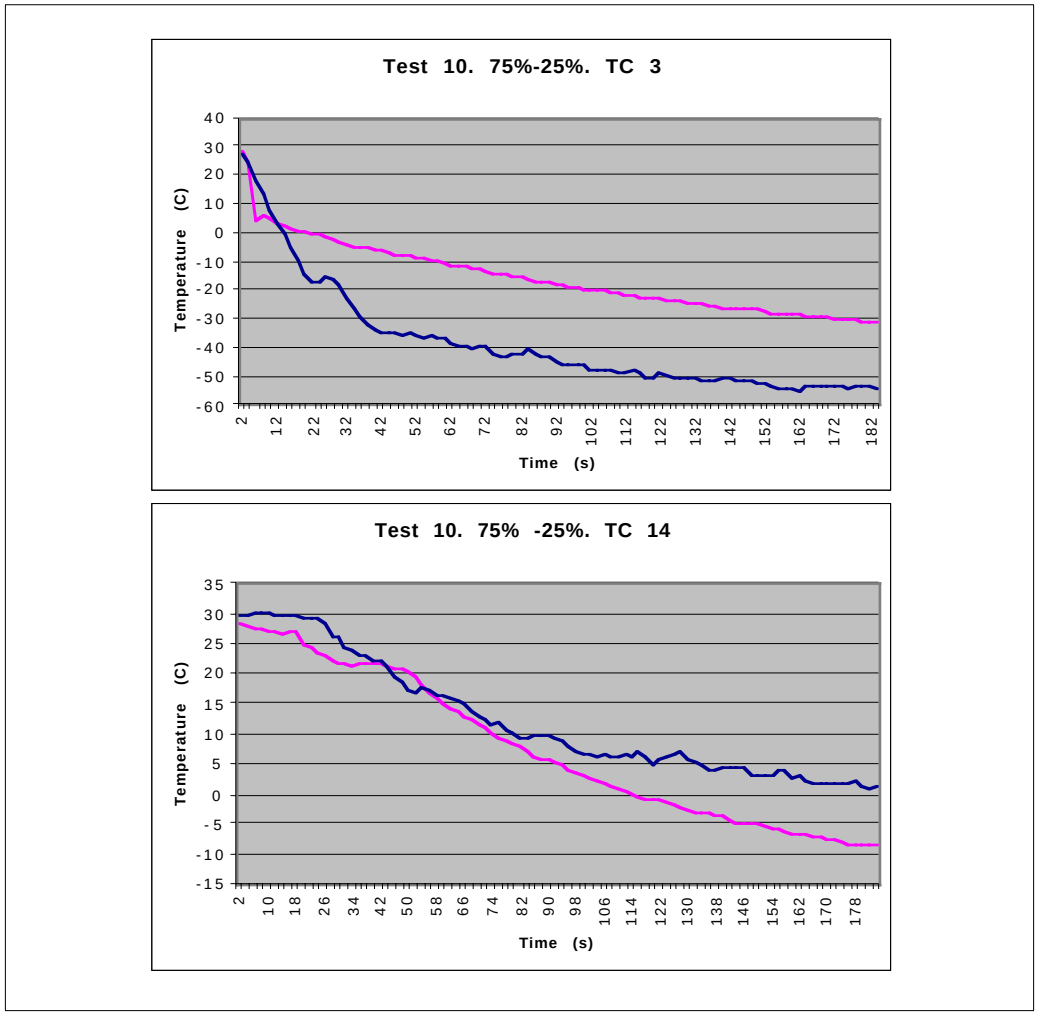

Figure 5.32 Evolution of Temperature.TC 3/S6, close to the pit, and TC4/S14, far from the pit. Blue:experimental data; Pink: simulation data

If our goal was to reach a good compromise for the thermocouples far from the pit, we see that now we are much closer to experimental data. We could still increase a little bit the proportion of flash-evaporation, but we will already do this for a more accurate model.

Conclusions The results of this model prove that the hypothesis that the latent heat of evaporation was missing in the ATLAS model, seems reasonable.

Apart from the symmetry aspect that the wall is implying, the problem of this model was that the heat flux was constant all along the wall. This is driving to too low temperatures for sensors that were located in high cotes far from the pit.

Nevertheless, this model was very useful to determine the proportion of flash-evaporation that took place in the dewar and pipe-line. This model lead us to a good approximation of this ratio, starting point for a better model.

We found out that there is another way of implementing energy sinks in the model without disturbing the flow. This model is the one presented in the next paragraphs.

5.5.3 One-Phase Flow with Energy Sinks

StarCD is allowing the implementation of energy sinks in such a way that is extracted straightforward from the energy balance and that is not disturbing the jet development. Altogether this model allows as an-easily non-uniform distribution of this heat sinks. This model is somehow a good compromise even though this is still a non-dynamic model.

Model Description

In order to get a simple model with the possibility of relatively high speed calculation, we implemented a model with an argon gas inlet and we distributed along the liquid jet (see figure 5.33) energy sinks that were extracting from the domain a quantity of energy equivalent to the latent heat of the liquid that evaporates into the room (total quantity of liquid argon minus the quantity of this argon that is suffering flash-evaporation).

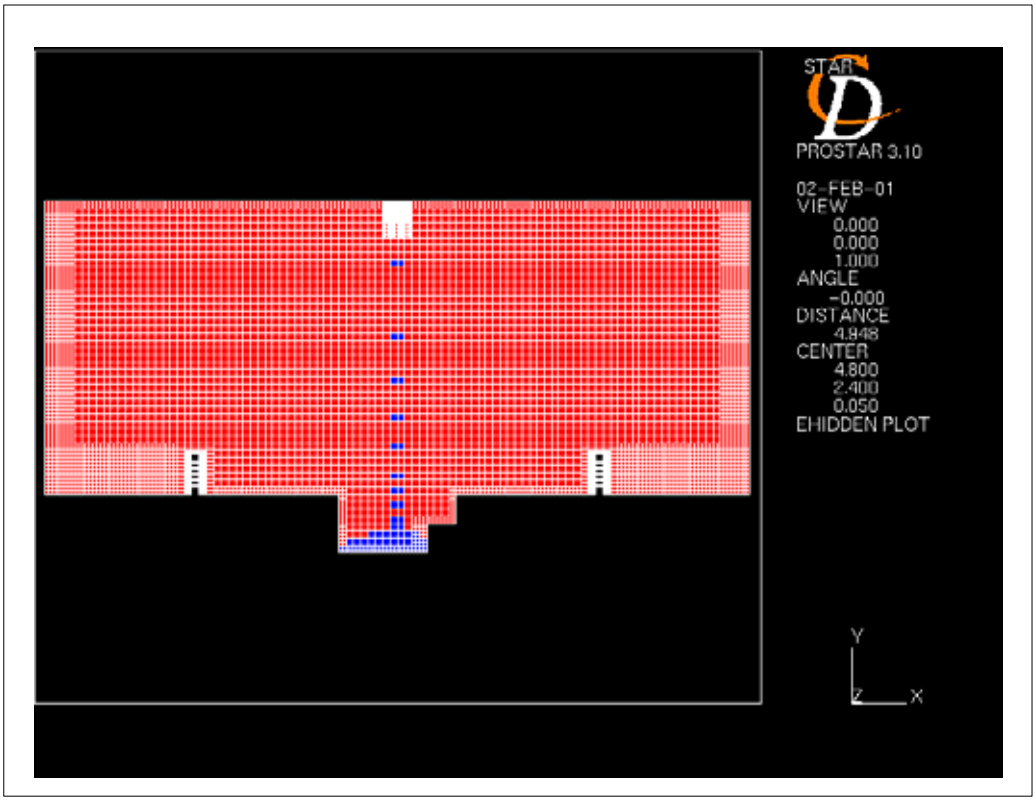

Figure 5.33 One-Phase Flow with Energy Sinks meshing and sinks distribution

These energy sinks are implemented via a user subroutine programmed in fortran, sorcen.f where we specify the quantity of heat in W/m^3 to be extracted from the room. To define the distribution of this sinks, we should define another type of fluid cells and then select them in the meshing.

The criteria used for the distribution of these sinks has to do with the ratio of volumes of the jet cone. This jet-cone is divided in three small ones of high equal to 1/3 of the total. Then we assign the quantity of energy to evacuate (the quantity of argon evaporating) proportionally to these volumes. We are assuming then that more evaporation is taking place in the pit of the room, which is certainly true, since pools of argon were forming.

The soren.f module was the following:

```
C***********************************************************************
      SUBROUTINE SORENT(S1P,S2P)
C     Source-term for enthalpy
C***********************************************************************
C-----------------------------------------------------------------------*
C     STAR RELEASE 3.100                                                *
C-----------------------------------------------------------------------*
      INCLUDE'comdb.inc'

      COMMON/USR001/INTFLG(100)

      INCLUDE'usrdat.inc'
      DIMENSION SCALAR(50)
      EQUIVALENCE(UDAT12(001), ICTID)
      EQUIVALENCE(UDAT03(001), CON)
      EQUIVALENCE(UDAT03(019), VOLP)
      EQUIVALENCE(UDAT04(001), CP)
      EQUIVALENCE(UDAT04(002), DEN)
      EQUIVALENCE(UDAT04(003), ED)
      EQUIVALENCE(UDAT04(004), HP)
      EQUIVALENCE(UDAT04(006), P)
      EQUIVALENCE(UDAT04(008), TE)
      EQUIVALENCE(UDAT04(009), SCALAR(01))
      EQUIVALENCE(UDAT04(059), U)
      EQUIVALENCE(UDAT04(060), V)
      EQUIVALENCE(UDAT04(061), W)
      EQUIVALENCE(UDAT04(062), VISM)
      EQUIVALENCE(UDAT04(063), VIST)
      EQUIVALENCE(UDAT04(007), T)
      EQUIVALENCE(UDAT04(067), X)
      EQUIVALENCE(UDAT04(068), Y)
      EQUIVALENCE(UDAT04(069), Z)
C-----------------------------------------------------------------------
C
C    This subroutine enables the user to specify a source term (per unit
C    volume) for enthalpy in linearized form:
C
C        Source = S1P-S2P*T, (W/m3)
C
C    in an arbitrary manner.
C    ** Parameters to be returned to STAR: S1P,S2P

C
C-----------------------------------------------------------------------
C
C     Sample coding: Fix temperature to the value of 300 K in solid
C                    No 3 (IMAT=-3)
C
C      IF(IMAT.EQ.-3) THEN
C        S1P=GREAT*300.
C        S2P=GREAT
C      ENDIF
C-----------------------------------------------------------------------
      IF(ICTID.EQ.4) THEN
         S1P=-1.0*W
         S2P=0.0
      ENDIF
      RETURN
      END
C
```

Results We refined the sensibility study that we had began with the Negative Flux Wall model, implementing now a ratio of 82% flash-evaporation and 18 % of liquid into the domain.

Here we present the results for a flow of 27,3 lLAr / min., so still Test 10. In the following figures we show experimental data, one-phase flow-ATLAS model and this new model with Energy Sinks. We present two groups of thermocouples, some close to the pit and some far from it.

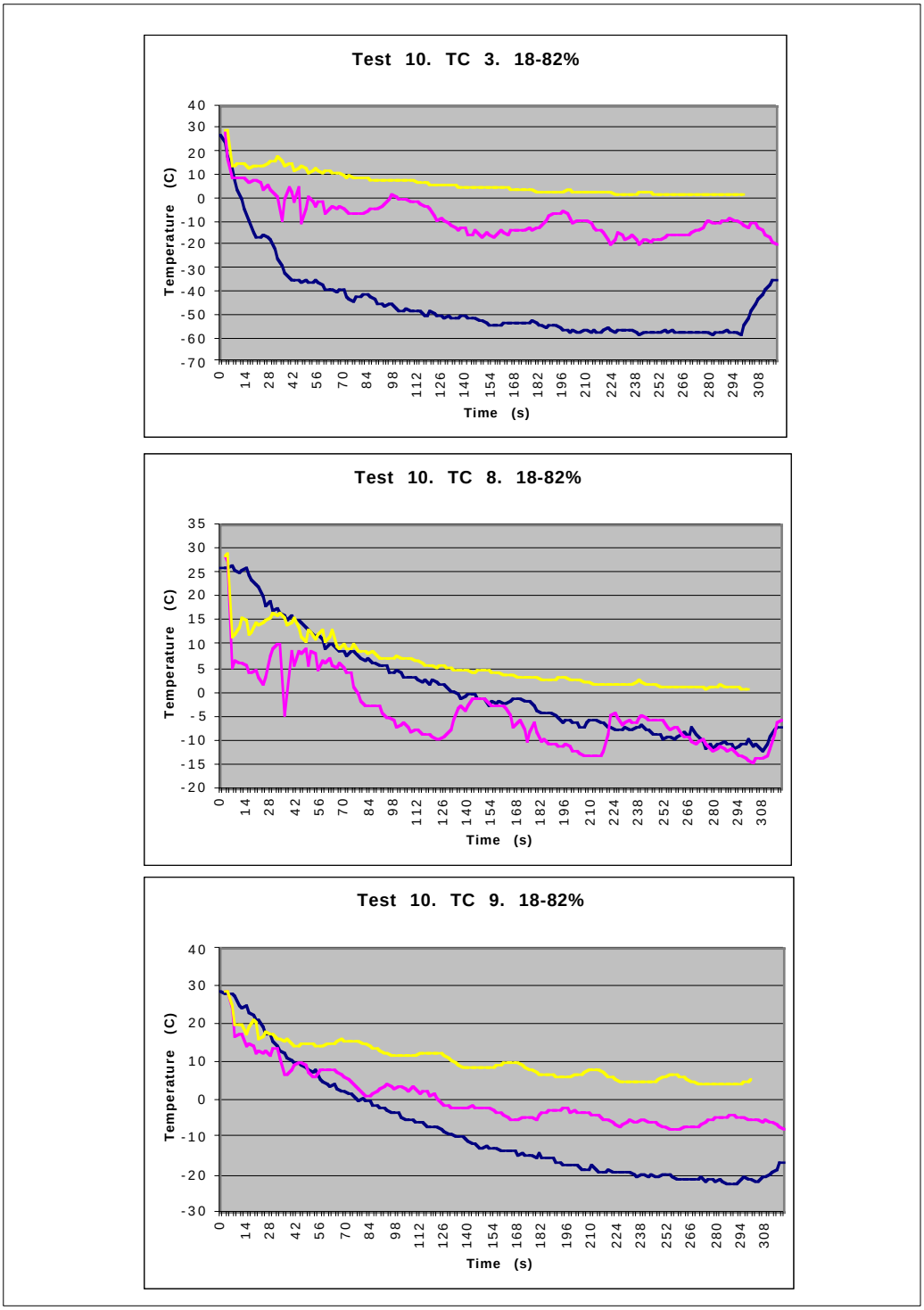

Figure 5.34 Evolution of Temperature.Thermocouples located far from the pit. Blue: experimental data; Pink:simulation One-Phase with Energy Sinks; Yellow: simulation One-Phase flow model

We observe how the new model is always improving the results. These thermocouples are all really close to the pit, and were the ones presenting more problems. Now we obtain acceptable results for TC 8 and TC9, improving on twenty degrees for the most complicated one, TC3, in the extraction grid.

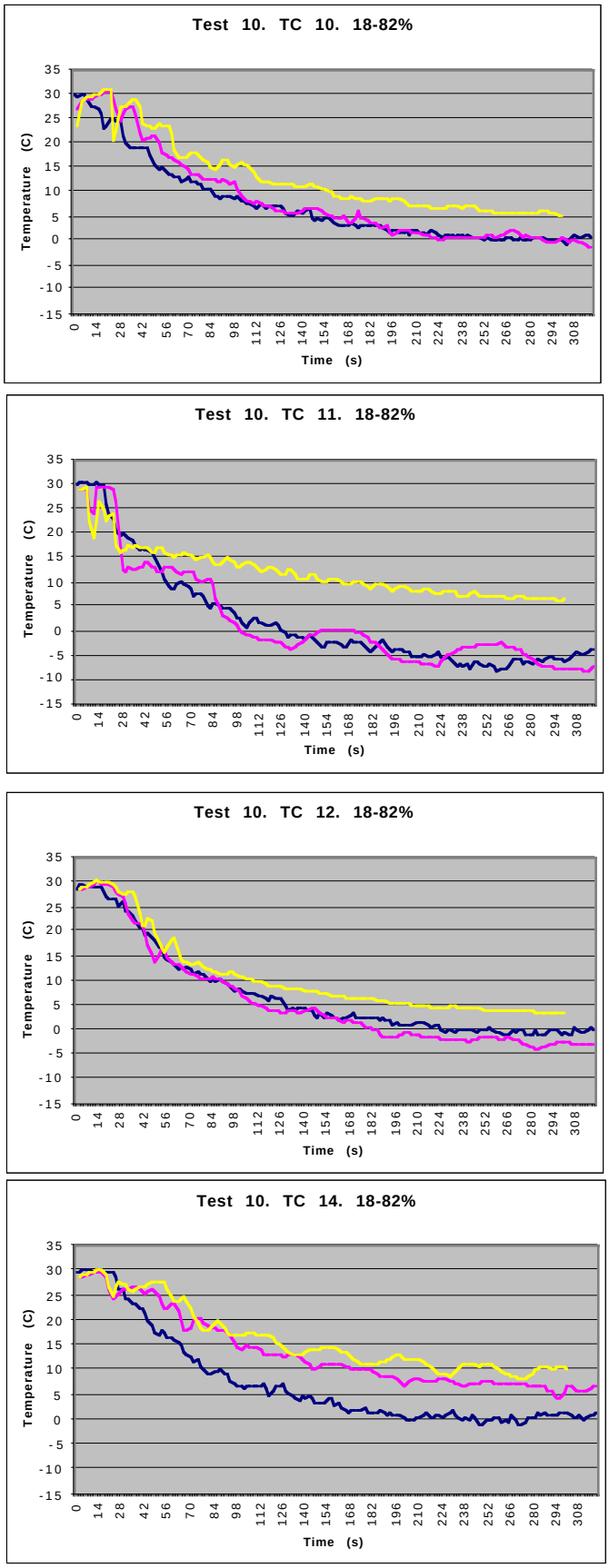

Figure 5.35 Evolution of Temperature.Thermocouples located far from the pit.Blue:experimental data; Pink: simulationOne-Phase with Energy Sinks; Yellow: simulation One-Phase flow model

In all the cases, the simulation with heat sinks is improving the predictions. The results are nearly coincident for some thermocouples, specially those far from the pit.

If we plot the results for all the thermocouples together, for Test 10, the outcome is the following:

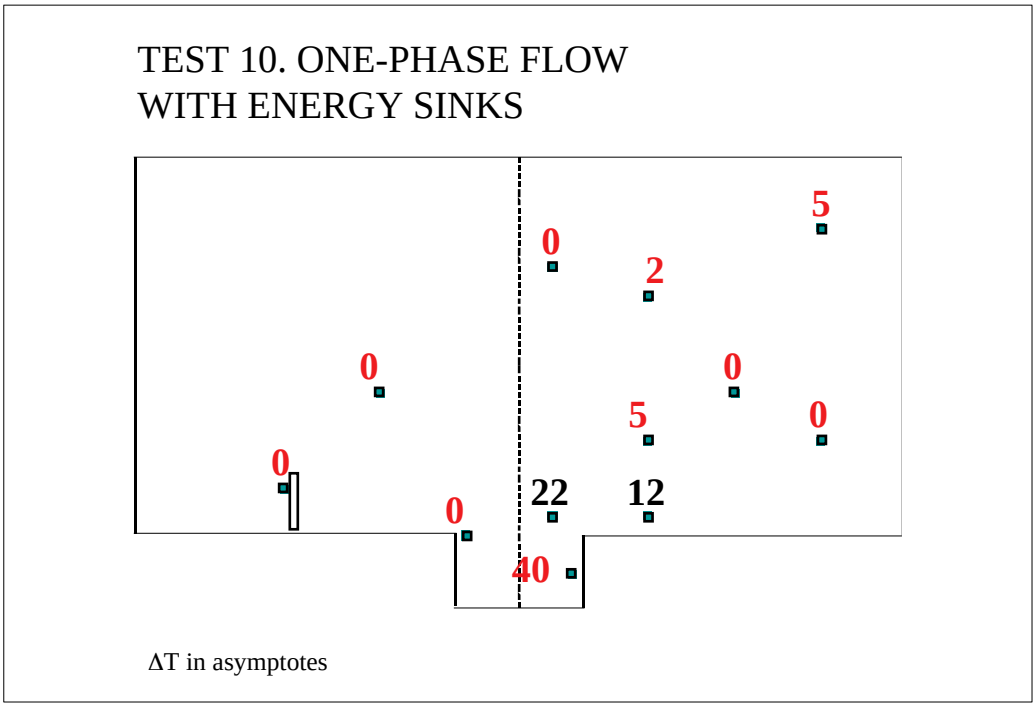

Figure 5.36 Test 10 One-Phase with Energy Sinks

We think that it is worth presenting all the results for the Test 8, 50 l LAr / s:

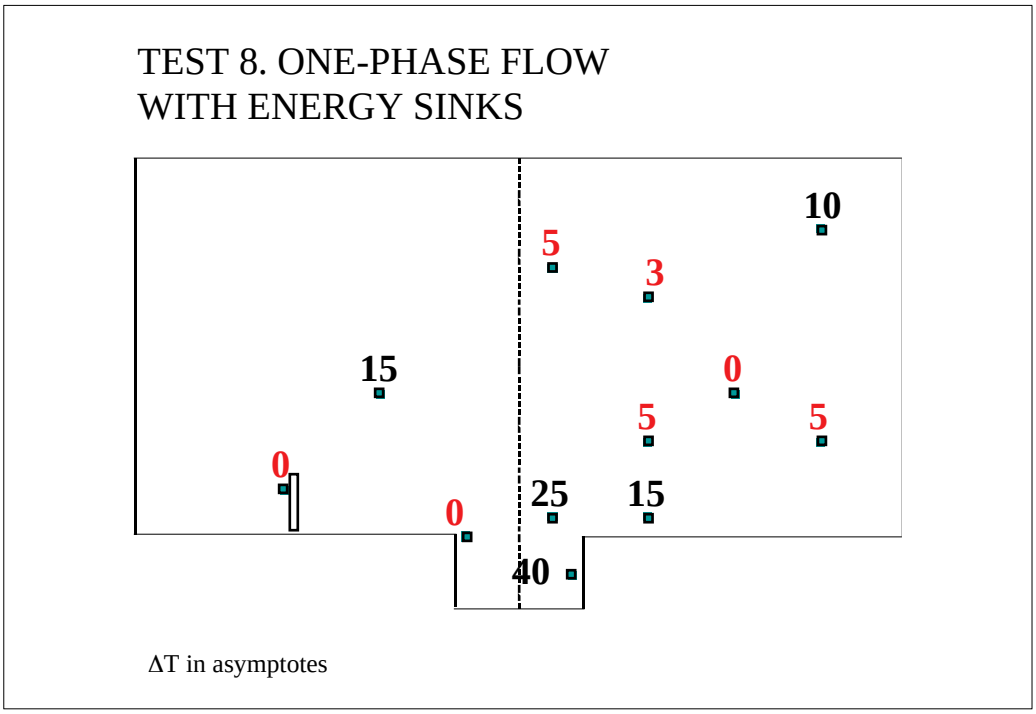

Figure 5.37 Test 8 One-Phase with Energy Sinks

This model has been implemented for nearly all the tests, always representing an improvement of the one-phase flow model. To see the results for all the Tests, please refer to Appendix B.

Conclusions

This model represents an improvement to the One-phase flow proposed for ATLAS.

As for the argon concentration distribution, we see how the curves remain the same for both models (with and without energy sinks); we could expect this, since the energy sinks are extracted straightly from the enthalpy equation. This is good, since the argon concentration was well predicted by the One-Phase model.

As for the temperature, this model is introducing a lot of improvement, reaching nearly coincident results for a lot of thermocouples. This is true for all the ranges of flows, even though we think the ratio of flash-evaporation should vary depending on the magnitude of the flow.

This model is not dynamic, but represents a good compromise between complexity-simplicity and accuracy in results.

5.6 Conclusions

The results showed that the simulated and experimental argon concentration distributions were very close, while for the simulated temperature distributions results were not very satisfactory. The experimental temperatures were always much lower than the ones calculated by the simulation. This, altogether with the fact that liquid argon was concentrating on the floor, lead us to think that we should modify the hypothesis of a one-phase flow and go for a two-phase model where the effects of the change of phase were taken into consideration.

At first, we tried to implement a new model with a combined input of droplets of liquid argon and gas argon (consequence of flash evaporation due to the pressure difference between the dewar and ambient), but finally we went for a one-phase flow with sinks of energy in order to simulate the latent heat of evaporation. This model is predicting very good results both for temperature and argon concentration distributions. However, there is a strong hypothesis that stands that the rate of flash-evaporation is around 85 %. This ratio is a critical factor, and is achieving good results for the whole range of flows that had been tested (4 l LAr / min. to 50 l LAr / min.).

This is the model that we implemented to study liquid argon spills in the ATLAS cavern, always being careful about the results and being aware of the weak points of the model.

Chapter 6

A New Model for ATLAS

In this chapter we present the results of implementing a one-phase flow model with sinks of energy for the ATLAS cryostat.

6.1 Goal

The goal of this chapter is to present some results of the implementation of the model proposed in the previous chapter, One-Phase flow with energy sinks, for the ATLAS cavern.

To begin with, we have implemented the *highest leak* we have used in the tests.

We have also implemented a liquid argon flow *similar* to an intermediate one of the tests. To establish the similarity we have taken into account the section dimensions of the room and the cavern, coming out a factor of 20.

Thirdly he have implemented an *extrapolation*, which would correspond to a 200 times this high flow.

Finally, we implemented a flow that in chapter 4 was defined as a critical accident in ATLAS, so as to determine the differences between the old and the new model.

6.2 Simulation results

The renormalized model for ATLAS has the same boundary conditions we have described in chapter 3, but now we introduce energy sinks distributed as shown in the following figure:

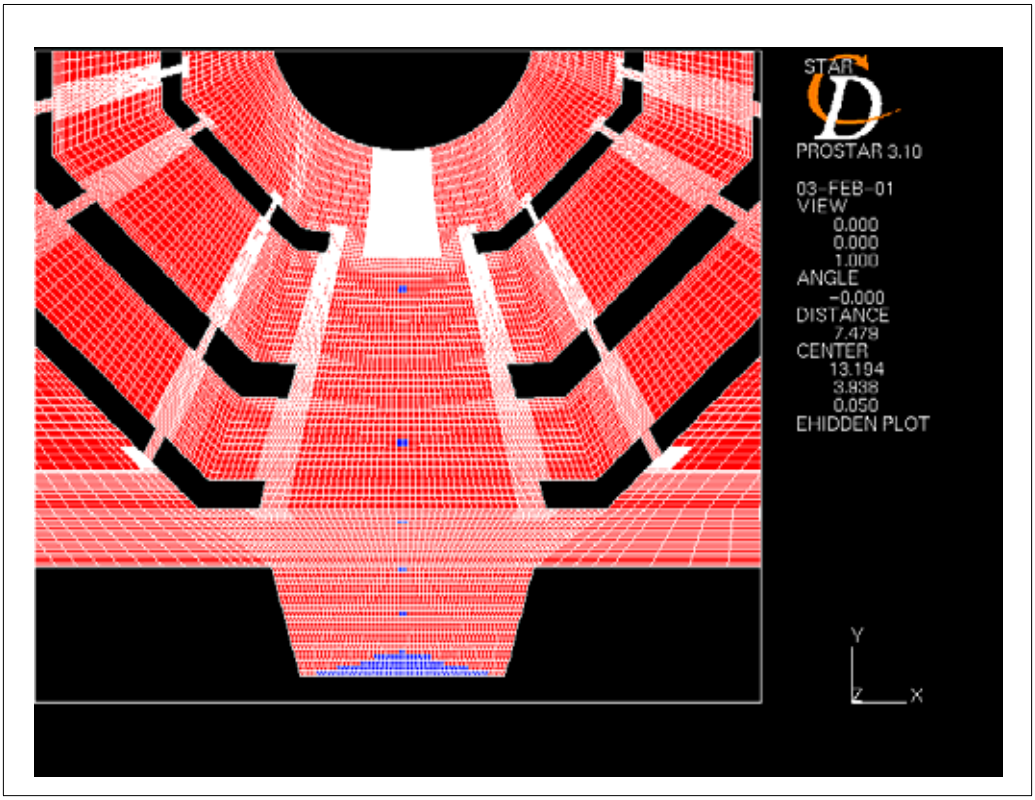

Figure 6.1 Energy sinks distribution in the renormalized ATLAS model

6.2.1 50 l LAr/min./0,834 l LAr/s

A flow of 50 l LAr / min. resulted to be catastrophic in the test room. We would like to know which consequences it would have for the ATLAS cavern.

The construction of the model is analogous to the methodology described in the previous chapters. A model with one-phase flow and a model with one-phase flow with sinks of energy have been simulated, for completeness.

One-Phase flow

This model, which considers the new specifications for ventilation and heat load, has an inlet of Argon characterised by the following parameters:

$v=0{,}2793257\ m/s$

$k=0{,}00117034\ m^2/s^2$

$\varepsilon=0{,}0036432\ m^2/s^3$

We show the results five minutes after the spill. As we see, this is a flow with nearly no consequences for the ATLAS cavern, both from the temperature and argon concentration point of view.

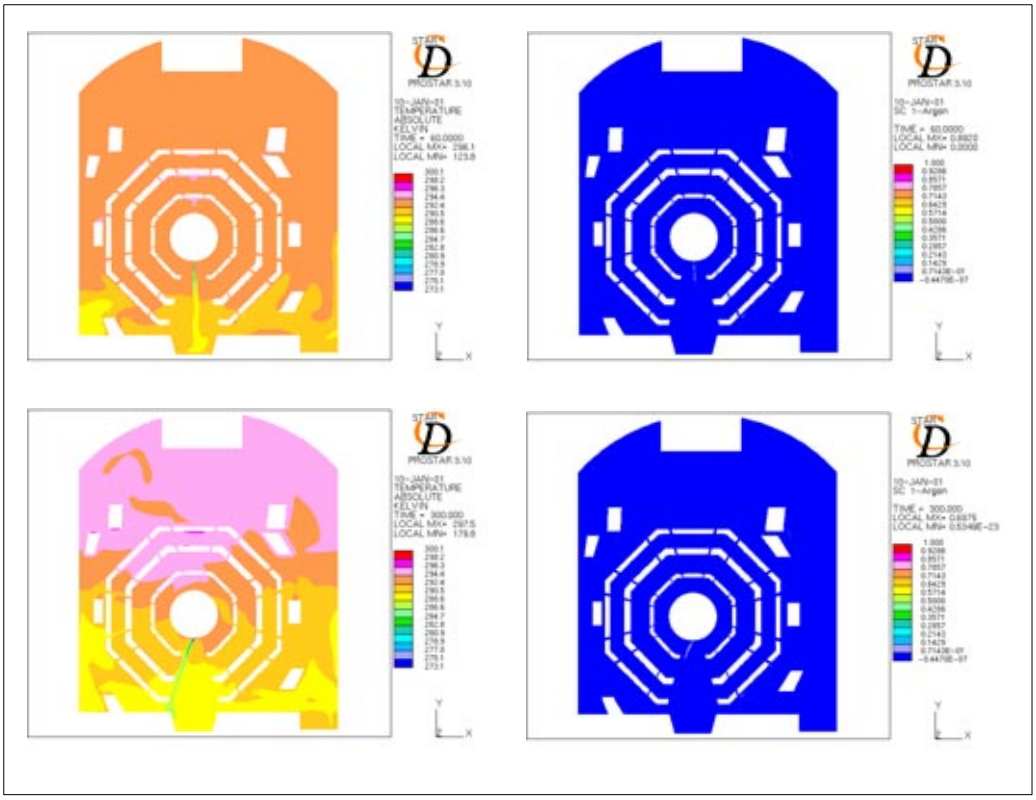

Figure 6.2 Temperature and Argon concentration distribution 1 and 5 minutes after the spill.

One-Phase flow with Energy Sinks

Taking into consideration that 82 % of the liquid is flash-evaporating, the latent heat of evaporation is of about 34 kW. Therefore, if we consider that these kW will be distributed within 140 cells of dimensions 0,07x0,112x45 m^3, then the heat sinks absorb 680 W / m^3.

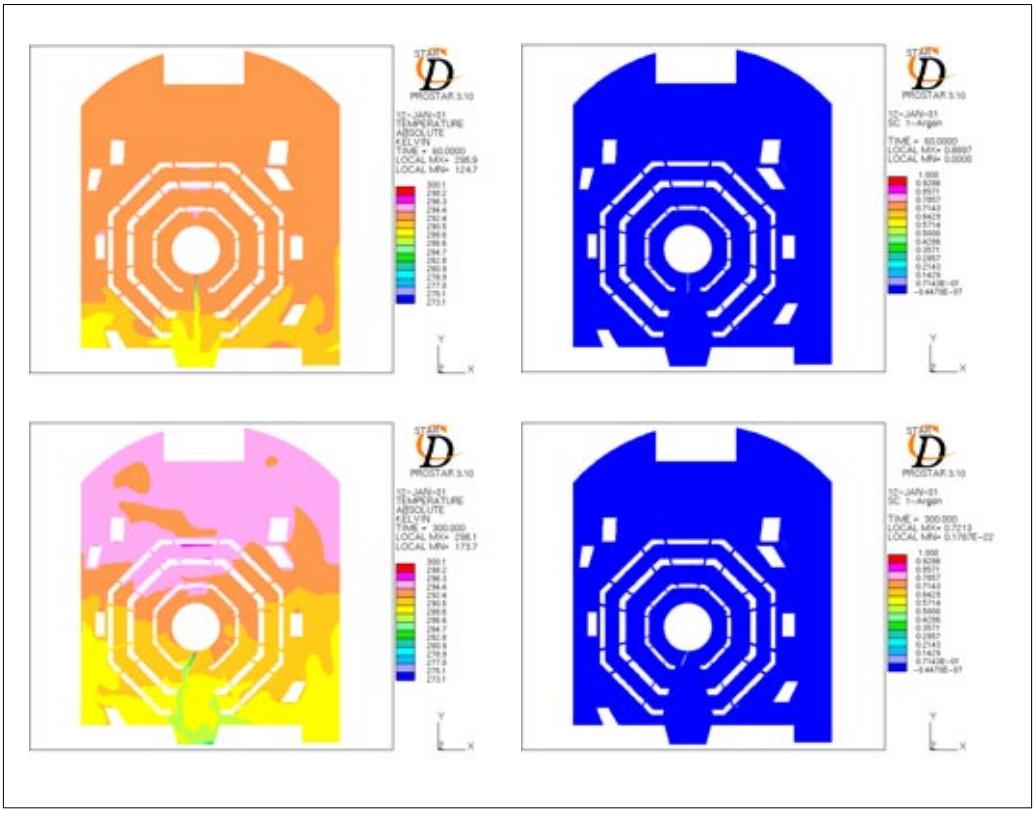

Figure 6.3 Temperature and argon concentration distributions 1 and 5 minutes after the spill

Even taking into account the change of phase, the temperatures reached are not dangerous. This kind of accident would allow workers to follow an evacuation plan without any problem. Besides, the mist cloud would be pretty small, since the temperatures are above the dew point of the air.

A flow which is catastrophic in the test room, has nearly no consequences in the ATLAS cavern.

6.2.2 9,3 l LAr/s

This flow represents a *similar* flow of the 27 l LAr / min. proposed in the experience. The similarity has been referred to the transversal dimensions of the chamber and ATLAS cavern. This ratio is of 20. Therefore we chose the closest flow we had already implemented for ATLAS, which is 9,3 l LAr / s, in order to have the one-phase flow simulation as a reference (Chapter 4).

Now we include the energy sinks. Considering the 82 % of flash-evaporation, the latent heat of evaporation of the liquid is about 375 kW. Distributing them in a similar way as before, the sinks of energy absorb 7.591 W / m^3.

The argon and the temperature distributions one and five minutes after the spill:

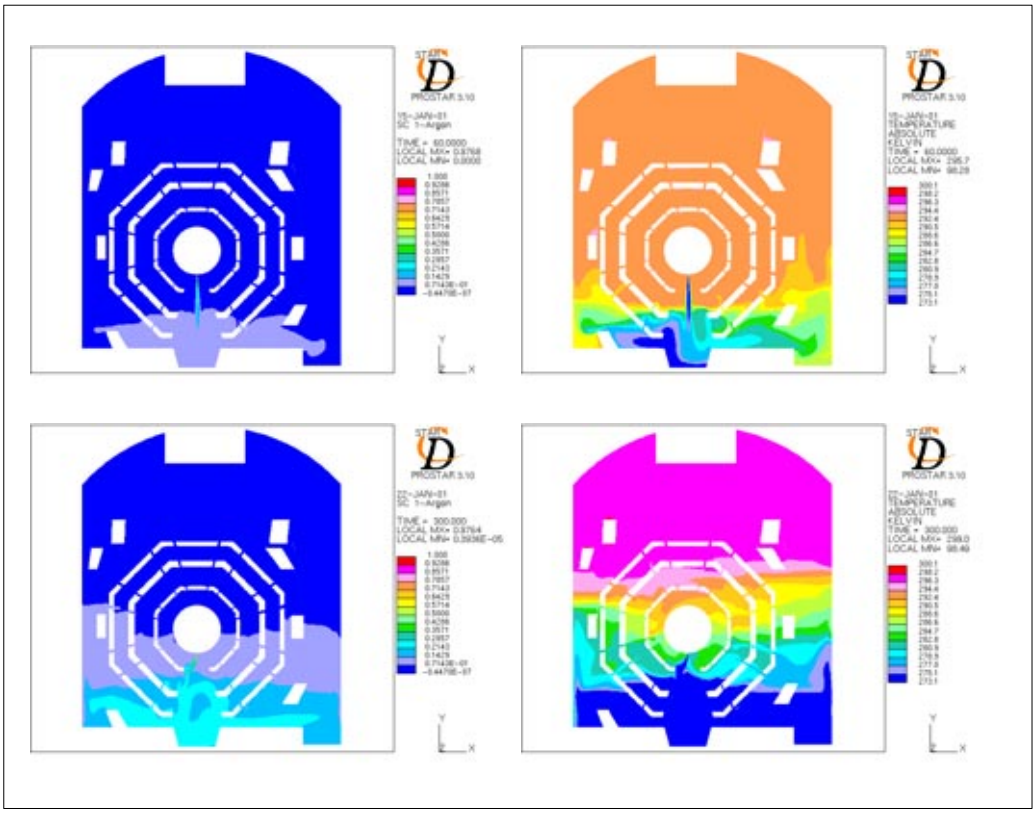

Figure 6.4 Argon concentration and Temperature distributions 1 and 5 minutes after the spill

This flow is far from being a catastrophic flow. People would escape easily during this kind of accident providing a good evacuation plan is defined.

6.2.3 17,46 l LAr/s

This flow, already shown in chapter two, was determining the limit of a critical flow, if we follow the criteria of considering non-critical a flow that does not reach dangerous argon concentrations or temperature within a reasonable time to evacuate the cavern. This was interesting to compare the results of the new model with energy sinks for this flow.

The sinks of energy were in this case of 14.251 W / m^3, and they are calculated the same way as we did before.

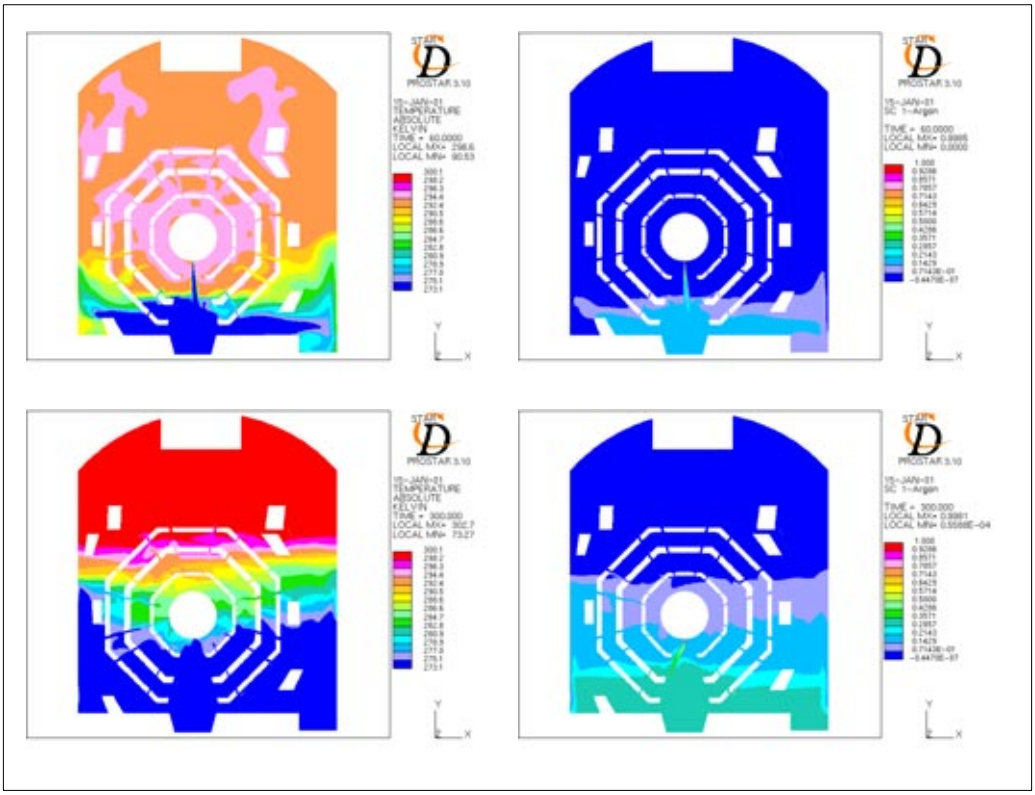

Figure 6.5 Temperature and Argon concentration distributions 1 and 5 minutes after the spill.

If we take a look again at the first results we obtained for the temperature distributions, and we compare them with the new ones (see figure in the following page), we see that the temperature has changed significantly.

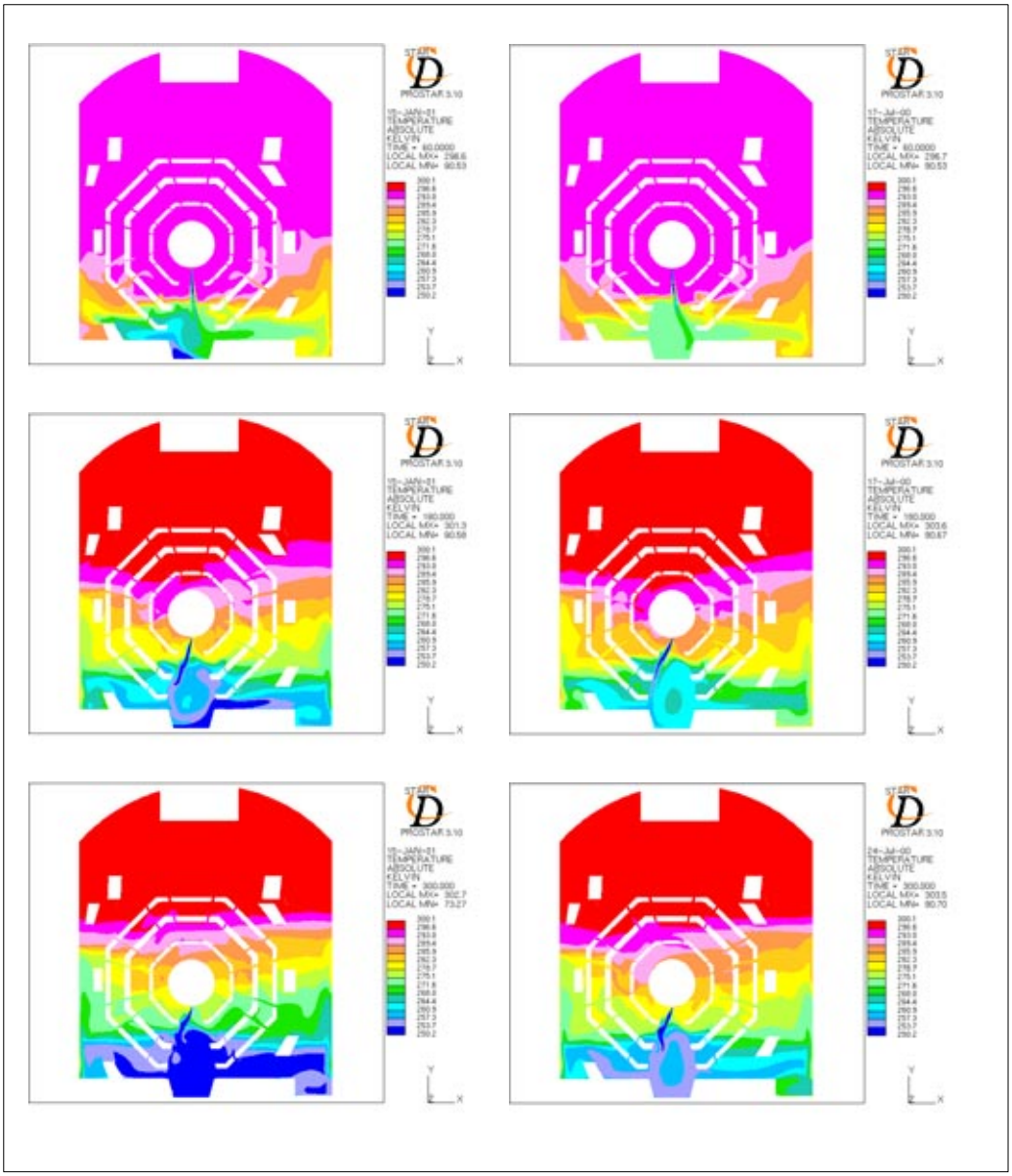

Figure 6.6 Temperature distribution comparison between one-phase flow with energy sinks (left) and one-phase flow model (right)

6.2.4 69,34 l LAr/s

In absolute values, this flow is 200 times bigger than an intermediate flow used in the tests. We can intuitively foresee this is an enormous flow. In this case, the energy sinks absorb 56.598 W/m^3.

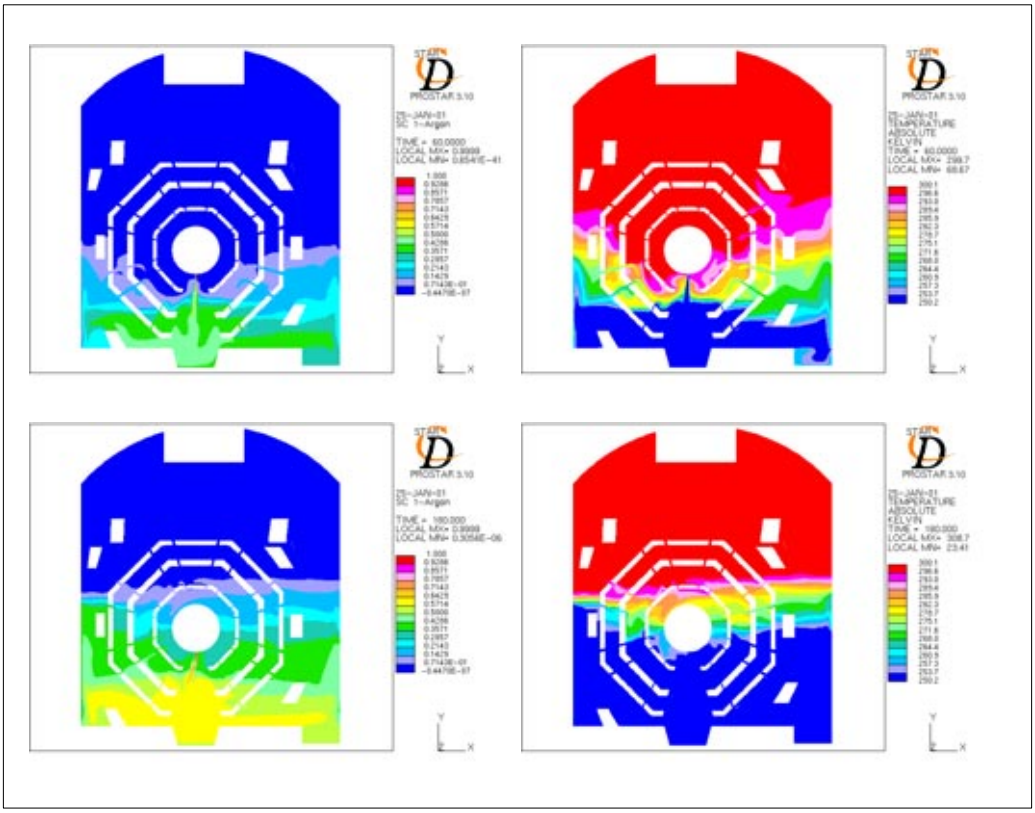

Figure 6.7 Argon concentration and Temperature distributions 1 and 3 minutes after the spill

This flow has catastrophic consequences, both from argon and temperature point of view.

6.3 Conclusions

As expected, the renormalization of the ATLAS model has very significant influence on the temperature distribution. The argon concentration remains the same as for the One-Phase flow model, which gave good predictions for argon, as demonstrated with the test.

The temperature distributions for the Two-Phase flow model show lower temperatures than for the One-Phase model. Even though these temperatures are very accurate in most locations, we have to be careful when it comes to interpreting the results in the retention pit.

The most important learnings from all these last simulations is that a flow which is catastrophic in the test room, has almost no consequences in the ATLAS cavern. Even five minutes after the accident, the temperatures are above 0 ^{o}C and above the dew point of the air, which means that no mist would prevent people from escaping.

A spill of 10 l LAr / s. corresponding to a *similar* flow to the 50 l LAr / min. in the ATLAS cavern (ratio of 20 between the cross sections) is far from being a catastrophic flow. People would escape easily during this kind of accident provided a good evacuation plan is defined.

During the experiment, we intuitively acquired the certitude that a catastrophic flow in the ATLAS cavern such as the one proposed as consequence of a rupture of a feedthrough is not realistic.

Chapter 7

Conclusions

The simulation of liquid argon spills in the ATLAS cavern allowed us to evaluate how much time people have to escape before the concentration of argon or room temperature creates a real risk of asphyxia or hypothermia. This is a crucial factor in the design of a good evacuation plan.

Our first studies were oriented towards a sensitivity on the flow, in order to analyze the consequences of intermediate flows. We wanted to determine what would be a *critical* flow, defining it as the biggest leak that would enable people to escape from the ground area following a safety evacuation plan that could not last more than two minutes. This happened at a flow of 18 l LAr / s. Bigger spills than this critical one would quickly create dangerous conditions, preventing people from escaping without dangerous injury. On the other hand, flows below 4 l LAr / s. are nearly absorbed by the pit ventilation.

A sensitivity study on the main elements of the model was also carried out. We wanted to define which were the elements of the model that really influenced argon concentration and temperature distributions. Firstly, we demonstrated that neither a variation in the ventilation flow rate nor the heat load significantly influenced the temperature or argon concentration distribution. Secondly, the hypothesis of an isothermal wall is not critical. This study also demonstrated how accurate the High-Reynolds model is, even though the mesh is too refined near some walls (where we could, possibly, implement a Low-Reynolds model). As for the spatial differencing schemes, the UD spatial differencing for speed, temperature and turbulence parameters is an appropriate and stable scheme.

Since all the previous simulations had been carried out for closed detector geometry and we know that the regular maintenance of the detector, as well as shorter accesses, will be done with the detector opened (long and short opening scenarios respectively), we found it necessary to recreate liquid argon spill accidents within this geometry. This implies the removal of the bottom muon chambers. This configuration of the detector does not disturb the flow motion towards the pit and therefore absorption by the pit extraction system is favorable in comparison to the closed detector scenario. This is especially relevant for small leaks. In an open detector scenario the argon pit plays an important role in preventing the argon from spreading.

However, all these results depend on the model's reliability. In order to validate these results, we carried out an experiment with various liquid argon spills.

This series of 11 tests (some of them were filmed) provided us with a large amount of valuable data and also allowed us to gain insight into the behavior of liquid argon when it is released from a pressurized dewar into ambient conditions. Since we tested a wide range of flows, we could see the results for both catastrophic and very small leaks.

We observed how quickly the mist spread into the room and we noticed how the surroundings of the inlet diffusers remained clear of this mist and pushed the argon cloud into the center, confining it to the pit. This was also observed afterwards in the simulations. This means that in the case of an accident asphyxiation could be prevented, if people stay near the diffusers.

Also in relation to ventilation, we could see how effective it was in evacuating the argon once the spill was over. Even though the quantity of argon did not reach the normal levels so quickly, the cloud of mist disappeared quite fast (even for huge flows).

We could hear the liquid argon rain falling and, after the cloud of mist had disappeared, we observed white traces on the isolation, proof of the formation of a small pool of liquid argon that did not instantaneously evaporate. This pointed to the existence of a two-phase flow, even though there was certainly a large amount of liquid that had evaporated in the dewar valve and pipeline (flash-evaporation).

The results of the test analysis showed that the simulated and experimental argon concentration distributions were very close, while for the simulated temperature distributions, results were not very satisfactory. The experimental temperatures were always much lower than the ones calculated by the simulation. This, together with the fact that the liquid argon was concentrated on the floor, led us to believe that we should modify the hypothesis of a one-phase flow and go for a two-phase model where the effects of the change of phase were taken into account.

Firstly, we tried to implement a new model with a combined input of liquid argon droplets and argon gas (the consequence of flash evaporation due to the pressure difference between the dewar and ambient), but finally we went for a one-phase flow with sinks of energy in order to simulate the latent heat of evaporation. This model predicted very good results for both temperature and argon concentration distributions. However, there is a strong hypothesis that the rate of flash-evaporation is around 85 %. This ratio is a critical factor and has achieved good results for the whole range of flows that have been tested (4 l LAr / min. to 50 l LAr / min.).

This is the model we implemented to study liquid argon spills in the ATLAS cavern, always being wary of the results and being aware of the model's weak points.

As expected, the renormalization of the ATLAS model had a very significant influence on temperature distribution. The argon concentration remains the same as in the One-Phase flow model, which gave good predictions for argon, as demonstrated by the test.

The temperature distributions for the Two-Phase flow model showed lower temperatures than for the One-Phase model. Even though these temperatures are

very accurate in most locations, we have to be careful when it comes to interpreting the results in the retention pit.

The most important lessons from these latest simulations is that a flow which is catastrophic in the test room has almost no consequences in the ATLAS cavern. Even five minutes after the accident, temperature was above 0 ^{o}C and above the dew point of air, which means there would be no mist to prevent people from escaping.

A spill of 10 l LAr / s. corresponding to a *similar* flow to the 50 l LAr / min. in the ATLAS cavern (ratio of 20 between the cross sections) is far from being a catastrophic flow. People could escape easily during this kind of accident, providing a good evacuation plan has been defined.

During the experiment, we became certain that a catastrophic flow in the ATLAS cavern, such as the one proposed following a rupture of a feedthrough, is not realistic.

The problem of mist seems to be more relevant than hypothermia or asphixia. Finally, we are facing a problem similar to a fire; it is not the high temperatures but the smoke, which should determine an evacuation plan.

Developing good models with Computed Fluid Dynamics codes requires a lot of experience as well as evolving a good sense of intuition. It is also time-consuming. A project like this one meant implementing 40 different models, about 35 GB of data and a total simulation time of aproximately 4 h , which represents a computational time of 12.000 h, 500 days.

Appendix A

ATLAS Models Figures

In this Appendix we collect all the evolution within time of temperature and argon concentrations for all the models described in chapter 4.

A.1 ATLAS models

A.1.1 184,43 l LAr/s. Open detector scenario

Q	**184,43 l LAr/s**				
Geometry	**Open detector scenario**				
Ventilation & Heat Load	**Old Specifications**				
Energy Sinks	**Non**				
Boundaries	*v (m/s)*	*k (m^2/s^2)*	*ε (m^2/s^3)*	*T (K)*	*ρ (kg/m^3)*
Argon Inlet	8,157	0,998	12,6	90	5,507
Exhaust fan	0,059	$5{,}364\ 10^{-5}$	$6{,}949\ 10^{-8}$	295	1,2
Left diffusor	0,138	$2{,}893\ 10^{-4}$	$4{,}044\ 10^{-6}$	290	1,2
Right top diffusor	0,083	1,016 10-4	7,012 10-7	290	1,2
Right bottom diffusor	0,138	$2{,}893\ 10^{-4}$	$4{,}044\ 10^{-6}$	290	1,2
Central pit extractor	0,167	$4{,}214\ 10^{-4}$	$1{,}527\ 10^{-5}$	295	1,2
Right pit extractor	0,046	$3{,}186\ 10^{-5}$	$3{,}284\ 10^{-7}$	295	1,2
Pit	292,5 K Isothermal				
Racks	3,7134 W / m^2 Constant heat flux				
Muon chambers	16,56 W / m^2 Constant heat flux				
Walls	292,5 K Isothermal				
Turbulence Model	K - E / R N G				
Differential schemes	*u,v*	*KE*	*ε*	*T*	*ρ*
Time	F u l l y I m p l i c i t				
Space	UD	UD	UD	UD	CD 0,8
Control					
Piso Correctors	5 to 9				
Max. COU number	78 to 90				
Mean COU number	1,7 to 2				
HDIFF	1 to 20 W				
Residual tolerance	0,01 for u,v,T,KE,ε,ρ / 0,001 for P				
Under-relaxation for P	0,8				
Precision	Double				
Simulated time	1 minute				
Folder	MODELO 6 / Alpha				

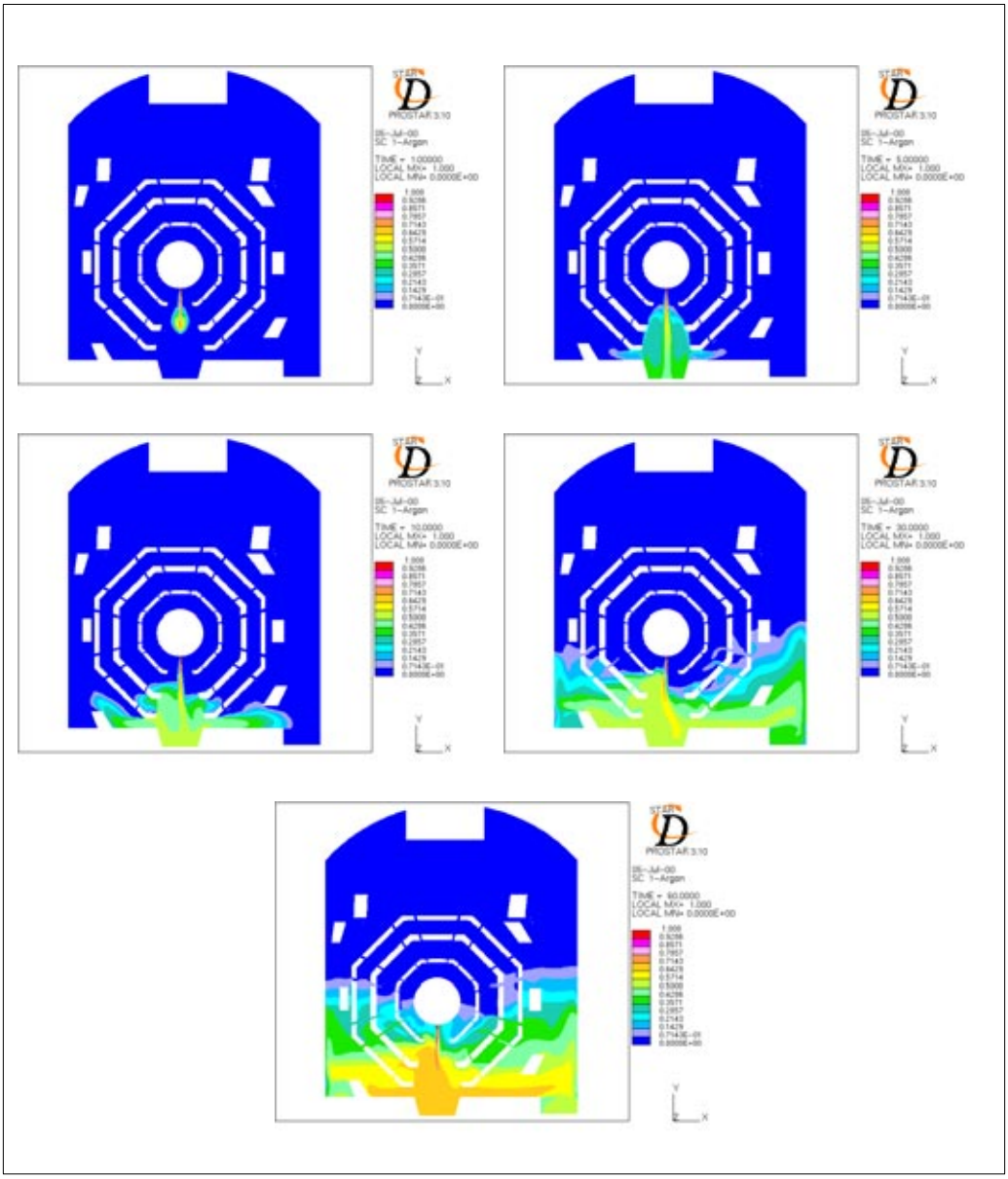

Figure A.1 Argon concentration 1,5,10,30,60 s after the spill

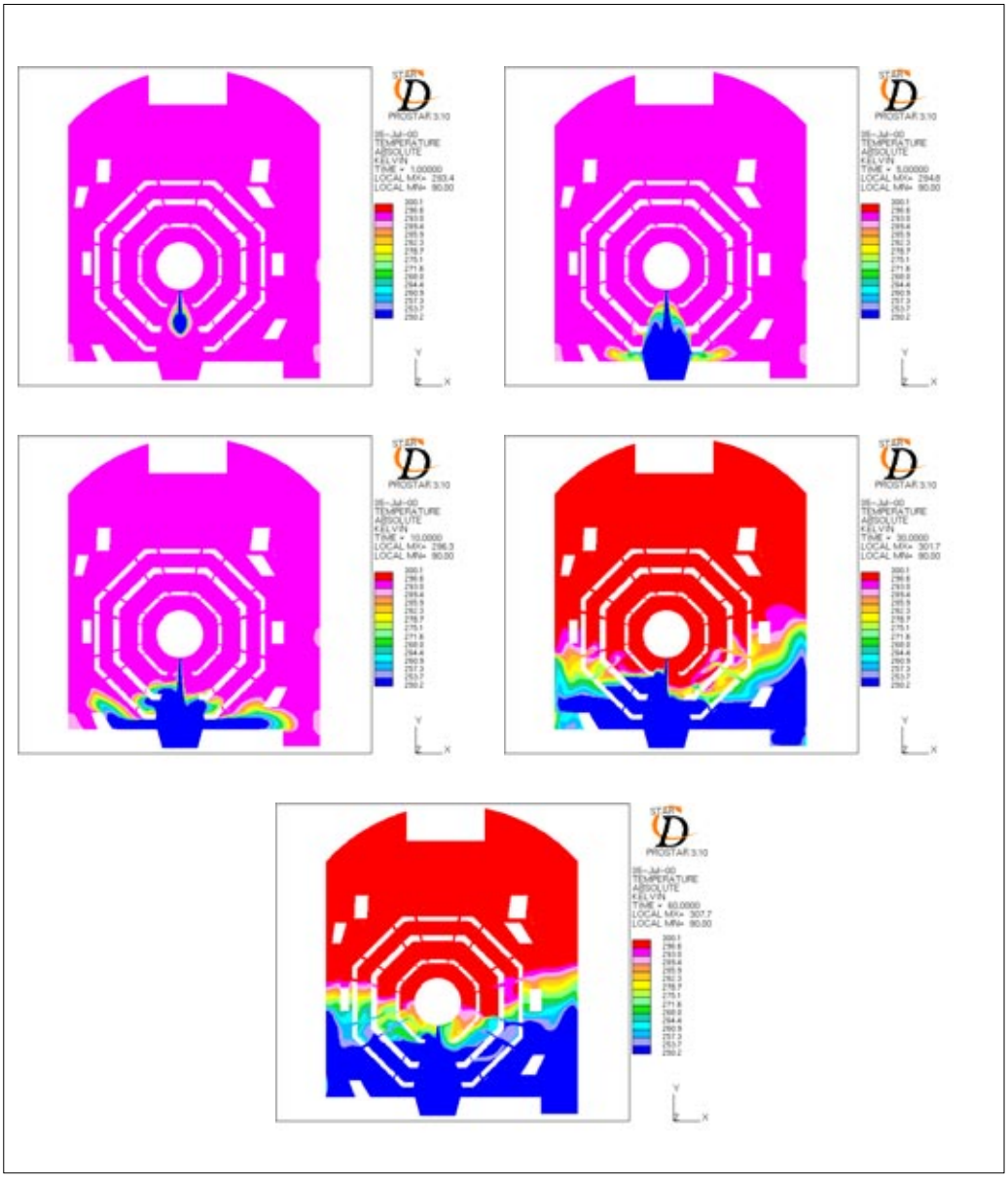

Figure A.2 Temperature distribution 1,5,10,30,60 s after the spill

A.1.2 69,34 l LAr/s. Open scenario geometry

Q	**69,34 l LAr/s**				
Geometry	**Open detector scenario**				
Ventilation & Heat Load	**New Specifications**				
Energy Sinks	**Non**				
Boundaries	*v (m/s)*	*k (m^2/s^2)*	*ε (m^2/s^3)*	*T (K)*	*ρ (kg/m^3)*
Argon Inlet	5,0	0,375	4,537	90	5,337
Exhaust fan	0,079	$9{,}53\ 10^{-5}$	$1{,}57\ 10^{-7}$	297	1,2
Left diffusor	0,185	$5{,}14\ 10^{-4}$	$9{,}18\ 10^{-6}$	290	1,2
Right top diffusor	0,082	$1{,}01\ 10^{-4}$	$7{,}01\ 10^{-7}$	290	1,2
Right bottom diffusor	0,185	$5{,}14\ 10^{-4}$	$9{,}18\ 10^{-6}$	290	1,2
Central pit extractor	0,167	$4{,}21\ 10^{-4}$	$1{,}52\ 10^{-5}$	297	1,2
Right pit extractor	0,046	$3{,}18\ 10^{-5}$	$3{,}28\ 10^{-7}$	297	1,2
Pit	293,6 K Isothermal				
Racks	6,34 W / m^2 Constant heat flux				
Muon chambers	29,78 W / m^2 Constant heat flux				
Walls	293,6 K Isothermal				
Turbulence Model	K - E / R N G				
Differential schemes	*u,v*	*KE*	*ε*	*T*	*ρ*
Time	Fully Implicit				
Space	UD	UD	UD	UD	CD 0,8
Control					
Piso Correctors	4 to 12				
Max. COU number	18 to 77				
Mean COU number	0,2 to 1,7				
HDIFF	0,2 to 11 W				
Residual tolerance	0,01 for u,v,T,KE,ε,ρ / 0,001 for P				
Under-relaxation for P	0,8				
Precision	Double				
Simulated time	5,5 minutes				
Folder	MODELO 9 / Alpha				

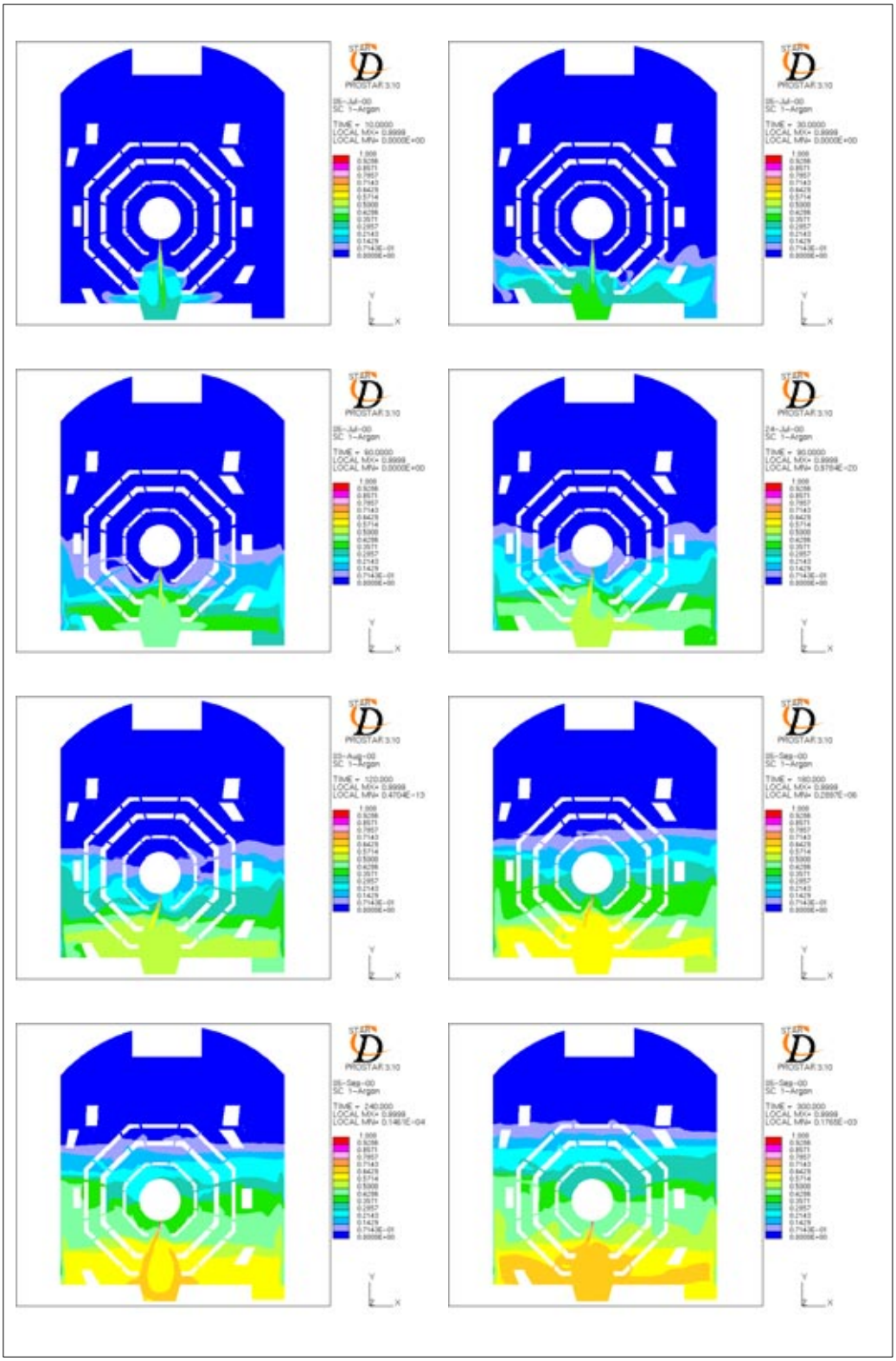

Figure A.3 Argon concentration after 10,30,60,90,120,180,240,300 s after the spill

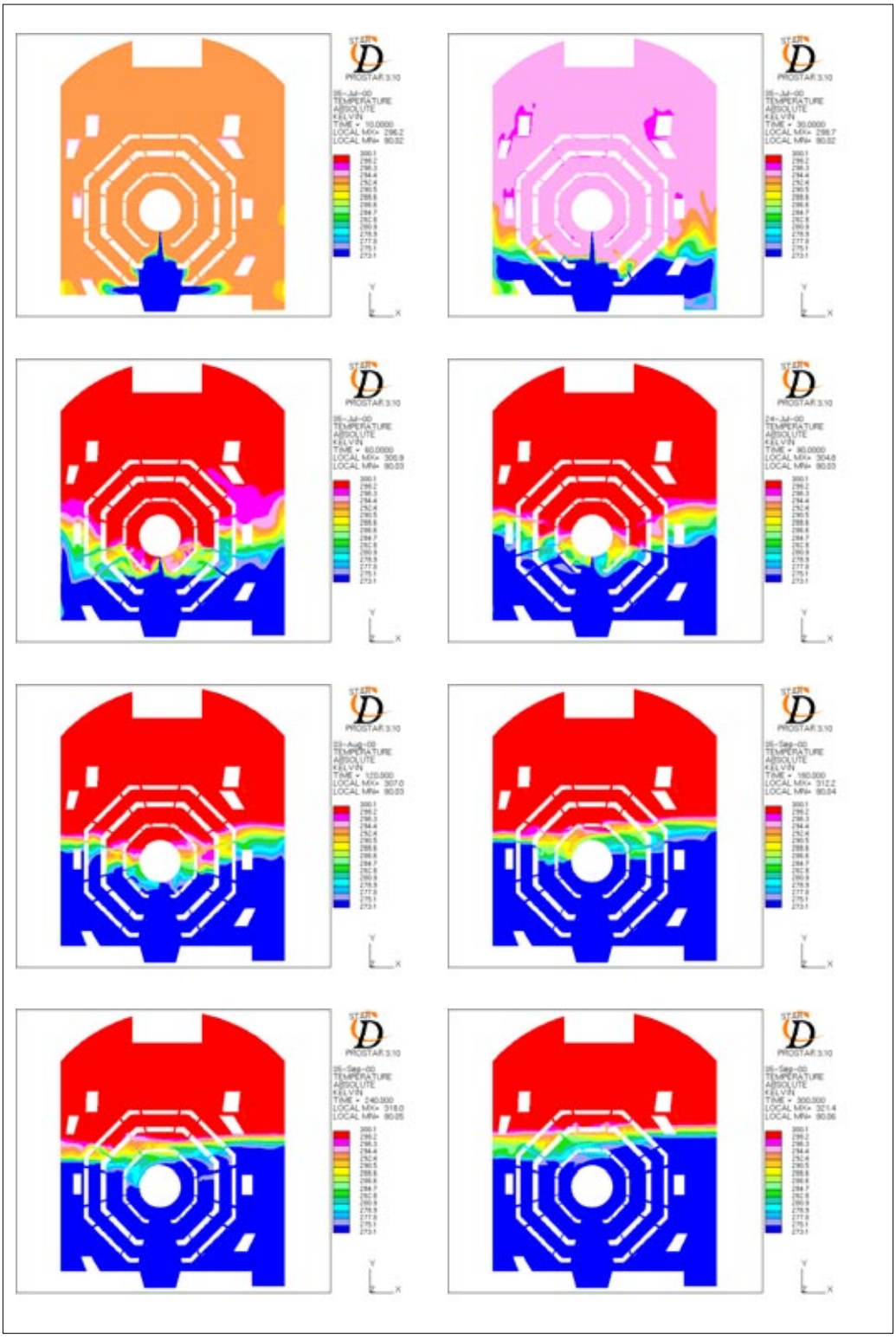

Figure A.4 Temperature distribution 10,30,60,90,120,180,240,300 s after the spill

A.1.3 26,08 l LAr/s. Open scenario geometry

Q	**26,08 l LAr/s**				
Geometry	**Open detector scenario**				
Ventilation & Heat Load	**Old Specifications**				
Energy Sinks	**Non**				
Boundaries	*v (m/s)*	*k (m^2/s^2)*	*ε (m^2/s^3)*	*T (K)*	*ρ (kg/m^3)*
Argon Inlet	3,0	0,135	1,562	90	5,507
Exhaust fan	0,059	$5{,}364\ 10^{-5}$	$6{,}949\ 10^{-8}$	295	1,2
Left diffusor	0,138	$2{,}893\ 10^{-4}$	$4{,}044\ 10^{-6}$	290	1,2
Right top diffusor	0,083	1,016 10-4	7,012 10-7	290	1,2
Right bottom diffusor	0,138	$2{,}893\ 10^{-4}$	$4{,}044\ 10^{-6}$	290	1,2
Central pit extractor	0,167	$4{,}214\ 10^{-4}$	$1{,}527\ 10^{-5}$	295	1,2
Right pit extractor	0,046	$3{,}186\ 10^{-5}$	$3{,}284\ 10^{-7}$	295	1,2
Pit	292,5 K Isothermal				
Racks	3,7134 W / m^2 Constant heat flux				
Muon chambers	16,56 W / m^2 Constant heat flux				
Walls	292,5 K Isothermal				
Turbulence Model	K - E / R N G				
Differential schemes	*u,v*	*KE*	*ε*	*T*	*ρ*
Time	F u l l y I m p l i c i t				
Space	UD	UD	UD	UD	CD 0,8
Control					
Piso Correctors	4 to 7				
Max. COU number	39 to 55				
Mean COU number	0,6 to 0,9				
HDIFF	1 to 2 W				
Residual tolerance	0,01 for u,v,T,KE,ε,ρ / 0,001 for P				
Under-relaxation for P	0,8				
Precision	Double				
Simulated time	2 minutes				
Folder	MODELO 11 / Alpha				

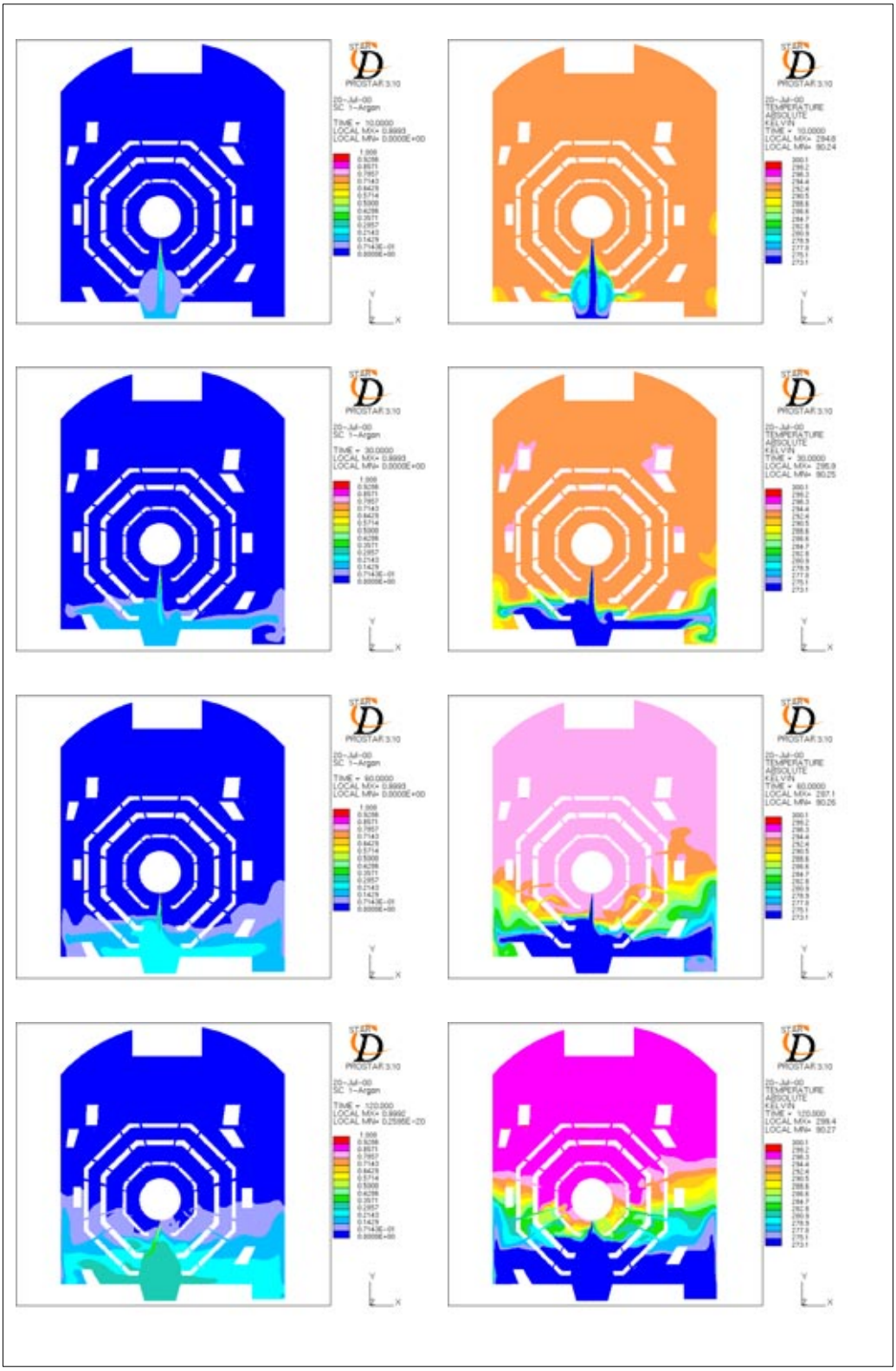

Figure A.5 Argon concentration and temperature distribution 10,30,60 and 120 s after the spill

A.1.4 17,46 l LAr/s. Open detector scenario

Q	**17,46 l LAr/s**				
Geometry	**Open detector scenario**				
Ventilation & Heat Load	**New Specifications**				
Energy Sinks	**Non**				
Boundaries	*v (m/s)*	*k (m^2/s^2)*	*ε (m^2/s^3)*	*T (K)*	*ρ (kg/m^3)*
Argon Inlet	2,5	0,0937	1,129	90	5,337
Exhaust fan	0,079	$9{,}53\ 10^{-5}$	$1{,}57\ 10^{-7}$	297	1,2
Left diffusor	0,185	$5{,}14\ 10^{-4}$	$9{,}18\ 10^{-6}$	290	1,2
Right top diffusor	0,082	$1{,}01\ 10^{-4}$	$7{,}01\ 10^{-7}$	290	1,2
Right bottom diffusor	0,185	$5{,}14\ 10^{-4}$	$9{,}18\ 10^{-6}$	290	1,2
Central pit extractor	0,167	$4{,}21\ 10^{-4}$	$1{,}52\ 10^{-5}$	297	1,2
Right pit extractor	0,046	$3{,}18\ 10^{-5}$	$3{,}28\ 10^{-7}$	297	1,2
Pit	293,6 K Isothermal				
Racks	6,34 W / m^2 Constant heat flux				
Muon chambers	29,78 W / m^2 Constant heat flux				
Walls	293,6 K Isothermal				
Turbulence Model	K - E / R N G				
Differential schemes	*u,v*	*KE*	*ε*	*T*	*ρ*
Time	F u l l y I m p l i c i t				
Space	UD	UD	UD	UD	CD 0,8
Control					
Piso Correctors	4 to 7				
Max. COU number	10 to 65				
Mean COU number	0,1 to 0,7				
HDIFF	0,2 to 4,8 W				
Residual tolerance	0,01 for u,v,T,KE,ε,ρ / 0,001 for P				
Under-relaxation for P	0,8				
Precision	Double				
Simulated time	10 minutes				
Folder	MODELO 12 / Alpha				

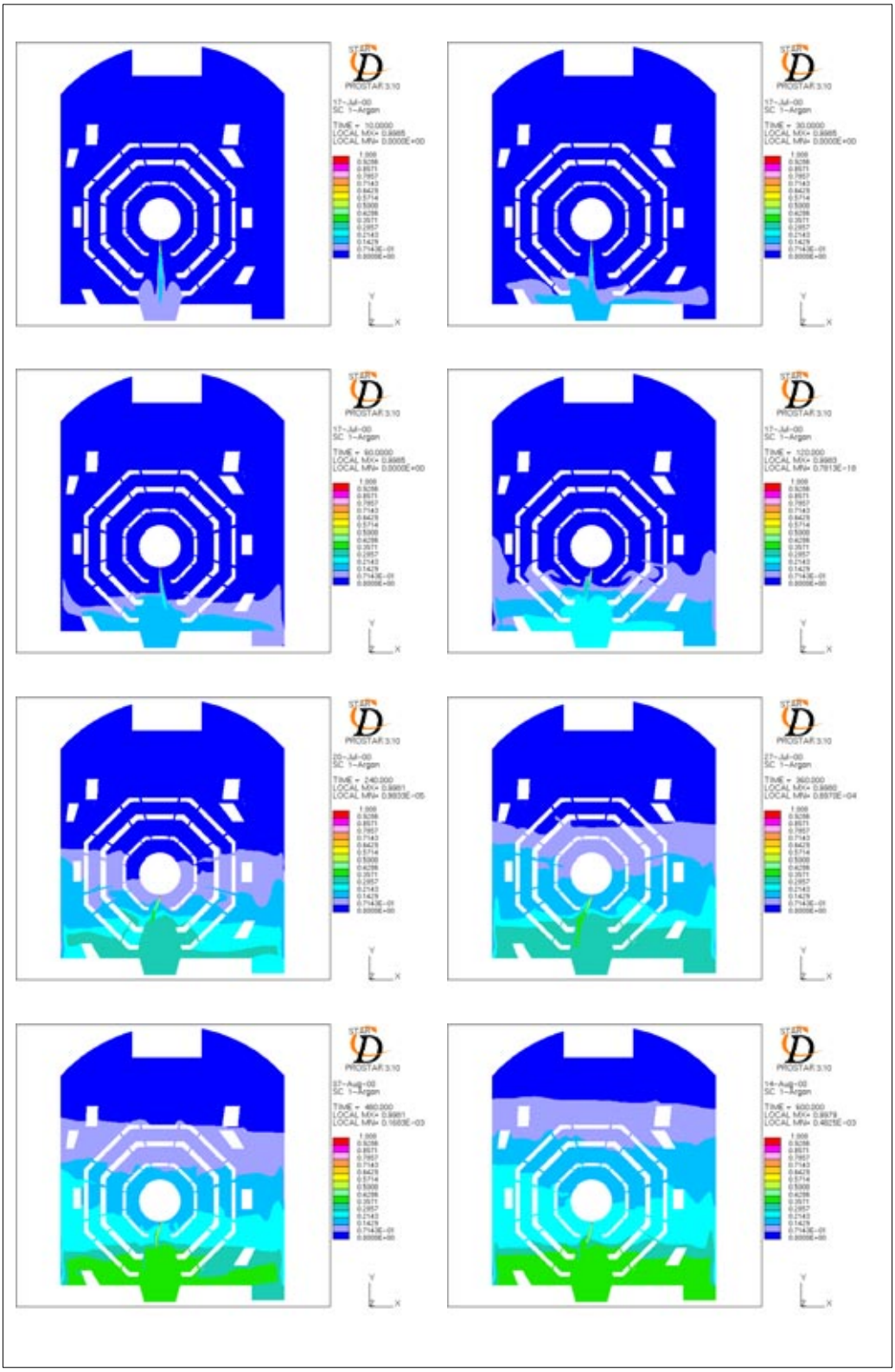

Figure A.6 Argon concentration 10,30,60,120,240,360,480,600 s after the spill

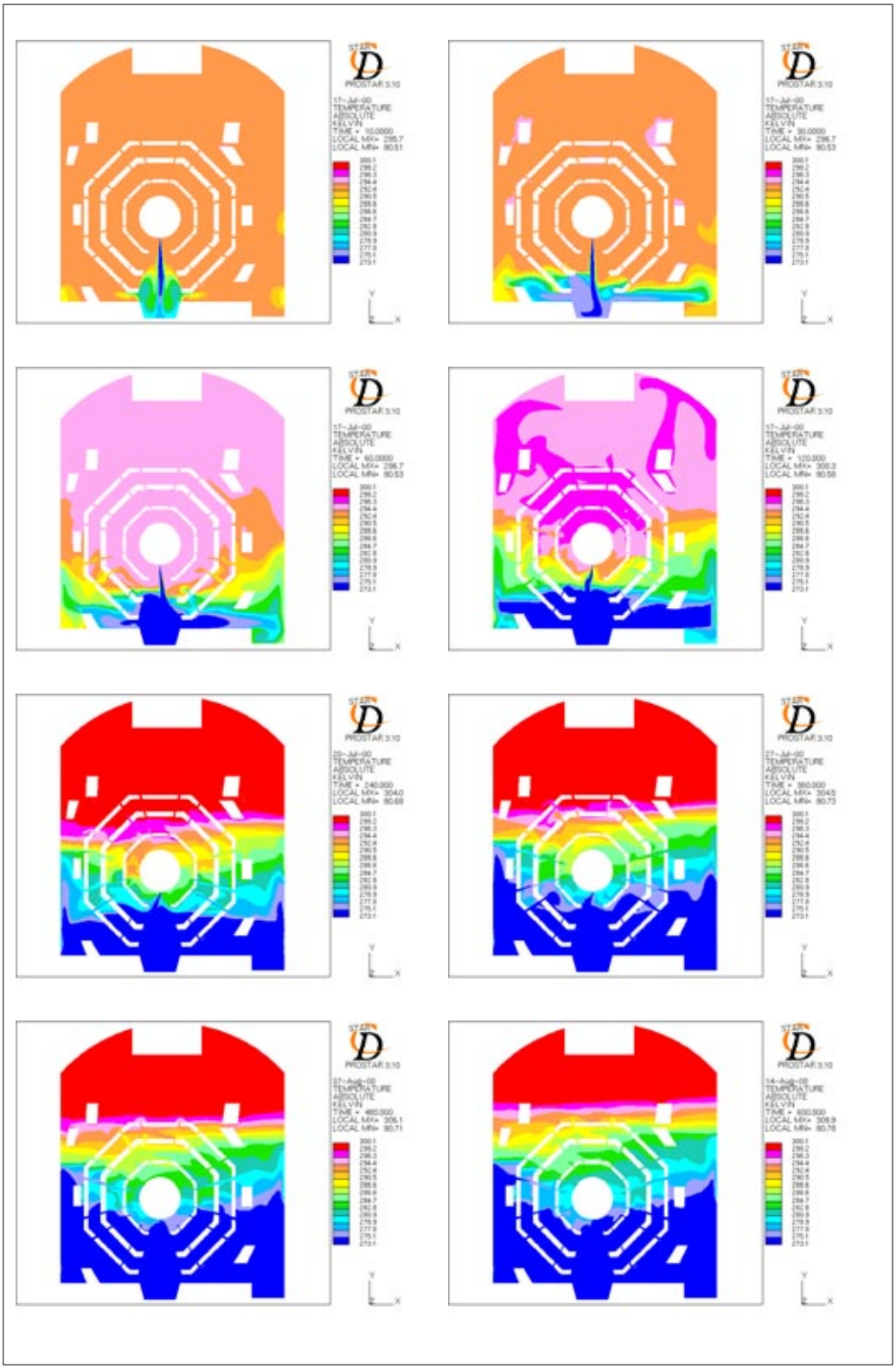

Figure A.7 Temperature distribution 10,30,60,120,240,480,600 s after the spill

A.1.5 12,39 l LAr/s.Closed detector scenario

Q	**12,39 l LAr/s**				
Geometry	**Closed detector scenario**				
Ventilation & Heat Load	**Old Specifications**				
Energy Sinks	**Non**				
Boundaries	*v (m/s)*	*k (m^2/s^2)*	*ε (m^2/s^3)*	*T (K)*	*ρ (kg/m^3)*
Argon Inlet	4,0	0,240	2,814	90	5,507
Exhaust fan	0,059	$5,364\ 10^{-5}$	$6,949\ 10^{-8}$	295	1,2
Left diffusor	0,138	$2,893\ 10^{-4}$	$4,044\ 10^{-6}$	290	1,2
Right top diffusor	0,083	1,016 10-4	7,012 10-7	290	1,2
Right bottom diffusor	0,138	$2,893\ 10^{-4}$	$4,044\ 10^{-6}$	290	1,2
Central pit extractor	0,167	$4,214\ 10^{-4}$	$1,527\ 10^{-5}$	295	1,2
Right pit extractor	0,046	$3,186\ 10^{-5}$	$3,284\ 10^{-7}$	295	1,2
Pit	292,5 K Isothermal				
Racks	3,7134 W / m^2 Constant heat flux				
Muon chambers	16,56 W / m^2 Constant heat flux				
Walls	292,5 K Isothermal				
Turbulence Model	K - E / R N G				
Differential schemes	*u,v*	*KE*	*ε*	*T*	*ρ*
Time	F u l l y I m p l i c i t				
Space	UD	UD	UD	UD	CD 0,8
Control					
Piso Correctors	5 to 7				
Max. COU number	35 to 50				
Mean COU number	0,82 to 1,2				
HDIFF	300 to 1000 W				
Residual tolerance	0,01 for u,v,T,KE,ε,ρ / 0,001 for P				
Under-relaxation for P	0,8				
Precision	Double				
Simulated time	6,5 minute				
Folder	MODELO 2 / Alpha				

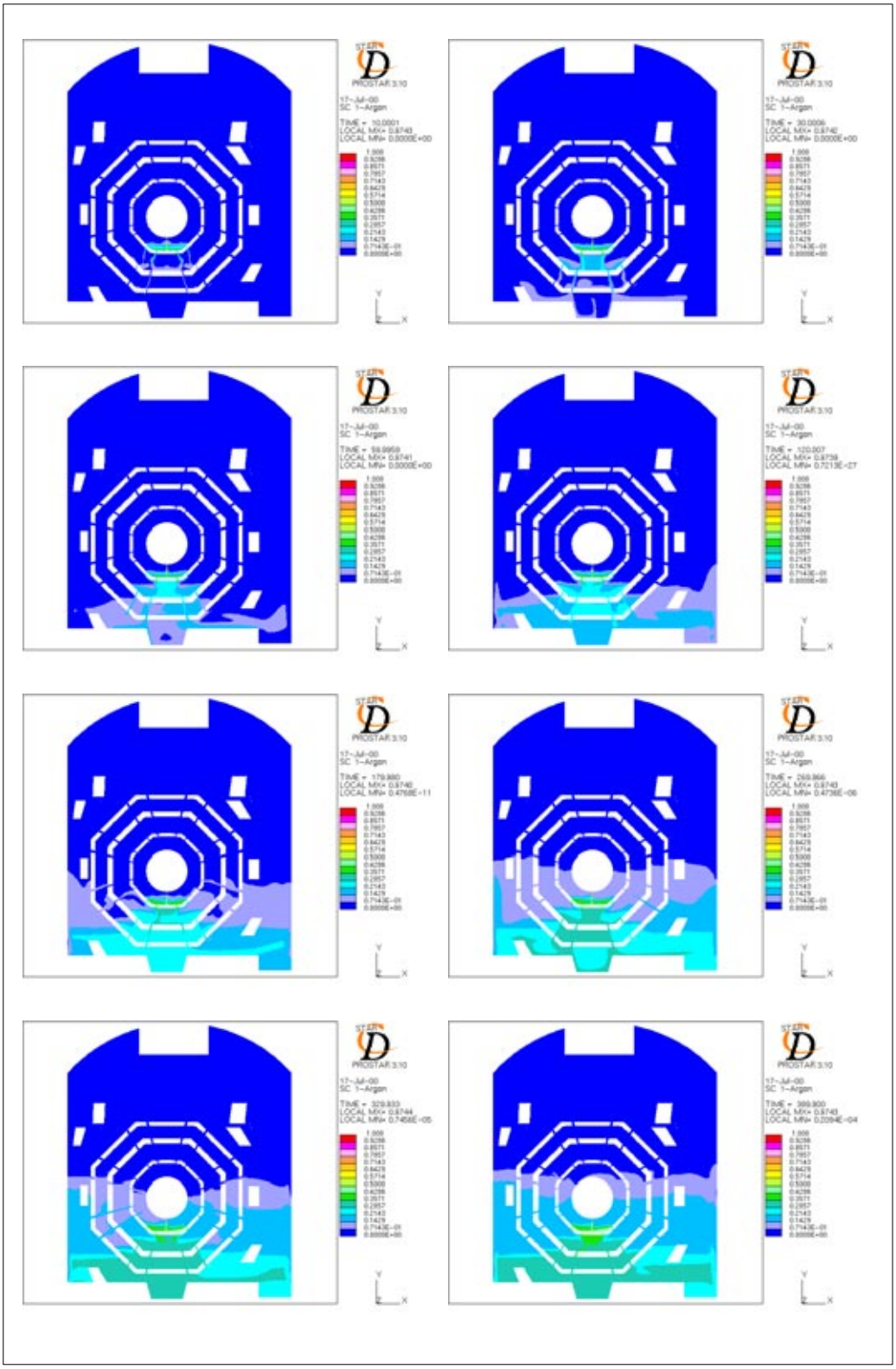

Figure A.8 Argon concentration 10,30,60,120,180,270,330,390 s after the spill

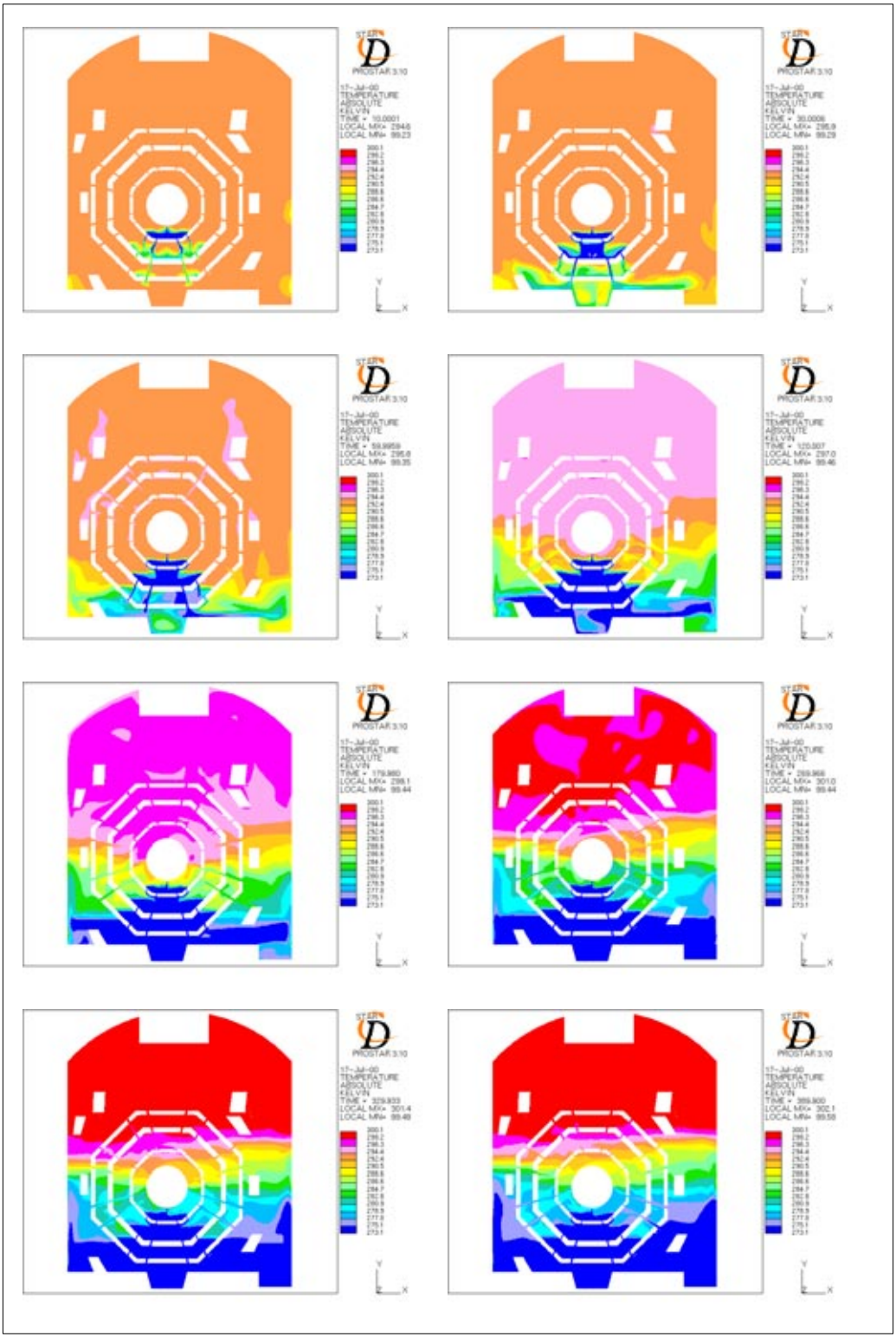

Figure A.9 Temperature distribution 10,30,60,120,180,270,330,390s after the spill

A.1.6 12,39 l LAr/s. Open Detector Scenario

Q	**12,39 l LAr/s**				
Geometry	**Open detector scenario**				
Ventilation & Heat Load	**New Specifications**				
Energy Sinks	**Non**				
Boundaries	*v (m/s)*	*k (m^2/s^2)*	*ε (m^2/s^3)*	*T (K)*	*ρ (kg/m^3)*
Argon Inlet	4,0	0,24	10,398	90	5,3375
Exhaust fan	0,079	$9{,}53\ 10^{-5}$	$1{,}57\ 10^{-7}$	297	1,2
Left diffusor	0,185	$5{,}14\ 10^{-4}$	$9{,}18\ 10^{-6}$	290	1,2
Right top diffusor	0,082	$1{,}01\ 10^{-4}$	$7{,}01\ 10^{-7}$	290	1,2
Right bottom diffusor	0,185	$5{,}14\ 10^{-4}$	$9{,}18\ 10^{-6}$	290	1,2
Central pit extractor	0,167	$4{,}21\ 10^{-4}$	$1{,}52\ 10^{-5}$	297	1,2
Right pit extractor	0,046	$3{,}18\ 10^{-5}$	$3{,}28\ 10^{-7}$	297	1,2
Pit	293,6 K Isothermal				
Racks	6,34 W / m^2 Constant heat flux				
Muon chambers	29,78 W / m^2 Constant heat flux				
Walls	293,6 K Isothermal				
Turbulence Model	K - E / R N G				
Differential schemes	*u,v*	*KE*	*ε*	*T*	*ρ*
Time	F u l l y I m p l i c i t				
Space	UD	UD	UD	UD	CD 0,8
Control					
Piso Correctors	5 to 7				
Max. COU number	10 to 65				
Mean COU number	0,1 to 0,7				
HDIFF	0,2 to 5 W				
Residual tolerance	0,01 for u,v,T,KE,ε,ρ / 0,001 for P				
Under-relaxation for P	0,8				
Precision	Double				
Simulated time	4 minutes				
Folder	MODELO 71 / Alpha				

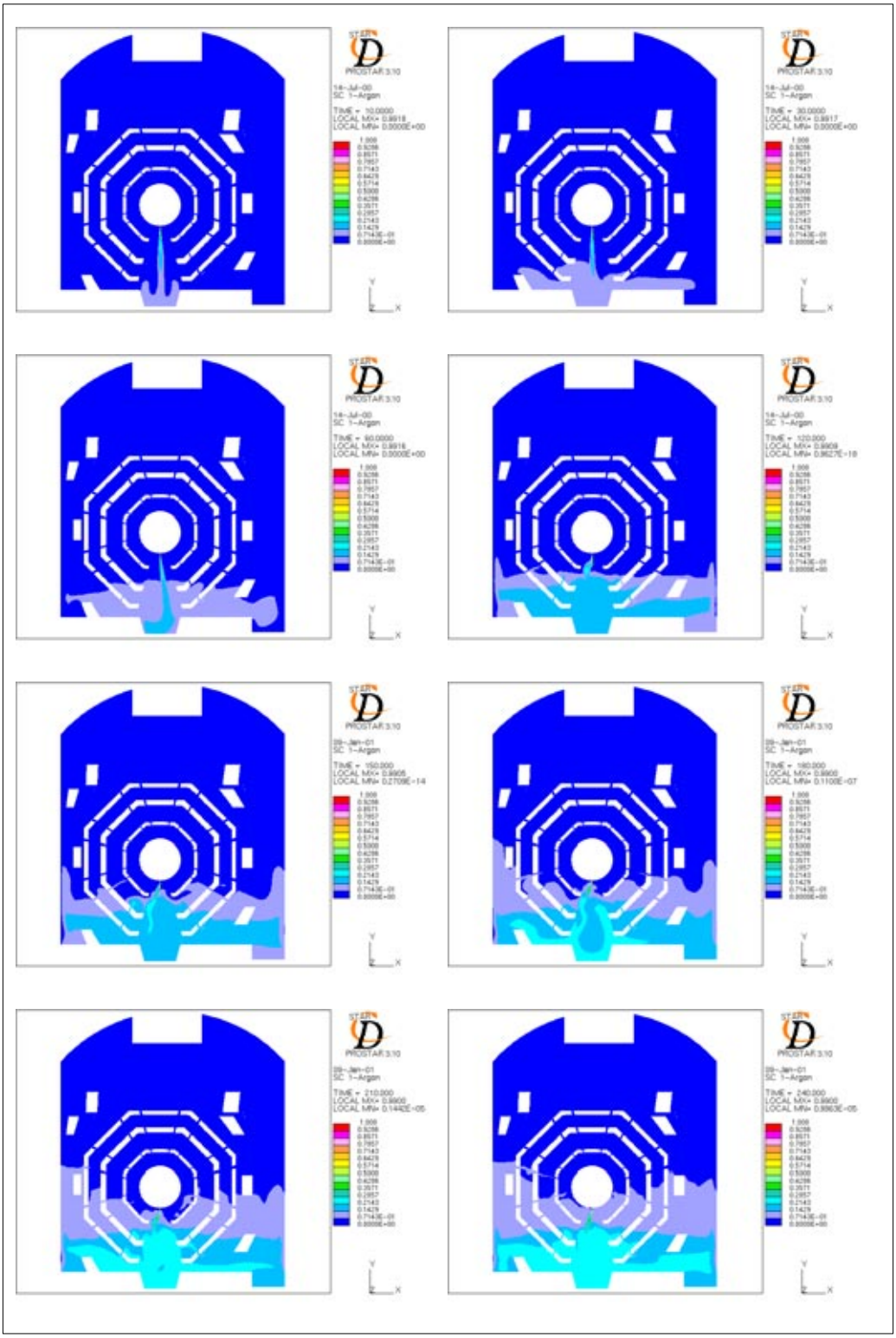

Figure A.10 Argon concentration and Temperature10,30,60,120,150,180,210,240 s after the spil

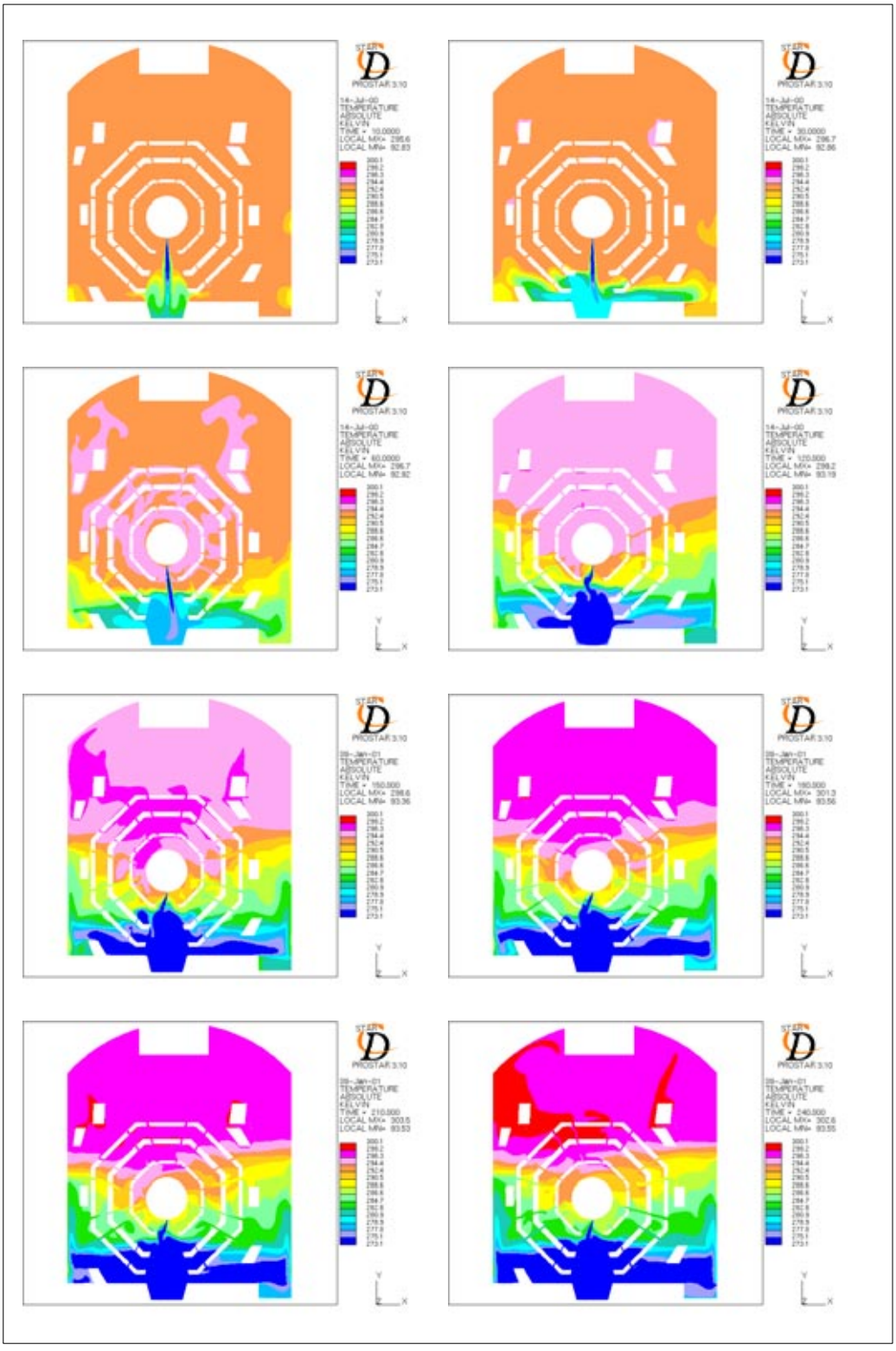

Figure A.11 Temperature distribution 10,30,60,120,150,180,210,240 s after the spill

A.1.7 9,3 l LAr/s. Open detector geometry

Q	**9,3 l LAr/s**				
Geometry	**Open detector scenario**				
Ventilation & Heat Load	**Old Specifications**				
Energy Sinks	**Non**				
Boundaries	*v (m/s)*	*k (m^2/s^2)*	*ε (m^2/s^3)*	*T (K)*	*ρ (kg/m^3)*
Argon Inlet	3,0	0,135	1,583	90	5,507
Exhaust fan	0,059	$5,364\ 10^{-5}$	$6,949\ 10^{-8}$	295	1,2
Left diffusor	0,138	$2,893\ 10^{-4}$	$4,044\ 10^{-6}$	290	1,2
Right top diffusor	0,083	1,016 10-4	7,012 10-7	290	1,2
Right bottom diffusor	0,138	$2,893\ 10^{-4}$	$4,044\ 10^{-6}$	290	1,2
Central pit extractor	0,167	$4,214\ 10^{-4}$	$1,527\ 10^{-5}$	295	1,2
Right pit extractor	0,046	$3,186\ 10^{-5}$	$3,284\ 10^{-7}$	295	1,2
Pit	292,5 K Isothermal				
Racks	3,7134 W / m^2 Constant heat flux				
Muon chambers	16,56 W / m^2 Constant heat flux				
Walls	292,5 K Isothermal				
Turbulence Model	K - E / R N G				
Differential schemes	*u,v*	*KE*	*ε*	*T*	*ρ*
Time	F u l l y I m p l i c i t				
Space	UD	UD	UD	UD	CD 0,8
Control					
Piso Correctors	4 to 5				
Max. COU number	9,8 to 12,2				
Mean COU number	around 0,35				
HDIFF	0,5 to 2,5 W				
Residual tolerance	0,01 for u,v,T,KE,ε,ρ / 0,001 for P				
Under-relaxation for P	0,8				
Precision	Double				
Simulated time	5 minutes				
Folder	MODELO 8 / Alpha				

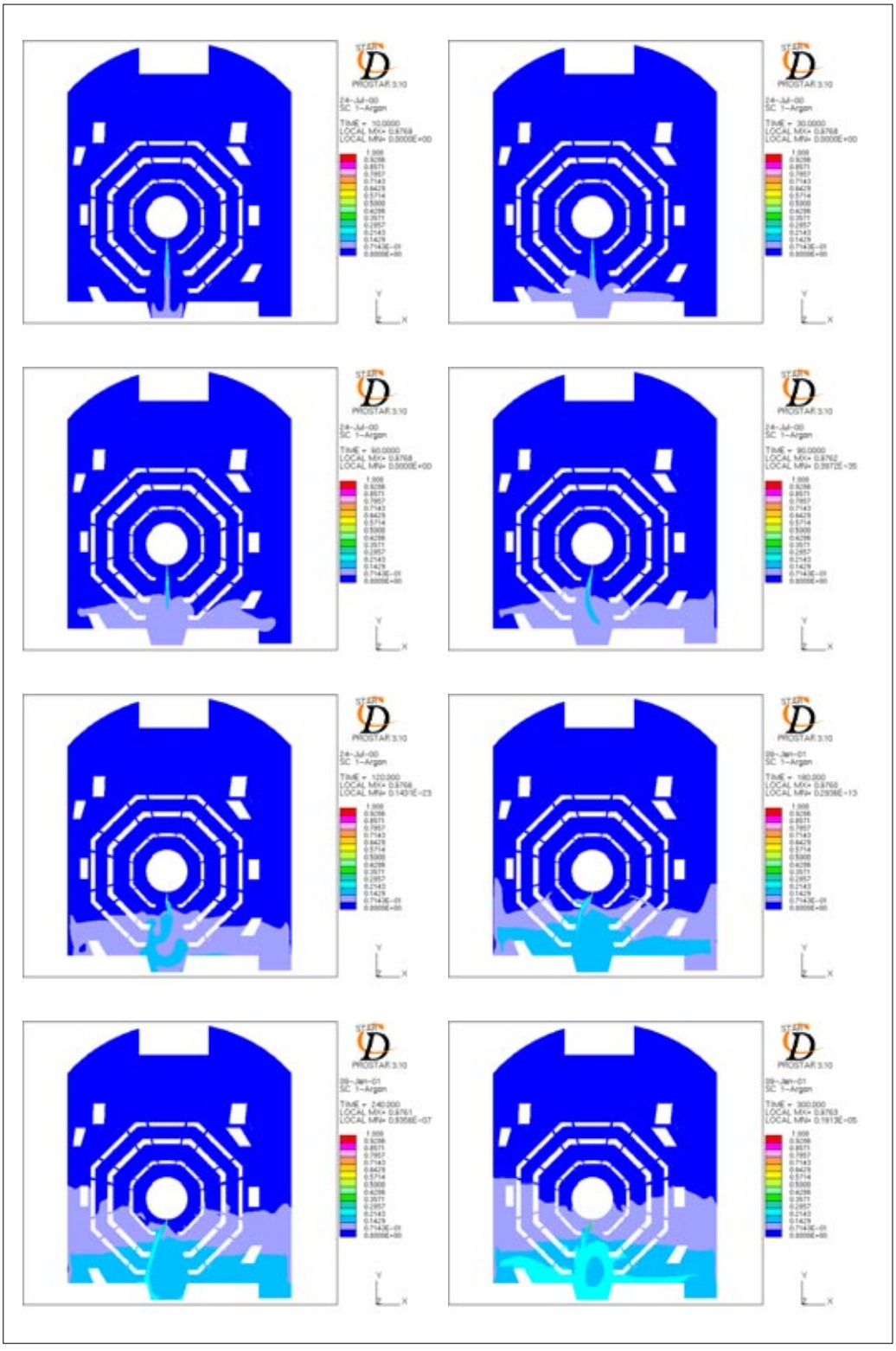

Figure A.12 Argon Concentration distribution 10,30,60,90,120,180,240,300 s after the spill

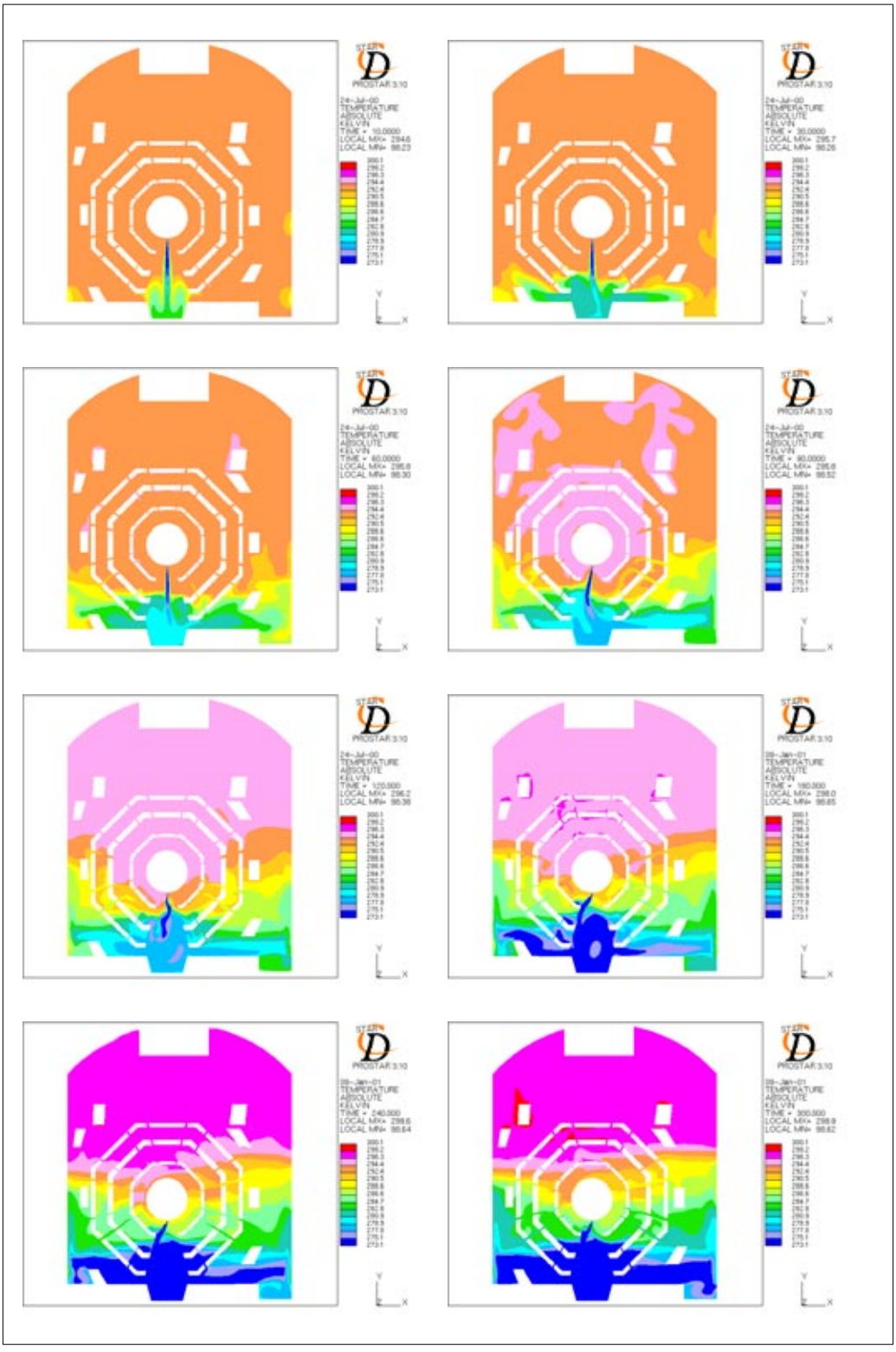

Figure A.13 Temperature distribution 10,30,60,90,120,180,240,300 s after the spill

A.1.8 3,79 l LAr/s. Closed detector geometry

Q	**3,79 l LAr/s**				
Geometry	**Open detector scenario**				
Ventilation & Heat Load	**Old Specifications**				
Energy Sinks	**Non**				
Boundaries	*v (m/s)*	*k (m^2/s^2)*	*ε (m^2/s^3)*	*T (K)*	*ρ (kg/m^3)*
Argon Inlet	1,22	0,022	0,302	90	5,507
Exhaust fan	0,059	$5{,}364\ 10^{-5}$	$6{,}949\ 10^{-8}$	295	1,2
Left diffusor	0,138	$2{,}893\ 10^{-4}$	$4{,}044\ 10^{-6}$	290	1,2
Right top diffusor	0,083	1,016 10-4	7,012 10-7	290	1,2
Right bottom diffusor	0,138	$2{,}893\ 10^{-4}$	$4{,}044\ 10^{-6}$	290	1,2
Central pit extractor	0,167	$4{,}214\ 10^{-4}$	$1{,}527\ 10^{-5}$	295	1,2
Right pit extractor	0,046	$3{,}186\ 10^{-5}$	$3{,}284\ 10^{-7}$	295	1,2
Pit	292,5 K Isothermal				
Racks	3,7134 W / m^2 Constant heat flux				
Muon chambers	16,56 W / m^2 Constant heat flux				
Walls	292,5 K Isothermal				
Turbulence Model	K - E / R N G				
Differential schemes	*u,v*	*KE*	*ε*	*T*	*ρ*
Time	F u l l y I m p l i c i t				
Space	UD	UD	UD	UD	CD 0,8
Control					
Piso Correctors	3 to 6				
Max. COU number	8 to 25				
Mean COU number	0,1 to 0,34				
HDIFF	0,1 to 0,4 W				
Residual tolerance	0,01 for u,v,T,KE,ε,ρ / 0,001 for P				
Under-relaxation for P	0,8				
Precision	Double				
Simulated time	5 minutes				
Folder	MODELO 5 / Alpha				

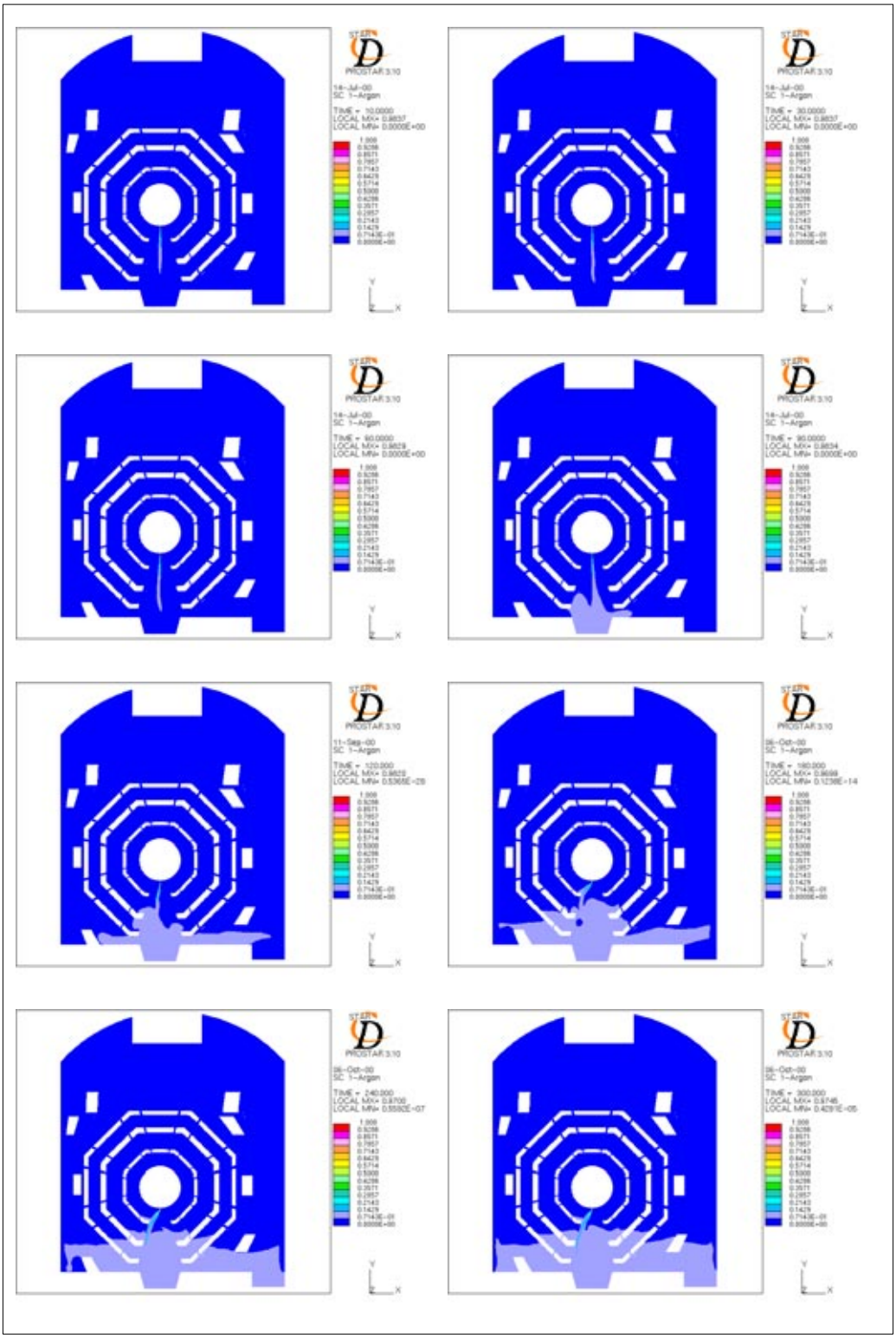

Figure A.14 Argon concentration 10,30,60,90,120,180,240,300 s after the spill

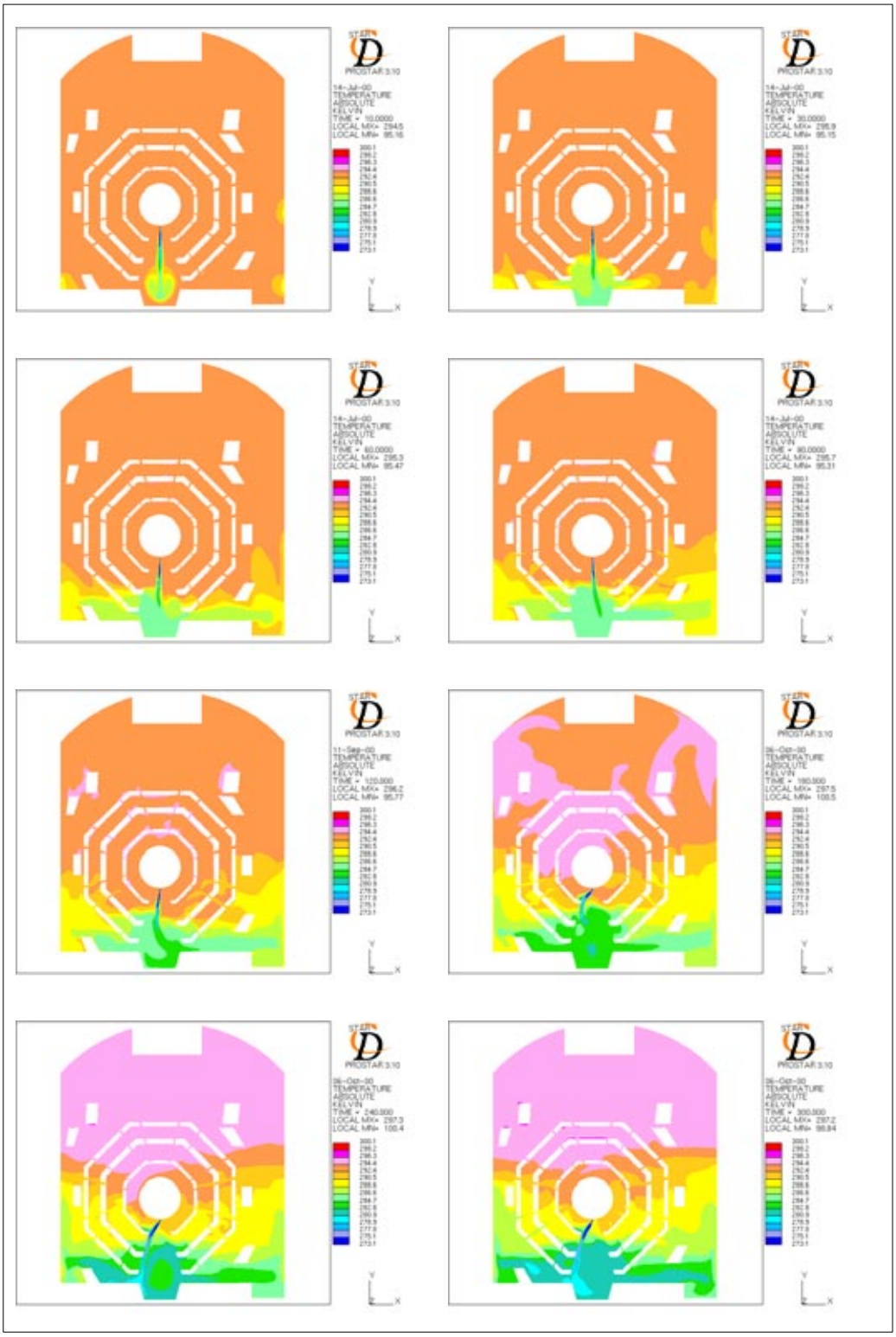

Figure A.15 Temperature distribution 10,30,60,90,120,180,240,300 s after the spill

A.1.9 3,28 l LAr/s. Closed detector scenario

Q	**3,28 l LAr/s**				
Geometry	**Closed detector scenario**				
Ventilation & Heat Load	**Old Specifications**				
Energy Sinks	**Non**				
Boundaries	*v (m/s)*	*k (m^2/s^2)*	*ε (m^2/s^3)*	*T (K)*	*ρ (kg/m^3)*
Argon Inlet	1,088	0,0177	0,2242	90	5,507
Exhaust fan	0,059	$5{,}364\ 10^{-5}$	$6{,}949\ 10^{-8}$	295	1,2
Left diffusor	0,138	$2{,}893\ 10^{-4}$	$4{,}044\ 10^{-6}$	290	1,2
Right top diffusor	0,083	1,016 10-4	7,012 10-7	290	1,2
Right bottom diffusor	0,138	$2{,}893\ 10^{-4}$	$4{,}044\ 10^{-6}$	290	1,2
Central pit extractor	0,167	$4{,}214\ 10^{-4}$	$1{,}527\ 10^{-5}$	295	1,2
Right pit extractor	0,046	$3{,}186\ 10^{-5}$	$3{,}284\ 10^{-7}$	295	1,2
Pit	292,5 K Isothermal				
Racks	3,7134 W / m^2 Constant heat flux				
Muon chambers	16,56 W / m^2 Constant heat flux				
Walls	292,5 K Isothermal				
Turbulence Model	K - E / R N G				
Differential schemes	*u,v*	*KE*	*ε*	*T*	*ρ*
Time	F u l l y I m p l i c i t				
Space	UD	UD	UD	UD	CD 0,8
Control					
Piso Correctors	3 to 4				
Max. COU number	2 to 25				
Mean COU number	1 to 1,7				
HDIFF	3 to 14 W				
Residual tolerance	0,01 for u,v,T,KE,ε,ρ / 0,001 for P				
Under-relaxation for P	0,8				
Precision	Double				
Simulated time	1,5 minutes				
Folder	MODELO 4 / Alpha				

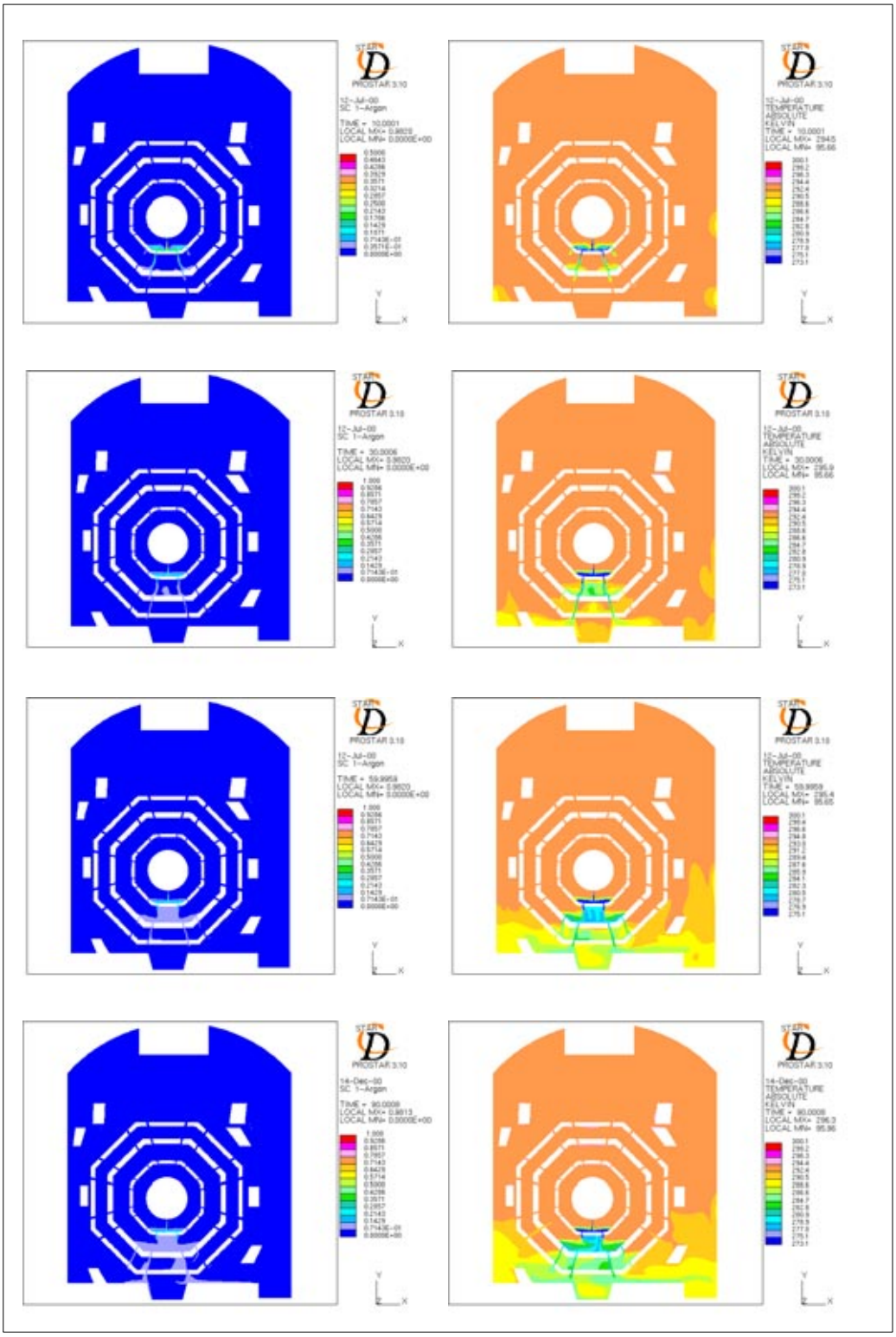

Figure A.16 Argon concentration and Tempertaure 10,30,60,90 s after the spill

A.1.10 50 l LAr/min. / 0,834 l LAr/s. Open detector scenario

Q	**0,834 l LAr/s**				
Geometry	**Open detector scenario**				
Ventilation & Heat Load	**New Specifications**				
Energy Sinks	**Non**				
Boundaries	*v (m/s)*	*k (m^2/s^2)*	*ε (m^2/s^3)*	*T (K)*	*ρ (kg/m^3)*
Argon Inlet	0,2783	0,00117	0,0036	90	5,3375
Exhaust fan	0,079	$9{,}53\ 10^{-5}$	$1{,}57\ 10^{-7}$	297	1,2
Left diffusor	0,185	$5{,}14\ 10^{-4}$	$9{,}18\ 10^{-6}$	290	1,2
Right top diffusor	0,082	$1{,}01\ 10^{-4}$	$7{,}01\ 10^{-7}$	290	1,2
Right bottom diffusor	0,185	$5{,}14\ 10^{-4}$	$9{,}18\ 10^{-6}$	290	1,2
Central pit extractor	0,167	$4{,}21\ 10^{-4}$	$1{,}52\ 10^{-5}$	297	1,2
Right pit extractor	0,046	$3{,}18\ 10^{-5}$	$3{,}28\ 10^{-7}$	297	1,2
Pit	293,6 K Isothermal				
Racks	6,34 W / m^2 Constant heat flux				
Muon chambers	29,78 W / m^2 Constant heat flux				
Walls	293,6 K Isothermal				
Turbulence Model	K - E / R N G				
Differential schemes	*u,v*	*KE*	*ε*	*T*	*ρ*
Time	F u l l y I m p l i c i t				
Space	UD	UD	UD	UD	CD 0,8
Control					
Piso Correctors	3 to 4				
Max. COU number	2 to 25				
Mean COU number	1 to 1,7				
HDIFF	3 to 50 W				
Residual tolerance	0,01 for u,v,T,KE,ε,ρ / 0,001 for P				
Under-relaxation for P	0,8				
Precision	Double				
Simulated time	5 minutes				
Folder	MODELO 1 / Linux				

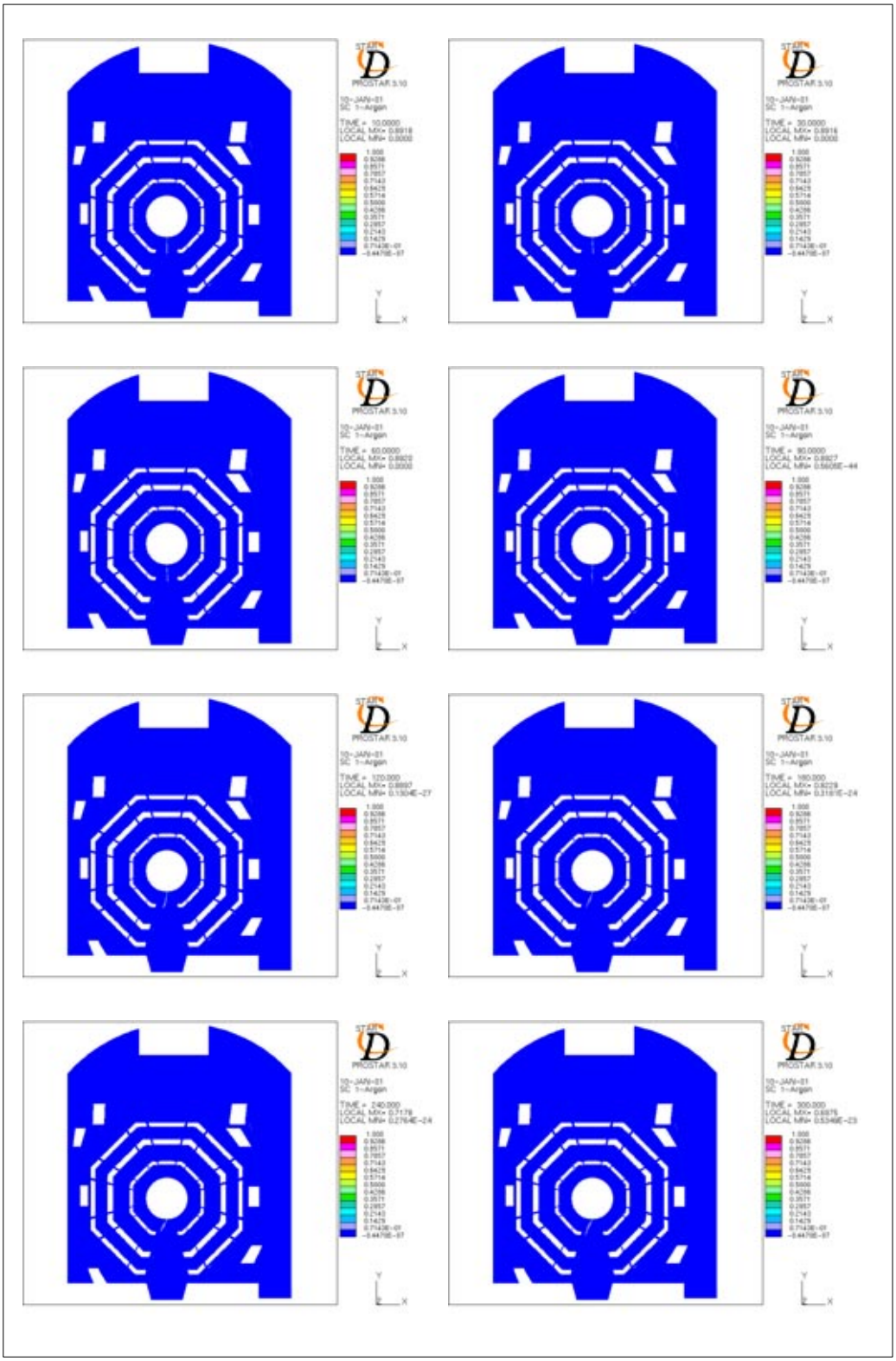

Figure A.17 Argon concentration 10,30,60,90,120,180,240,300 s after the spill

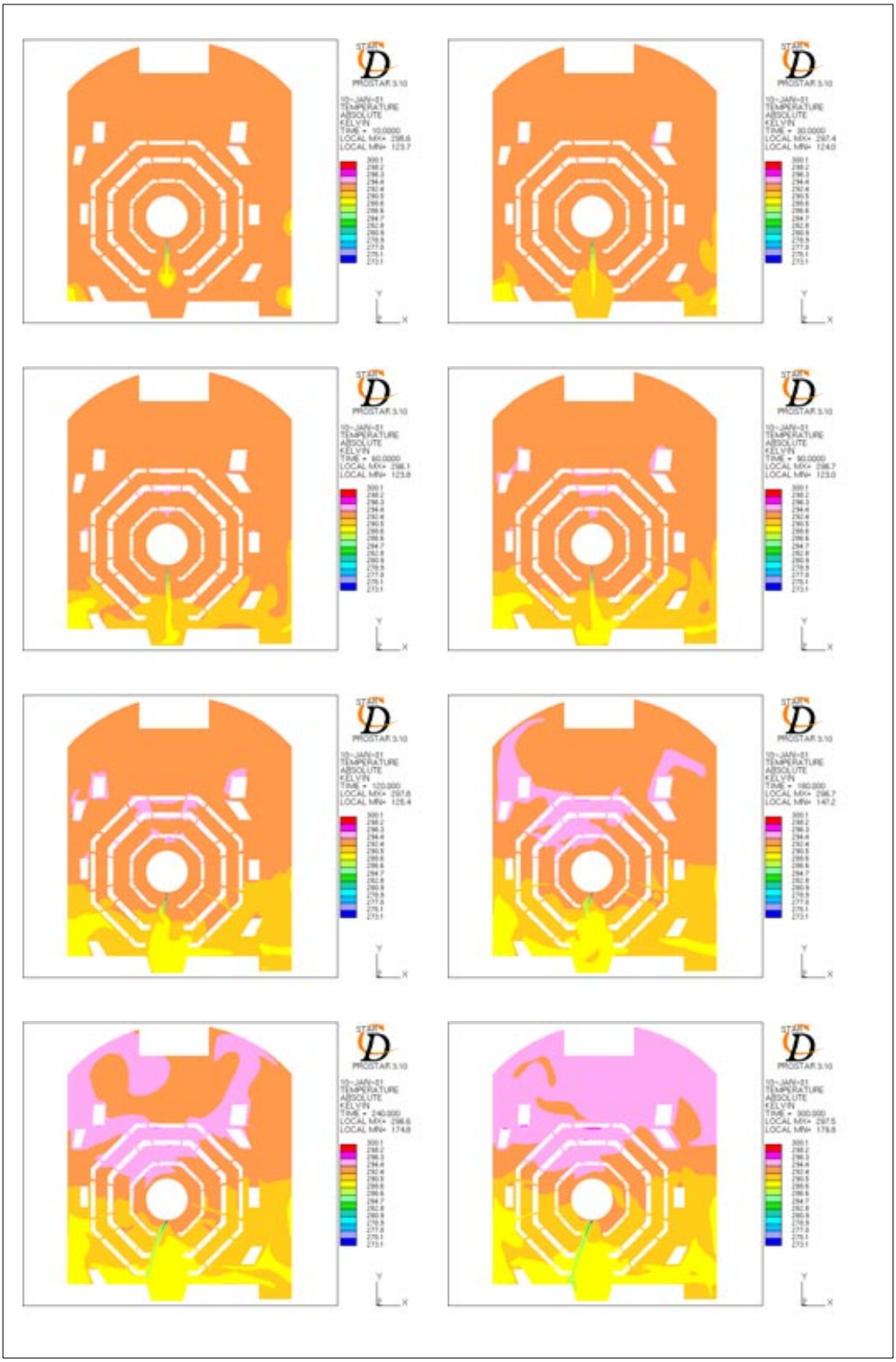

Figure A.18 Temperature distribution 10,30,60,90,120,180,240 and 300s after the spill

A.2 Study of critical elements of the model

A.2.1 Old versus New Specifications

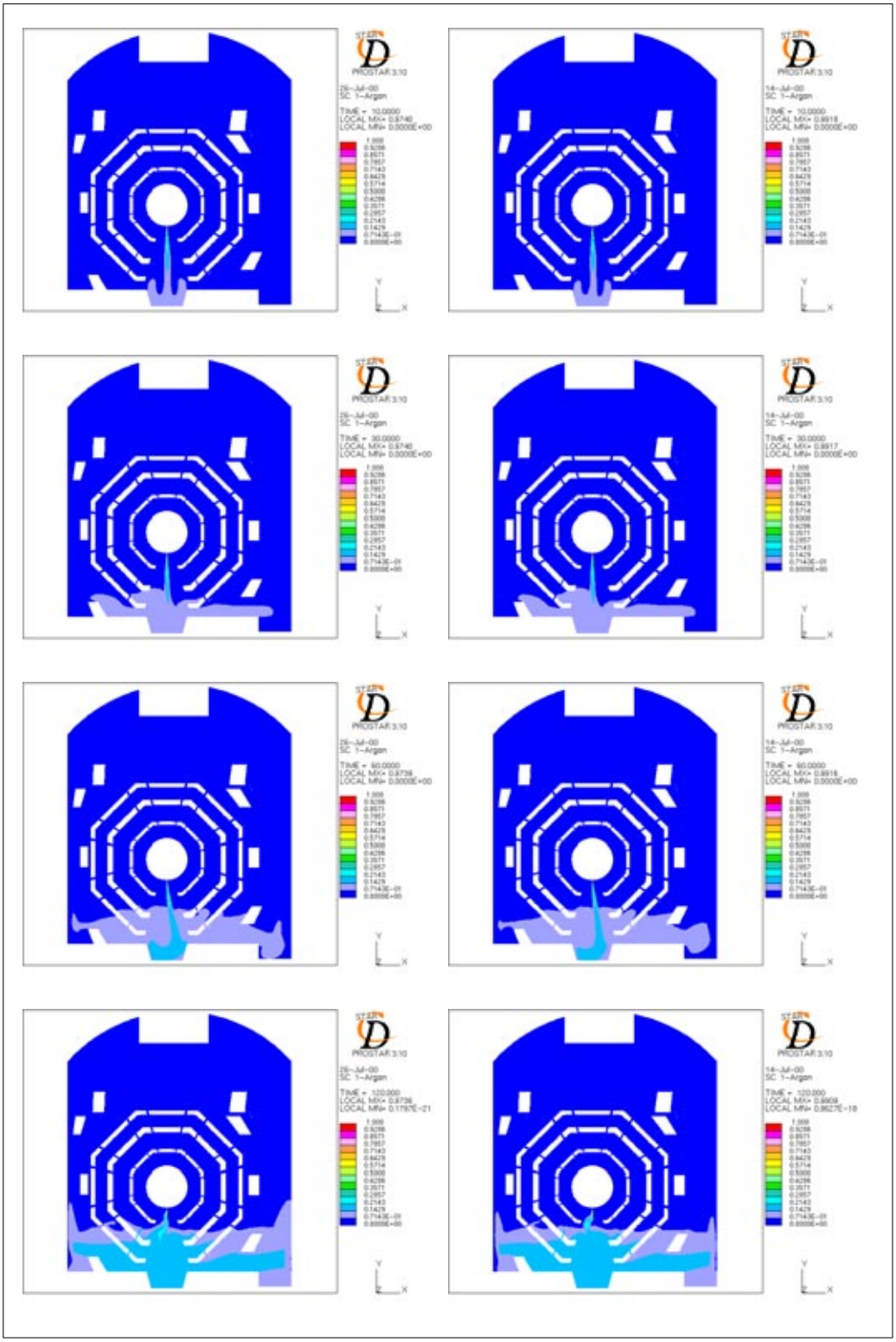

Figure A.19 Argon concentration comparison between Old (left) and New (right) specifications

Old versus New Specifications

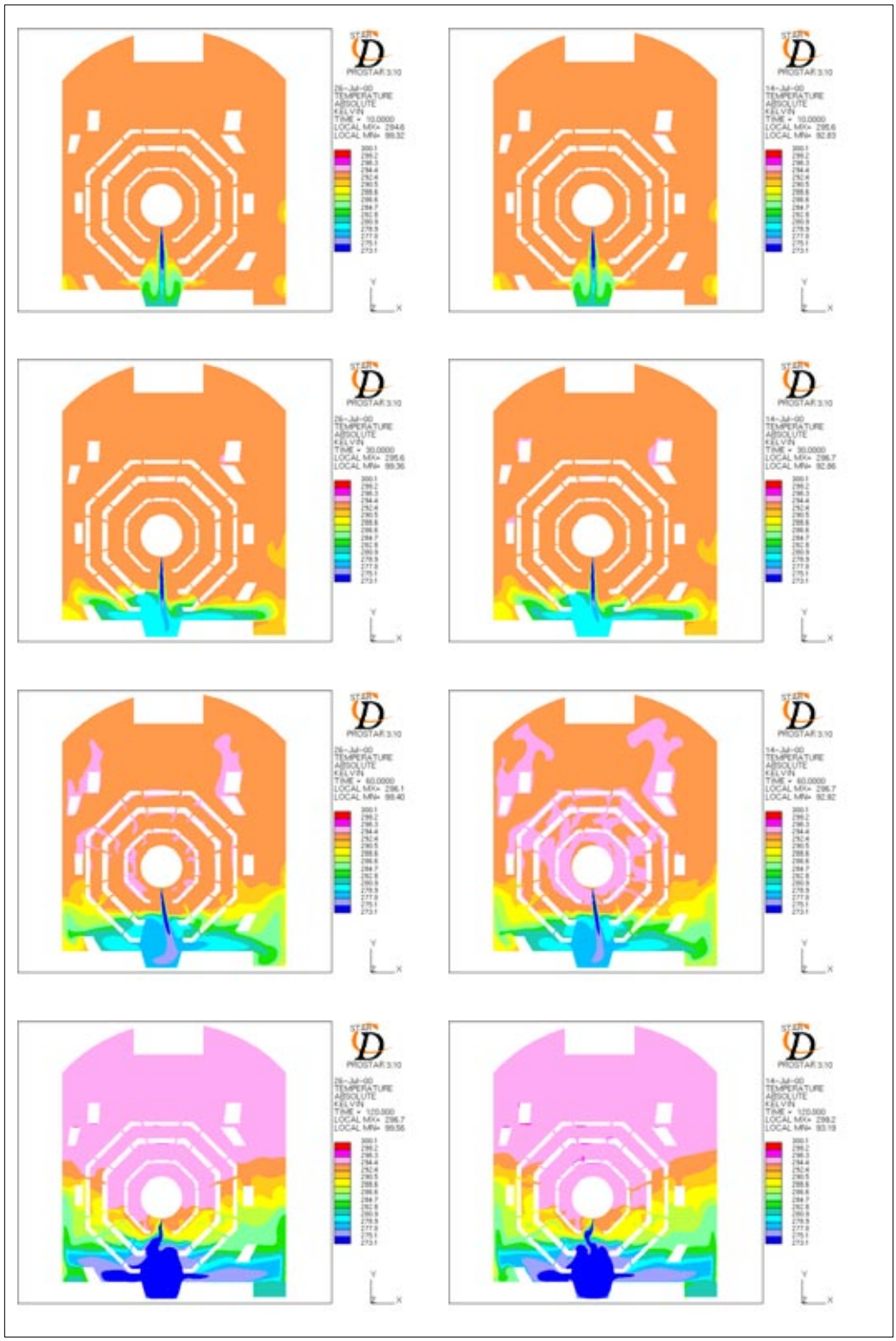

Figure A.20 Temperature distribution comparison between Old (left) and New (right) specifications

A.2.2 Heat Load vs. No Heat Load

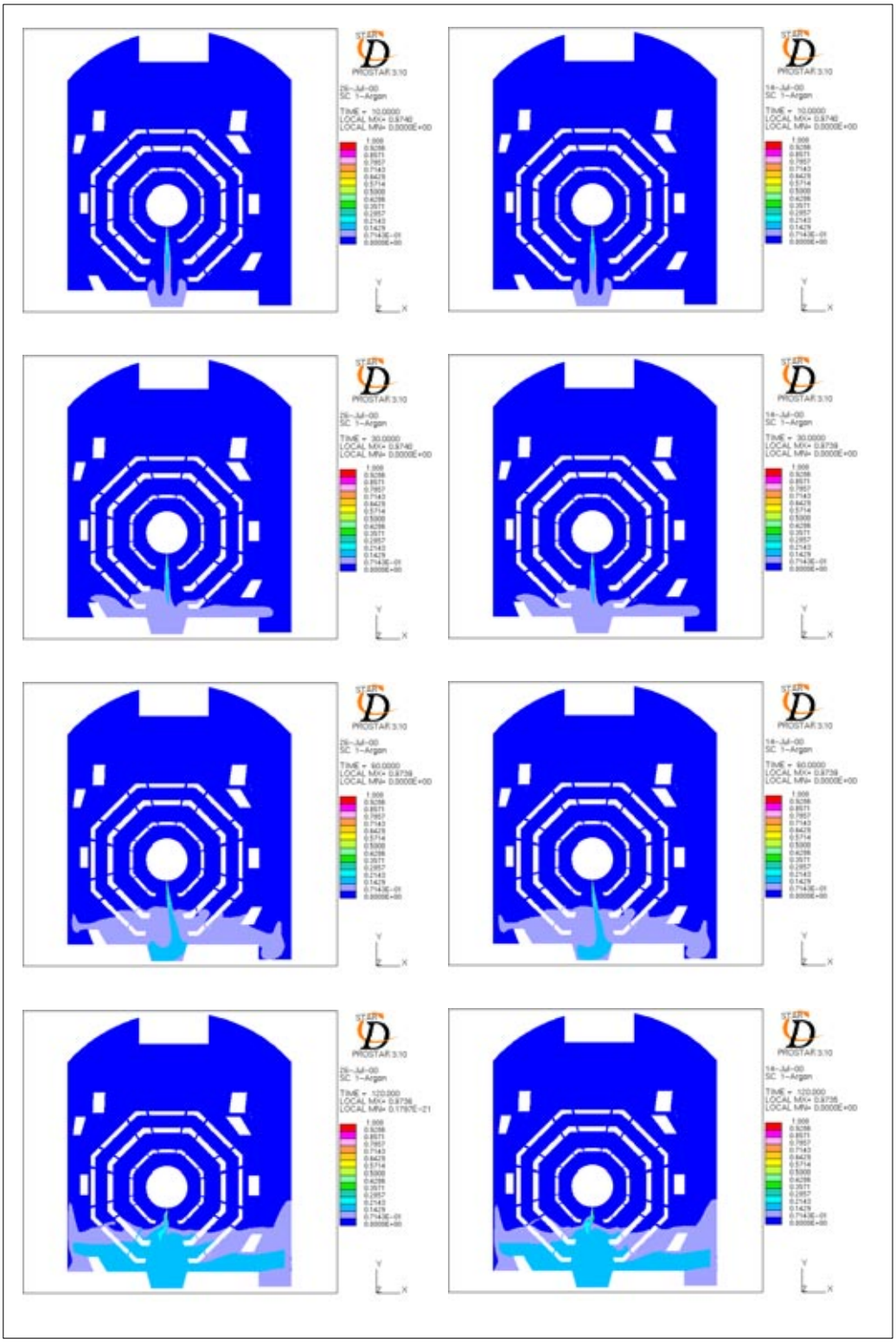

Figure A.21 Argon comparison between a model with Heat Load of 100 kW (left) and a model with no heat load at all (right) - pit, muon chambers and racks adiabatic walls

**Heat Load vs.
No Heat Load**

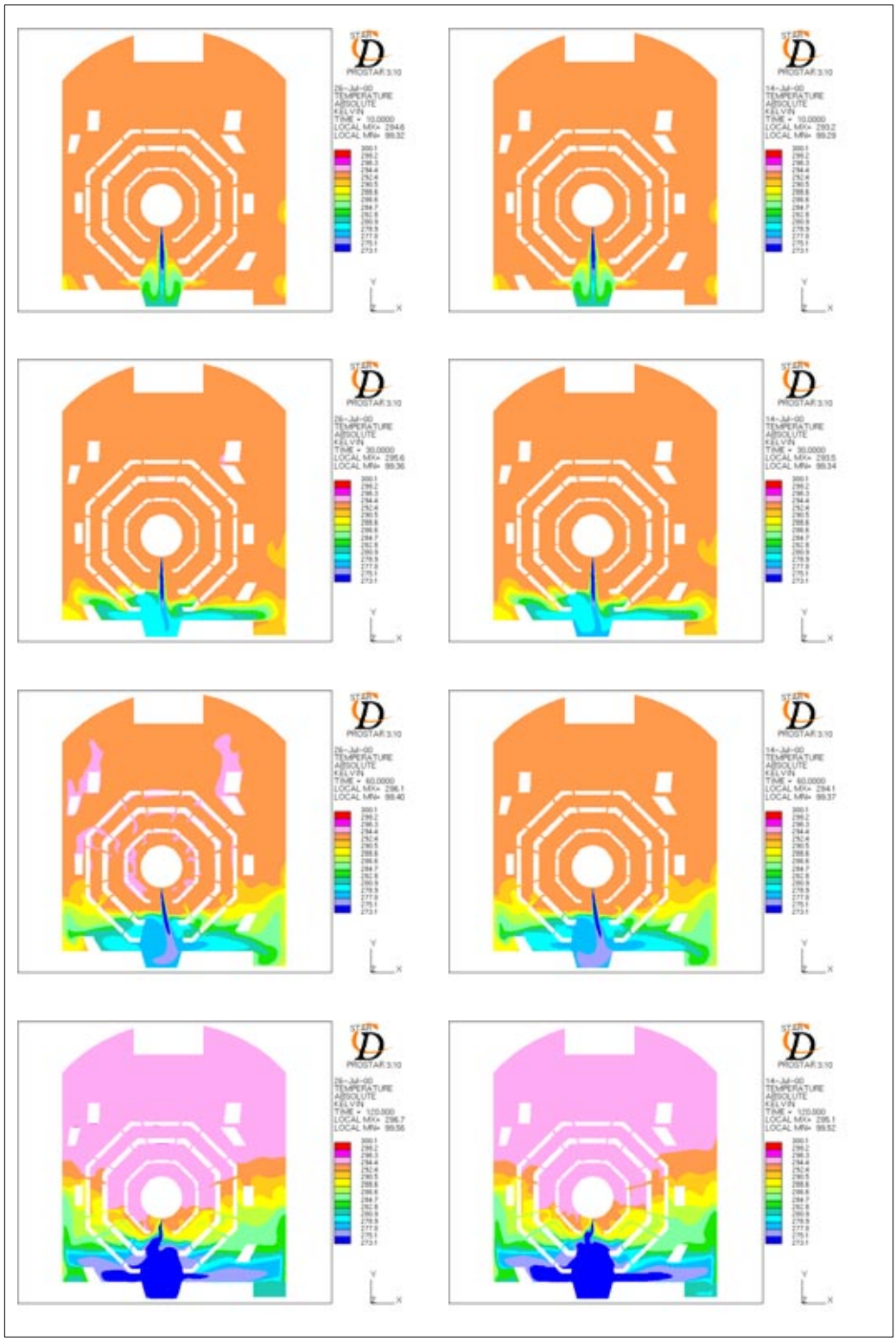

Figure A.22 Temperature comparison between a model with Heat Load of 100 kW (left) and a model with no heat load at all (right) - pit, muon chambers and racks adiabatic walls

A.2.3 k-ε/RNG vs. Low Reynolds

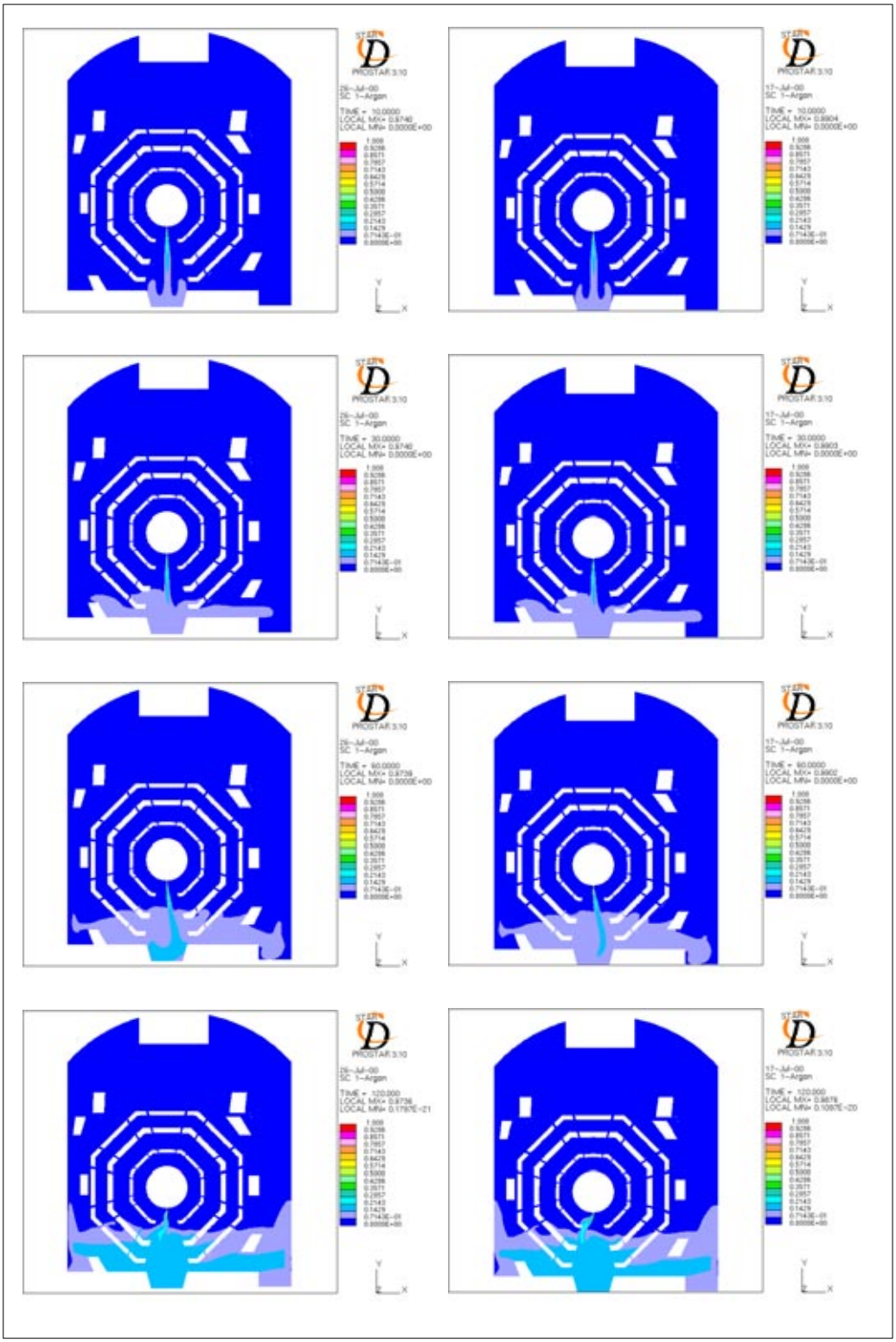

Figure A.23 Argon comparison between a model with K-ε/RNG turbulence model (left) and a model with Low Reynolds turbulence model

k-ε/RNG vs. Low Reynolds

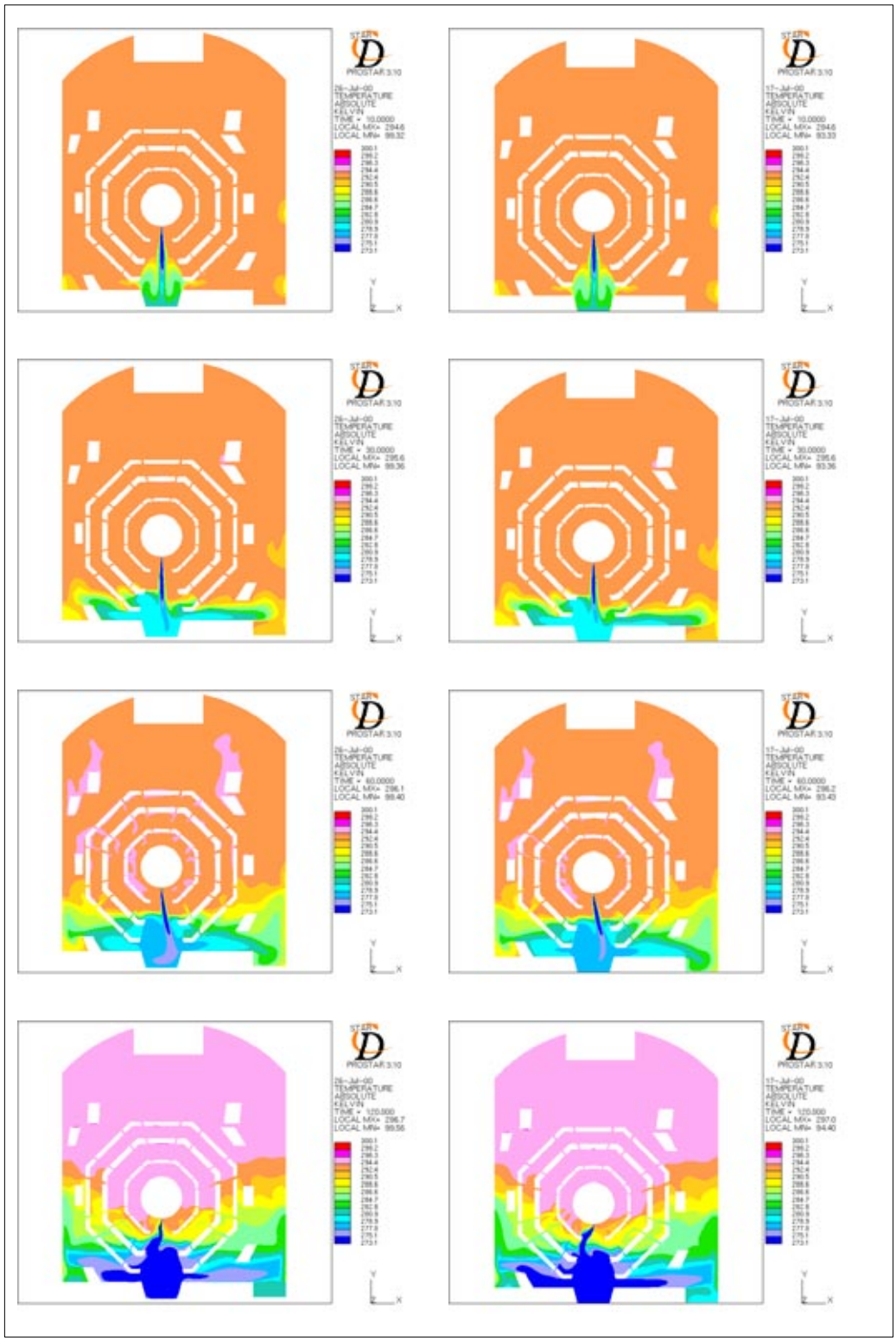

Figure A.24 Temperature comparison between a model with K-ε/RNG turbulence model (left) and a model with Low Reynolds turbulence model

A.2.4 UD vs MARS 0,5

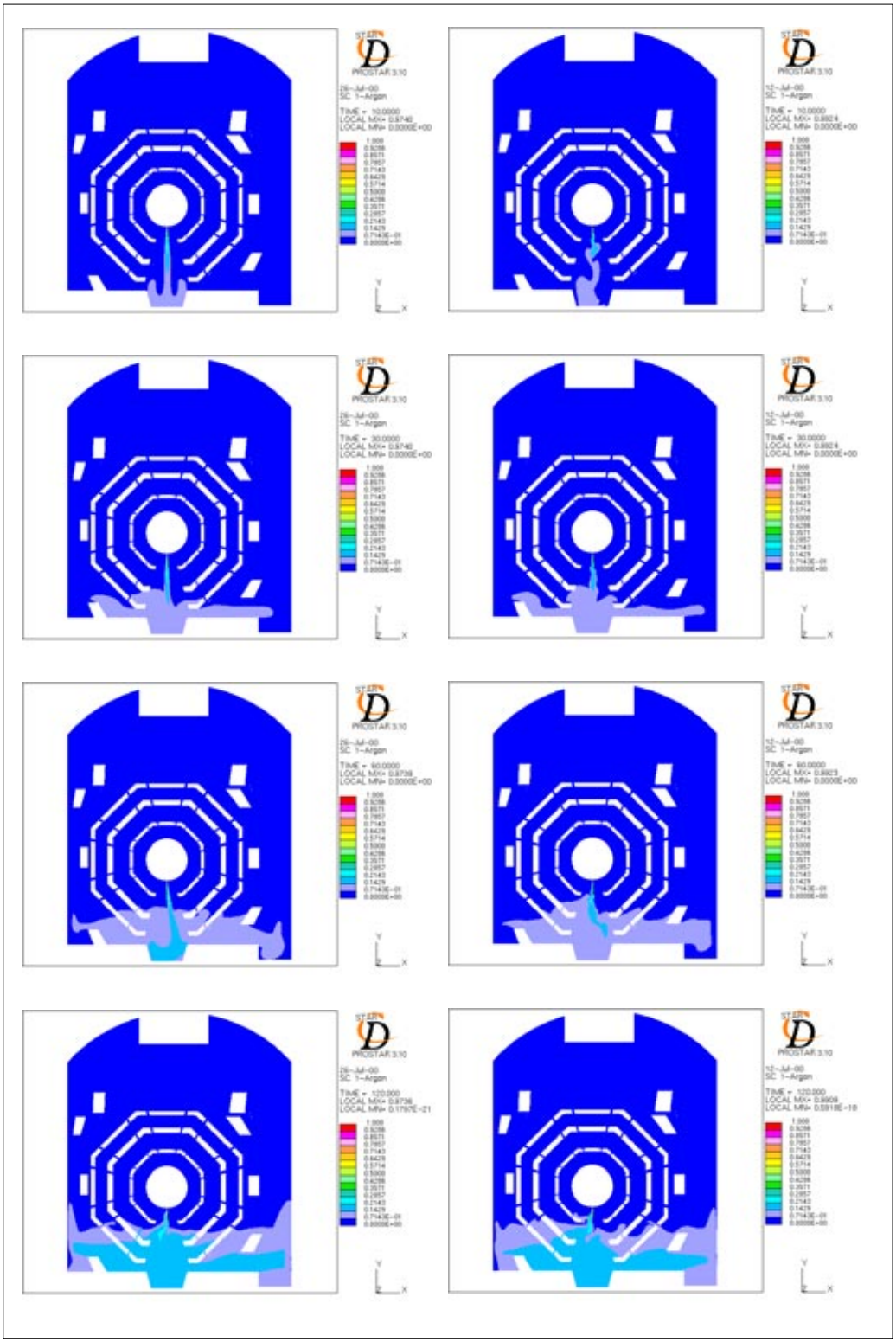

Figure A.25 Argon comparison between a model with a UD differential scheme (left) and a model with MARS 0,5 differential scheme for u,v, T, k, ε

UD vs MARS 0,5

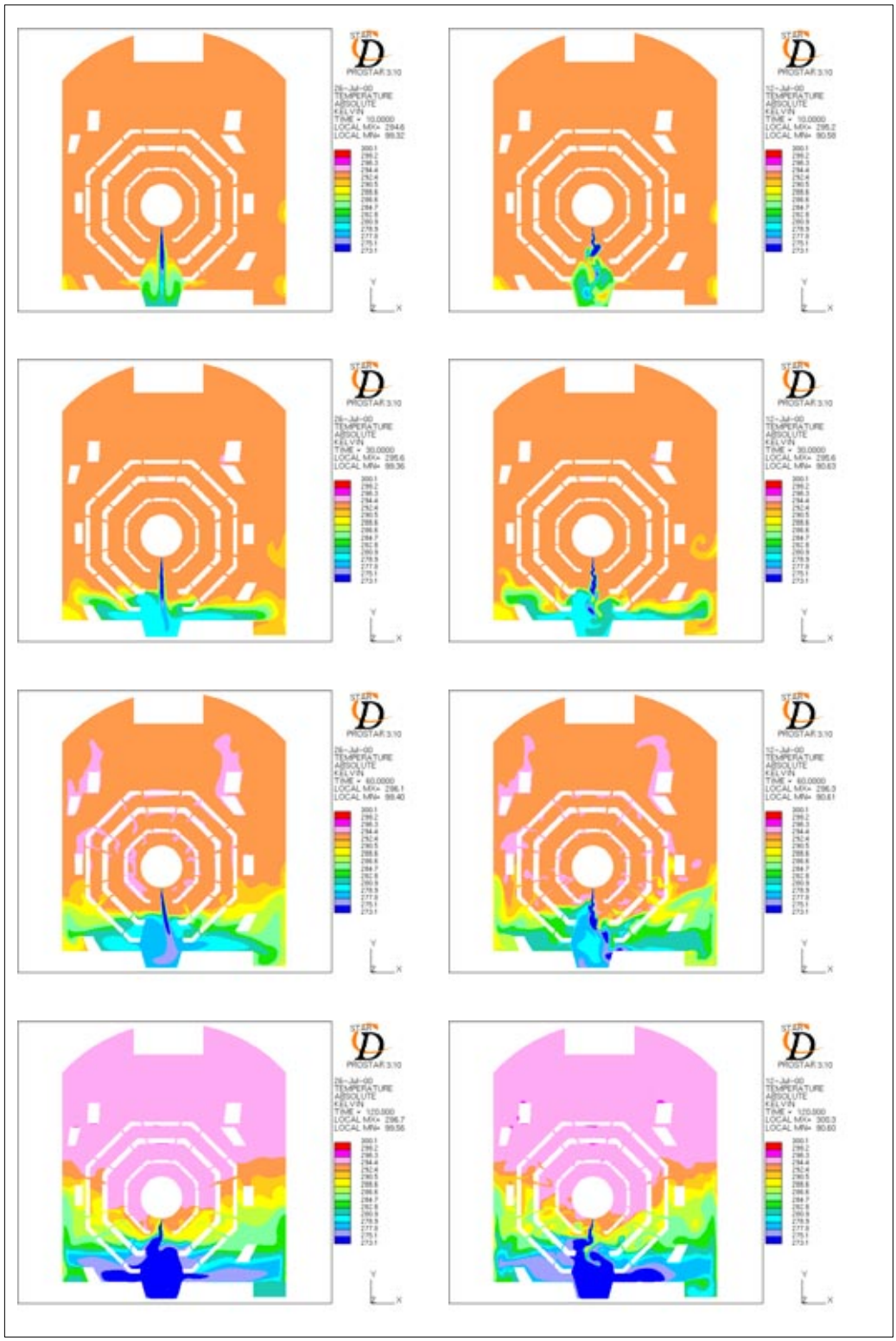

Figure A.26 Temperature comparison between a model with a UD differential scheme (left) and a model with MARS 0,5 differential scheme for u,v, T, k, ε

A.2.5 Isothermal vs Adiabatic Pit

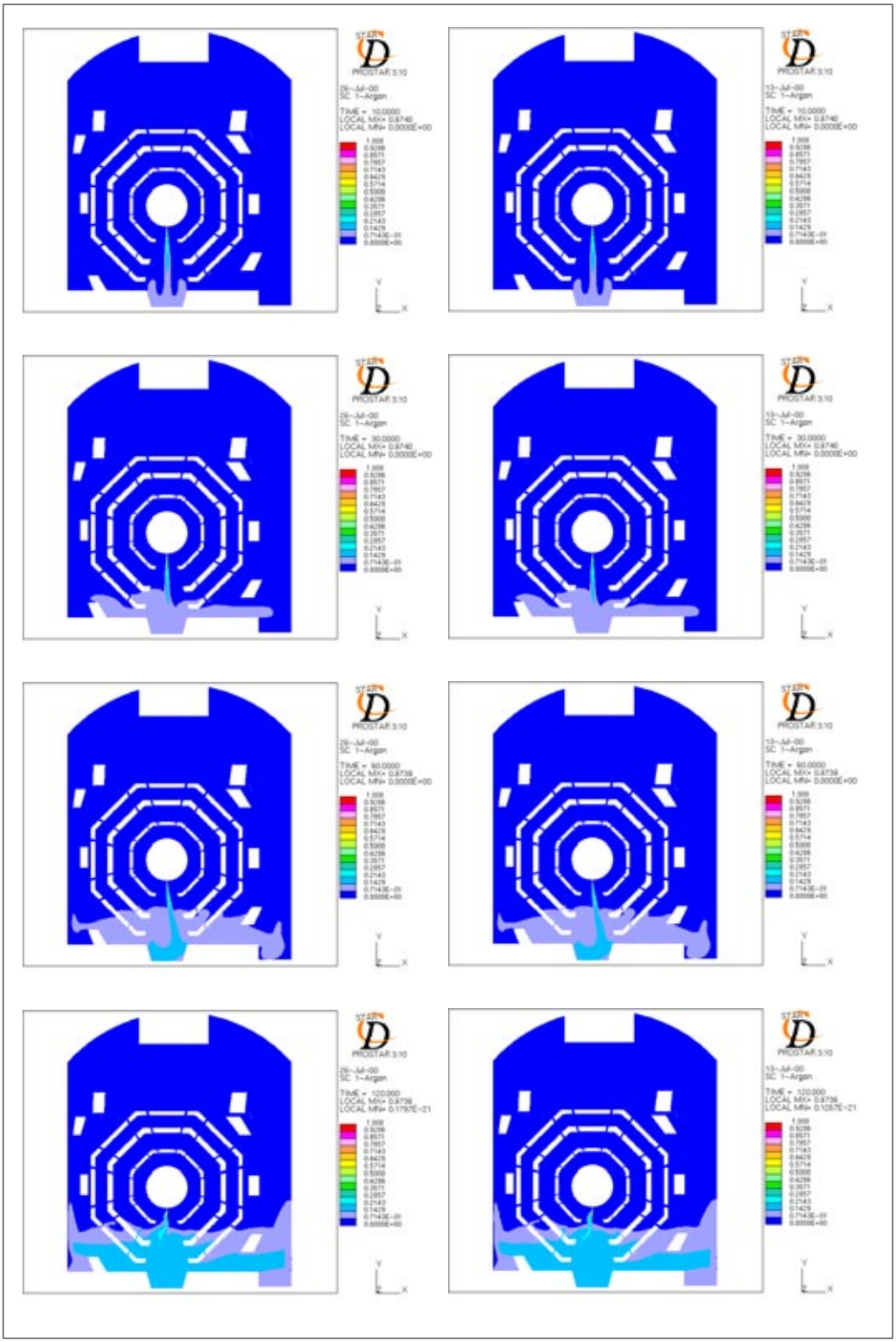

Figure A.27 Argon comparison between a model with an isothermal pit (left) and a model with an adiabatic pit

Isothermal vs Adiabatic Pit

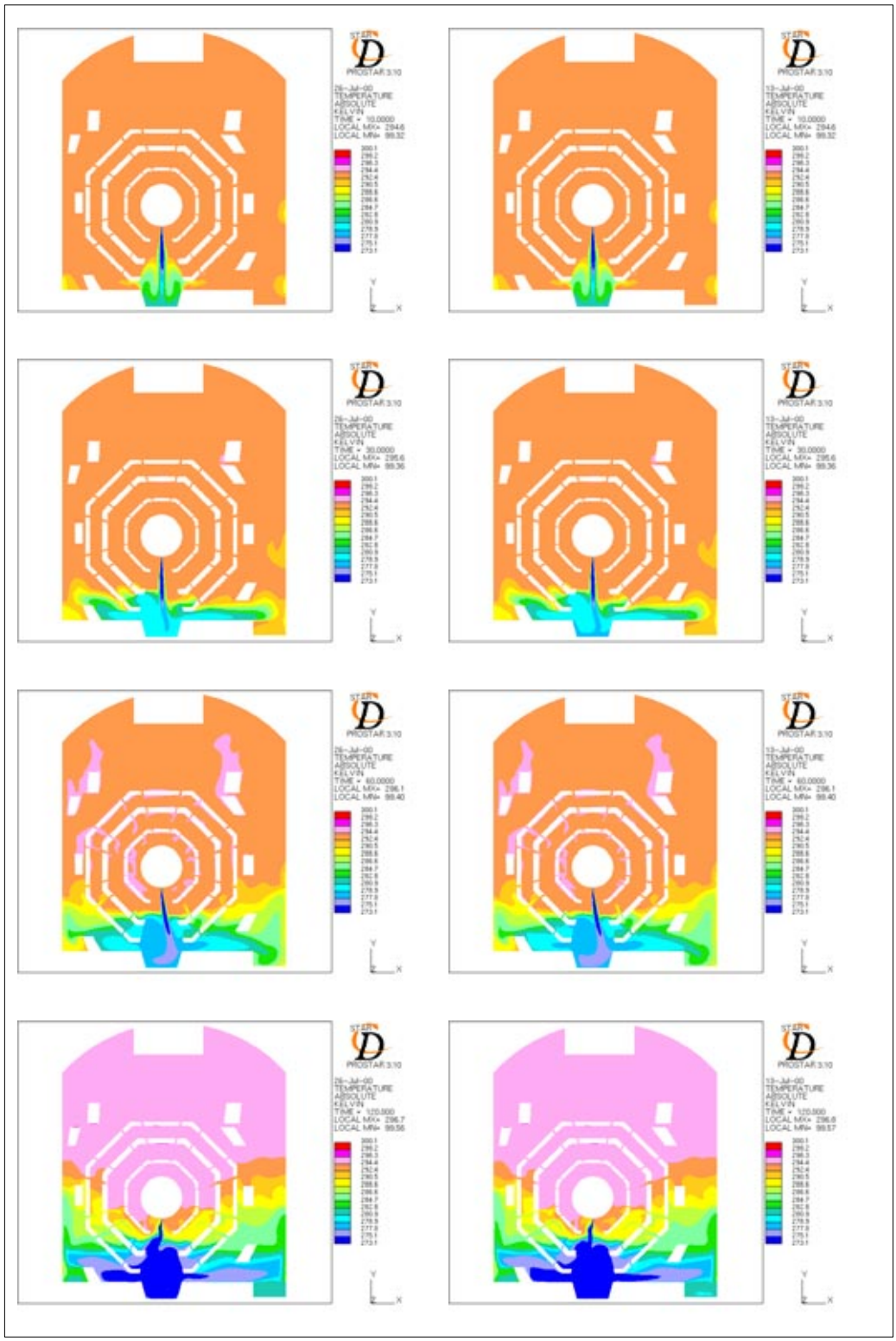

Figure A.28 Temperature comparison between a model with an isothermal pit (left) and a model with an adiabatic pit

Appendix B

Liquid Argon Spill Tests Figures

In this Appendix we collect all kind of data related to the Liquid Argon Spill Tests, described in Chapter 5. We show the results of the simulations previous to the tests as well as all the curves comparing the simulations and the experimental data, for the different models implemented.

B.1 Previous simulations

B.1.1 Flow of 11,13 l LAr/min.

Q	**11,13 l LAr/min**				
Geometry	**Test scenario**				
Energy Sinks	**Non**				
Boundaries	*v (m/s)*	*k (m^2/s^2)*	*ε (m^2/s^3)*	*T (K)*	*ρ (kg/m^3)*
Argon Inlet	0,5	0,0037	0,0187	90	5,3375
Exhaust fan	0,164	$4{,}070\ 10^{-4}$	$4{,}309\ 10^{-5}$	291,15	1,2
Ceiling extraction	0,20	0,0006	1,446 10-^{5}	291,15	1,2
Right and left diffusors	0,185	$5{,}144\ 10^{-4}$	$1{,}836\ 10^{-5}$	290	1,2
Walls	290,6 K Isothermal				
Heat Load	131,6 W / m^2 Constant heat flux				
Turbulence Model	K - E / R N G				
Differential schemes	*u,v*	*KE*	*ε*	*T*	*ρ*
Time	F u l l y I m p l i c i t				
Space	UD	UD	UD	UD	CD 0,8
Control					
Piso Correctors	3 to 5				
Max. COU number	0,3				
Mean COU number	0,05 to 0,1				
HDIFF	0,2 to 1 W				
Residual tolerance	0,01 for u,v,T,KE,ε,ρ / 0,001 for P				
Under-relaxation for P	0,8				
Relaxation factors	v-0,7 / KE-0,7 / P-1,0 / T-0,95 / ρ-0,5				
Precision	Double				
Simulated time	10 minutes				
Folder	EXPER 4 / Alpha				

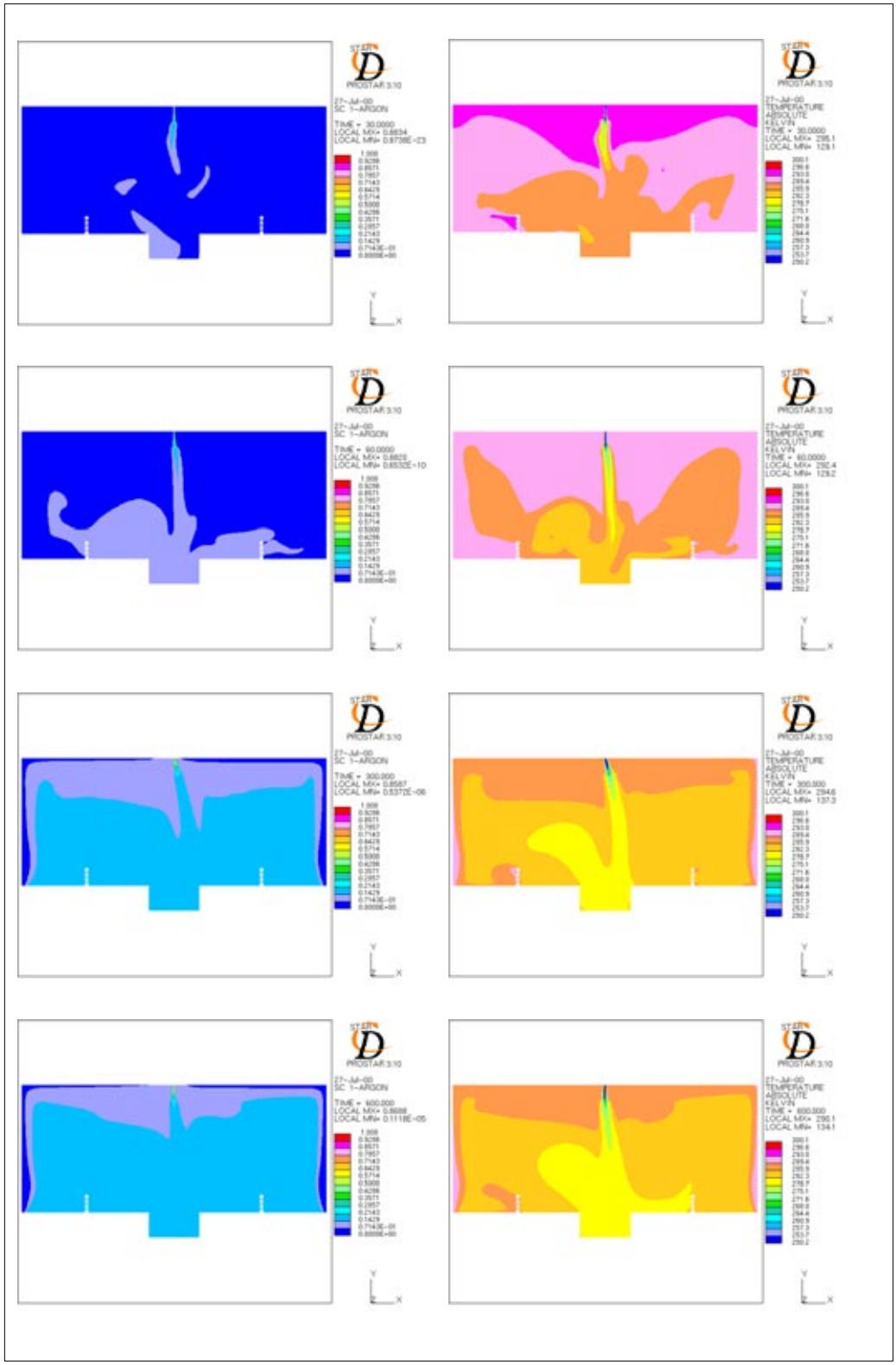

Figure 7.1 Argon concentration and Temperature for a flow of 11,13 l LAr/min. 30,60,300 and 600 s after the spill

B.1.2 Flow of 15,6 l LAr/min.

Q	**15,6 l LAr/min**				
Geometry	**Test scenario**				
Energy Sinks	**Non**				
Boundaries	*v (m/s)*	*k (m^2/s^2)*	*ε (m^2/s^3)*	*T (K)*	*ρ (kg/m^3)*
Argon Inlet	0,7	0,0073	0,0495	90	5,3375
Exhaust fan	0,164	$4{,}070\ 10^{-4}$	$4{,}309\ 10^{-5}$	291,15	1,2
Ceiling extraction	0,2	0,0006	1,446 10-^{5}	291,15	1,2
Right and left diffusors	0,185	$5{,}144\ 10^{-4}$	$1{,}836\ 10^{-5}$	290	1,2
Walls	290,6 K Isothermal				
Heat Load	131,6 W / m^2 Constant heat flux				
Turbulence Model	K - E / R N G				
Differential schemes	*u,v*	*KE*	*ε*	*T*	*ρ*
Time	Fully Implicit				
Space	UD	UD	UD	UD	CD 0,8
Control					
Piso Correctors	3 to 6				
Max. COU number	0,2				
Mean COU number	0,02				
HDIFF	0 to 0,9				
Residual tolerance	0,01 for u,v,T,KE,ε,ρ / 0,001 for P				
Under-relaxation for P	0,8				
Relaxation factors	v-0,7 / KE-0,7 / P-1,0 / T-0,95 / ρ-0,5				
Precision	Double				
Simulated time	10 minutes				
Folder	EXPER 3 / Alpha				

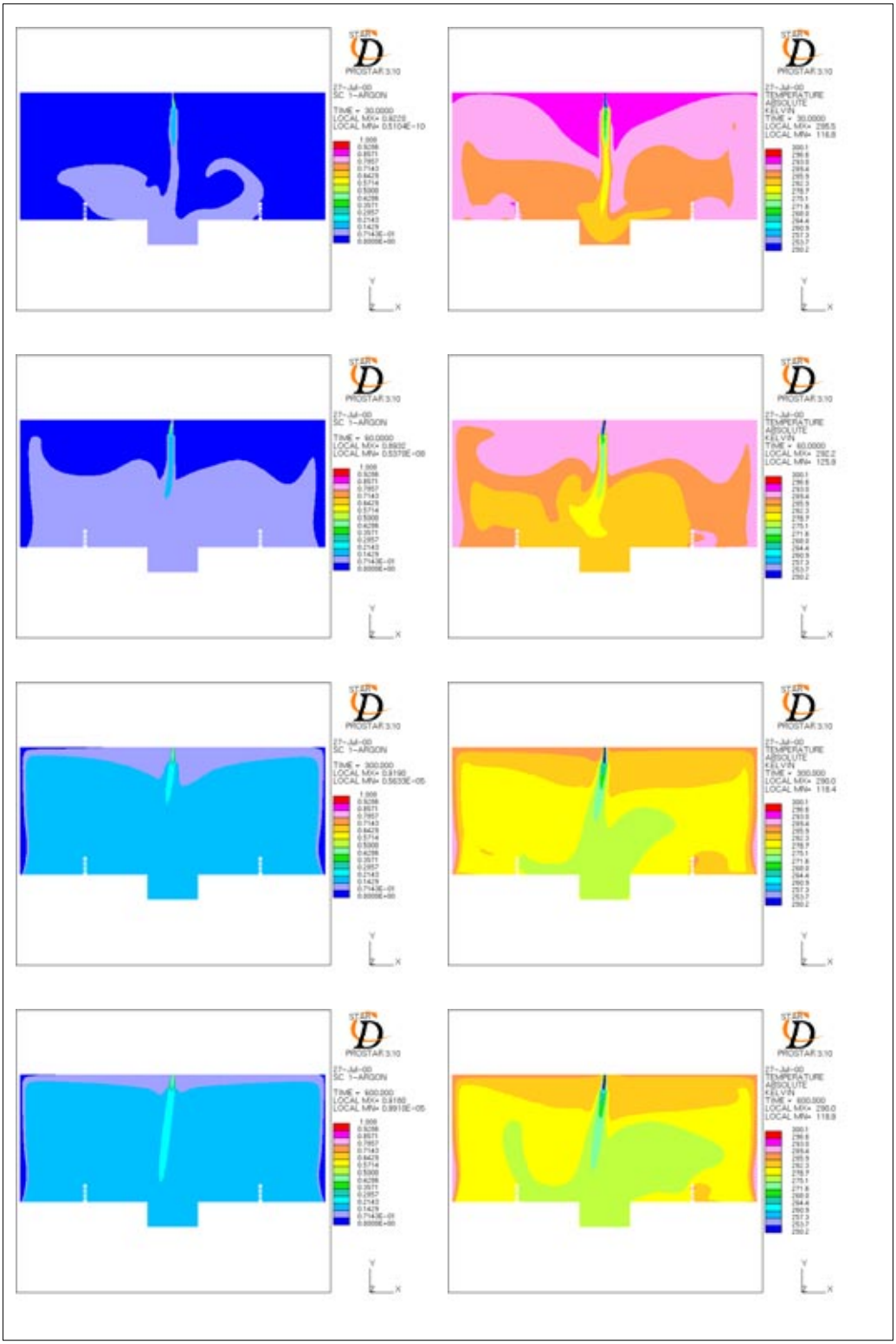

Figure B.1 Argon concentration and Temperature for a flow of 15,6 l LAr/min. 30,60,300 and 600 s after the spill

B.1.3 Flow of 22,26 l LAr/min.

Q	**22,26 l LAr/min**				
Geometry	**Test scenario**				
Energy Sinks	**Non**				
Boundaries	*v (m/s)*	*k (m^2/s^2)*	*ε (m^2/s^3)*	*T (K)*	*ρ (kg/m^3)*
Argon Inlet	1,0	0,0150	0,1446	90	5,3375
Exhaust fan	0,164	$4{,}070\ 10^{-4}$	$4{,}309\ 10^{-5}$	291,15	1,2
Ceiling extraction	0,2	0,0006	1,446 10-^{5}	291,15	1,2
Right and left diffusors	0,185	$5{,}144\ 10^{-4}$	$1{,}836\ 10^{-5}$	290	1,2
Walls	290,6 K Isothermal				
Heat Load	131,6 W / m^2 Constant heat flux				
Turbulence Model	K - E / R N G				
Differential schemes	*u,v*	*KE*	*ε*	*T*	*ρ*
Time	Fully Implicit				
Space	UD	UD	UD	UD	CD 0,8
Control					
Piso Correctors	3 to 4				
Max. COU number	0,1 to 2,5				
Mean COU number	0,05 to 0,2				
HDIFF	0,2 to 1 W				
Residual tolerance	0,01 for u,v,T,KE,ε,ρ / 0,001 for P				
Under-relaxation for P	0,8				
Relaxation factors	v-0,7 / KE-0,7 / P-1,0 / T-0,95 / ρ-0,5				
Precision	Double				
Simulated time	10 minutes				
Folder	EXPER 2 / Alpha				

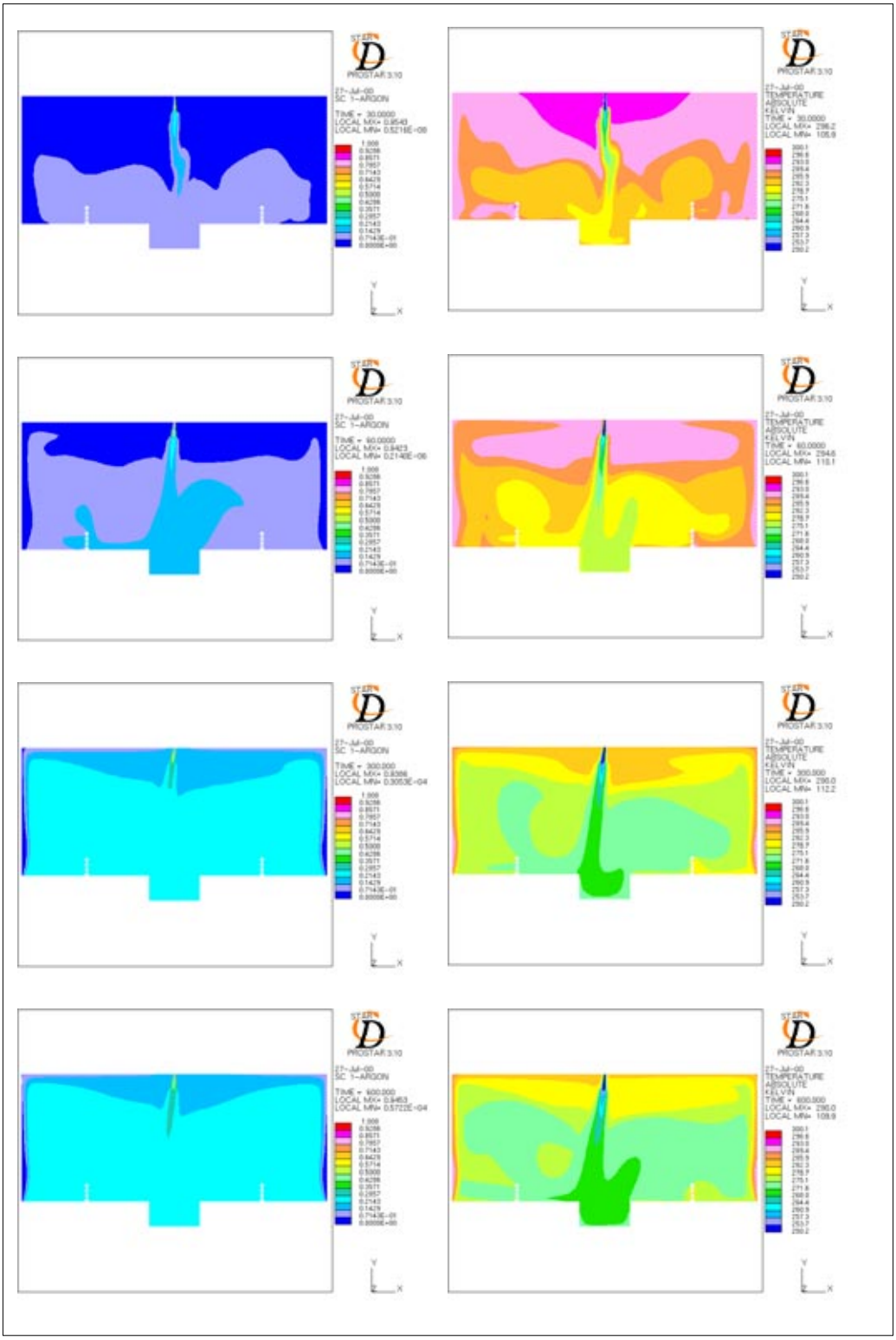

Figure 7.2 Argon concentration and Temperature for a flow of 22,26 l LAr/min. 30,60,300 and 600 s after the spill

B.1.4 Flow of 44,52 l LAr/min.

Q	**44,52 l LAr/min**				
Geometry	**Test scenario**				
Energy Sinks	**Non**				
Boundaries	*v (m/s)*	*k (m^2/s^2)*	*ε (m^2/s^3)*	*T (K)*	*ρ (kg/m^3)*
Argon Inlet	2,0	0,06	1,1568	90	5,3375
Exhaust fan	0,164	$4{,}070\ 10^{-4}$	$4{,}309\ 10^{-5}$	291,15	1,2
Ceiling extraction	0,2	0,0006	1,446 10-^{5}	291,15	1,2
Right and left diffusors	0,185	$5{,}144\ 10^{-4}$	$1{,}836\ 10^{-5}$	290	1,2
Walls	290,6 K Isothermal				
Heat Load	131,6 W / m^2 Constant heat flux				
Turbulence Model	K - E / R N G				
Differential schemes	*u,v*	*KE*	*ε*	*T*	*ρ*
Time	Fully Implicit				
Space	UD	UD	UD	UD	CD 0,8
Control					
Piso Correctors	3 to 7				
Max. COU number	3 to 6				
Mean COU number	0,2 to 0,4				
HDIFF	0,7 to 3 W				
Residual tolerance	0,01 for u,v,T,KE,ε,ρ / 0,001 for P				
Under-relaxation for P	0,8				
Relaxation factors	v-0,7 / KE-0,7 / P-1,0 / T-0,95 / ρ-0,5				
Precision	Double				
Simulated time	10 minutes				
Folder	EXPER 1 / Alpha				

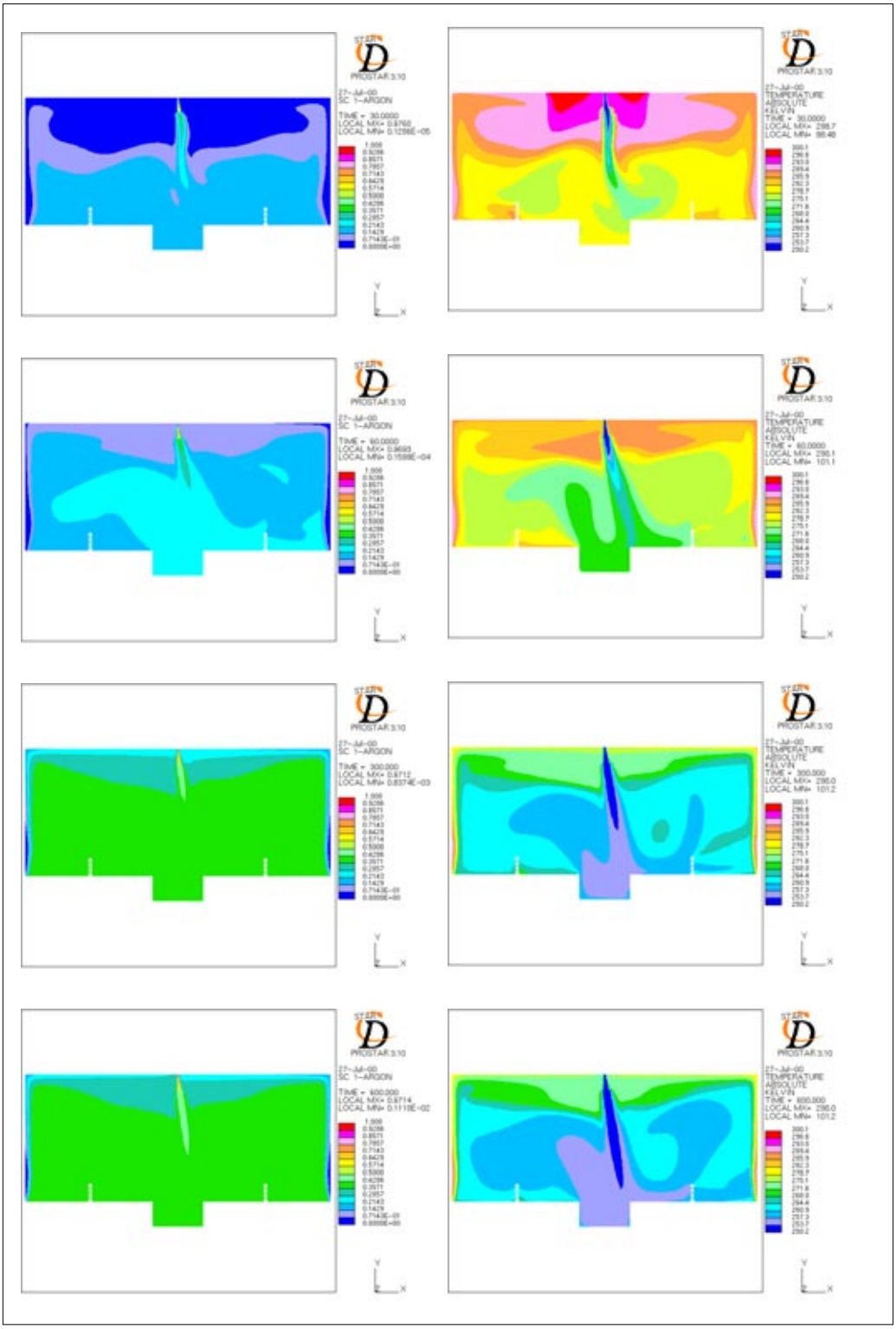

Figure 7.3 Argon concentration and Temperature for a flow of 44,52 l LAr/min. 30,60,300 and 600 s after the spill

B.1.5 Flow of 66,78 l LAr/min.

Q	**66,78 l LAr/min**				
Geometry	**Test scenario**				
Energy Sinks	**Non**				
Boundaries	*v (m/s)*	*k (m^2/s^2)*	*ε (m^2/s^3)*	*T (K)*	*ρ (kg/m^3)*
Argon Inlet	3,0	0,135	3,904	90	5,3375
Exhaust fan	0,164	$4{,}070\ 10^{-4}$	$4{,}309\ 10^{-5}$	291,15	1,2
Ceiling extraction	0,2	0,0006	1,446 10-^{5}	291,15	1,2
Right and left diffusors	0,185	$5{,}144\ 10^{-4}$	$1{,}836\ 10^{-5}$	290	1,2
Walls	290,6 K Isothermal				
Heat Load	131,6 W / m^2 Constant heat flux				
Turbulence Model	K - E / R N G				
Differential schemes	*u,v*	*KE*	*ε*	*T*	*ρ*
Time	Fully Implicit				
Space	UD	UD	UD	UD	CD 0,8
Control					
Piso Correctors	3 to 4				
Max. COU number	2,8 to 3				
Mean COU number	0,2				
HDIFF	1 to 2,5 W				
Residual tolerance	0,01 for u,v,T,KE,ε,ρ / 0,001 for P				
Under-relaxation for P	0,8				
Relaxation factors	v-0,7 / KE-0,7 / P-1,0 / T-0,95 / ρ-0,5				
Precision	Double				
Simulated time	10 minutes				
Folder	EXPER 0 / Alpha				

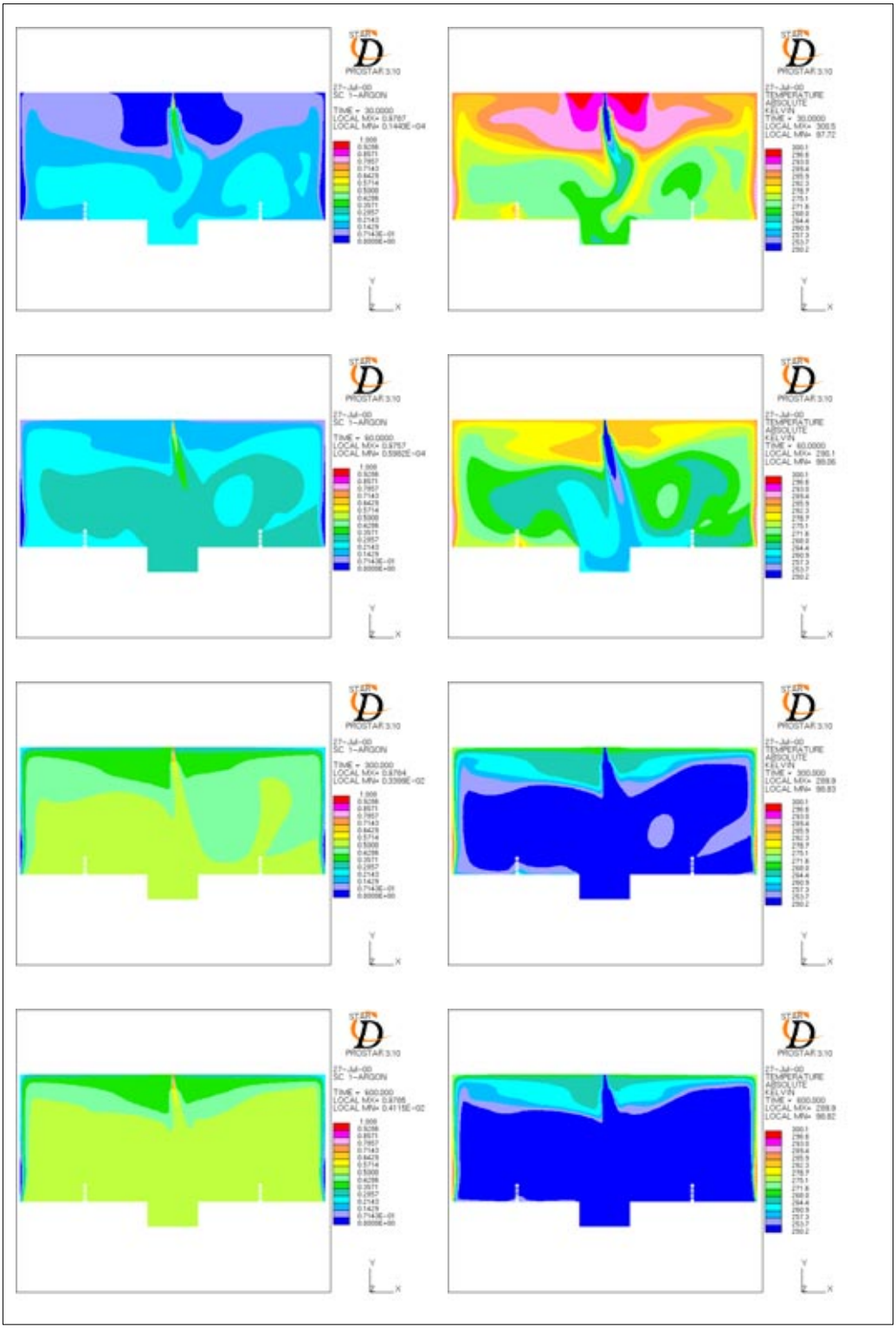

Figure 7.4 Argon concentration and Temperature for a flow of 66,78 l LAr/min. 30,60,300 and 600 s after the spill

B.2 Test simulations

B.2.1 Test 4. 4,99 l LAr/min.

TEST 4
One-Phase Flow

Q	**4,99 l LAr/min**				
Geometry	**Test scenario**				
Energy Sinks	**Non**				
Boundaries	*v (m/s)*	*k (m^2/s^2)*	*ε (m^2/s^3)*	*T (K)*	*ρ (kg/m^3)*
Argon Inlet	0,224	$7{,}52\ 10^{-4}$	$1{,}62\ 10^{-3}$	90	5,337
Exhaust fan	0,412	$2{,}55\ 10^{-3}$	$1{,}35\ 10^{-3}$	299	1,2
Ceiling extraction	0,197	$5{,}85\ 10^{-4}$	$1{,}40\ 10^{-5}$	301	1,2
Right and left diffusors	0,161	$3{,}91\ 10^{-4}$	$1{,}0\ 10^{-5}$	300	1,2
Walls	295,7 K Isothermal				
Heat Load	131,6 W / m^2 Constant heat flux				
Turbulence Model	K - E / R N G				
Differential schemes	*u,v*	*KE*	*ε*	*T*	*ρ*
Time	F u l l y I m p l i c i t				
Space	UD	UD	UD	UD	CD 0,8
Control					
Piso Correctors	3 to 6				
Max. COU number	0,13 to 0,56				
Mean COU number	0,02 to 0,06				
HDIFF	0 to 0,2 W				
Residual tolerance	0,01 for u,v,T,KE,ε,ρ / 0,001 for P				
Under-relaxation for P	0,8				
Relaxation factors	v-0,7 / KE-0,7 / P-1,0 / T-0,95 / ρ-0,5				
Precision	Double				
Simulated time	10 minutes and 10 seconds				
Folder	TEST 4 / Alpha				

TEST 4
One-Phase Flow

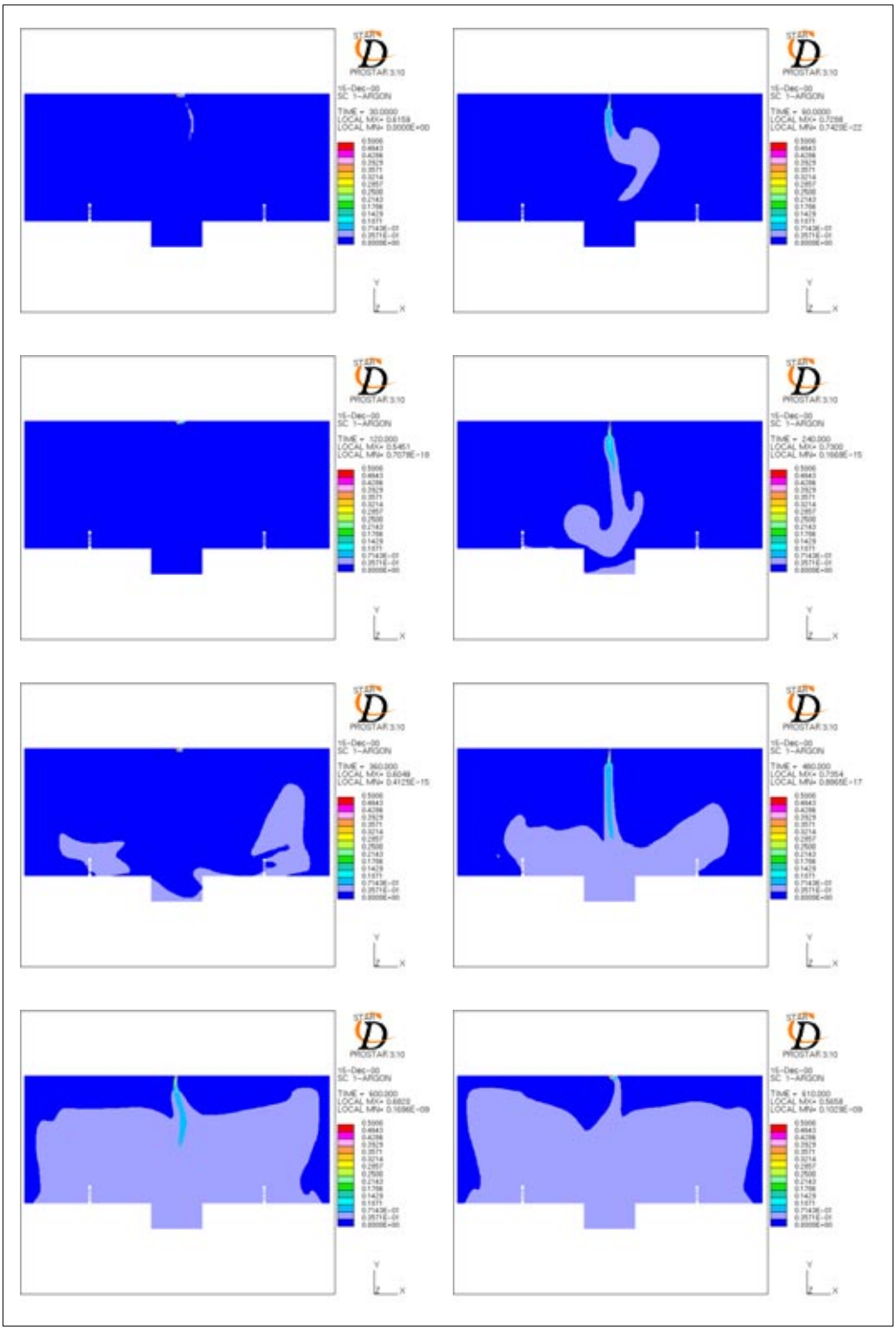

Figure B.2 Argon concentration 30,60,120,240,360,480,600 and 610 s after the spill

TEST 4
One-Phase Flow

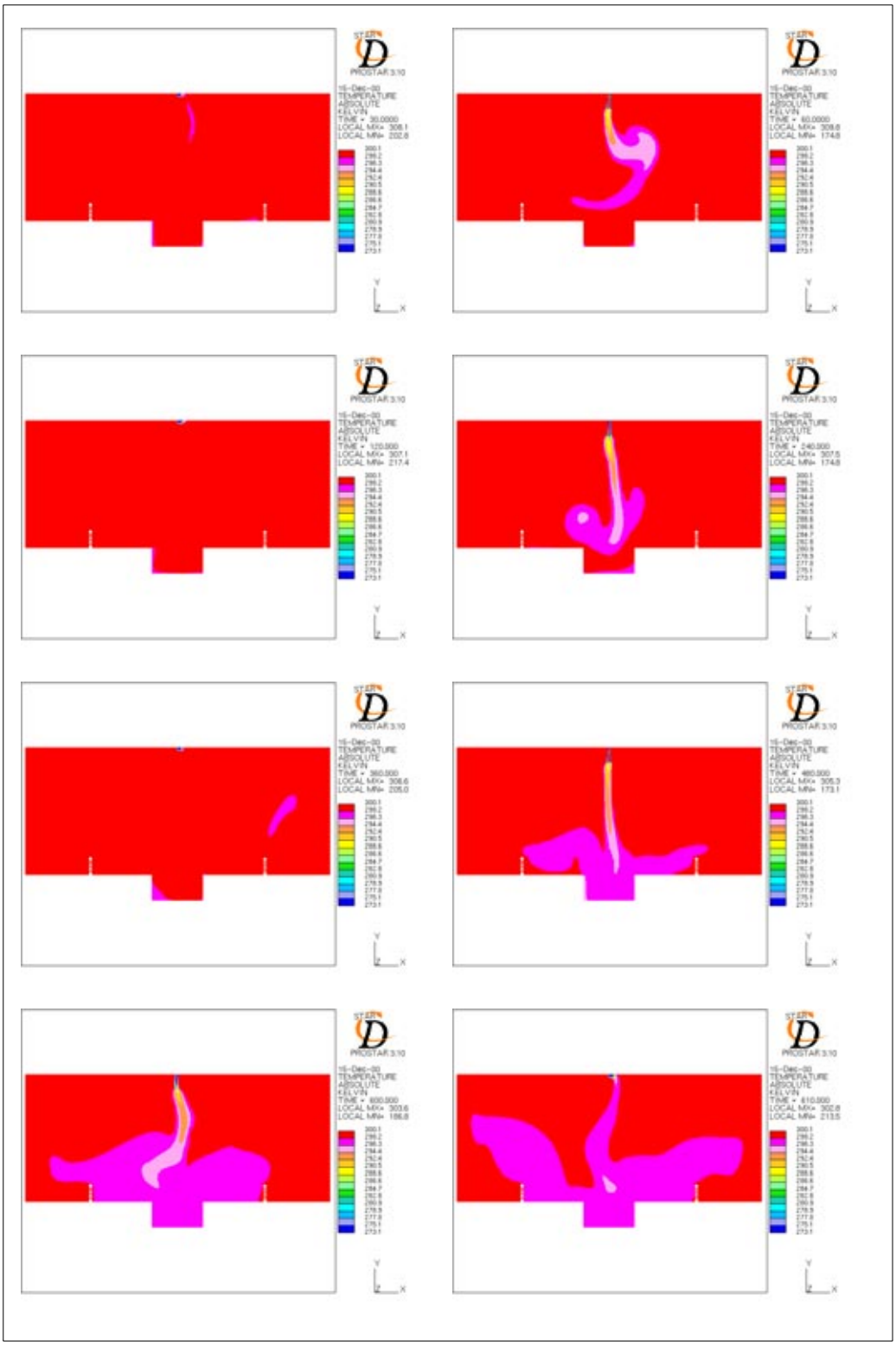

Figure B.3 Temperature distribution 30,60,120,240,360,480,600 and 610 s after the spill

TEST4
One-Phase with Energy Sinks

Q	**4,99 l LAr/min**				
Geometry	**Test scenario**				
Energy Sinks	**Yes: 3,353 kW / 1.397 W/m^3**				
Boundaries	*v (m/s)*	*k (m^2/s^2)*	*ε (m^2/s^3)*	*T (K)*	*ρ (kg/m^3)*
Argon Inlet	0,224	7,52 10^{-4}	1,62 10^{-3}	90	5,337
Exhaust fan	0,412	2,55 10^{-3}	1,35 10^{-3}	299	1,190
Ceiling extraction	0,197	5,85 10^{-4}	1,40 10^{-5}	301	1,190
Right and left diffusors	0,161	3,91 10^{-4}	1,0 10^{-5}	300	1,190
Walls	295,7 K Isothermal				
Heat Load	131,6 W / m^2 Constant heat flux				
Turbulence Model	K - E / R N G				
Differential schemes	*u,v*	*KE*	*ε*	*T*	*ρ*
Time	F u l l y I m p l i c i t				
Space	UD	UD	UD	UD	CD 0,8
Control					
Piso Correctors	3 to 5				
Max. COU number	1,3 to 2				
Mean COU number	0,1 to 0,2				
HDIFF	0,1 to 0,5 W				
Residual tolerance	0,01 for u,v,T,KE,ε,ρ / 0,001 for P				
Under-relaxation for P	0,8				
Relaxation factors	v-0,7 / KE-0,7 / P-1,0 / T-0,95 / ρ-0,5				
Precision	Double				
Simulated time	10 minutes and 10 seconds				
Folder	TEST SINKS 4 / Linux				

TEST 4
One-Phase with Energy Sinks

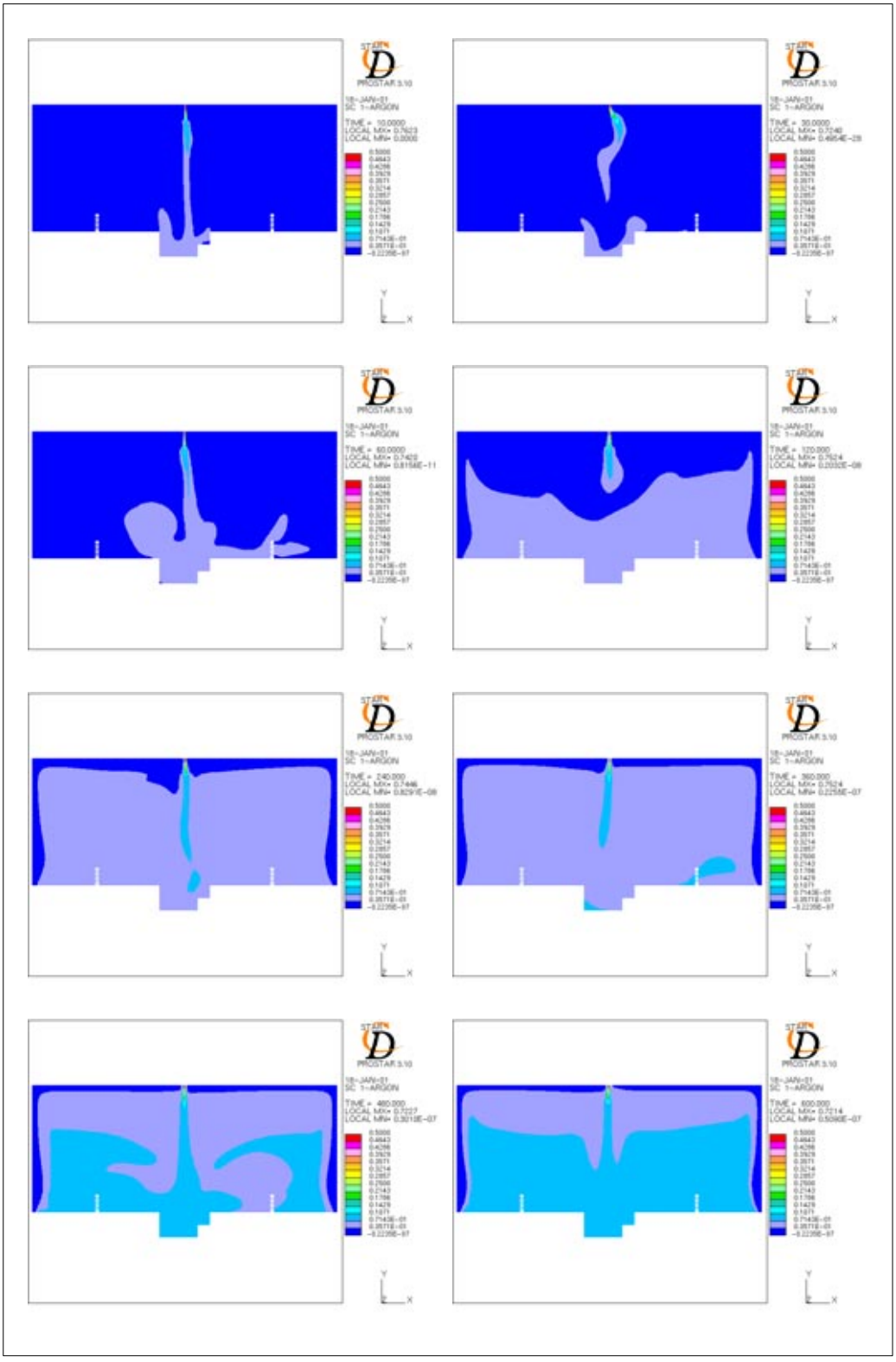

Figure B.4 Argon concentration distributions 10,30,60,120,240,360,480 and 600 s after the spill

TEST 4
One-Phase with Energy Sinks

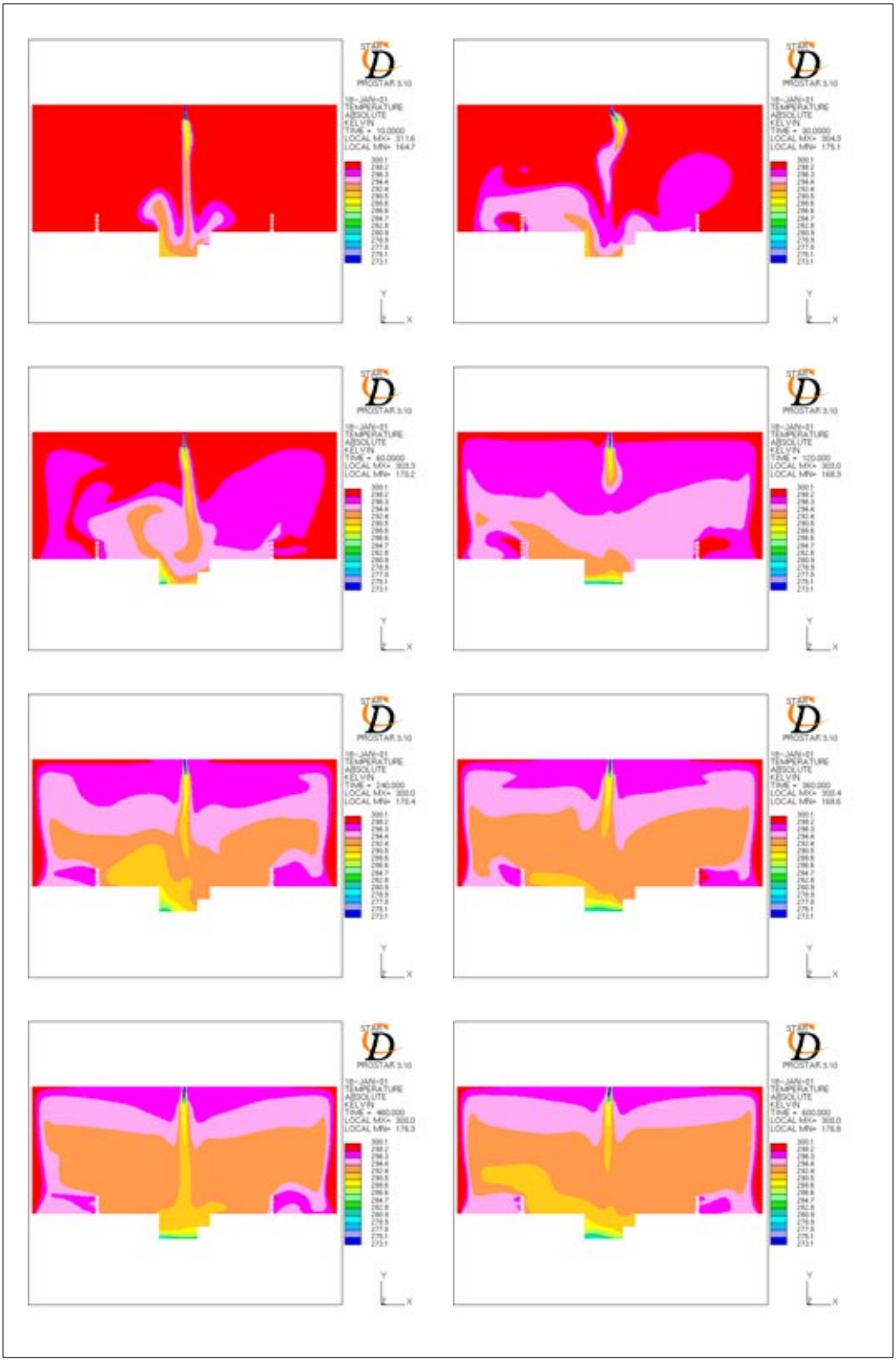

Figure B.5 Temperature distributions 10,30,60,120,240,360,480 and 600 s after the spill

TEST 4
Comparison

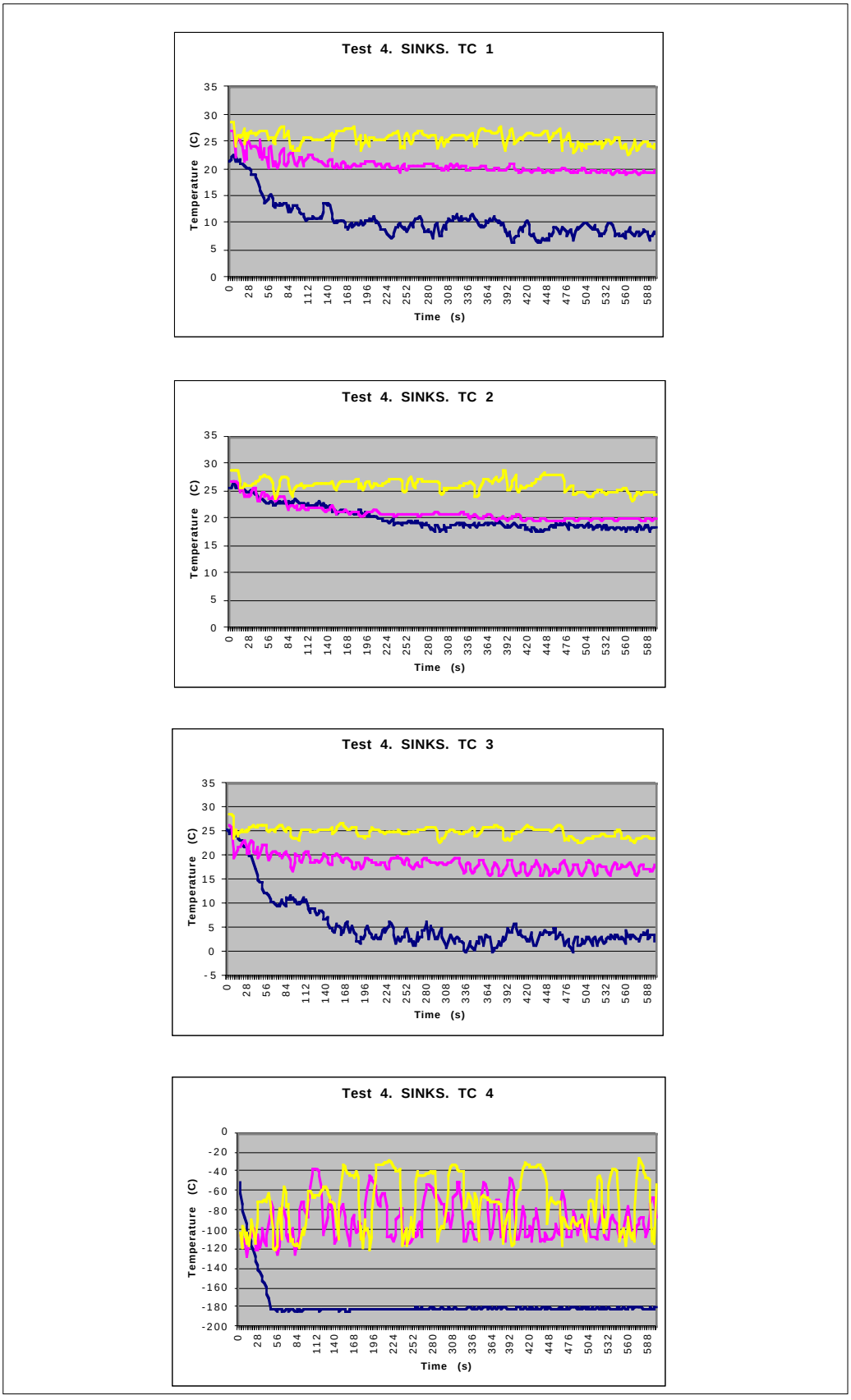

Figure B.6 Temperature comparison. Blue: Experiment, Yellow: One-phase, Pink: Energy sinks

TEST 4
Comparison

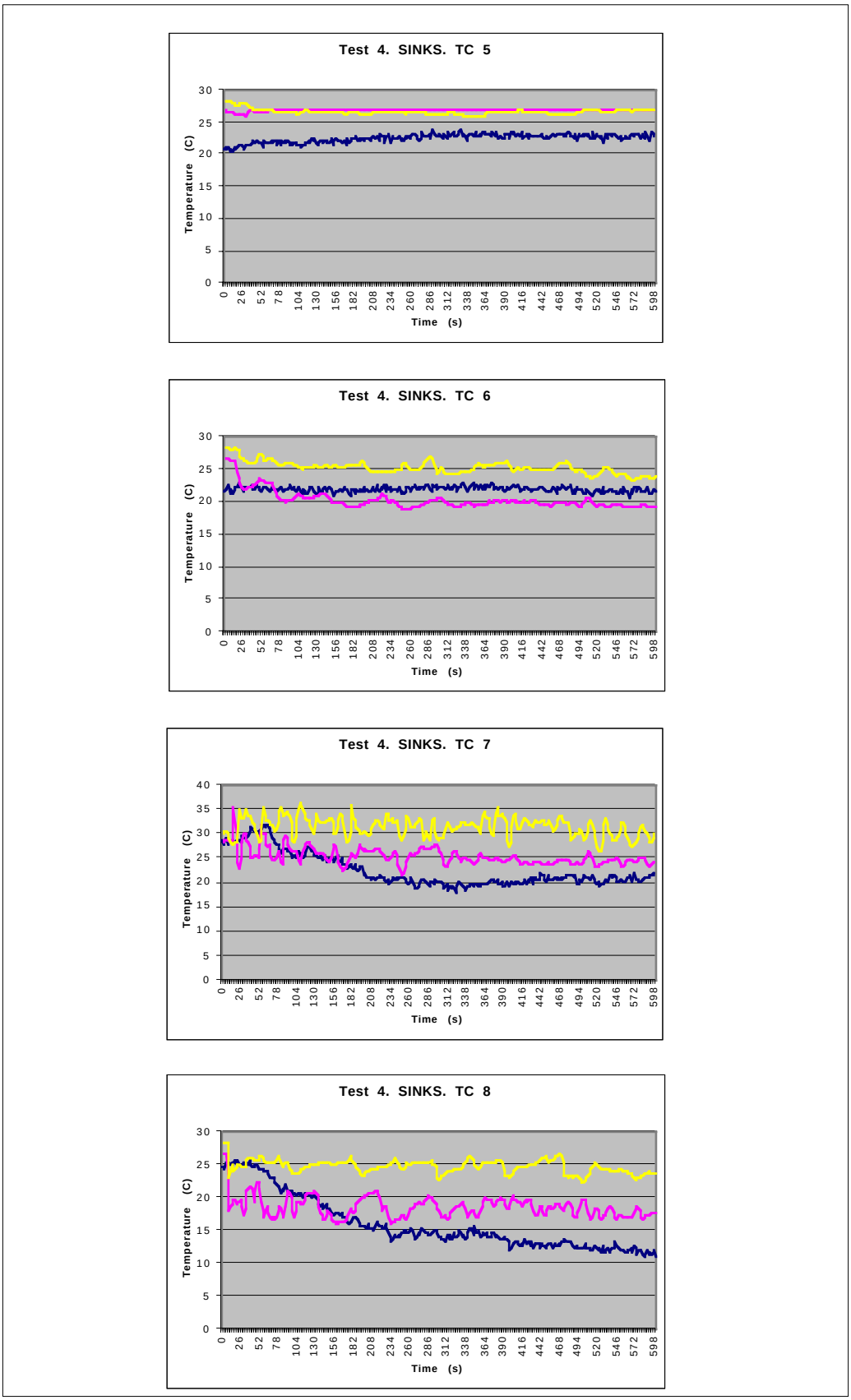

Figure B.7 Temperature comparison. Blue: Experiment, Yellow: One-phase, Pink: Energy sinks

TEST 4
Comparison

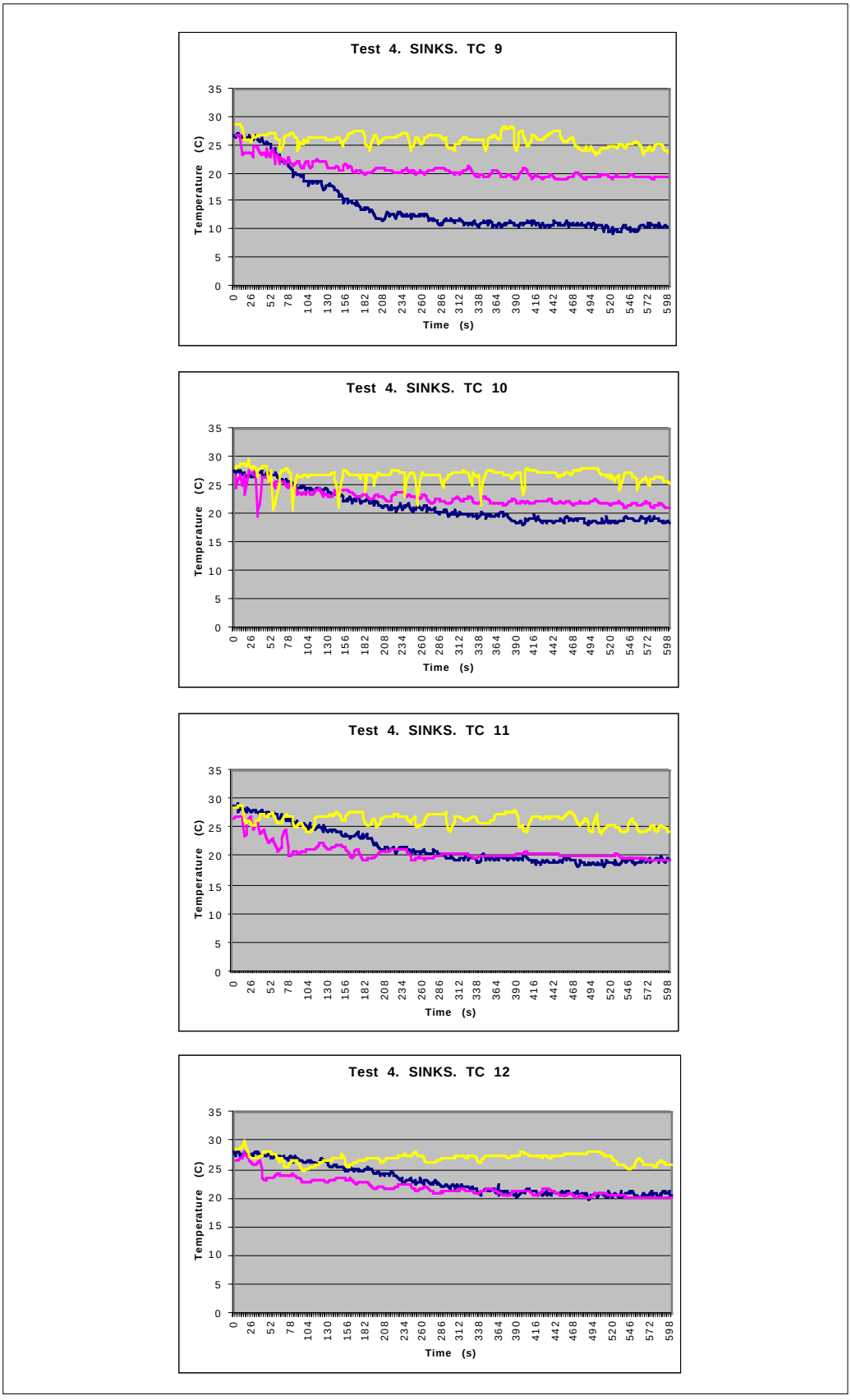

Figure B.8 Temperature comparison. Blue: Experiment, Yellow: One-phase, Pink: Energy sinks

TEST 4
Comparison

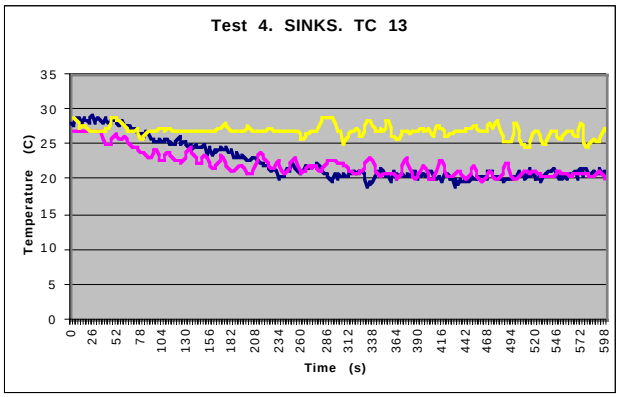

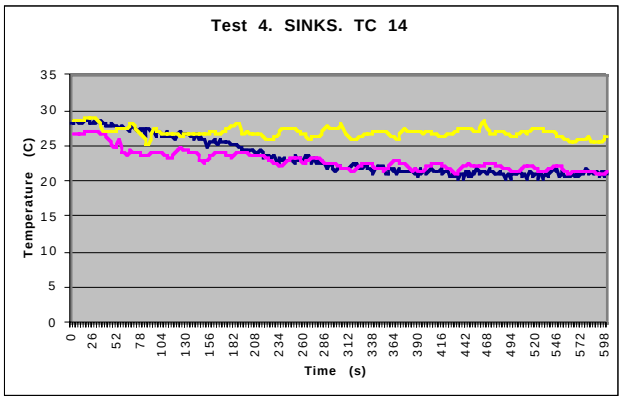

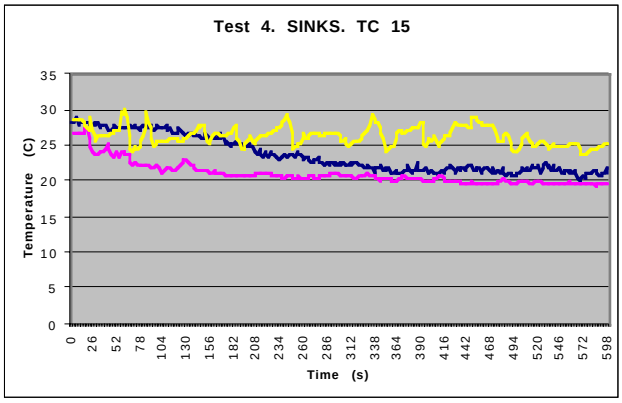

Figure B.9 Temperature comparison. Blue: Experiment, Yellow: One-phase, Pink: Energy sinks

TEST 4
Comparison

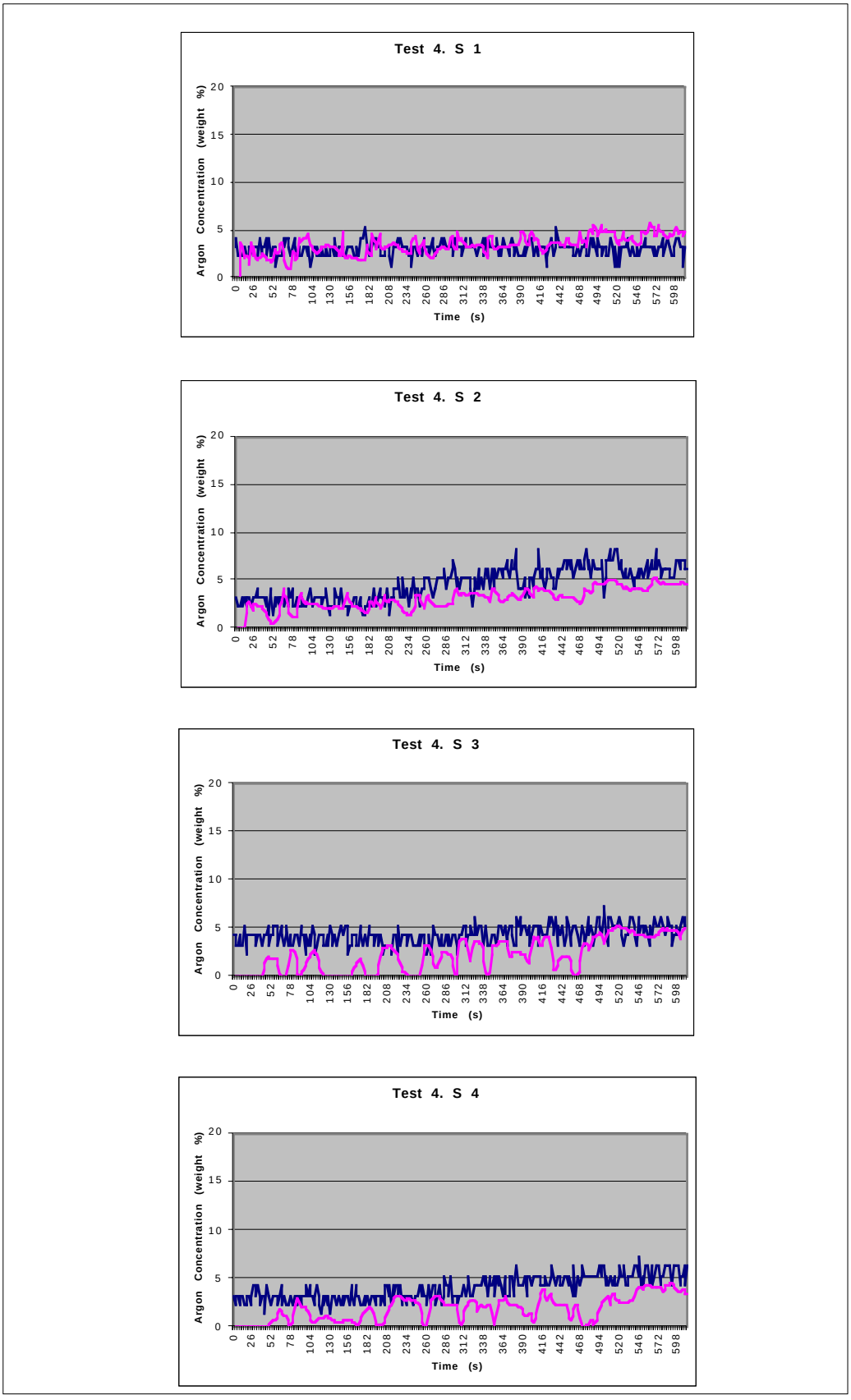

Figure B.10 Argon concentration comparison. Blue: Experiment; Pink: Energy sinks/One-phase

TEST 4
Comparison

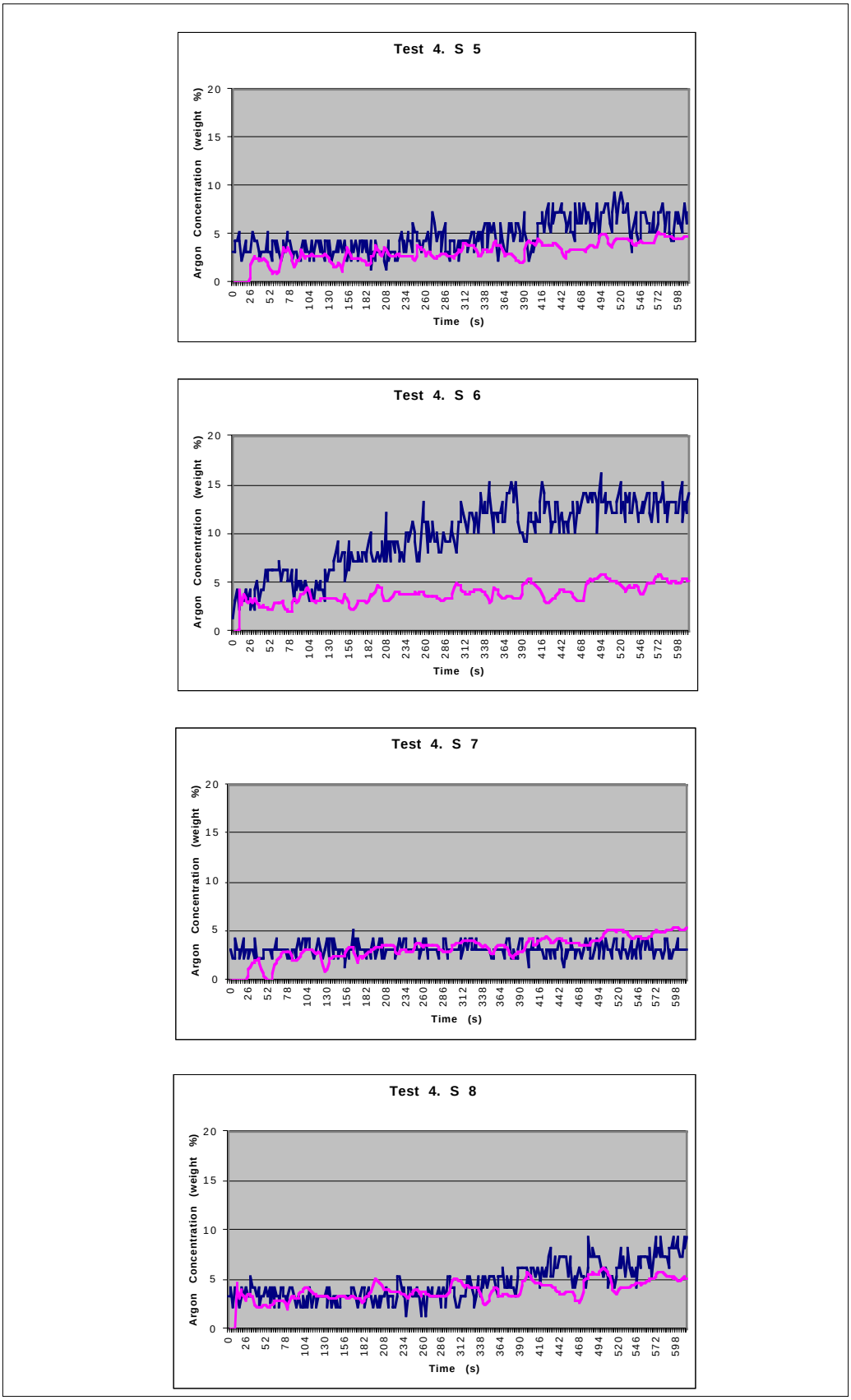

Figure B.11 Argon concentration comparison. Blue: Experiment; Pink: Energy sinks/One-phase

TEST 4
Comparison

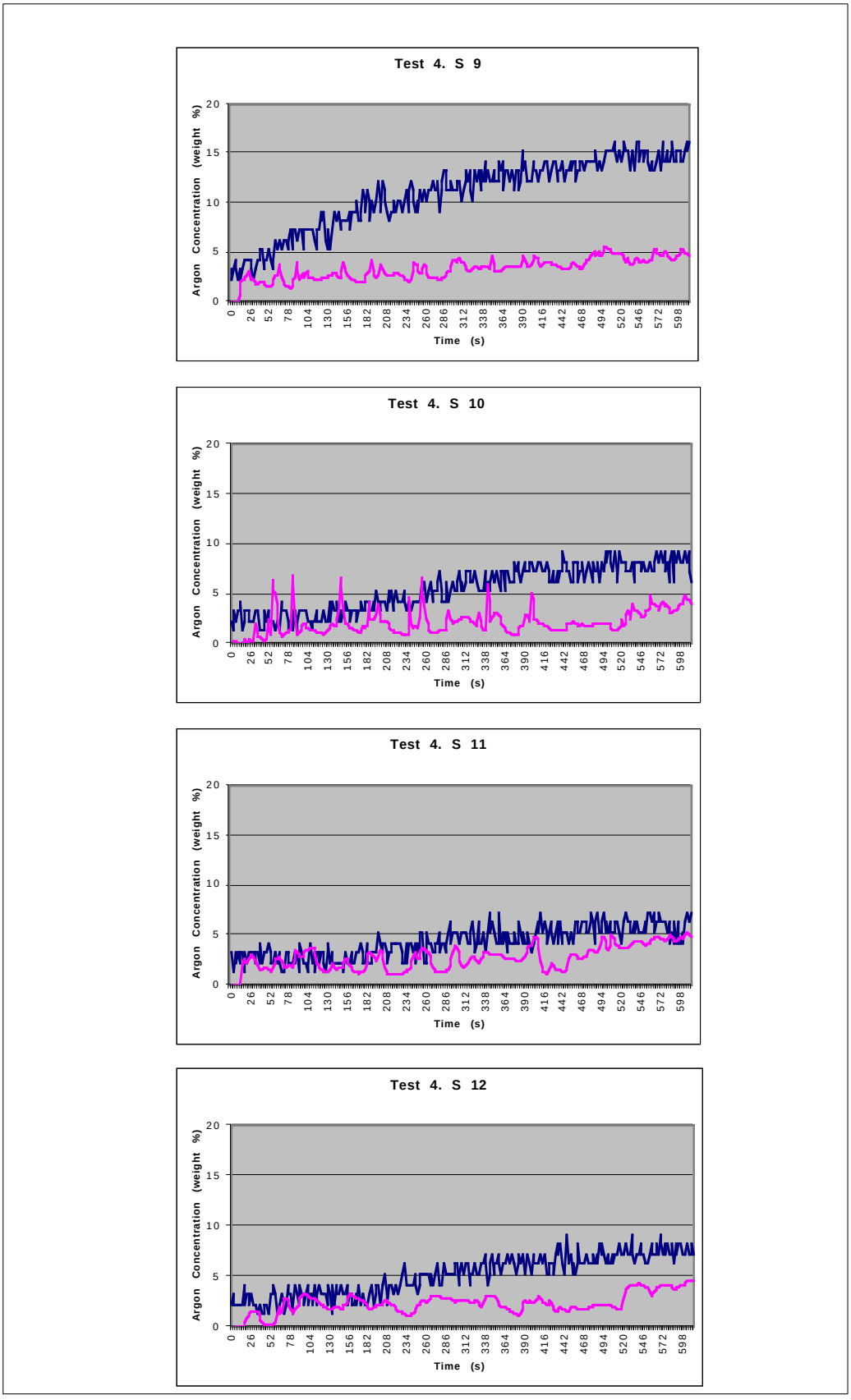

Figure B.12 Argon concentration comparison. Blue: Experiment; Pink: Energy sinks/One-phase

B.2.2 Test 5. 8,73 l LAr/min.

TEST 5*
One-Phase Flow

Q	**8,73 l LAr/min**				
Geometry	**Test scenario**				
Energy Sinks	**Non**				
Boundaries	*v (m/s)*	*k (m^2/s^2)*	*ε (m^2/s^3)*	*T (K)*	*ρ (kg/m^3)*
Argon Inlet	0,3921	$2{,}306\ 10^{-3}$	$8{,}714\ 10^{-3}$	90	5,337
Exhaust fan	No ventilation				
Ceiling extraction	0,0153	$3{,}54\ 10^{-6}$	$5{,}245\ 10^{-7}$	299	1,2
Right and left diffusors	No ventilation				
Walls	294,1 K Isothermal				
Heat Load	131,6 W / m^2 Constant heat flux				
Turbulence Model	K - E / R N G				
Differential schemes	*u,v*	*KE*	*ε*	*T*	*ρ*
Time	Fully Implicit				
Space	UD	UD	UD	UD	CD 0,8
Control					
Piso Correctors	3				
Max. COU number	0,5 to 1				
Mean COU number	0,05 to 0,1				
HDIFF	0,1 W				
Residual tolerance	0,01 for u,v,T,KE,ε,ρ / 0,001 for P				
Under-relaxation for P	0,8				
Relaxation factors	v-0,7 / KE-0,7 / P-1,0 / T-0,95 / ρ-0,5				
Precision	Double				
Simulated time	11 minutes and 12 seconds				
Folder	TEST 5 / Linux				

* During the performance of this test without ventilation we could appreciate a big quantity of argon cooling through the door. Besides, the ceiling extraction was difficult to evaluate in this case. Therefore it was difficult to model this test. This results in bad predictions from the simulation, as we see in the Temperature evolution we show in the following pages. This is the reason why we do not show the argon concentration curves .

TEST 5
One-Phase Flow

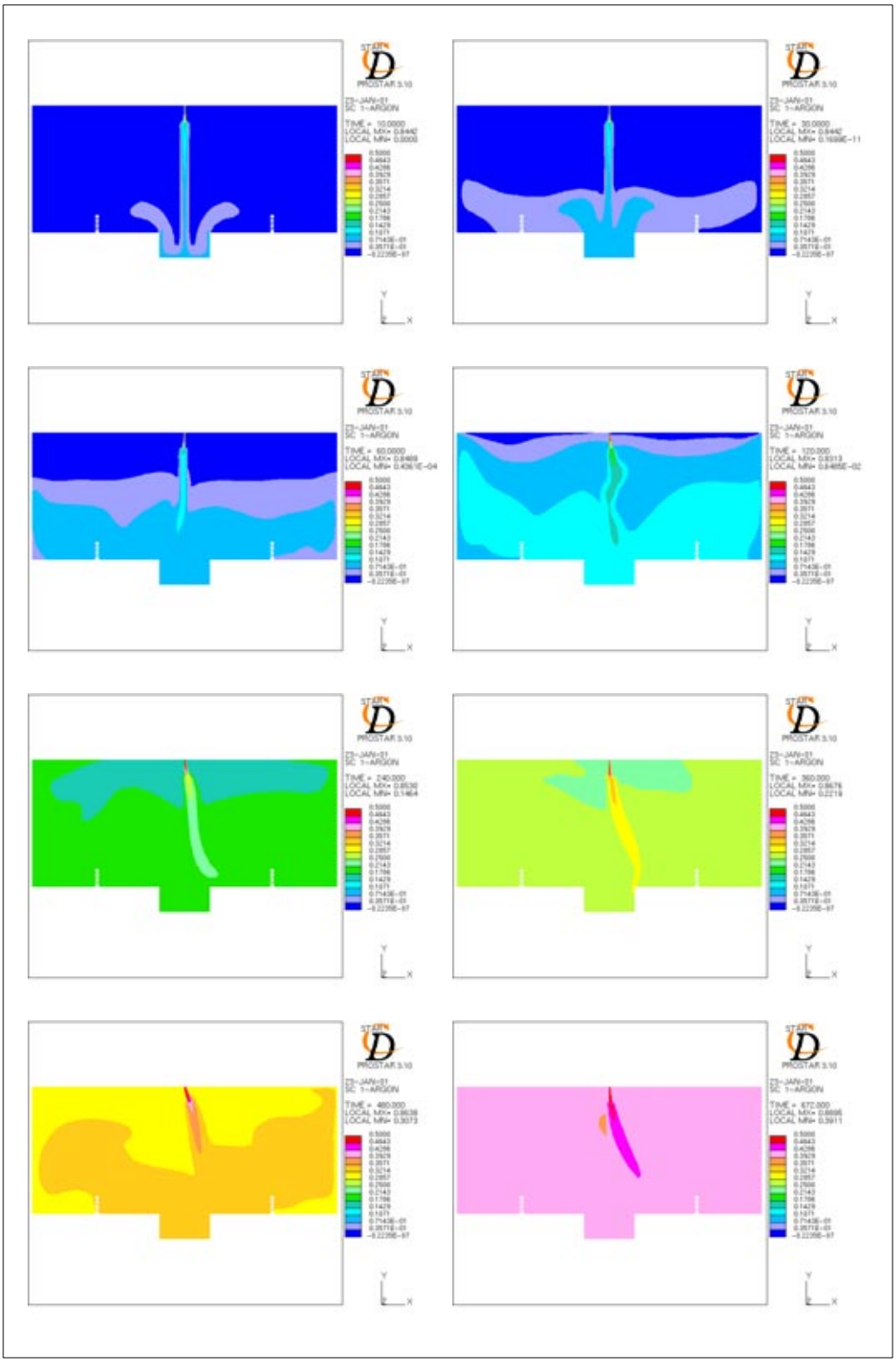

Figure B.13 Argon concentration distribution 10,30,60,120,240,360,480 and 672 s after the spill

TEST 5
One-Phase Flow

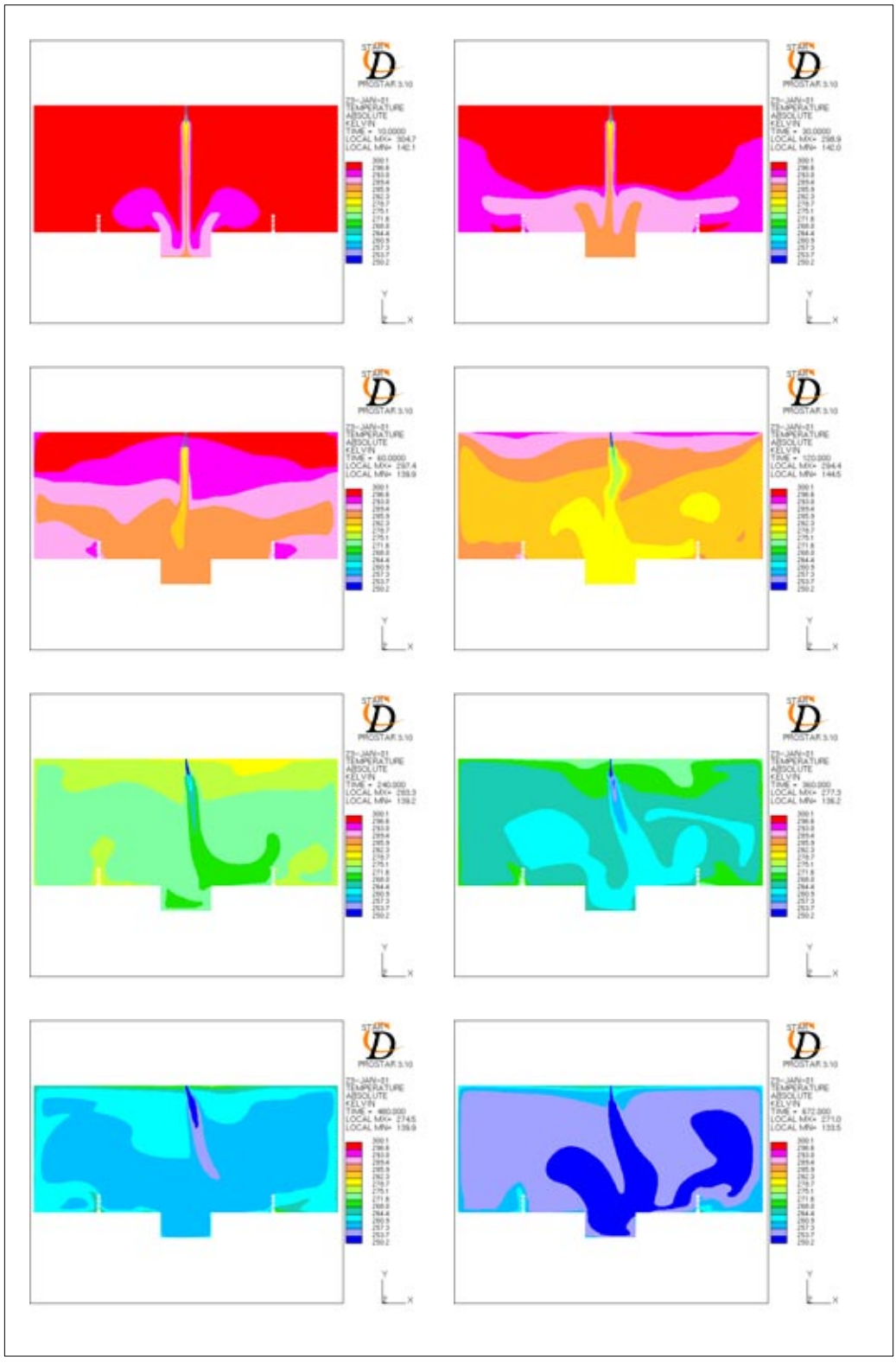

Figure B.14 Temperature distribution 10,30,60,120,240,360,480 and 672 s after the spill

TEST 5
Comparison

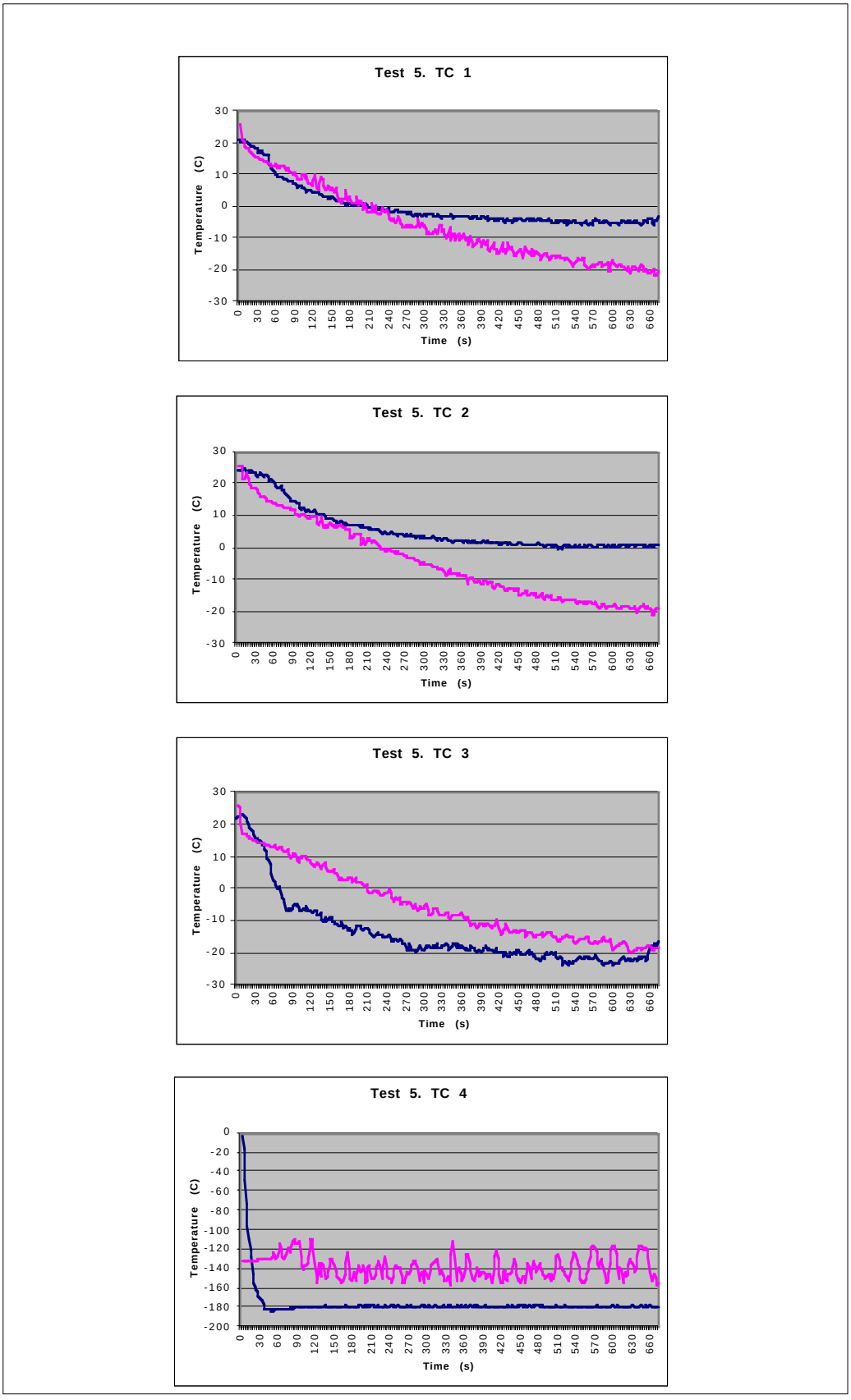

Figure B.15 Temperature comparison. Blue: Experiment; Pink: One-phase

TEST 5
Comparison

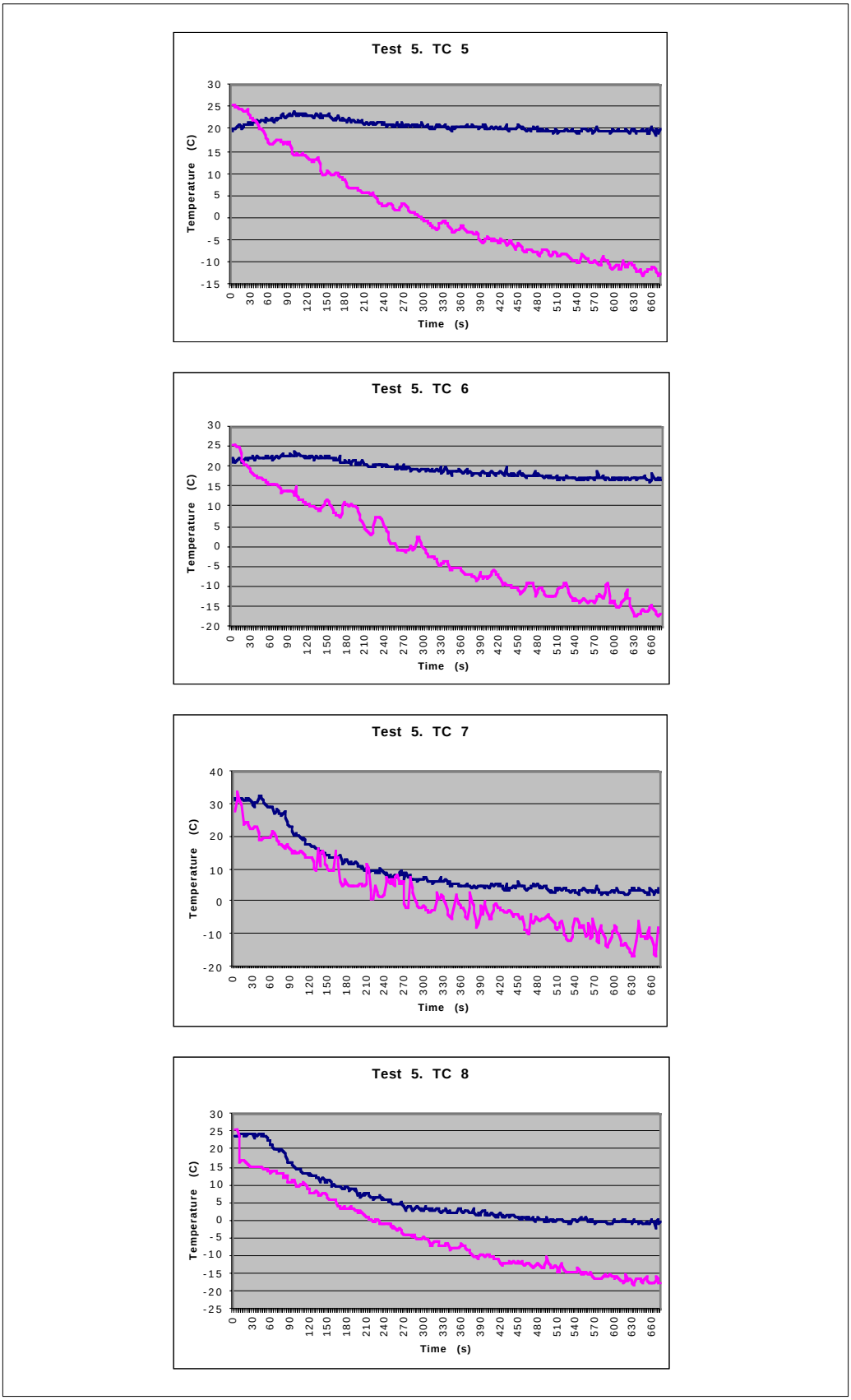

Figure B.16 Temperature comparison. Blue: Experiment; Pink: One-phase

TEST 5
Comparison

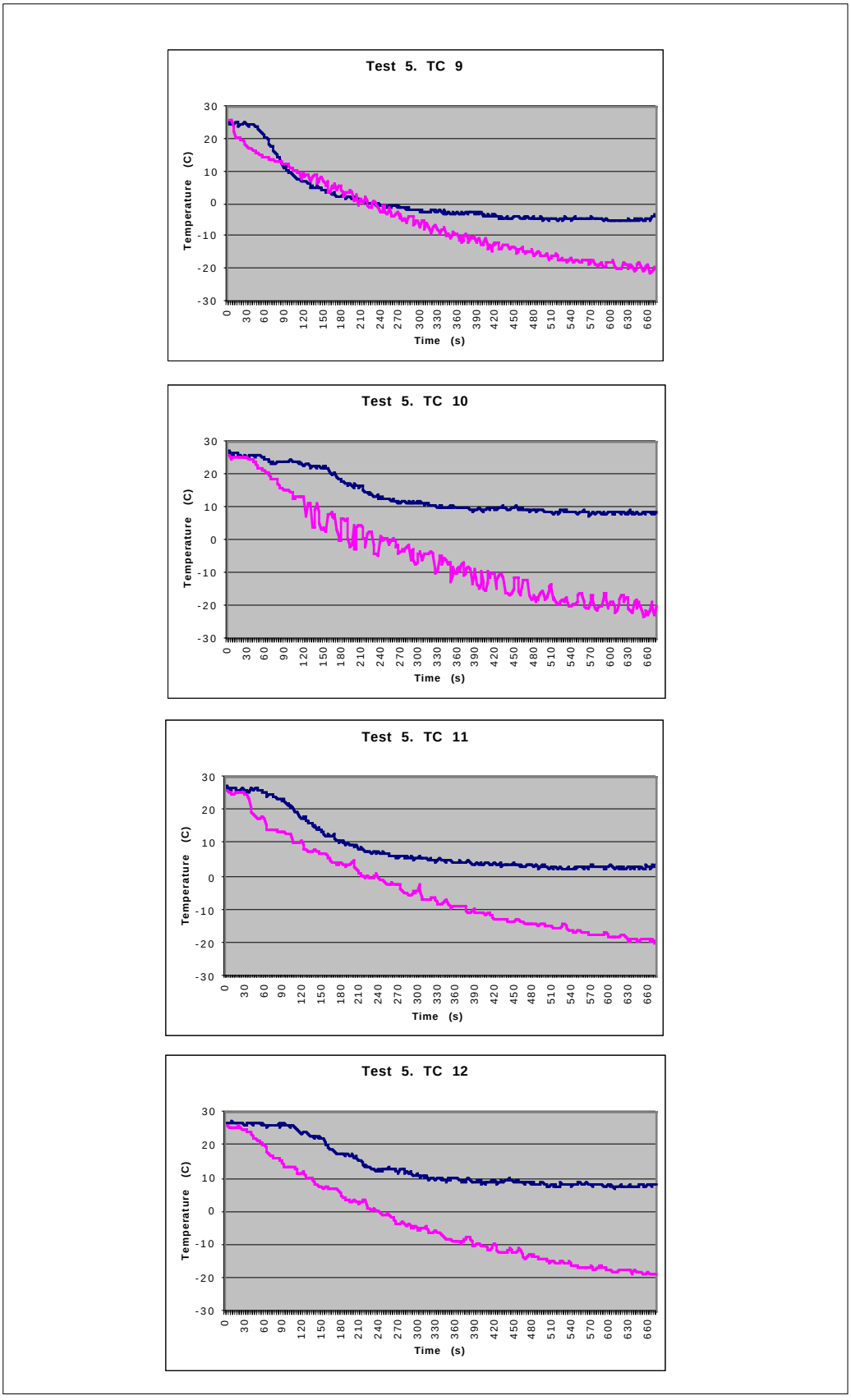

Figure B.17 Temperature comparison. Blue: Experiment; Pink: One-phase

TEST 5
Comparison

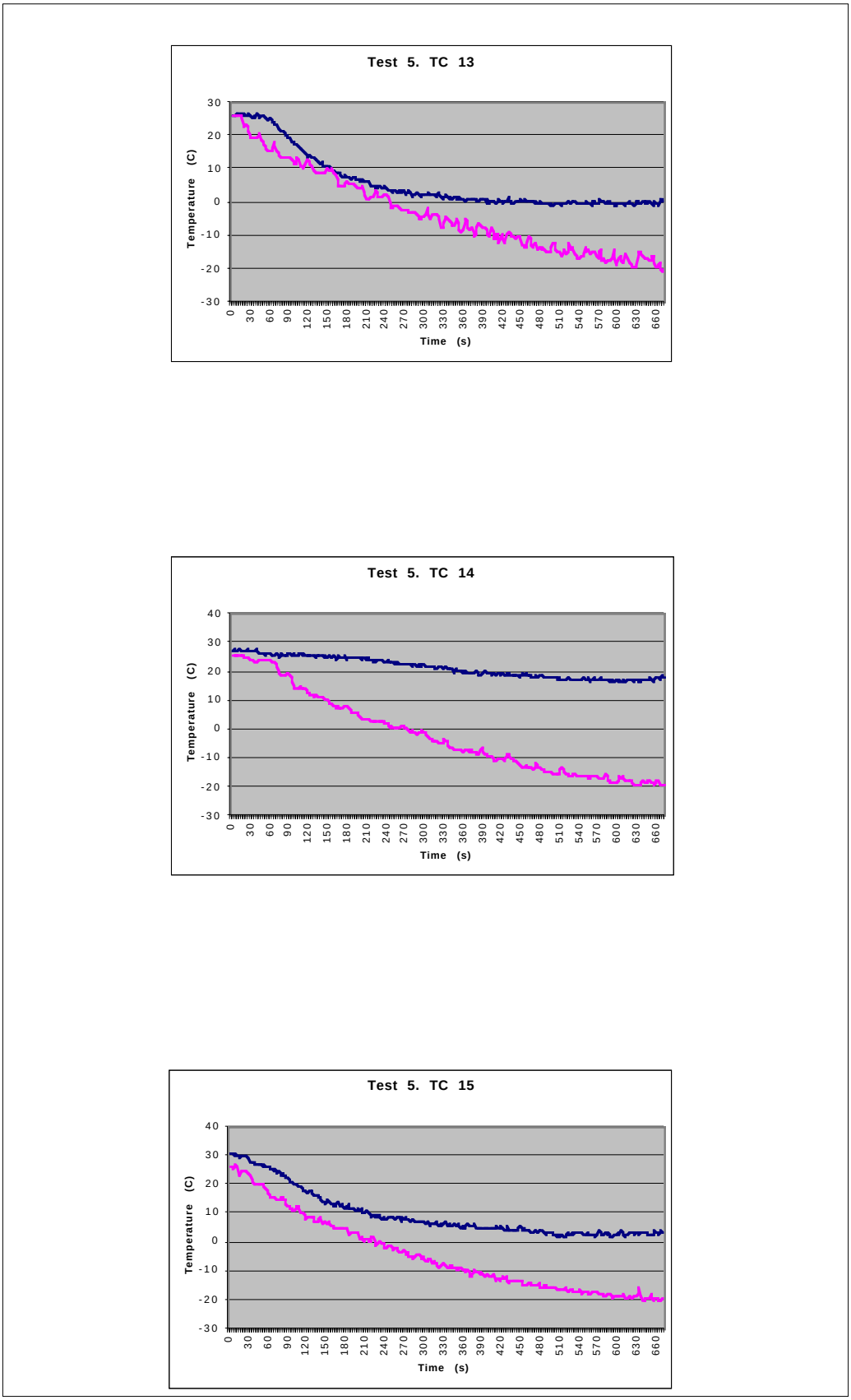

Figure B.18 Temperature comparison. Blue: Experiment; Pink: One-phase

B.2.3 Test 6. 3,72 l LAr/min

TEST 6*
One-Phase Flow

Q	**3,72 l LAr/min**				
Geometry	**Test scenario**				
Energy Sinks	**Non**				
Boundaries	*v (m/s)*	*k (m^2/s^2)*	*ε (m^2/s^3)*	*T (K)*	*ρ (kg/m^3)*
Argon Inlet	0,167	$4{,}19\ 10^{-4}$	$6{,}76\ 10^{-3}$	90	5,337
Exhaust fan	0,412	$2{,}55\ 10^{-3}$	$1{,}35\ 10^{-3}$	292	1,2
Ceiling extraction	0,197	$5{,}85\ 10^{-4}$	$1{,}40\ 10^{-5}$	300	1,2
Right and left diffusors	0,161	$3{,}91\ 10^{-4}$	$1{,}0\ 10^{-5}$	300	1,2
Walls	293,7 K Isothermal				
Heat Load	131,6 W / m^2 Constant heat flux				
Turbulence Model	K - E / R N G				
Differential schemes	*u,v*	*KE*	*ε*	*T*	*ρ*
Time	Fully Implicit				
Space	UD	UD	UD	UD	CD 0,8
Control					
Piso Correctors	3 to 6				
Max. COU number	0,1 to 0,4				
Mean COU number	0,02 to 0,05				
HDIFF	0,1 to 0,2 W				
Residual tolerance	0,01 for u,v,T,KE,ε,ρ / 0,001 for P				
Under-relaxation for P	0,8				
Relaxation factors	v-0,7 / KE-0,7 / P-1,0 / T-0,95 / ρ-0,5				
Precision	Double				
Simulated time	21 minutes and 24 seconds				
Folder	TEST 6 / Alpha				

* This flow is very similar to Test 4 and therefore it was not implemented with Energy Sinks. This is the reason why we do not show the comparison curves but just the simulation results.

TEST 6
One-Phase Flow

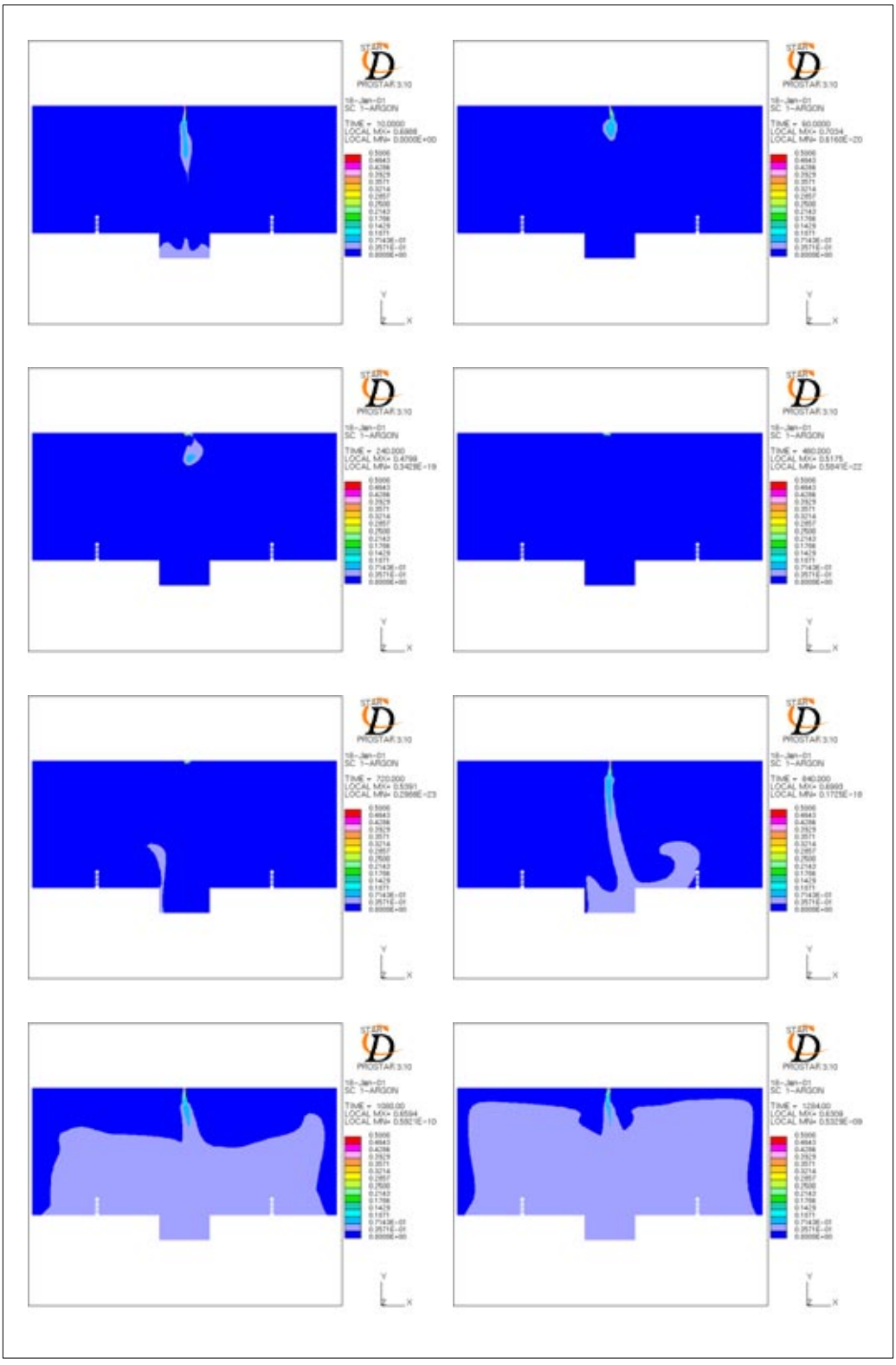

Figure B.19 Argon concentration distribution 10,60,240,480,720,840,1080 and 1284 s after the spill

TEST 6
One-Phase Flow

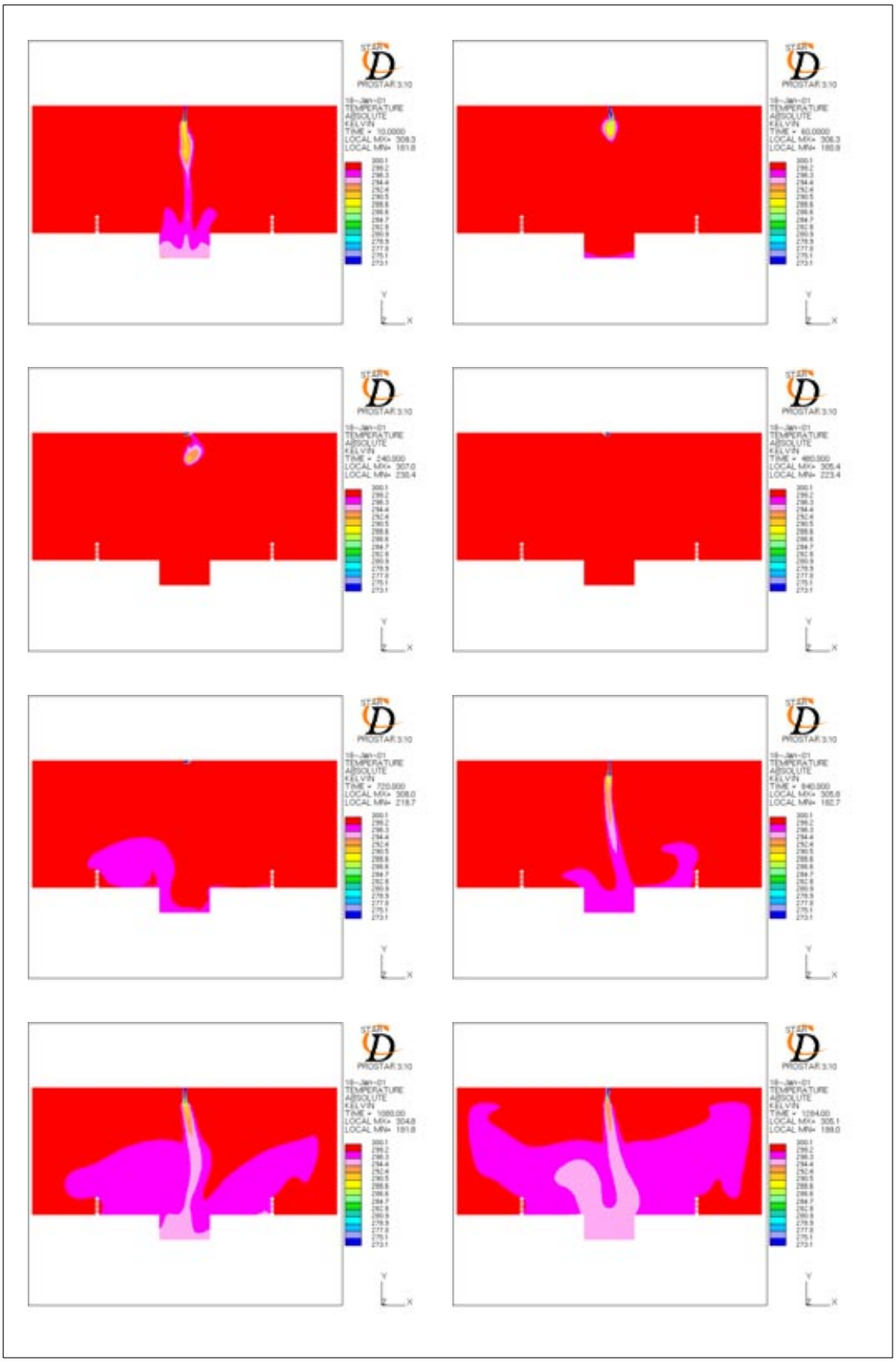

Figure B.20 Temperature distribution 10,60,240,480,720,840,1080 and 1284 s after the spill

B.2.4 Test 7. 17,78 l LAr/min.

TEST 7
One-Phase Flow

Q	**17,78 l LAr/min**				
Geometry	**Test scenario**				
Energy Sinks	**Non**				
Boundaries	*v (m/s)*	*k (m^2/s^2)*	*ε (m^2/s^3)*	*T (K)*	*ρ (kg/m^3)*
Argon Inlet	0,798	$9{,}56\ 10^{-3}$	0,073	90	5,337
Exhaust fan	0,412	$2{,}55\ 10^{-3}$	$1{,}35\ 10^{-3}$	300	1,2
Ceiling extraction	0,197	$5{,}85\ 10^{-4}$	$1{,}40\ 10^{-5}$	301	1,2
Right and left diffusors	0,161	$3{,}91\ 10^{-4}$	$1{,}0\ 10^{-5}$	301	1,2
Walls	297,9 K Isothermal				
Heat Load	131,6 W / m^2 Constant heat flux				
Turbulence Model	K - E / R N G				
Differential schemes	*u,v*	*KE*	*ε*	*T*	*ρ*
Time	F u l l y I m p l i c i t				
Space	UD	UD	UD	UD	CD 0,8
Control					
Piso Correctors	3 to 6				
Max. COU number	0,7 to 2,5				
Mean COU number	0,01 to 0,2				
HDIFF	0 to 7 W				
Residual tolerance	0,01 for u,v,T,KE,ε,ρ / 0,001 for P				
Under-relaxation for P	0,8				
Relaxation factors	v-0,7 / KE-0,7 / P-1,0 / T-0,95 / ρ-0,5				
Precision	Double				
Simulated time	11 minutes and 12 seconds				
Folder	TEST 7 / Alpha				

TEST 7
One-Phase Flow

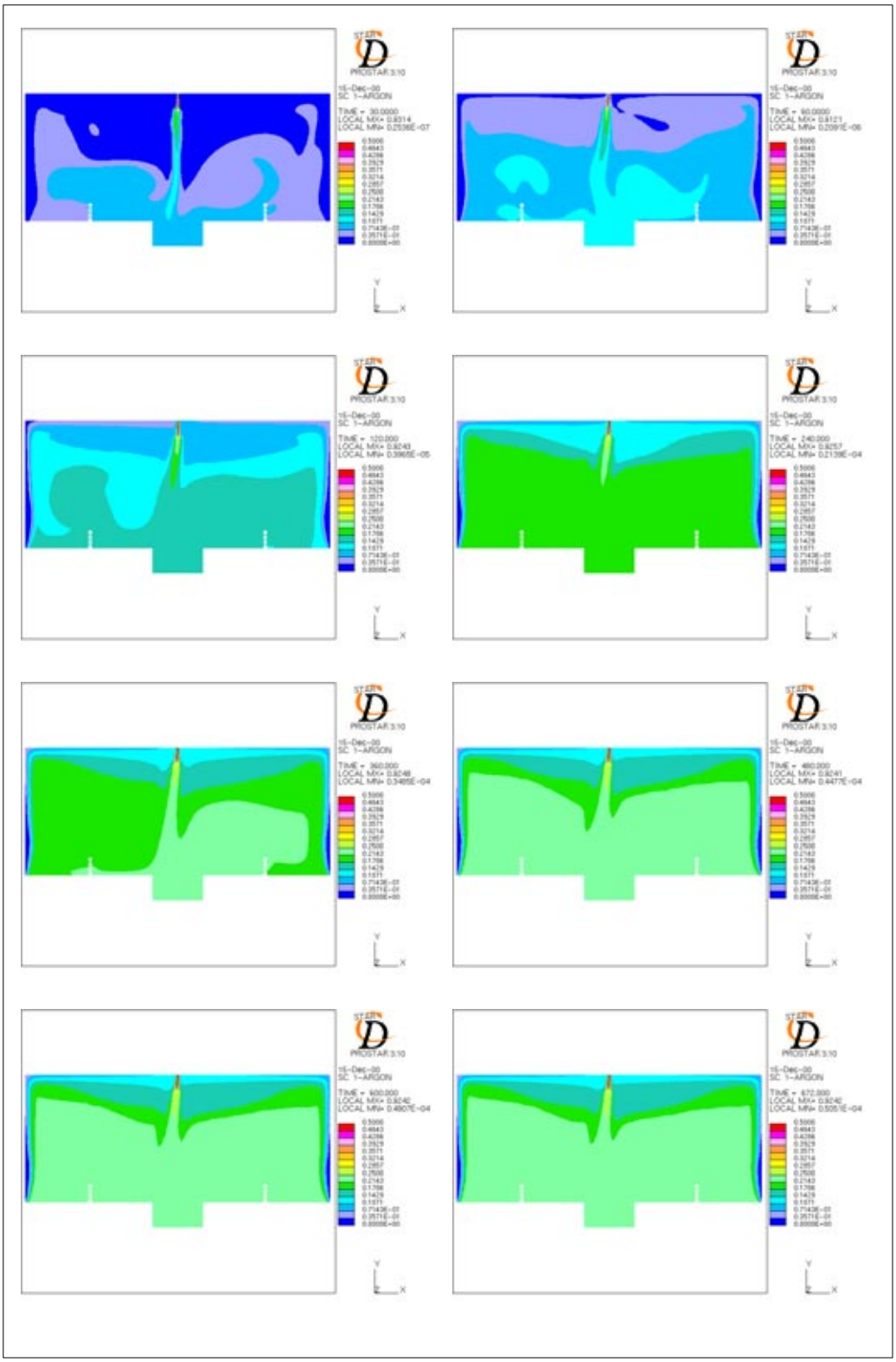

Figure B.21 Argon concentration 30,60,120,240,360,480,600 and 672 s after the spill

TEST 7
One-Phase Flow

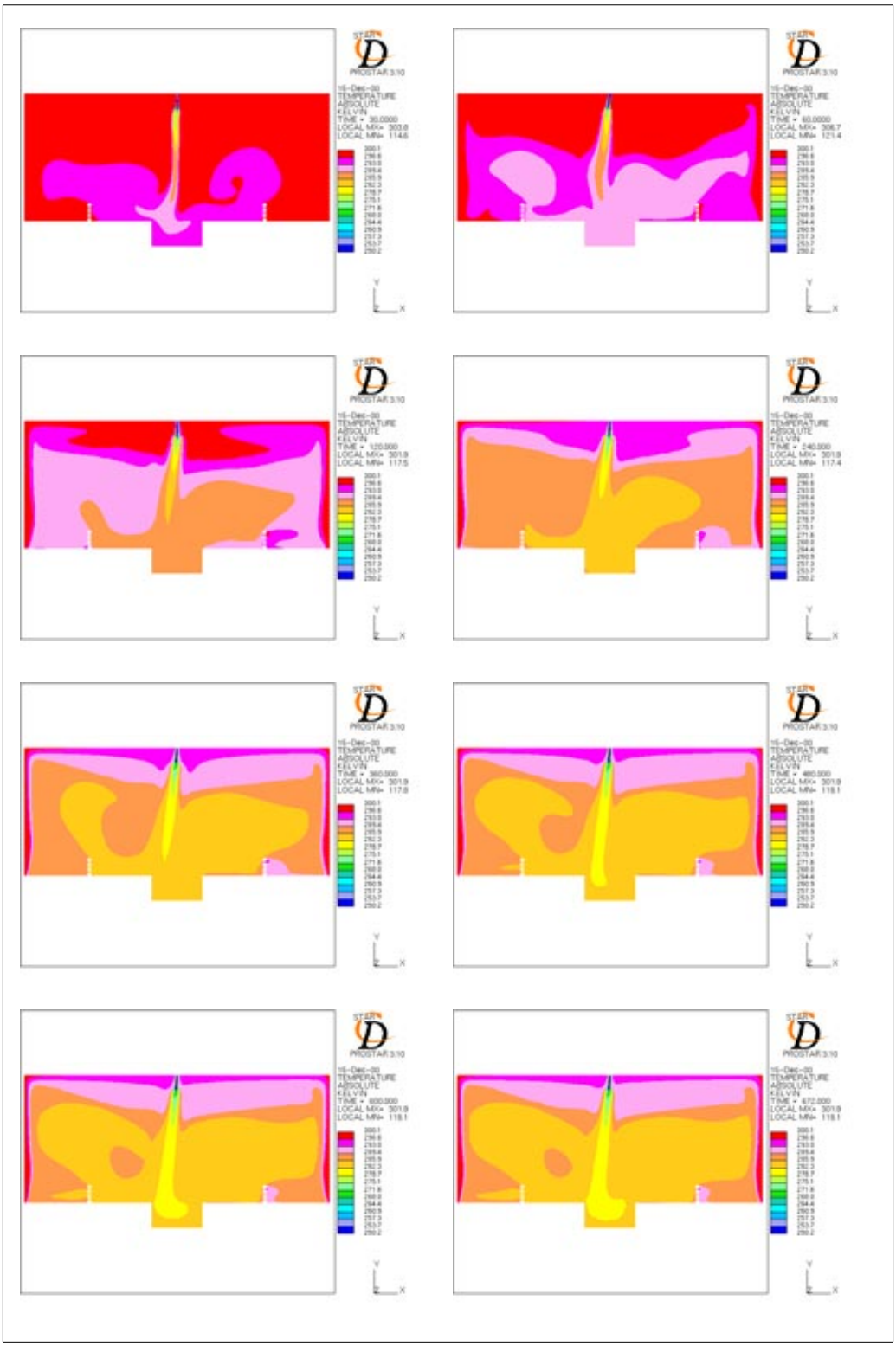

Figure B.22 Temperature distribution 30,60,120,240,360,480,600 and 672 s after the spill

TEST 7
One-Phase with Energy Sinks

Q	**17,78 l LAr/min**				
Geometry	**Test scenario**				
Energy Sinks	**Yesm: 11,94 kW / 4977,8 W/m^3**				
Boundaries	*v (m/s)*	*k (m^2/s^2)*	*ε (m^2/s^3)*	*T (K)*	*ρ (kg/m^3)*
Argon Inlet	0,798	9,56 10^{-3}	0,073	90	5,337
Exhaust fan	0,412	2,55 10^{-3}	1,35 10^{-3}	300	1,2
Ceiling extraction	0,197	5,85 10^{-4}	1,40 10^{-5}	301	1,2
Right and left diffusors	0,161	3,91 10^{-4}	1,0 10^{-5}	301	1,2
Walls	297,9 K Isothermal				
Heat Load	131,6 W / m^2 Constant heat flux				
Turbulence Model	K - E / R N G				
Differential schemes	*u,v*	*KE*	*ε*	*T*	*ρ*
Time	F u l l y I m p l i c i t				
Space	UD	UD	UD	UD	CD 0,8
Control					
Piso Correctors	3				
Max. COU number	0,6 to 3				
Mean COU number	0,1 to 0,2				
HDIFF	0,2 to 2 W				
Residual tolerance	0,01 for u,v,T,KE,ε,ρ / 0,001 for P				
Under-relaxation for P	0,8				
Relaxation factors	v-0,7 / KE-0,7 / P-1,0 / T-0,95 / ρ-0,5				
Precision	Double				
Simulated time	11 minutes and 12 seconds				
Folder	TEST SINKS 7 / Linux				

TEST 7
One-Phase with Energy Sinks

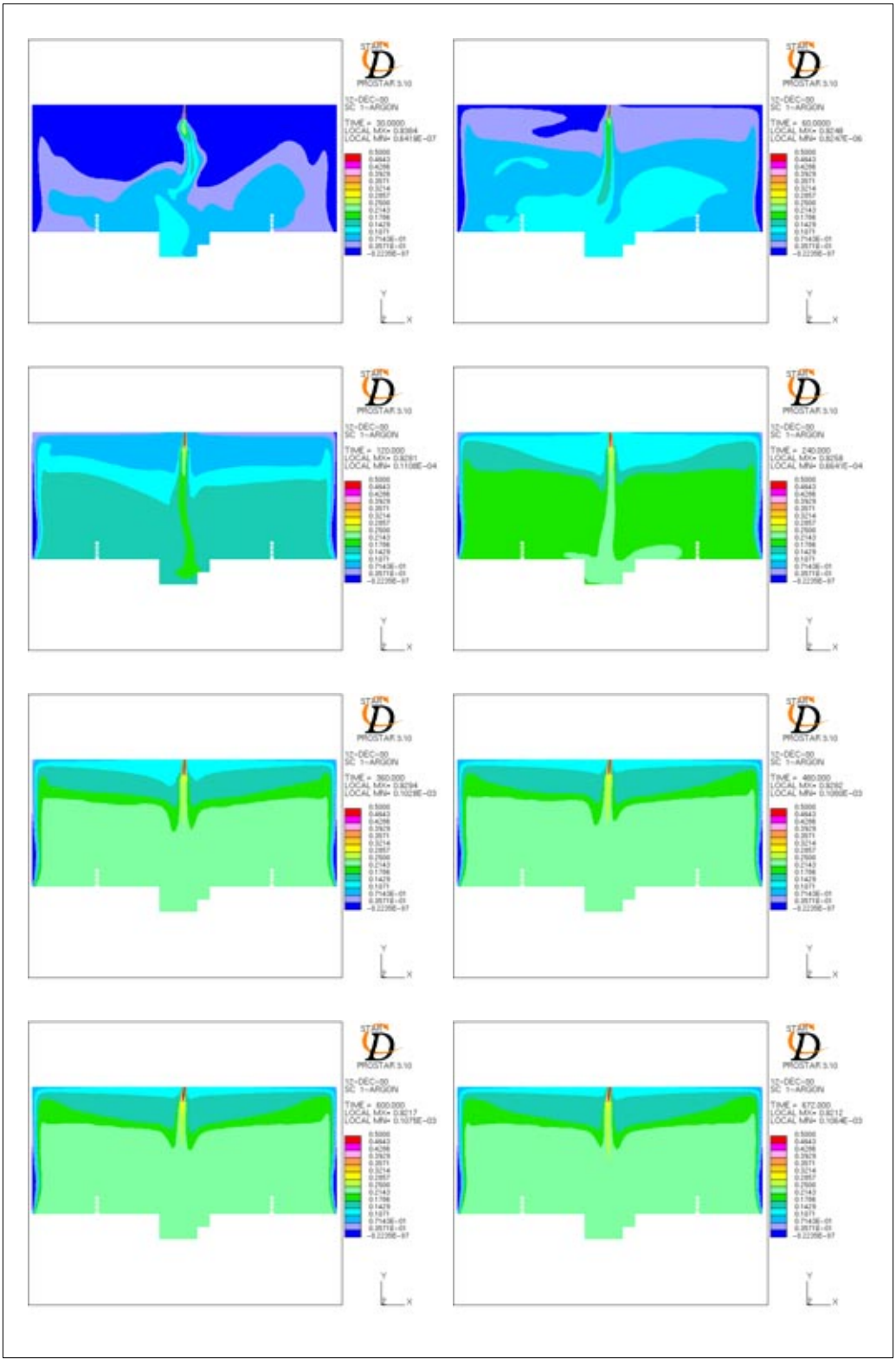

Figure B.23 Argon concentration distribution 30,60,120,240,360,480,600 and 672 s after the spill

TEST 7
One-Phase with Energy Sinks

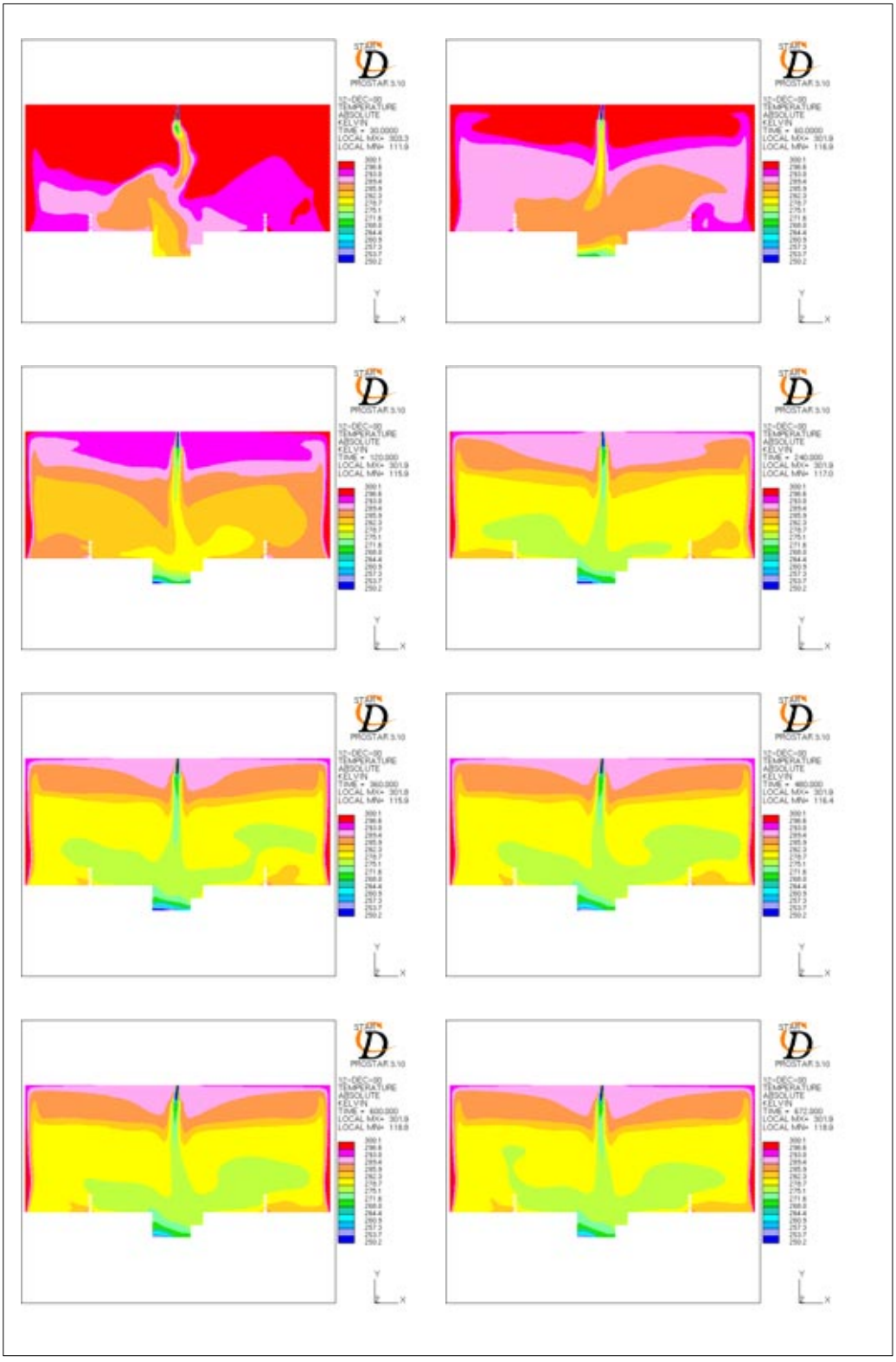

Figure B.24 Temperature distribution 30,60,120,240,360,480,600 and 672 s after the spill

Test 7
Comparison

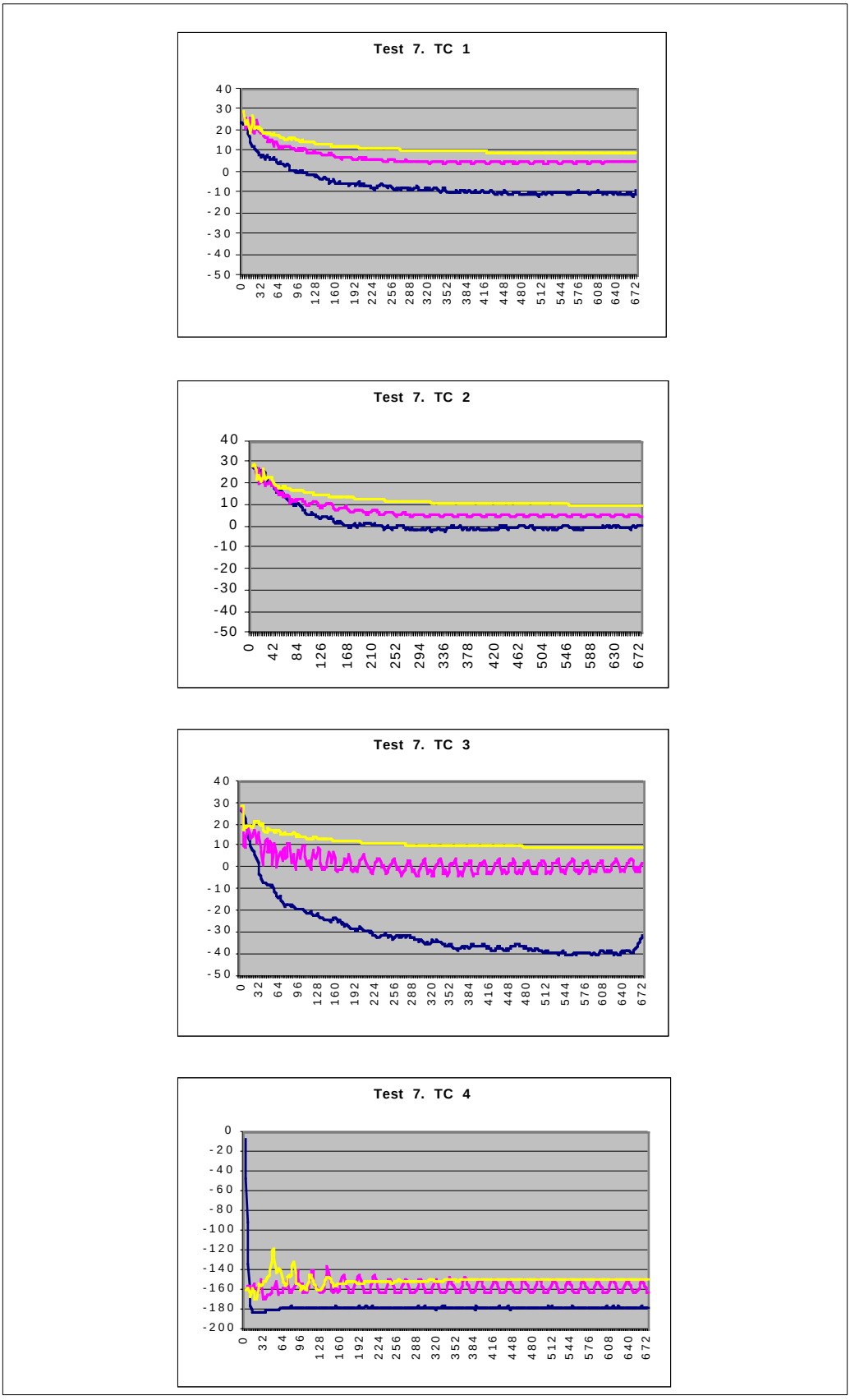

Figure B.25 Temperature comparison. Blue: Experiment; Yellow: One-phase, Pink: Energy sinks

Test 7
Comparison

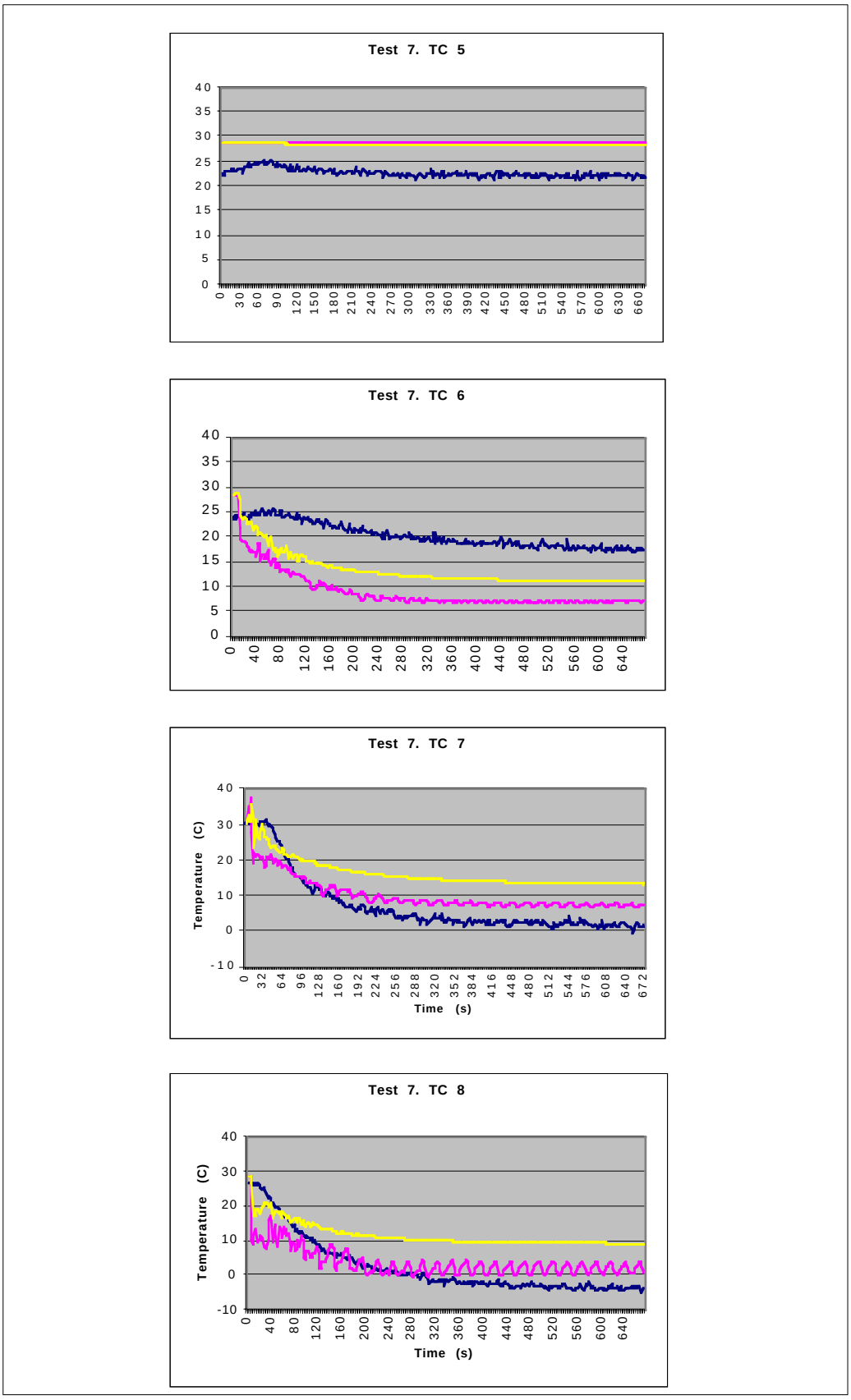

Figure B.26 Temperature comparison. Blue: Experiment; Yellow: One-phase, Pink: Energy sinks

Test 7
Comparison

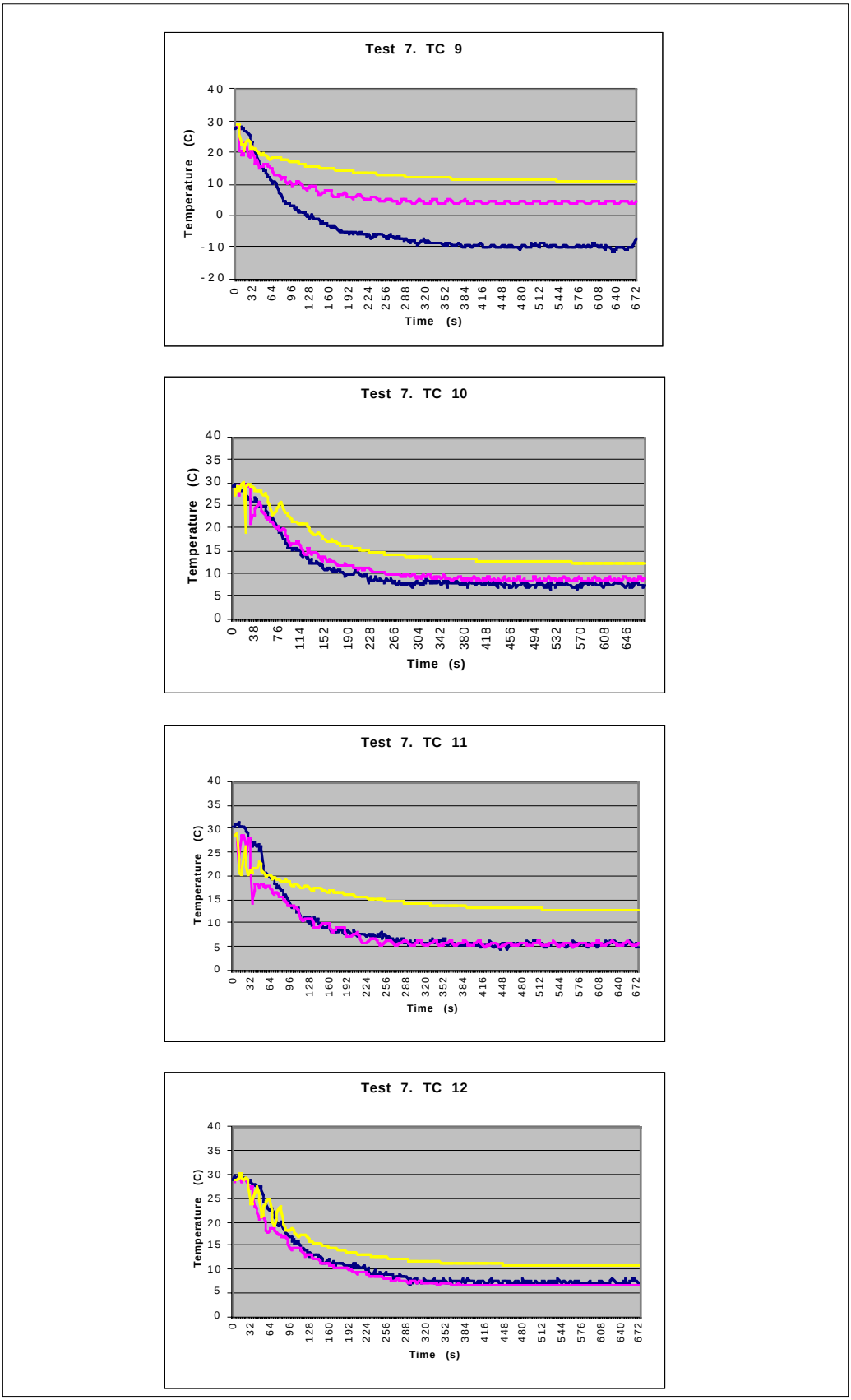

Figure B.27 Temperature comparison. Blue:experiment; Yellow: One-phase, Pink:Energy sinks

Test 7
Comparison

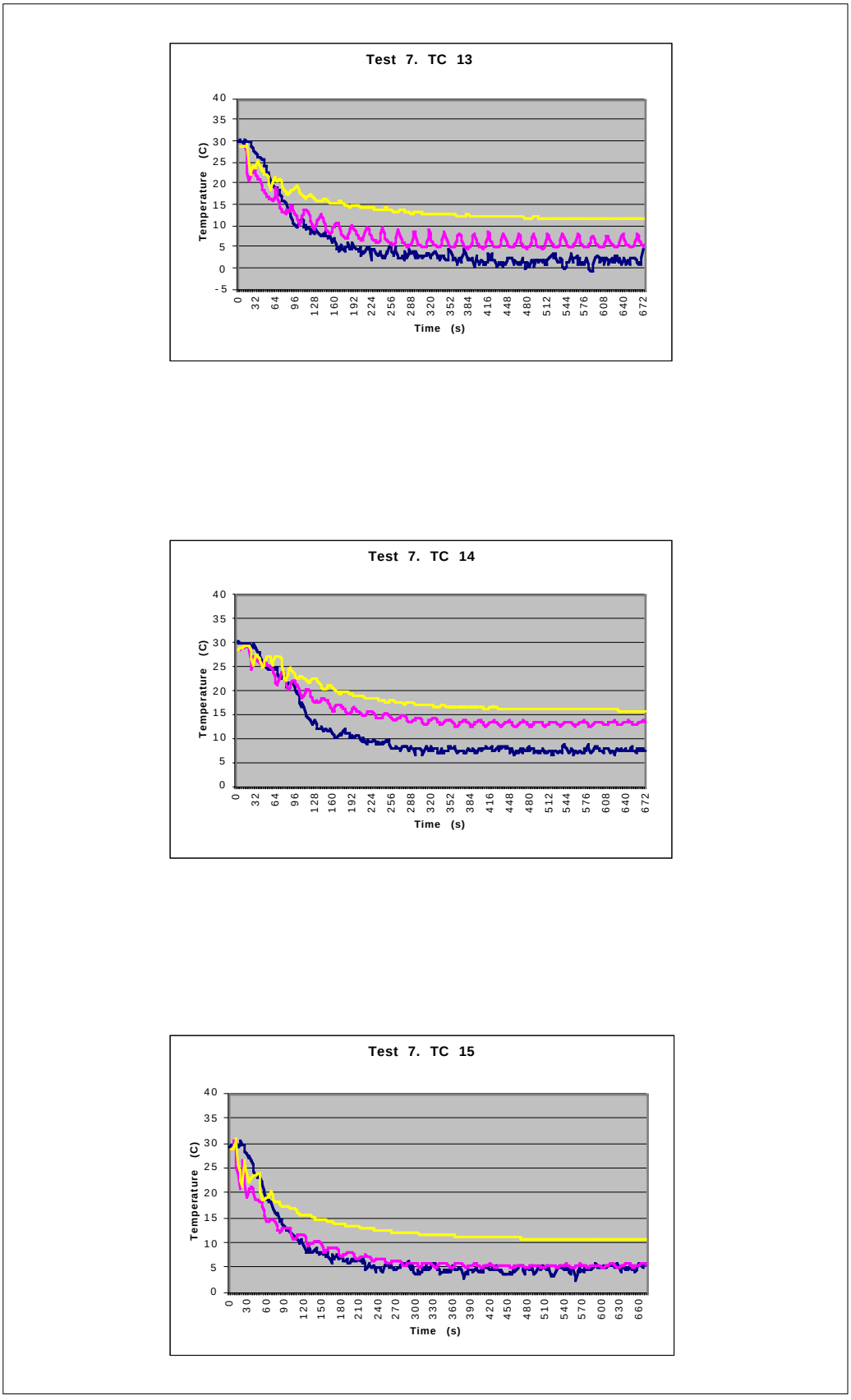

Figure B.28 Temperature comparison. Blue: Experiment; Yellow: One-phase, Pink: Energy sinks

Test 7
Comparison

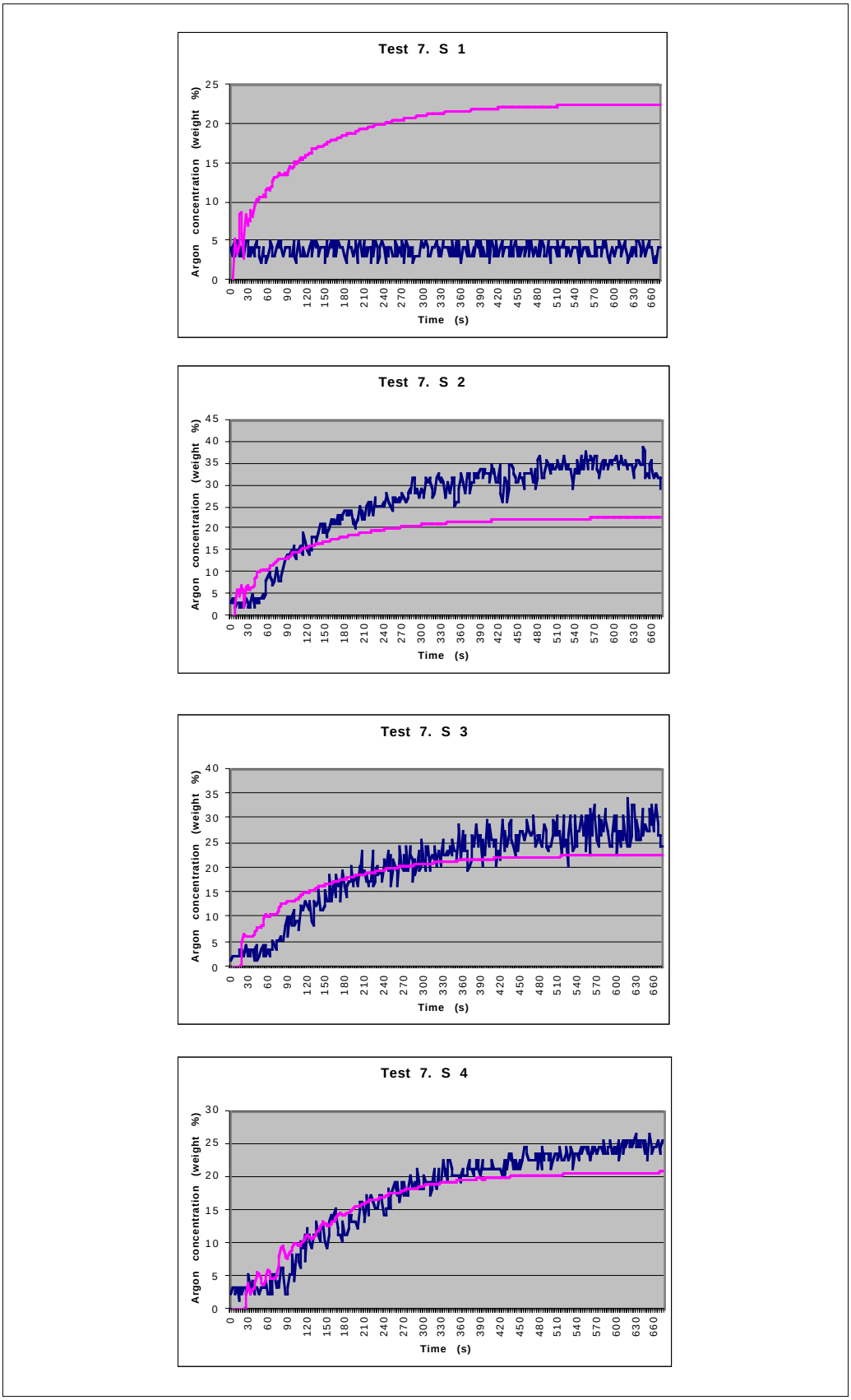

Figure B.29 Argon concentration comparison. Blue: Experiment; Pink: Energy sinks/One-Phase

Test 7
Comparison

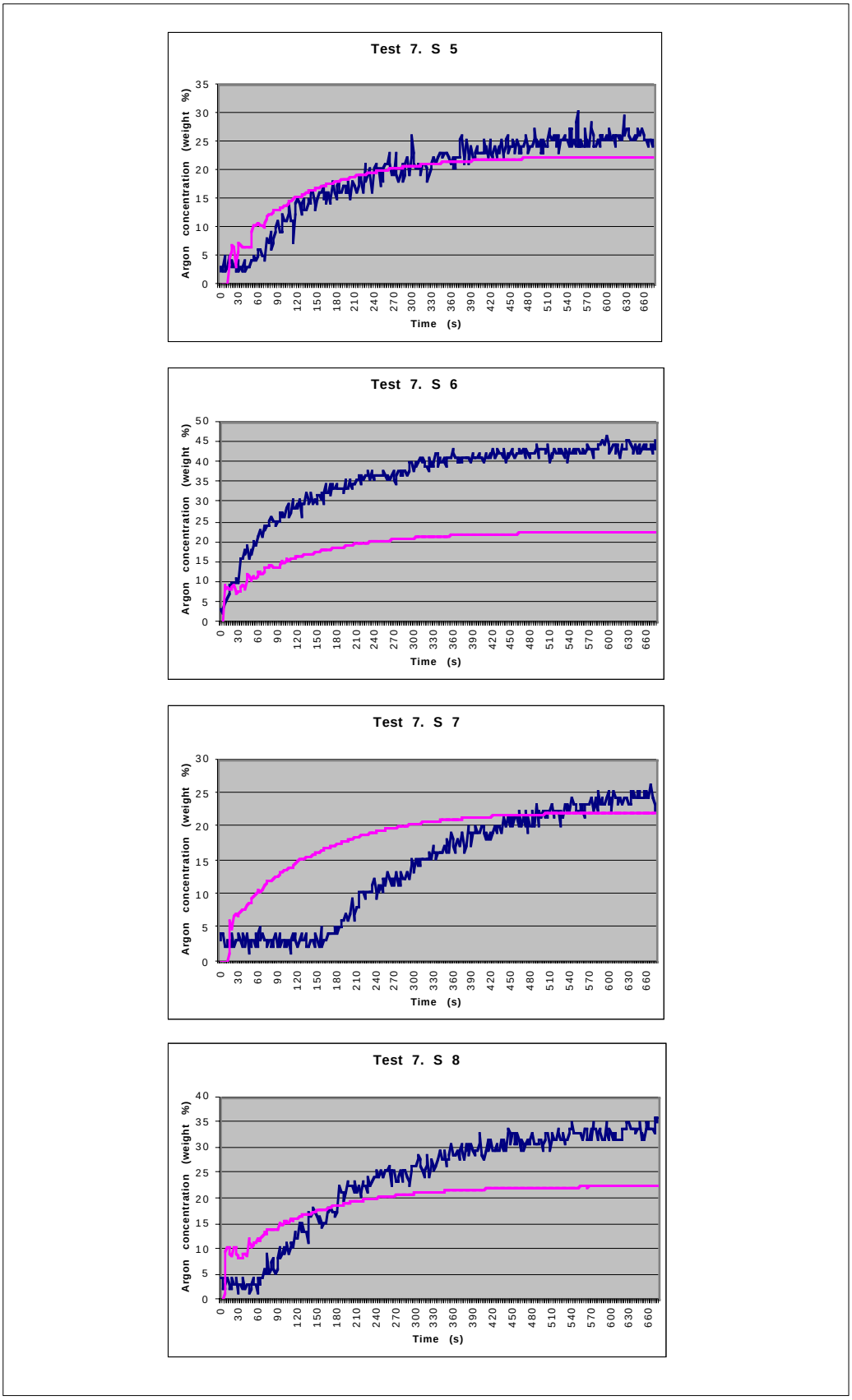

Figure B.30 Argon concentration comparison. Blue: Experiment; Pink: Energy sinks/One-Phase

Test 7
Comparison

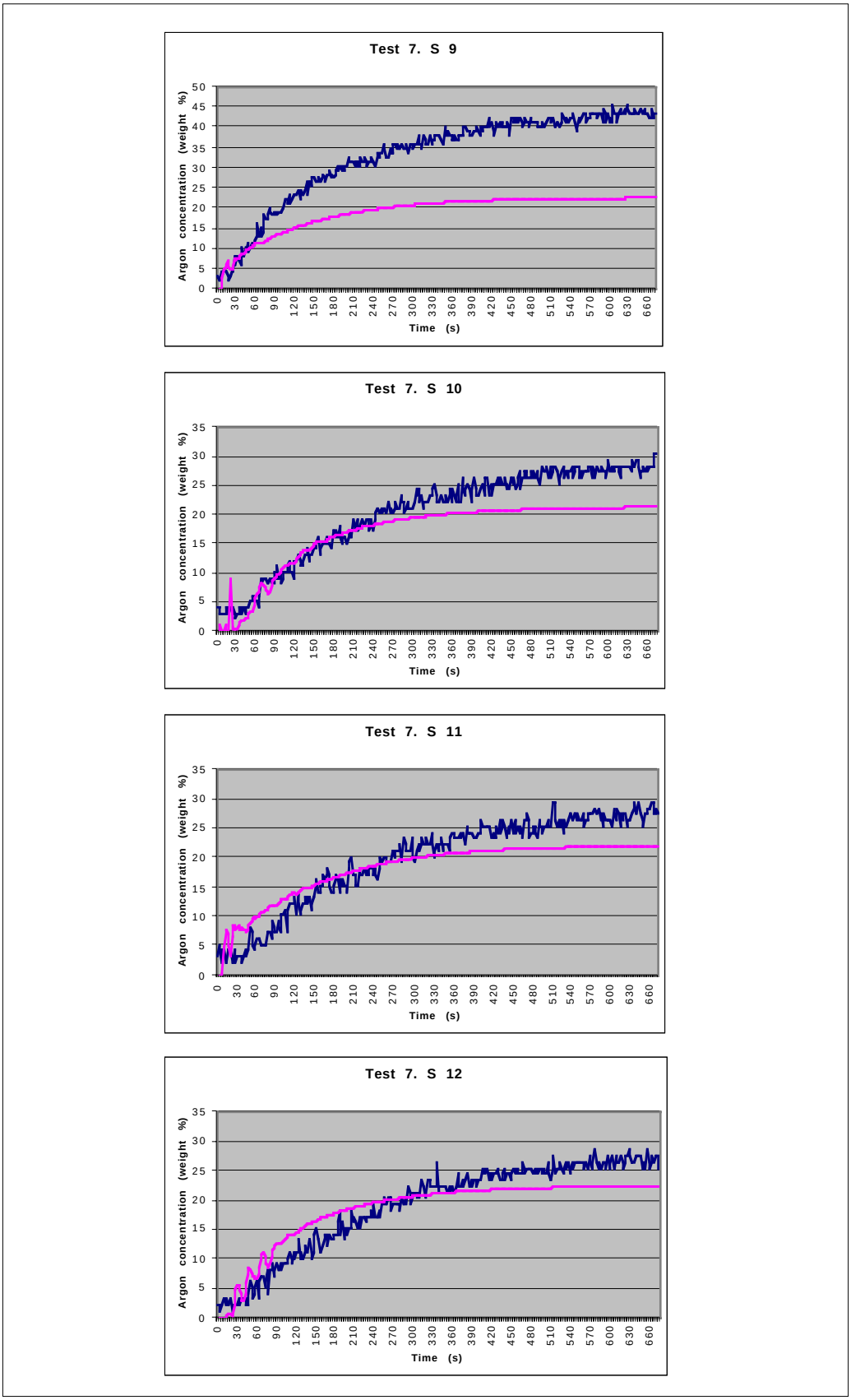

Figure B.31 Argon concentration comparison. Blue: Experiment; Pink: Energy sinks/One-Phase

B.2.5 Test 8. 50,0 l Lar/min.

TEST 8
One-Phase Flow

Q	**50,0 l LAr/min**				
Geometry	**Test scenario**				
Energy Sinks	**Non**				
Boundaries	*v (m/s)*	*k (m^2/s^2)*	*ε (m^2/s^3)*	*T (K)*	*ρ (kg/m^3)*
Argon Inlet	2,245	0,075	1,638	90	5,337
Exhaust fan	0,412	$2,55\ 10^{-3}$	$1,35\ 10^{-3}$	299	1,2
Ceiling extraction	0,197	$5,85\ 10^{-4}$	$1,40\ 10^{-5}$	300	1,2
Right and left diffusors	0,161	$3,91\ 10^{-4}$	$1,0\ 10^{-5}$	300	1,2
Walls	296,7 K Isothermal				
Heat Load	131,6 W / m^2 Constant heat flux				
Turbulence Model	K - E / R N G				
Differential schemes	*u,v*	*KE*	*ε*	*T*	*ρ*
Time	F u l l y I m p l i c i t				
Space	UD	UD	UD	UD	CD 0,8
Control					
Piso Correctors	3 to 4				
Max. COU number	2,4 to 3				
Mean COU number	around 0,2				
HDIFF	0,2 to 2 W				
Residual tolerance	0,01 for u,v,T,KE,ε,ρ / 0,001 for P				
Under-relaxation for P	0,8				
Relaxation factors	v-0,7 / KE-0,7 / P-1,0 / T-0,95 / ρ-0,5				
Precision	Double				
Simulated time	4 minutes and 12 seconds				
Folder	TEST 8 / Alpha				

TEST 8
One-phase flow

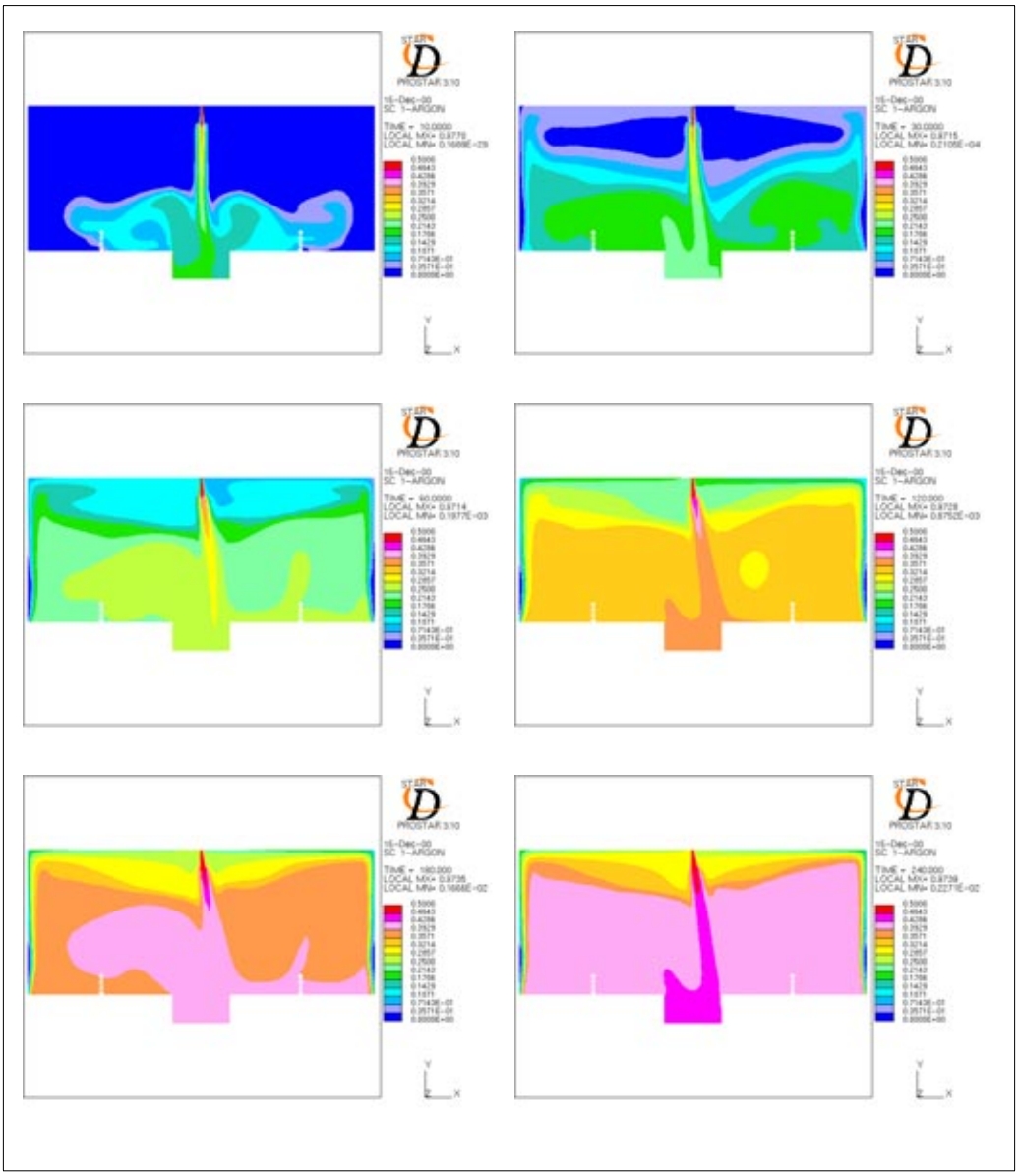

Figure B.32 Argon concentration 10,30,60,120,180 and 240 s after the spill

TEST 8
One-phase flow

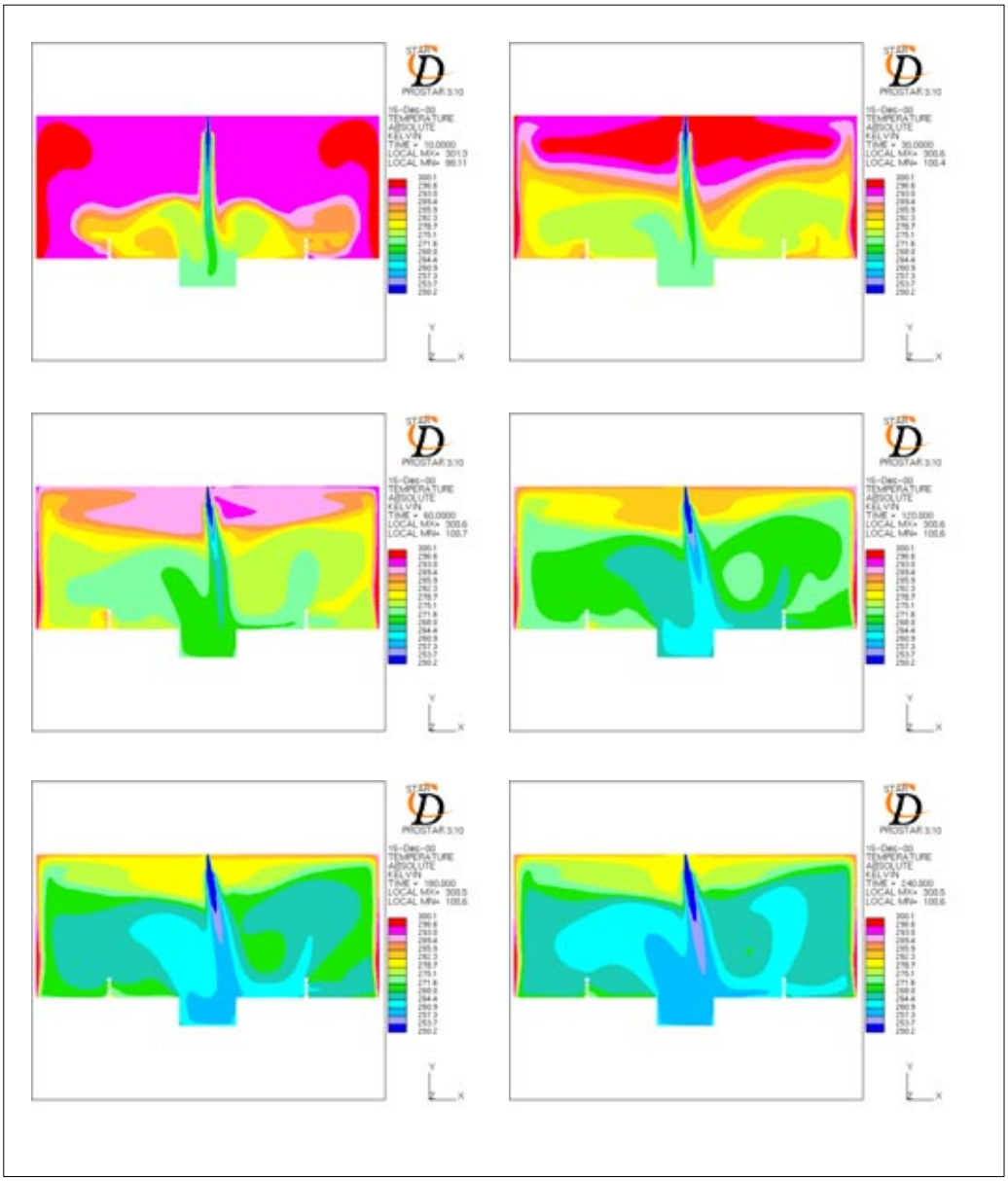

Figure B.33 Temperature distribution 10,30,60,120,180,240 s after the spill

TEST 8
One-Phase Flow
3D Geometry

Q	**50,0 l LAr/min**				
Geometry	**Test scenario, 3D**				
Energy Sinks	**Non**				
Boundaries	*v (m/s)*	*k (m^2/s^2)*	*ε (m^2/s^3)*	*T (K)*	*ρ (kg/m^3)*
Argon Inlet	21,56	6,973	289,83	90	5,337
Exhaust fan	1,981	$5{,}88\ 10^{-2}$	0,149	299	1,2
Ceiling extraction	0,197	$5{,}85010^{-4}$	$1{,}40\ 10^{-5}$	300	1,2
Right and left diffusors	1,259	$2{,}38\ 10^{-2}$	$4{,}81\ 10^{-3}$	300	1,2
Walls	296,7 K Isothermal				
Heat Load	131,6 W / m^2 Constant heat flux				
Turbulence Model	K - E / R N G				
Differential schemes	*u,v*	*KE*	*ε*	*T*	*ρ*
Time	F u l l y I m p l i c i t				
Space	UD	UD	UD	UD	CD 0,8
Control					
Piso Correctors	2 to 5				
Max. COU number	6 to 20				
Mean COU number	0,1 to 0,2				
HDIFF	25 to 1900 W				
Residual tolerance	0,01 for u,v,T,KE,ε,ρ / 0,001 for P				
Under-relaxation for P	0,8				
Relaxation factors	v-0,7 / KE-0,7 / P-1,0 / T-0,95 / ρ-0,5				
Precision	Double				
Simulated time	4 minutes and 12 seconds				
Folder	TEST 8 3D / Alpha				

TEST 8
One-Phase Flow
3D Geometry

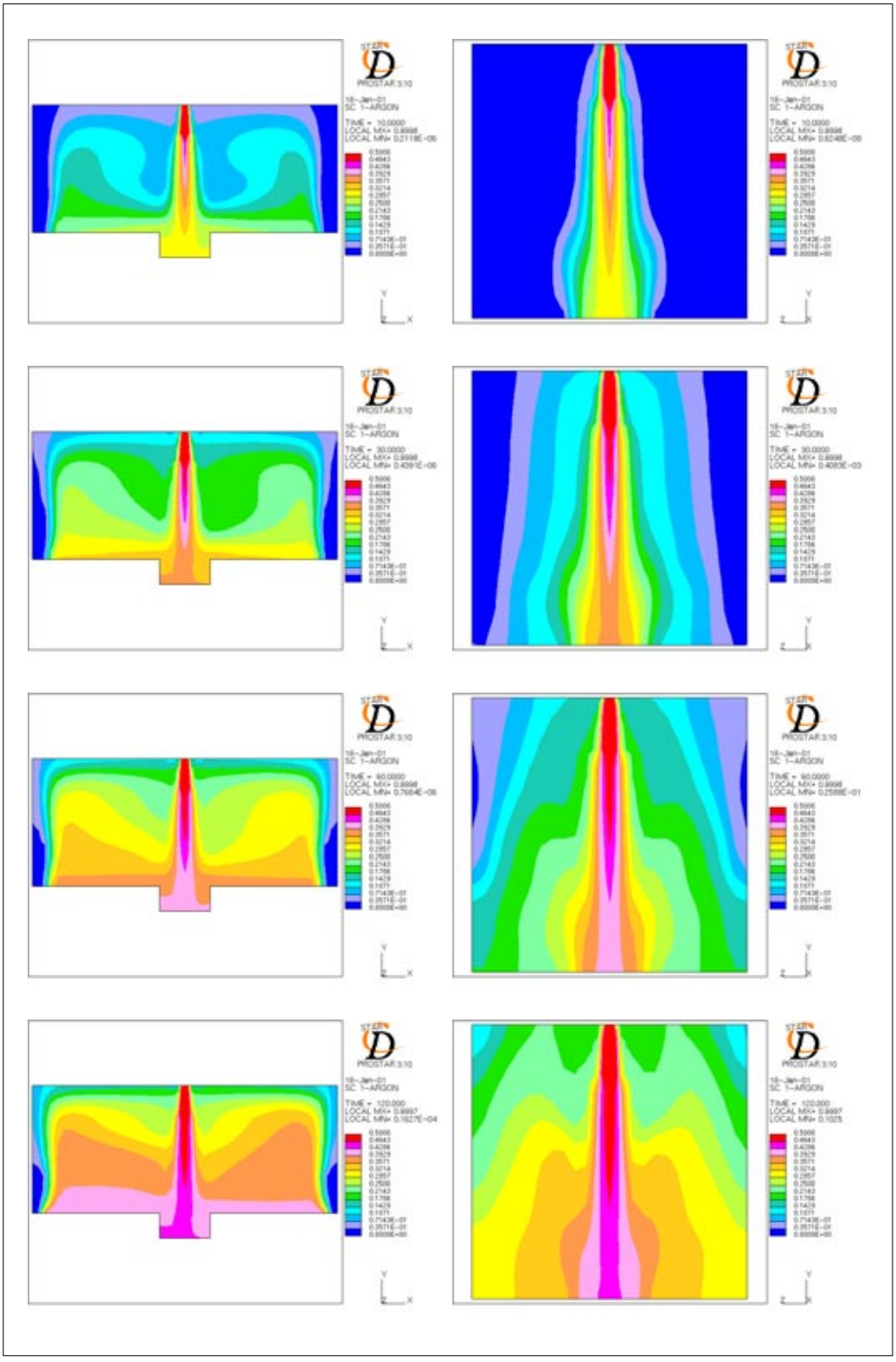

Figure B.34 Argon concentration distribution 10,30,60 and 120 s after the spill. Sections

TEST 8
One-Phase Flow
3D Geometry

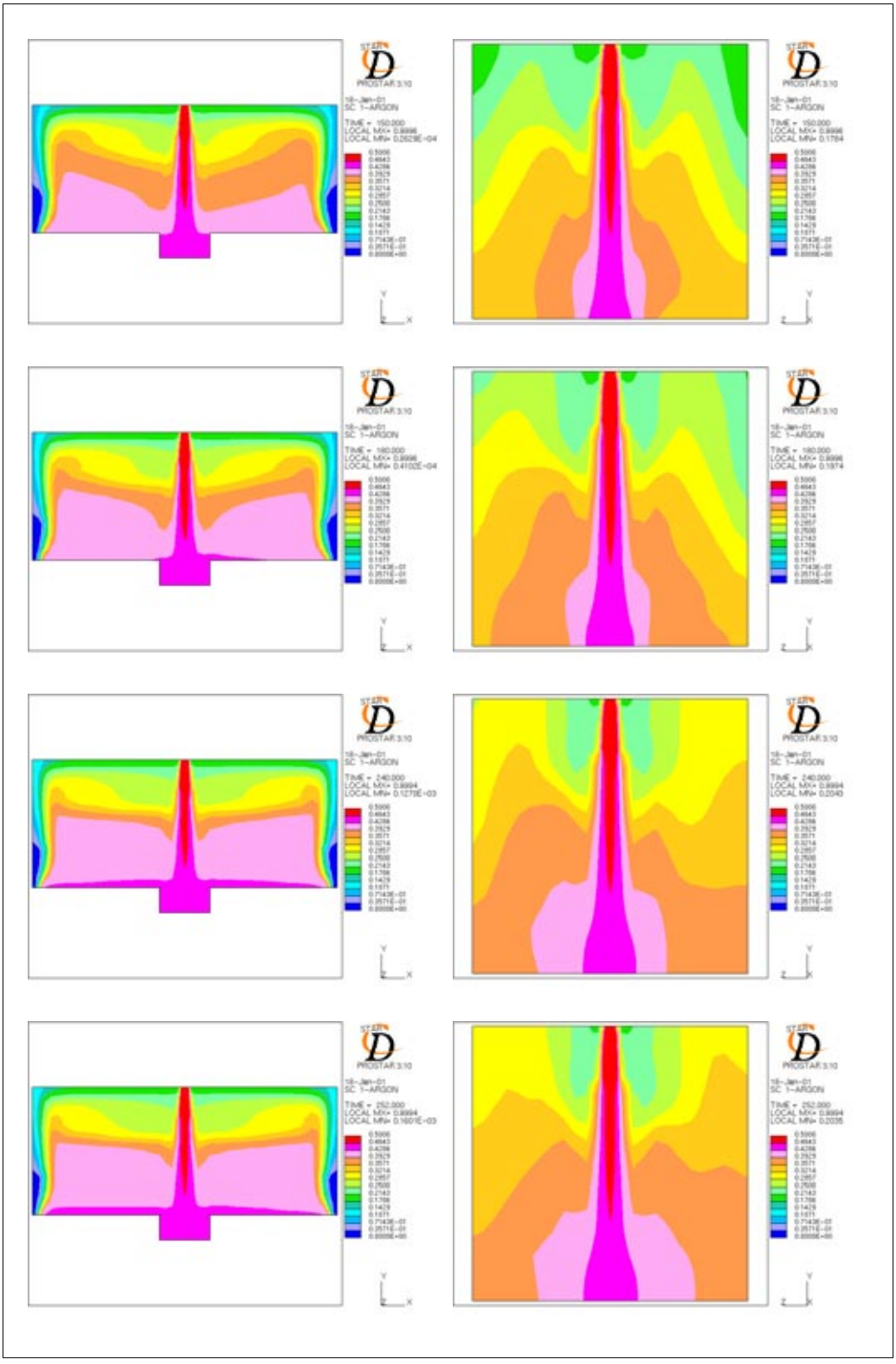

Figure B.35 Argon concentration distribution 150,180,240 adn 252 s after the spill. Sections

TEST 8
One-Phase Flow
3D Geometry

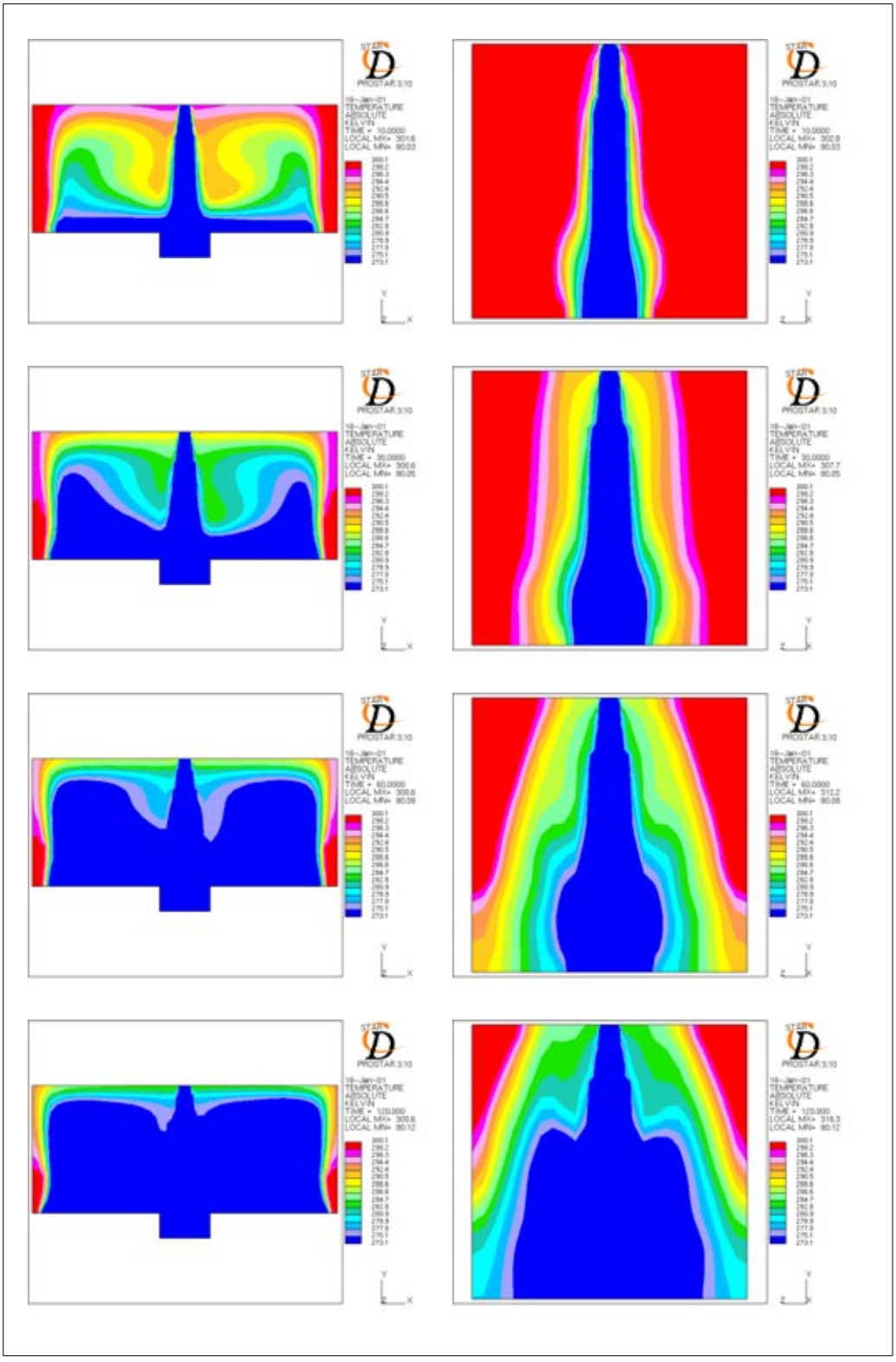

Figure B.36 Temperature distribution10,30,60 and 120 s after the spill. Sections

TEST 8
One-Phase Flow
3D Geometry

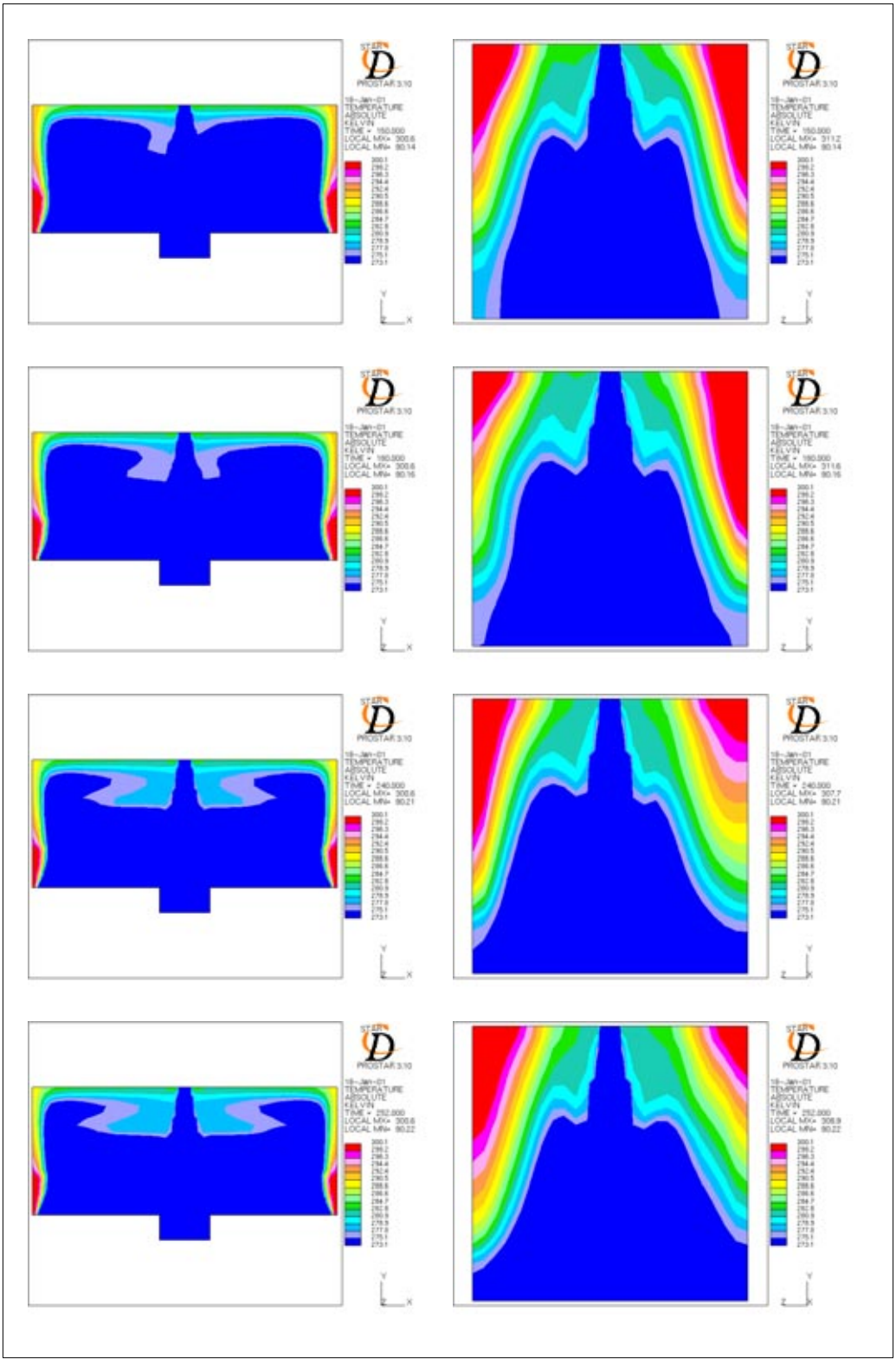

Figure B.37 Temperature distribution150,180,240 and 252 s after the spill. Sections

TEST 8
One-Phase with Energy Sinks

Q	**50,0 l LAr/min**				
Geometry	**Test scenario**				
Energy Sinks	**Yes: 33,6 kW / 13.998,5 W/m^3**				
Boundaries	*v (m/s)*	*k (m^2/s^2)*	*ε (m^2/s^3)*	*T (K)*	*ρ (kg/m^3)*
Argon Inlet	2,245	0,075	1,638	90	5,337
Exhaust fan	0,412	$2{,}55\ 10^{-3}$	$1{,}35\ 10^{-3}$	299	1,2
Ceiling extraction	0,197	$5{,}85\ 10^{-4}$	$1{,}40\ 10^{-5}$	300	1,2
Right and left diffusors	0,161	$3{,}91\ 10^{-4}$	$1{,}0\ 10^{-5}$	300	1,2
Walls	296,7 K Isothermal				
Heat Load	131,6 W / m^2 Constant heat flux				
Turbulence Model	K - E / R N G				
Differential schemes	*u,v*	*KE*	*ε*	*T*	*ρ*
Time	F u l l y I m p l i c i t				
Space	UD	UD	UD	UD	CD 0,8
Control					
Piso Correctors	3 to 4				
Max. COU number	1 to 4				
Mean COU number	0,1 to 0,2				
HDIFF	0,1 to 3 W				
Residual tolerance	0,01 for u,v,T,KE,ε,ρ / 0,001 for P				
Under-relaxation for P	0,8				
Relaxation factors	v-0,7 / KE-0,7 / P-1,0 / T-0,95 / ρ-0,5				
Precision	Double				
Simulated time	4 minutes and 12 seconds				
Folder	TEST SINKS 8 / Alpha				

TEST 8
One-phase with Energy Sinks

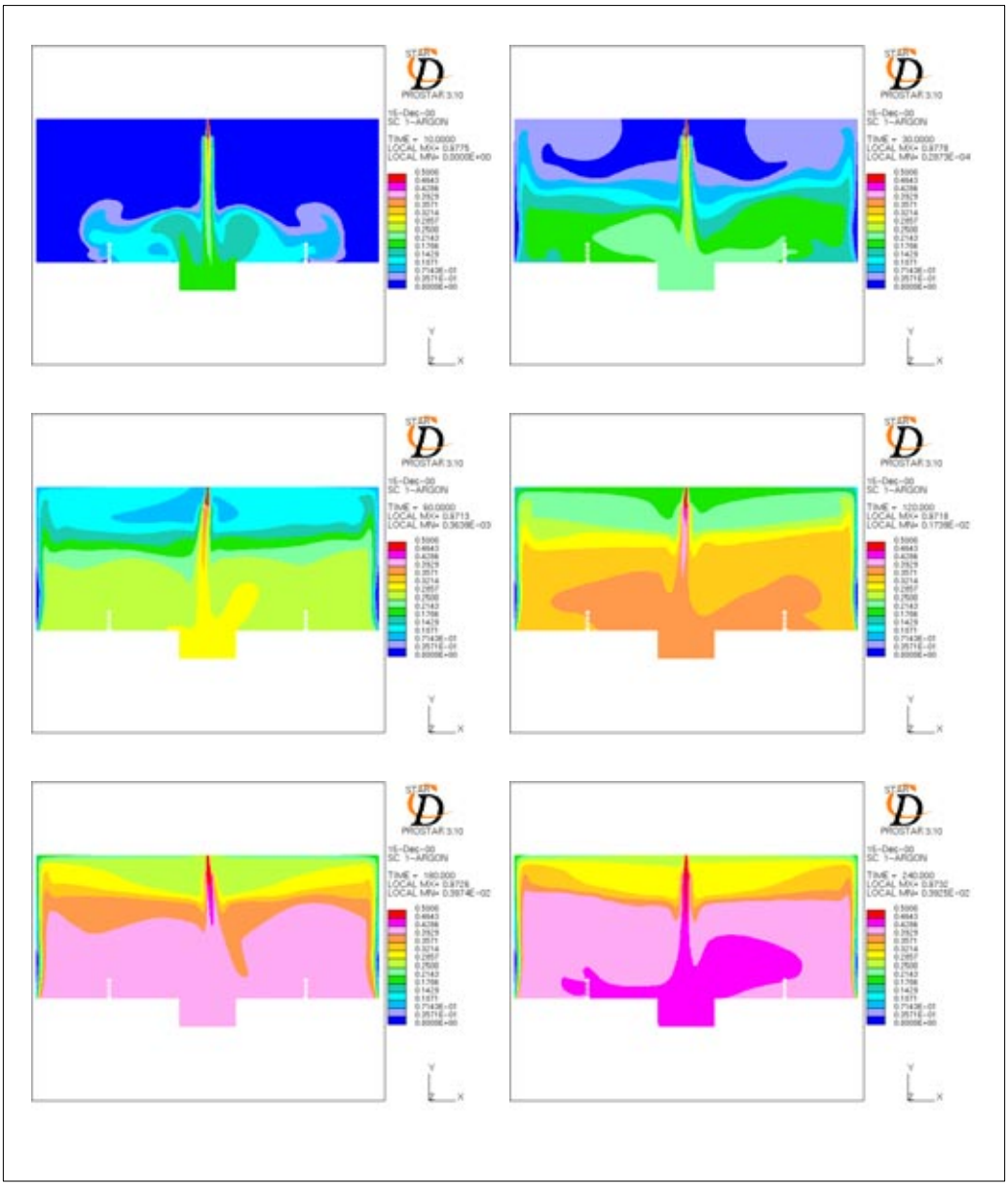

Figure B.38 Argon concentration 10,30,60,120,180 and 240 s after the spill

TEST 8
One-phase with Energy Sinks

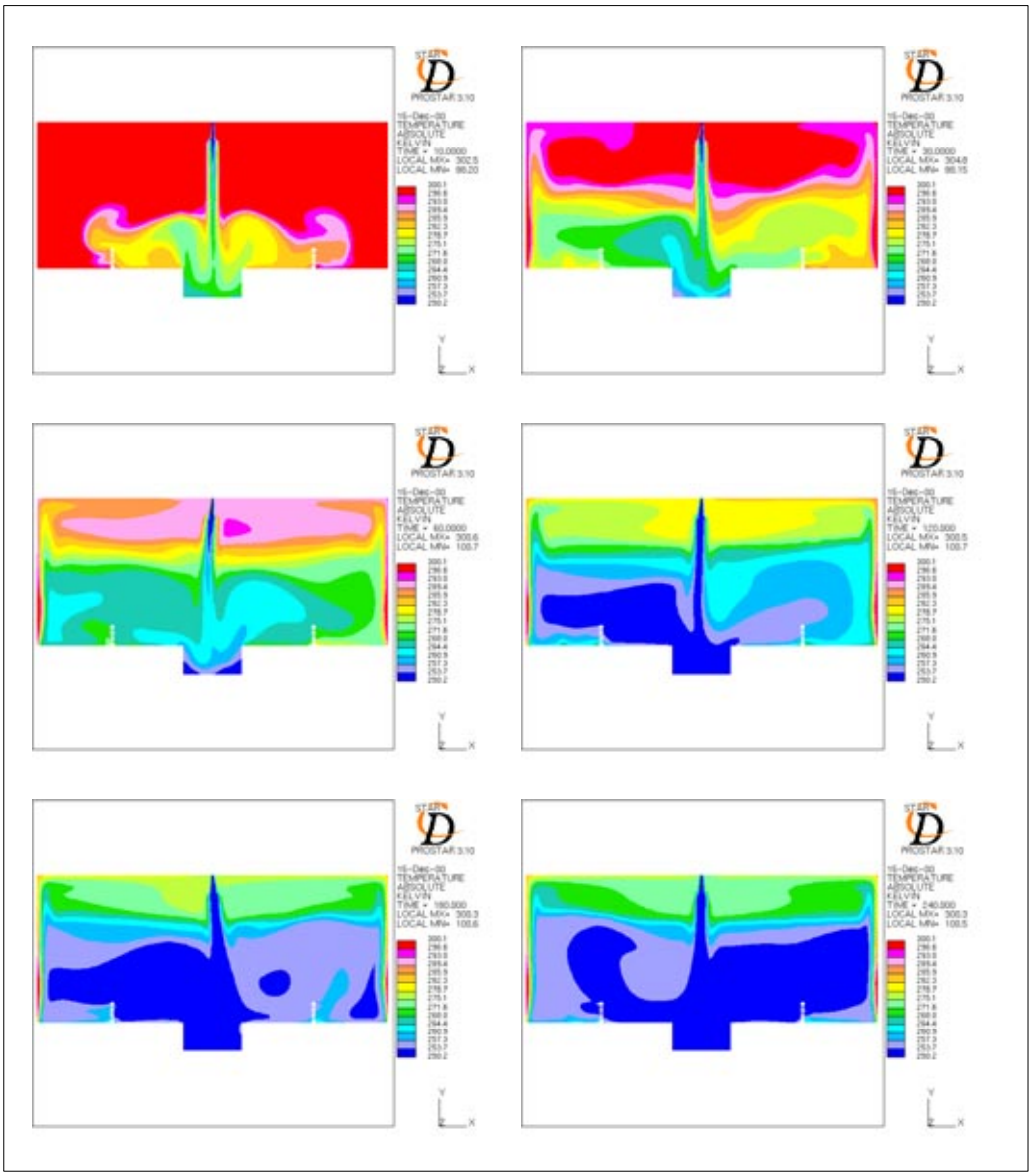

Figure B.39 Temperature distribution 10,30,60,120,180,240 s after the spill

TEST 8
Comparison

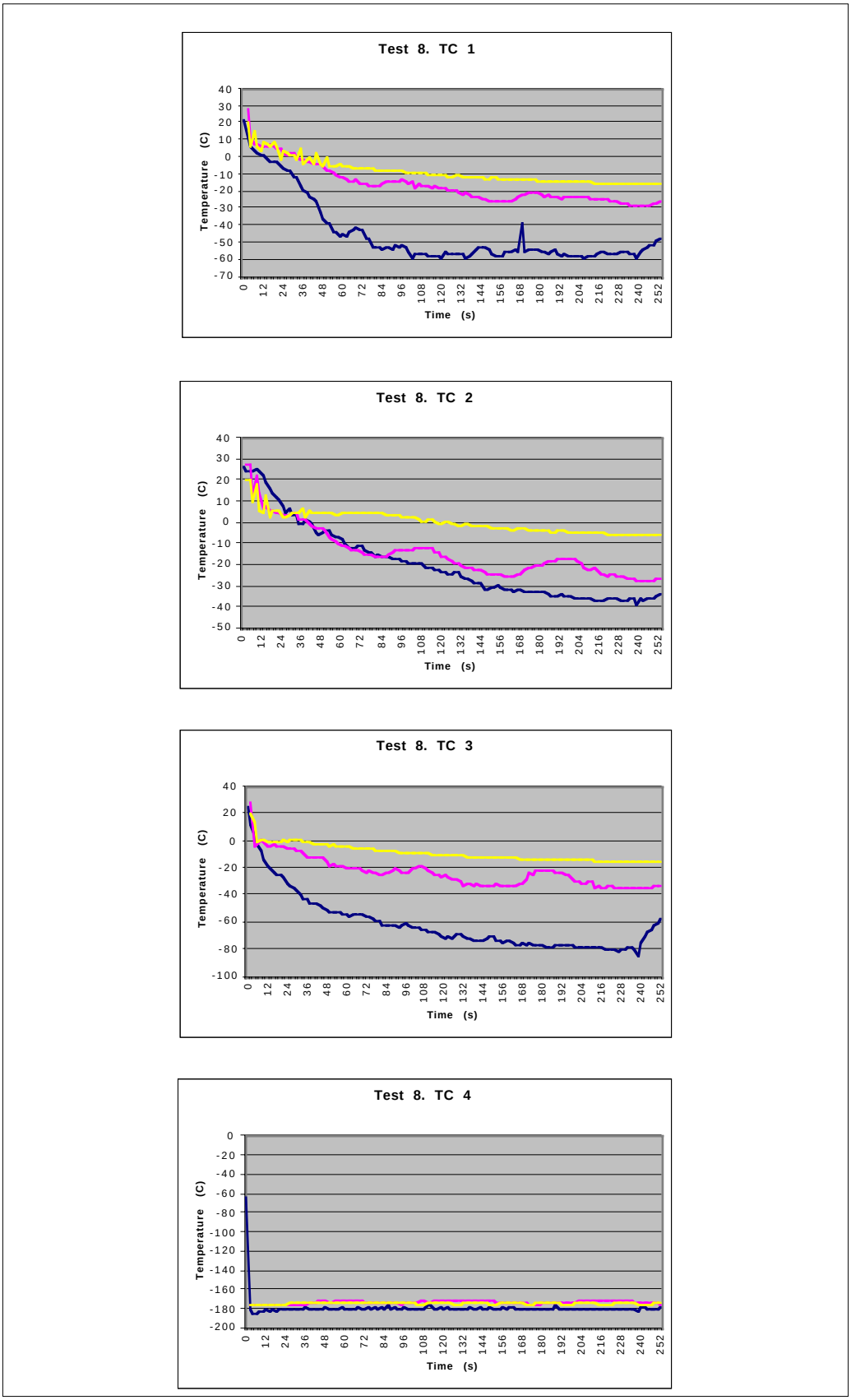

Figure B.40 Temperature comparison. Blue: Experiment, Yellow: One-phase, Pink: Energy Sinks

TEST 8
Comparison

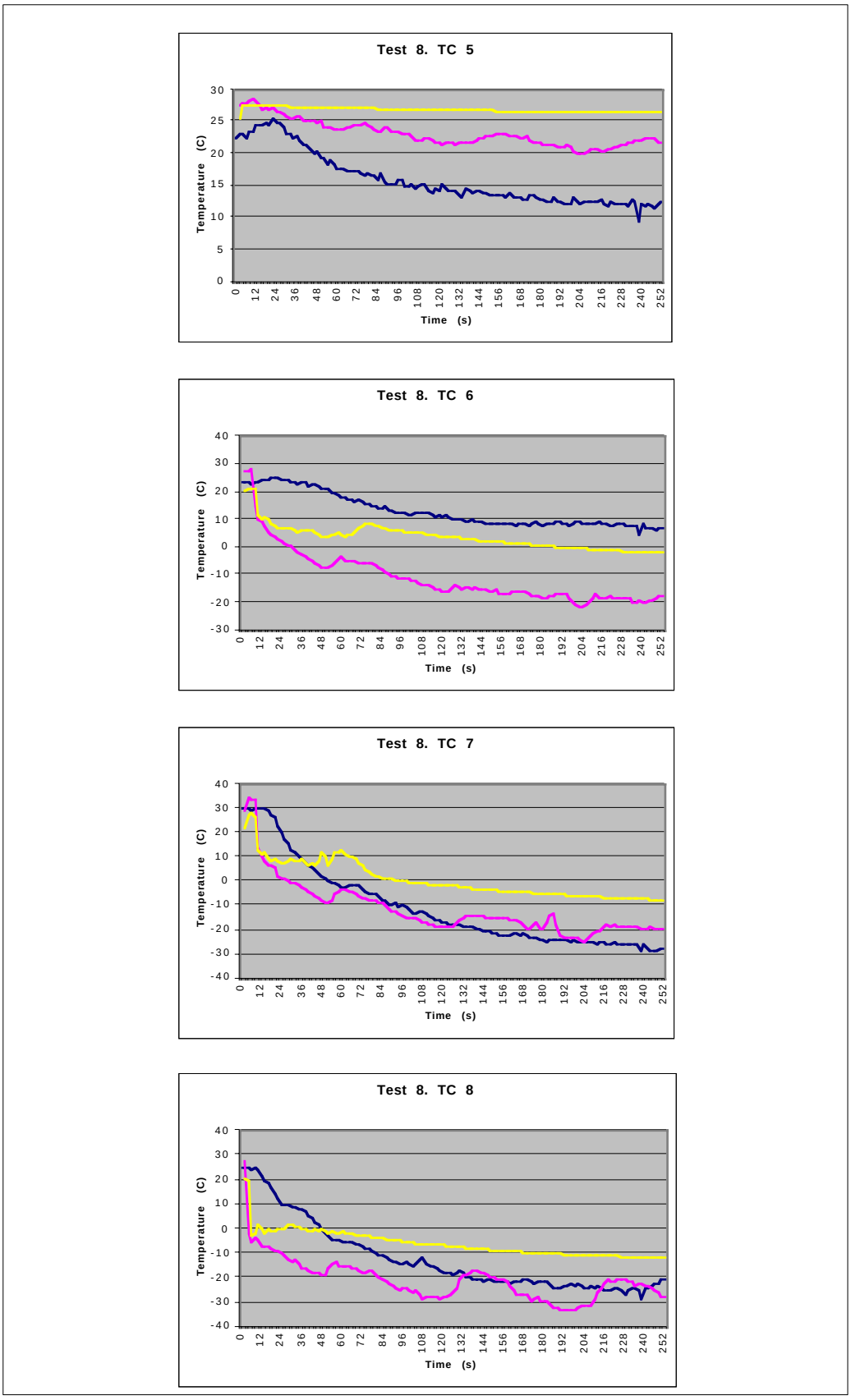

Figure B.41 Temperature comparison. Blue: Experiment, Yellow: One-phase, Pink: Energy Sinks

TEST 8
Comparison

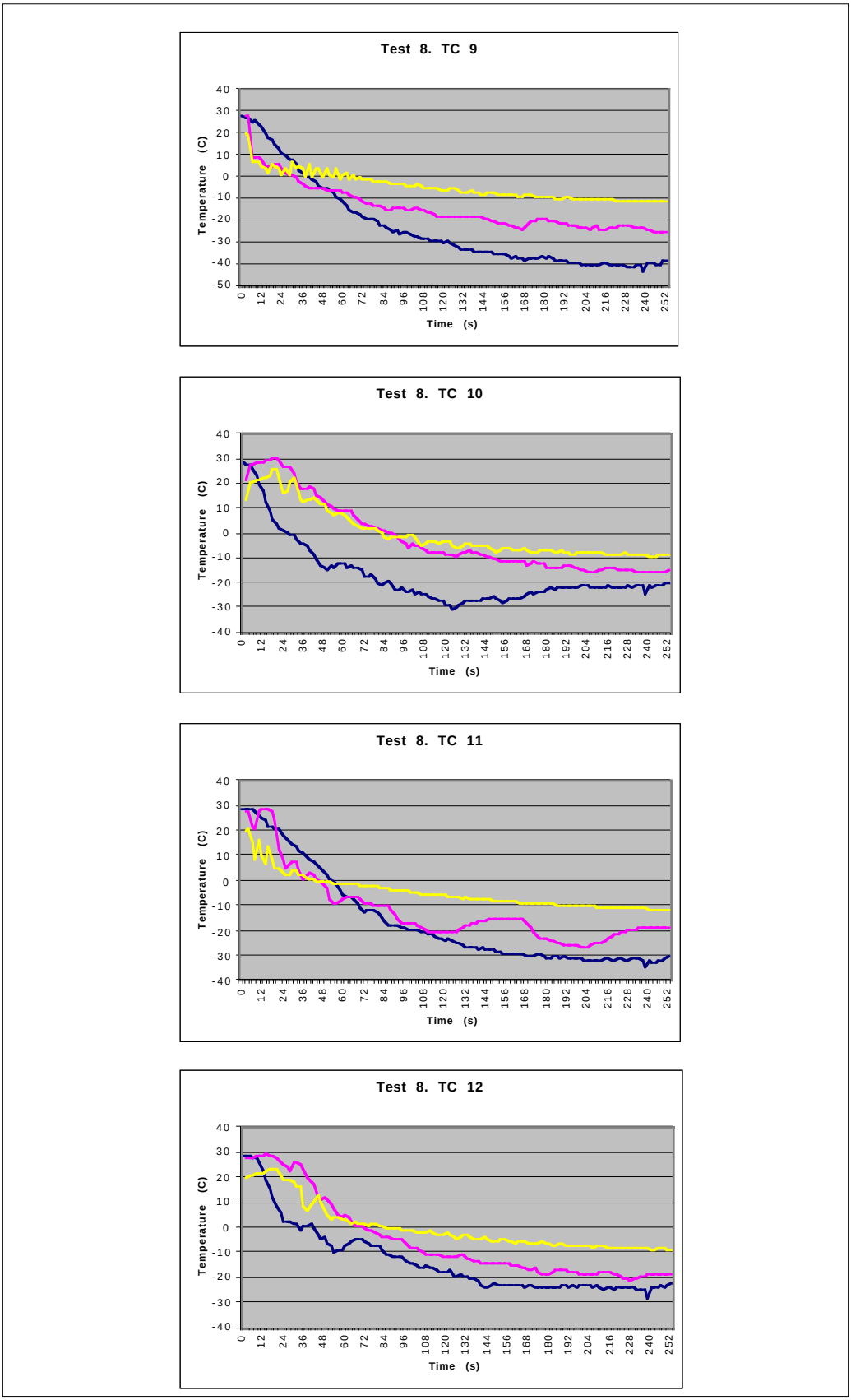

Figure B.42 Temperature comparison. Blue: Experiment, Yellow: One-phase, Pink: Energy Sinks

TEST 8
Comparison

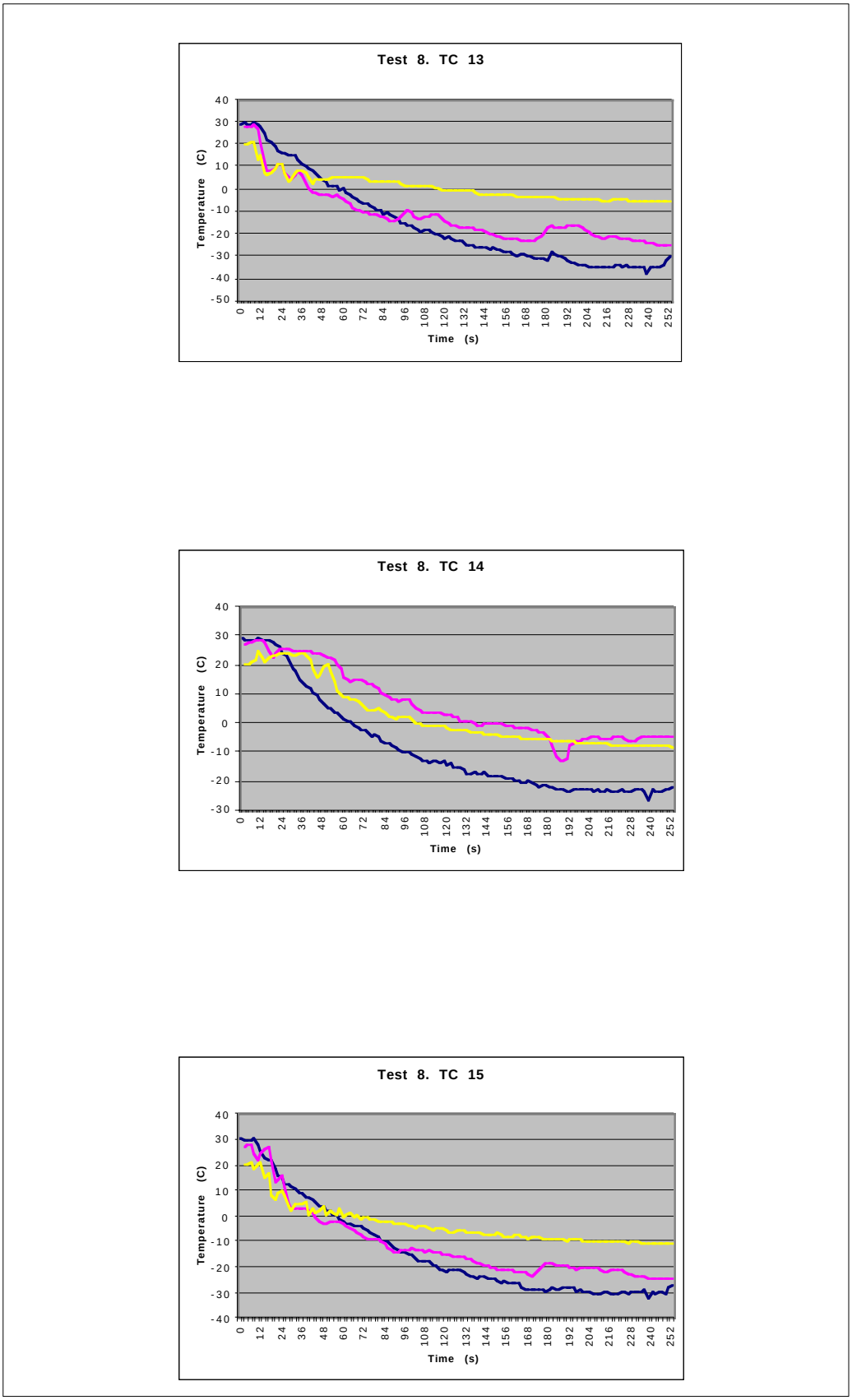

Figure B.43 Temperature comparison. Blue: Experiment, Yellow: One-phase, Pink: Energy Sinks

TEST 8
Comparison

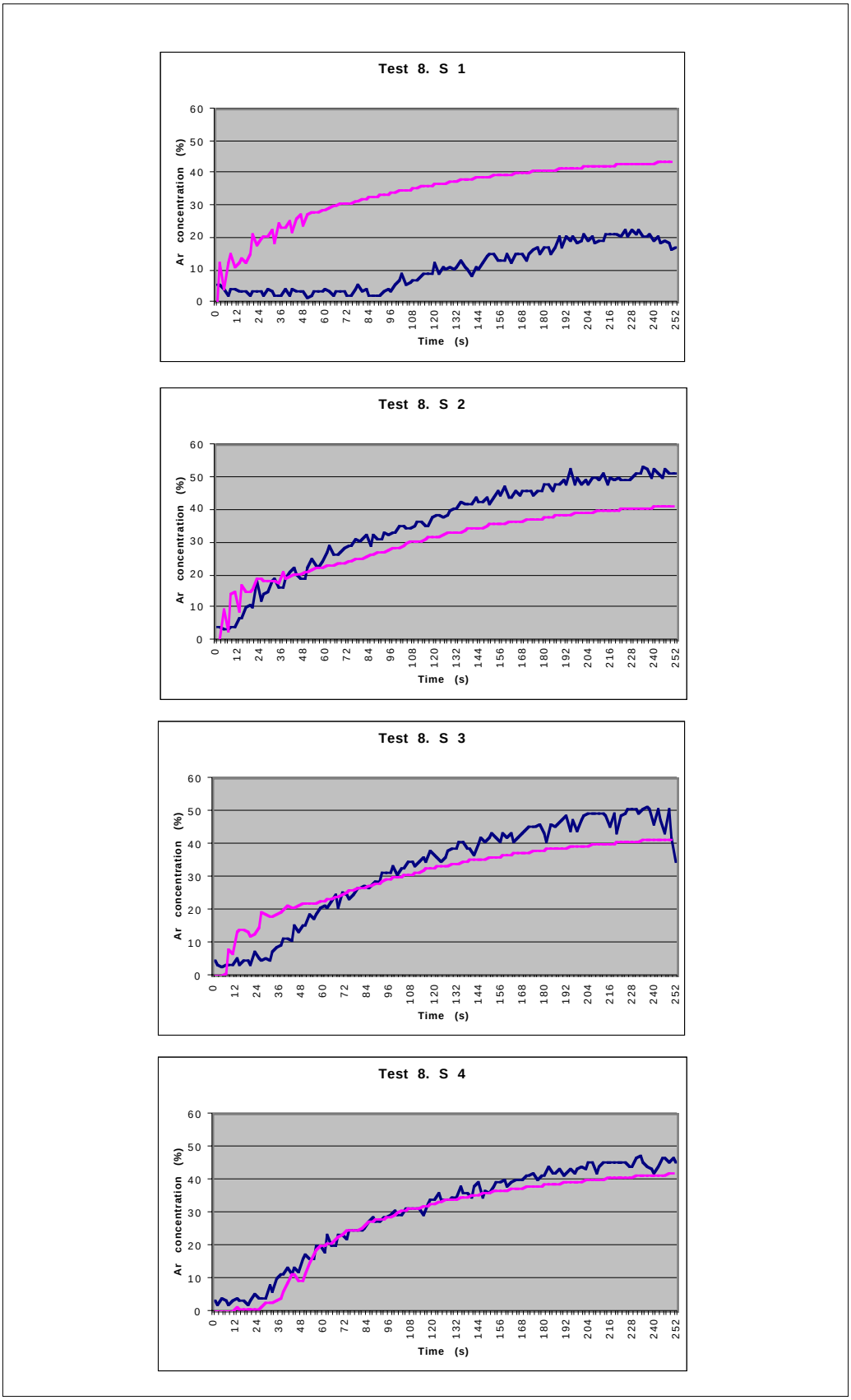

Figure B.44 Argon concentration comparison. Blue: Experiment; Pink: Energy sinks/One-phase flow

TEST 8
Comparison

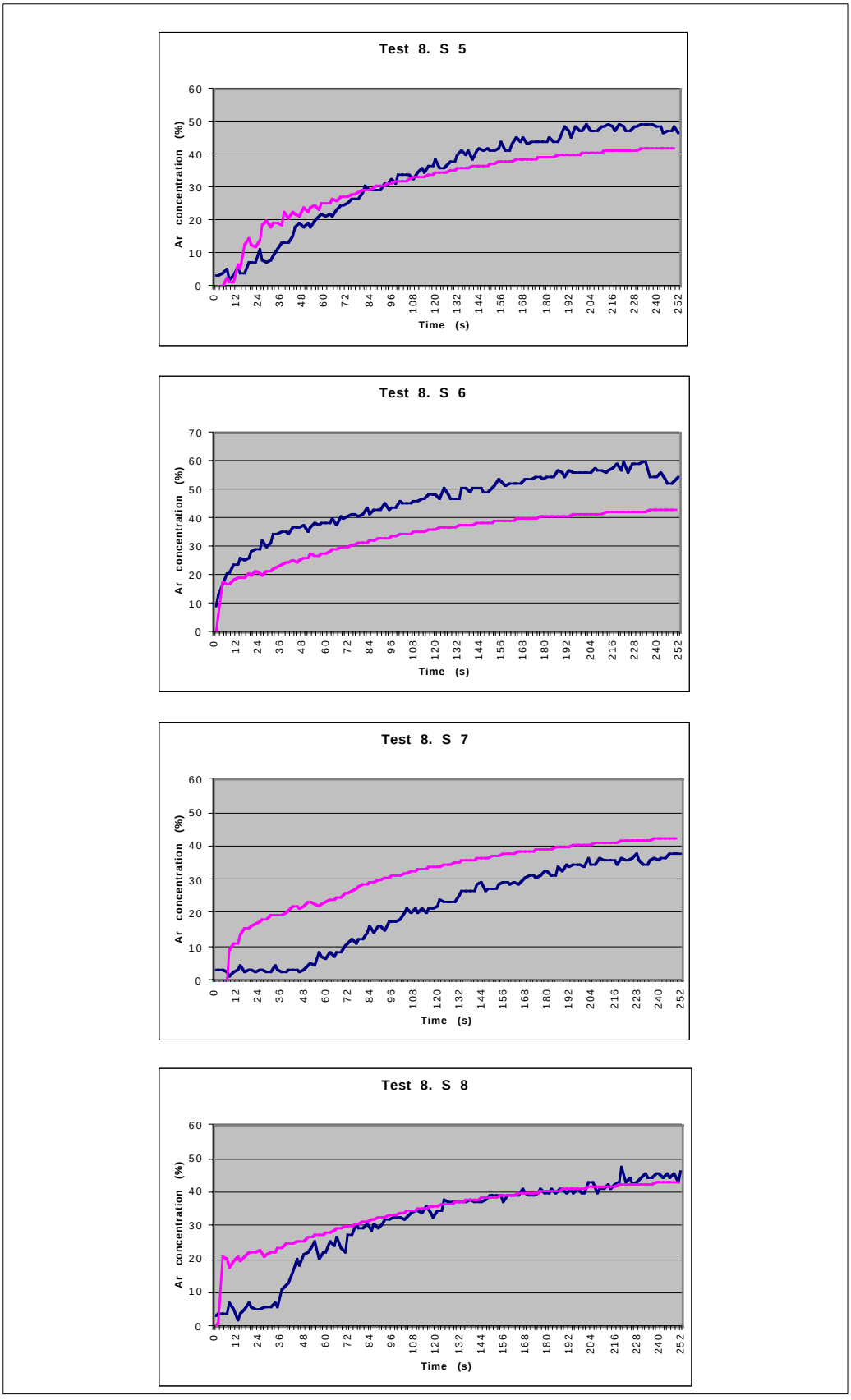

Figure B.45 Argon concentration comparison. Blue: Experiment; Pink: Energy sinks/One-phase flow

TEST 8
Comparison

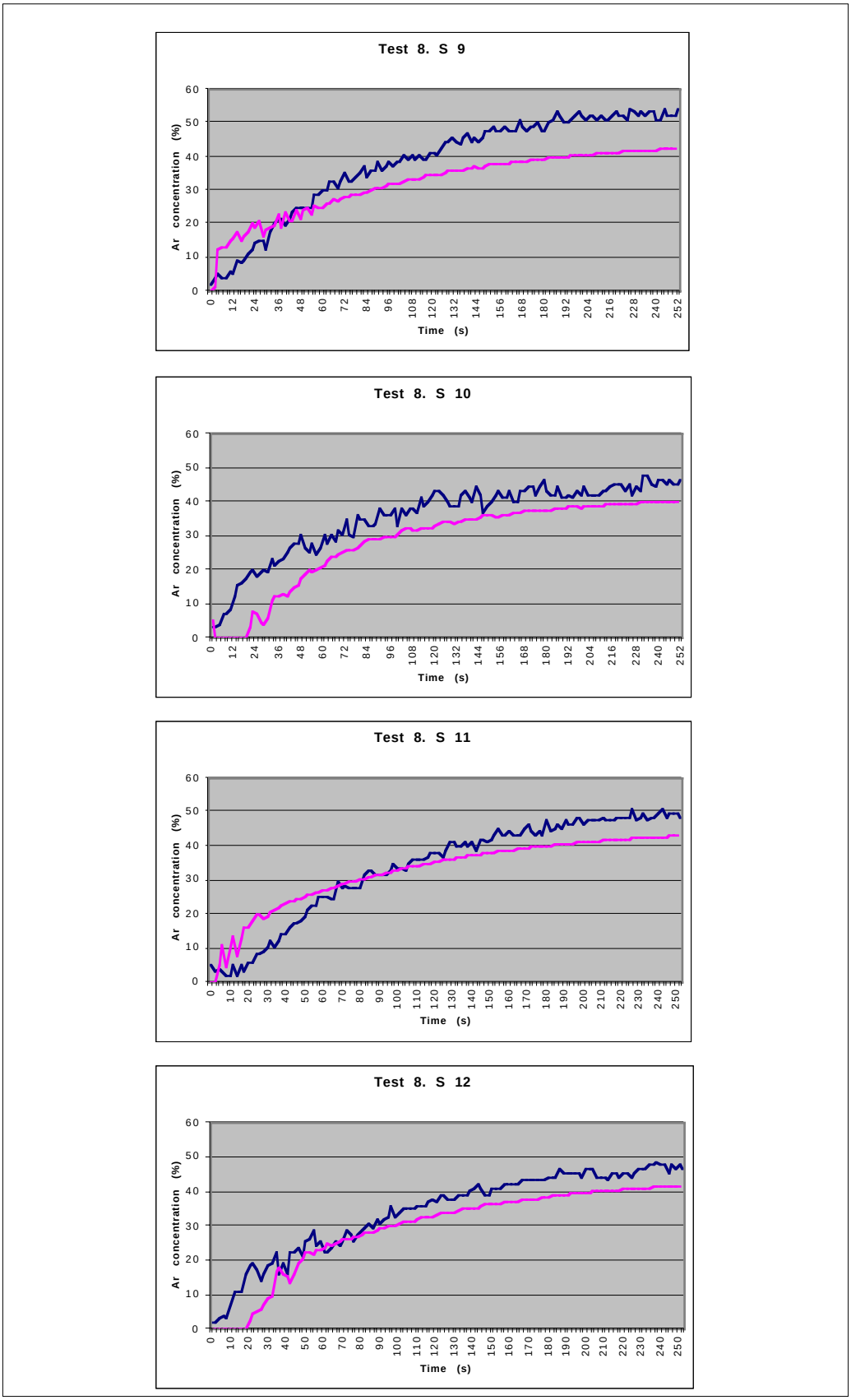

Figure B.46 Argon concentration comparison. Blue: Experiment; Pink: Energy sinks/One-phase flow

B.2.6 Test 9. 10,42 l LAr/min.

TEST 9*
One-Phase Flow

Q	**10,42 l LAr/min**				
Geometry	**Test scenario**				
Energy Sinks	**Non**				
Boundaries	*v (m/s)*	*k (m^2/s^2)*	*ε (m^2/s^3)*	*T (K)*	*ρ (kg/m^3)*
Argon Inlet	0,468	$3{,}28\ 10^{-3}$	0,014	90	5,337
Exhaust fan	No ventilation				
Ceiling extraction	0,018	$5{,}04\ 10^{-6}$	$1{,}12\ 10^{-8}$	300	1,2
Right and left diffusors	No ventilation				
Walls	298,5 K Isothermal				
Heat Load	131,6 W / m^2 Constant heat flux				
Turbulence Model	K - E / R N G				
Differential schemes	*u,v*	*KE*	*ε*	*T*	*ρ*
Time	Fully Implicit				
Space	UD	UD	UD	UD	CD 0,8
Control					
Piso Correctors	4 to 7				
Max. COU number	0,7 to 1				
Mean COU number	0,05 to 0,1				
HDIFF	0,05 to 1 W				
Residual tolerance	0,01 for u,v,T,KE,ε,ρ / 0,001 for P				
Under-relaxation for P	0,8				
Relaxation factors	v-0,7 / KE-0,7 / P-1,0 / T-0,95 / ρ-0,5				
Precision	Double				
Simulated time	10 minutes and 46 seconds				
Folder	TEST 9 / Alpha				

* During the performance of this test without ventilation we could appreciate a big quantity of argon cooling through the door. Besides, the ceiling extraction was difficult to evaluate in this case. Therefore it was difficult to model this test. This results in bad predictions from the simulation, as we see in the Temperature evolution we show in the following pages. This is the reason why we do not show the argon concentration curves .

TEST 9
One-Phase Flow

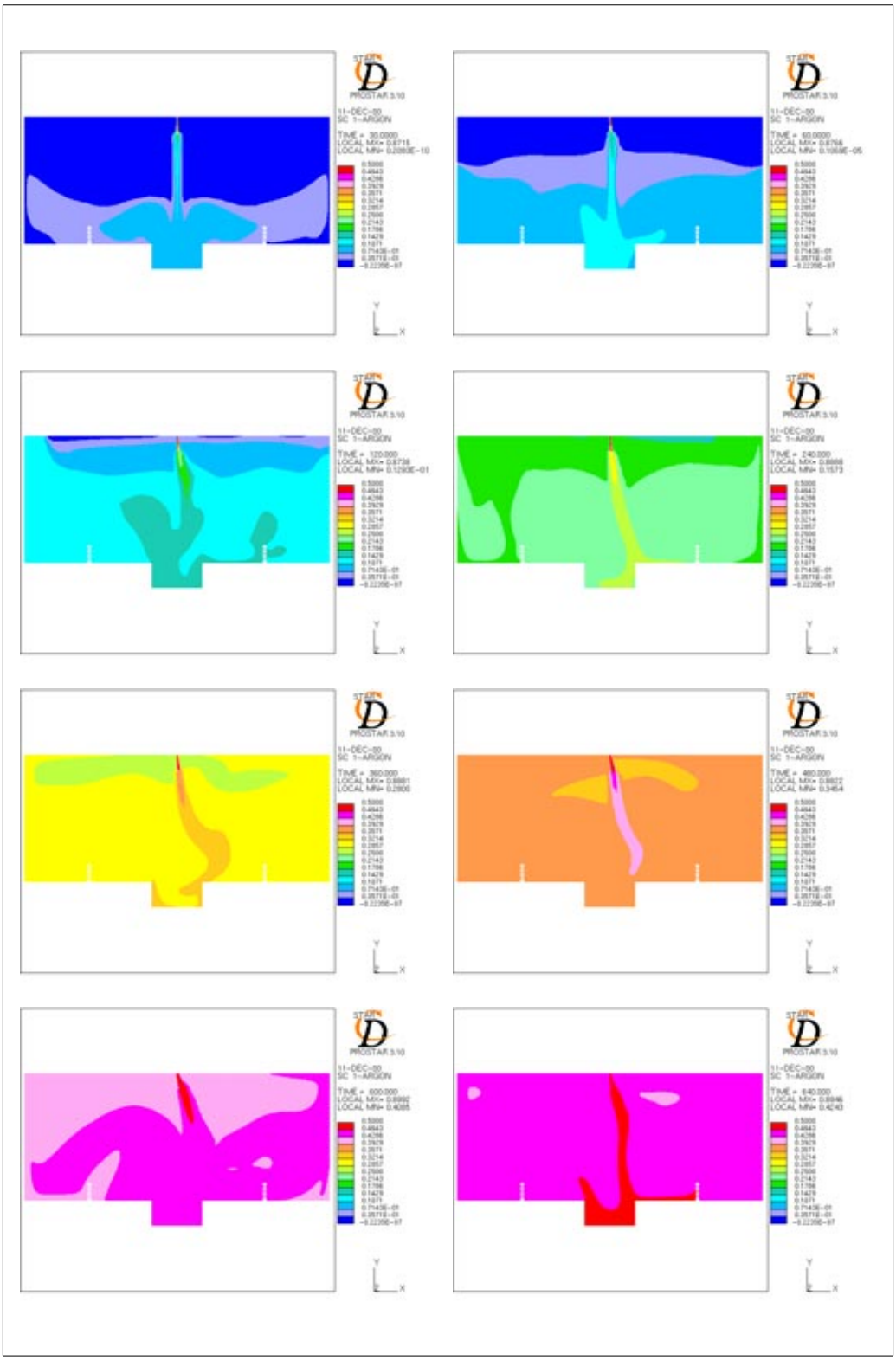

Figure B.47 Argon concentration 10,30,60,120,240,360,480,600 and 640 s after the spill

TEST 9
One-Phase Flow

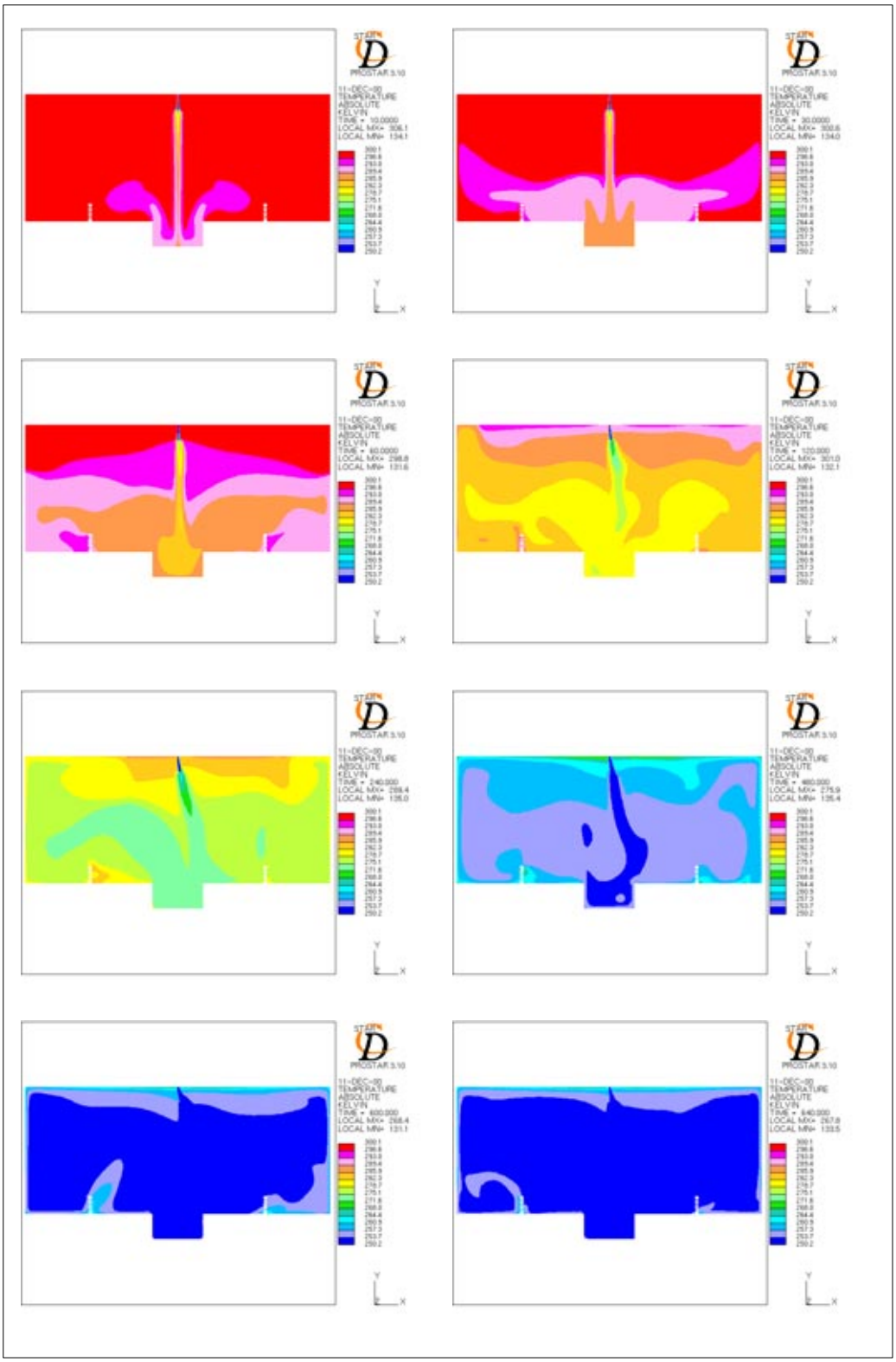

Figure B.48 Temperature distribution 10,30,60,120,240,360,480,600 and 640s after the spill

TEST 9
Comparison

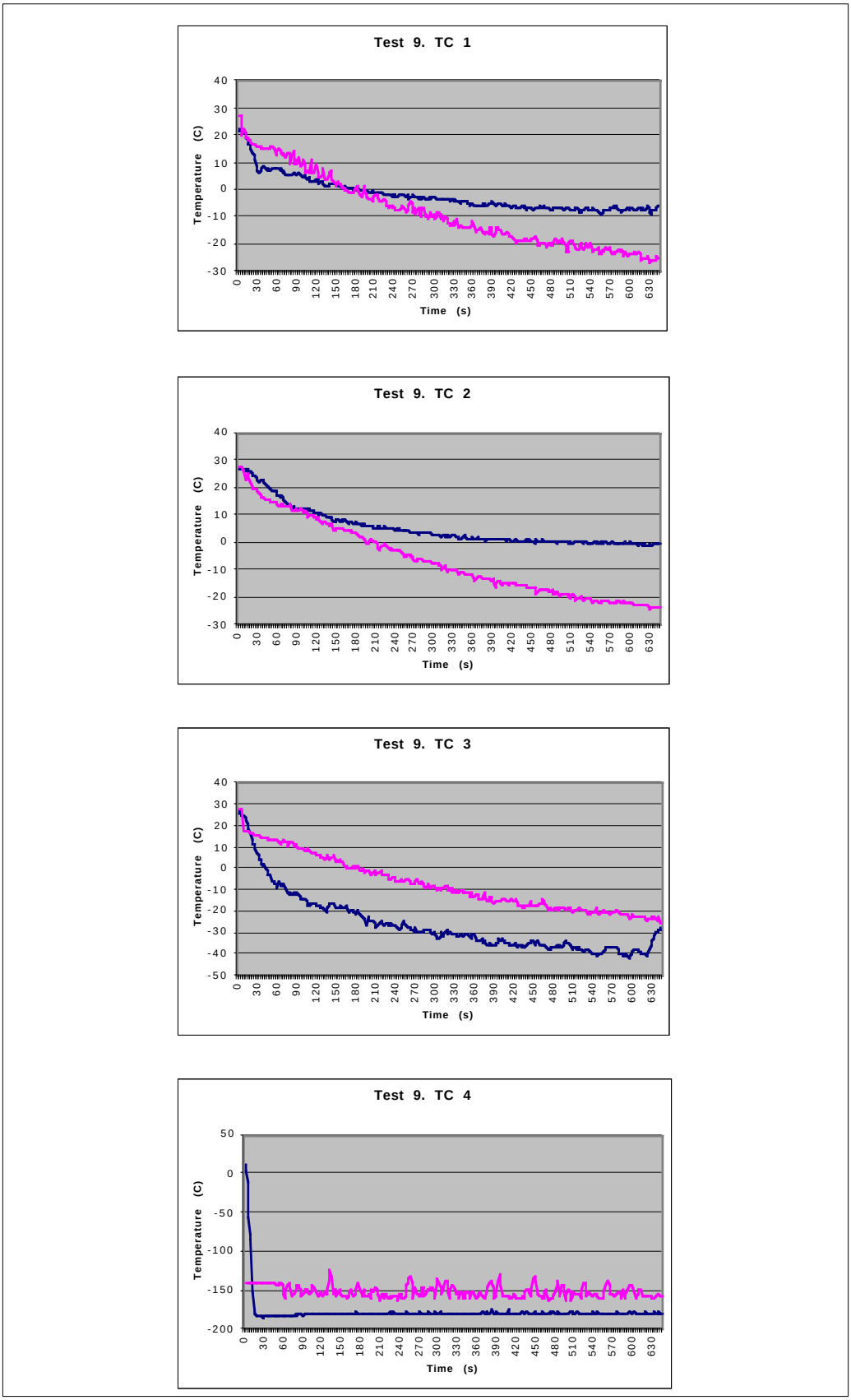

Figure B.49 Temperature comparison. Blue: Experiment, Pink: One-phase

TEST 9
Comparison

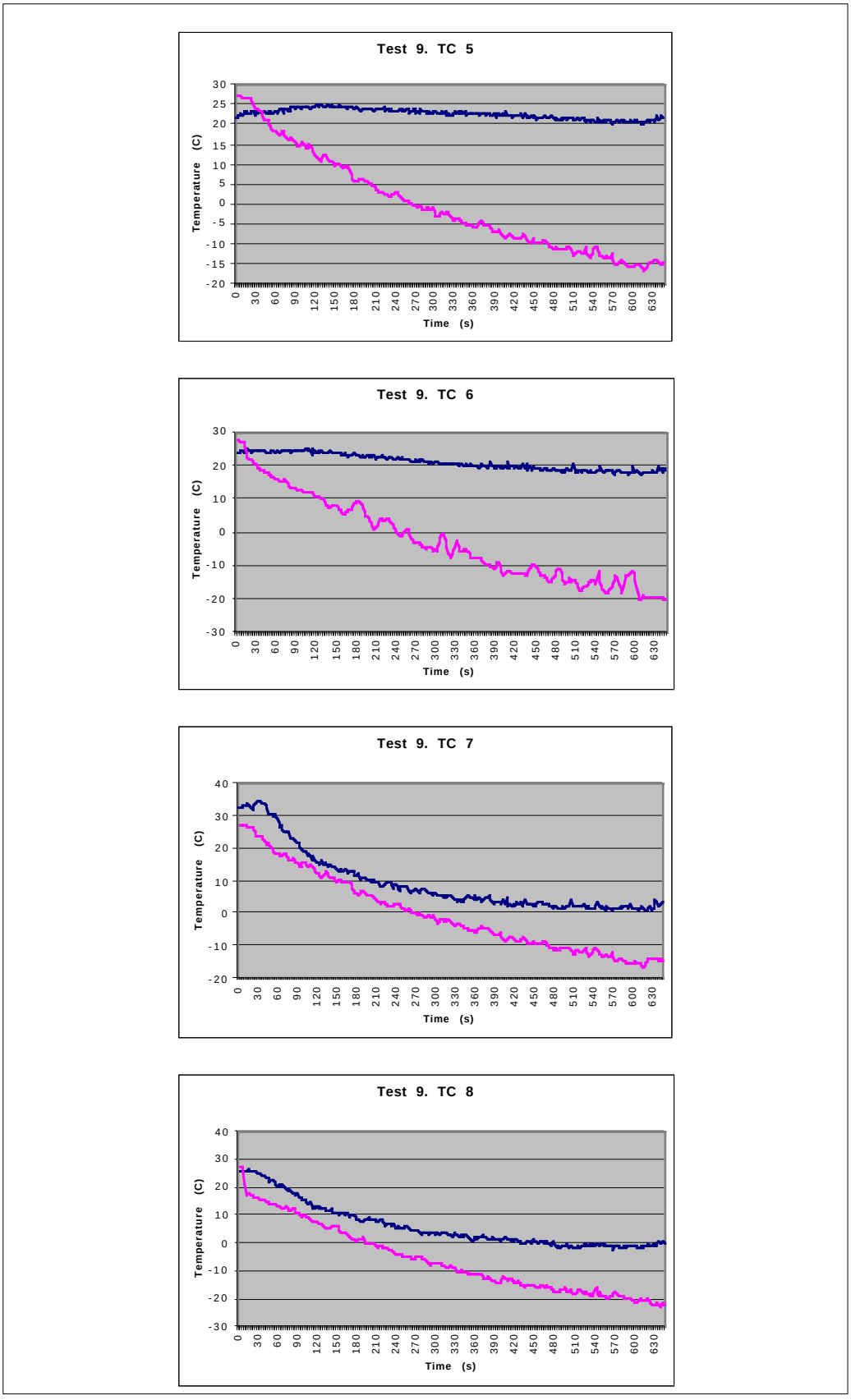

Figure B.50 Temperature comparison. Blue: Experiment, Pink: One-Phase

TEST 9
Comparison

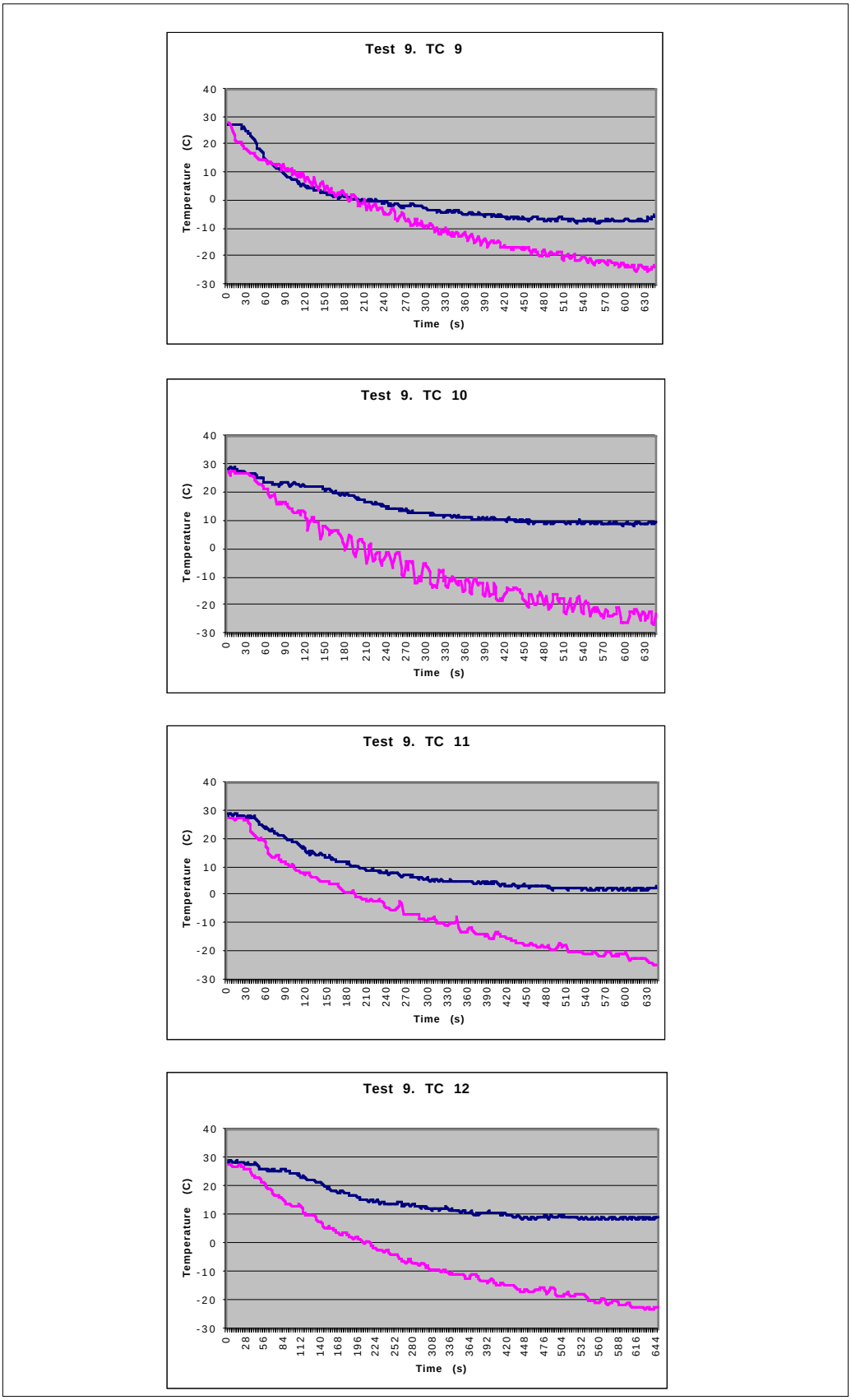

Figure B.51 Temperature comparison. Blue: Experiment, Pink: One-Phase

TEST 9
Comparison

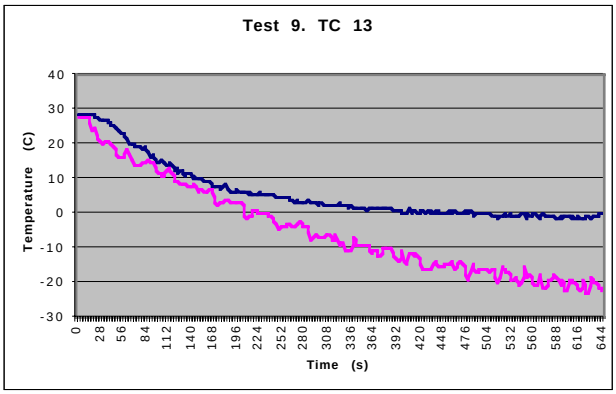

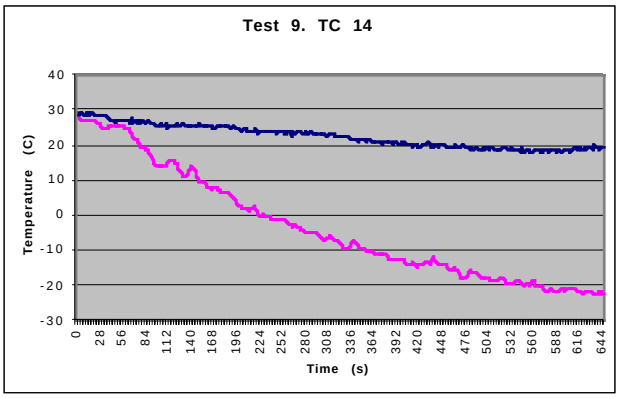

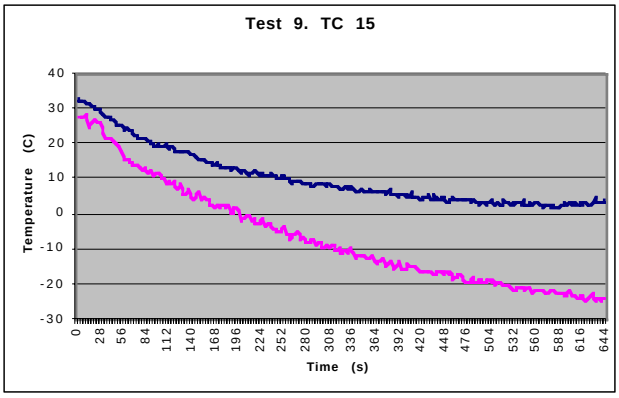

Figure B.52 Temperature comparison. Blue: Experiment, Pink: One-Phase

B.2.7 Test 10. 27,33 l LAr/min.

TEST 10
One-Phase Flow

Q	**27,33 l LAr/min**				
Geometry	**Test scenario**				
Energy Sinks	**Non**				
Boundaries	*v (m/s)*	*k (m^2/s^2)*	*ε (m^2/s^3)*	*T (K)*	*ρ (kg/m^3)*
Argon Inlet	1,227	0,022	0,267	90	5,337
Exhaust fan	0,412	$2,55\ 10^{-3}$	$1,35\ 10^{-3}$	299	1,2
Ceiling extraction	0,197	$5,85\ 10^{-4}$	$1,40\ 10^{-5}$	301	1,2
Right and left diffusors	0,161	$3,91\ 10^{-4}$	$1,0\ 10^{-5}$	301	1,2
Walls	296,6 K Isothermal				
Heat Load	131,6 W / m^2 Constant heat flux				
Turbulence Model	K - E / R N G				
Differential schemes	*u,v*	*KE*	*ε*	*T*	*ρ*
Time	F u l l y I m p l i c i t				
Space	UD	UD	UD	UD	CD 0,8
Control					
Piso Correctors	3 to 6				
Max. COU number	0,7 to 2,5				
Mean COU number	0,02 to 0,2				
HDIFF	0,05 to 0,8 W				
Residual tolerance	0,01 for u,v,T,KE,ε,ρ / 0,001 for P				
Under-relaxation for P	0,8				
Relaxation factors	v-0,7 / KE-0,7 / P-1,0 / T-0,95 / ρ-0,5				
Precision	Double				
Simulated time	5 minutes and 18 seconds				
Folder	TEST 10 / Alpha				

TEST 10
One-Phase flow

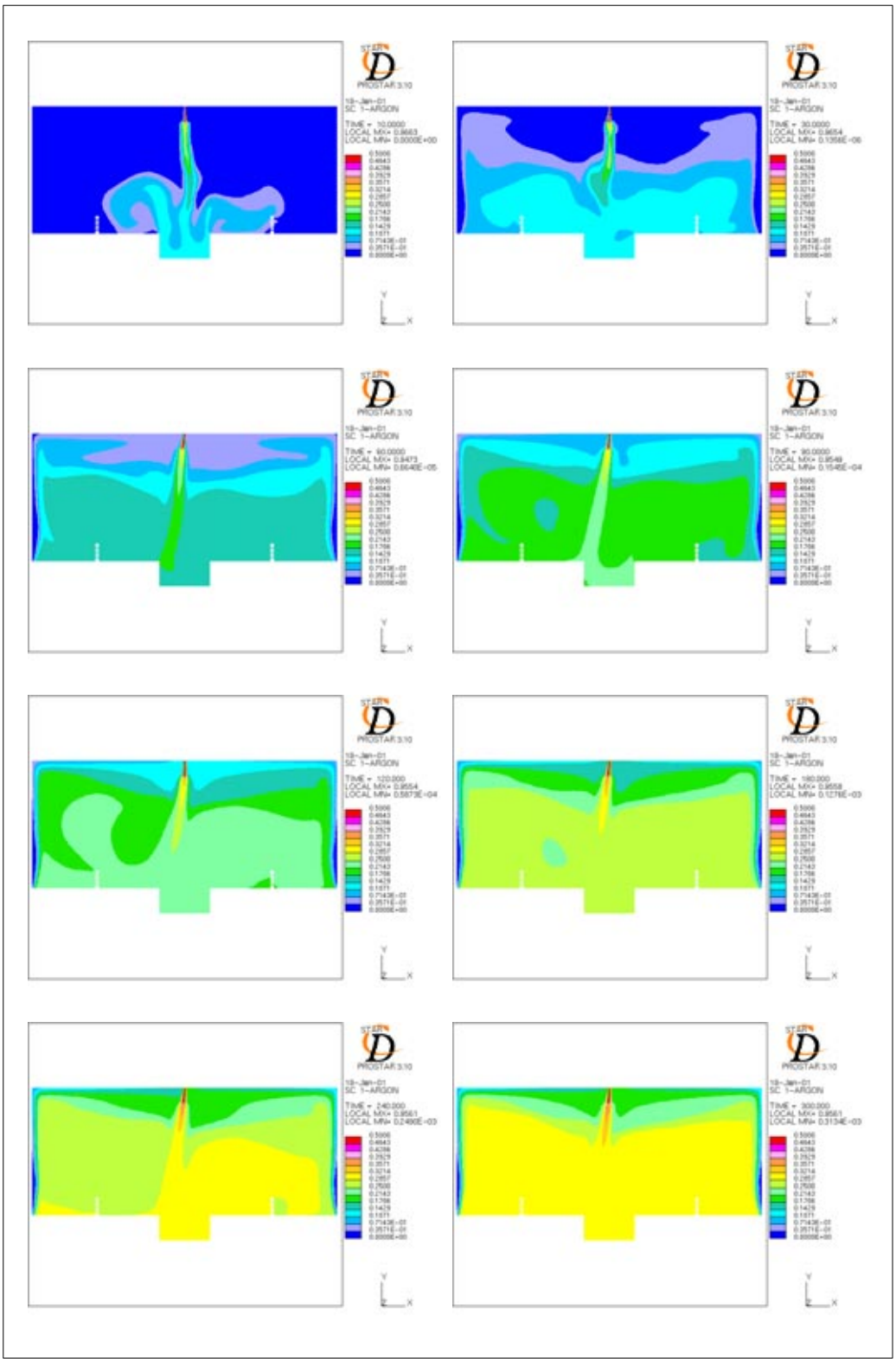

Figure B.53 Argon Concentration. 10,30,60,90,120,180,240 and 300 s after the spill

TEST 10
One-Phase flow

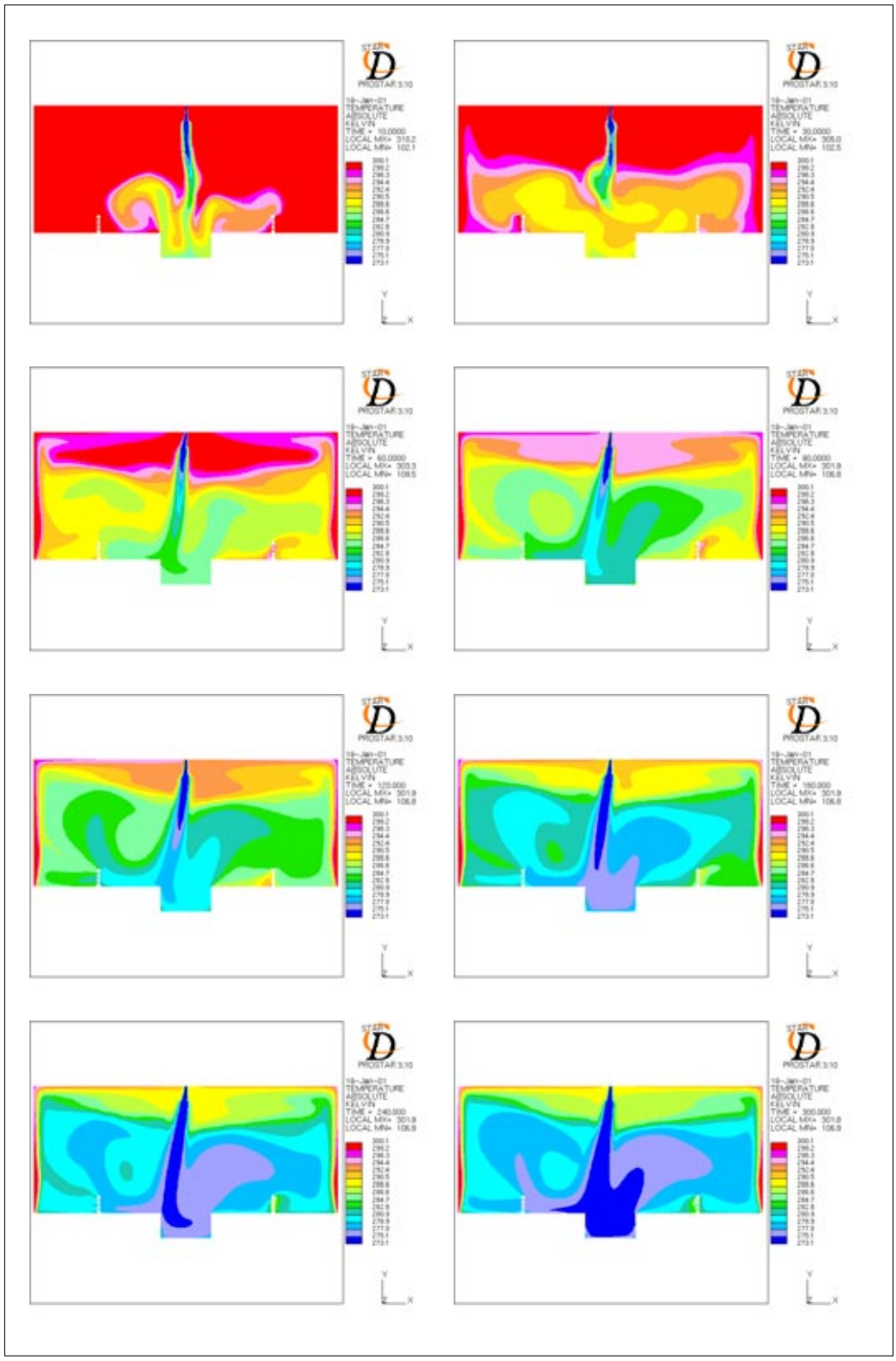

Figure B.54 Temperature distribution 10,30,60,90,120,180,240 and 300 s after the spill

TEST 10
One-Phase with Energy Sinks

Q	**27,33 l LAr/min**				
Geometry	**Test scenario**				
Energy Sinks	**Yes: 18,37 kW / 7652 W/m^3**				
Boundaries	*v (m/s)*	*k (m^2/s^2)*	*ε (m^2/s^3)*	*T (K)*	*ρ (kg/m^3)*
Argon Inlet	1,227	0,022	0,267	90	5,337
Exhaust fan	0,412	$2{,}55\ 10^{-3}$	$1{,}35\ 10^{-3}$	299	1,2
Ceiling extraction	0,197	$5{,}85\ 10^{-4}$	$1{,}40\ 10^{-5}$	301	1,2
Right and left diffusors	0,161	$3{,}91\ 10^{-4}$	$1{,}0\ 10^{-5}$	301	1,2
Walls	296,6 K Isothermal				
Heat Load	131,6 W / m^2 Constant heat flux				
Turbulence Model	K - E / R N G				
Differential schemes	*u,v*	*KE*	*ε*	*T*	*ρ*
Time	F u l l y I m p l i c i t				
Space	UD	UD	UD	UD	CD 0,8
Control					
Piso Correctors	3 to 4				
Max. COU number	0,6 to 3				
Mean COU number	0,1 to 0,2				
HDIFF	0,1 to 5 W				
Residual tolerance	0,01 for u,v,T,KE,ε,ρ / 0,001 for P				
Under-relaxation for P	0,8				
Relaxation factors	v-0,7 / KE-0,7 / P-1,0 / T-0,95 / ρ-0,5				
Precision	Double				
Simulated time	5 minutes and 18 seconds				
Folder	TEST SINKS 10 / Alpha				

TEST 10
One-phase with Energy Sinks

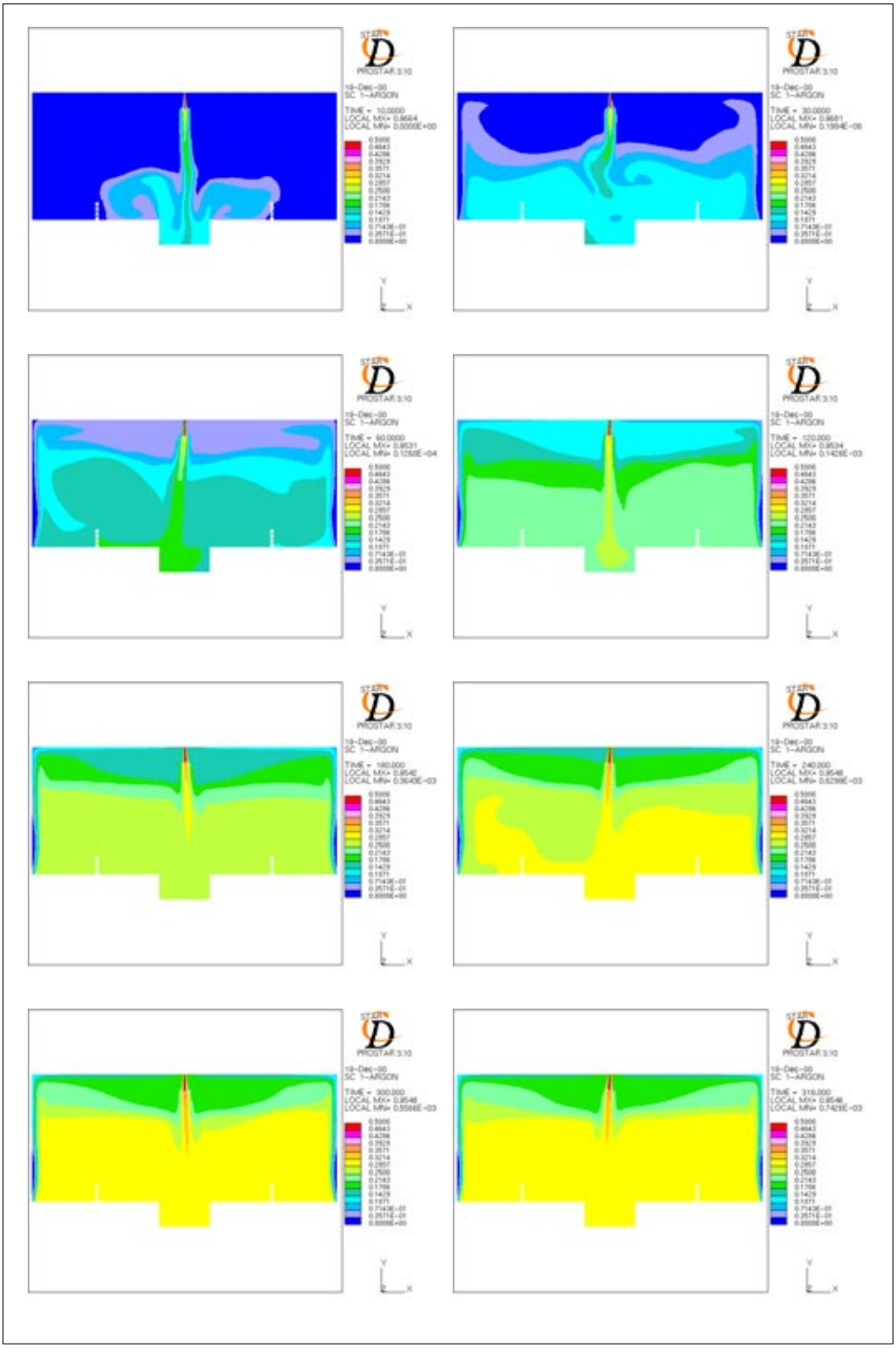

Figure B.55 Argon concentration 10,30,60,120,180,240,300 and 318 s after the spill

TEST 10
One-phase with Energy Sinks

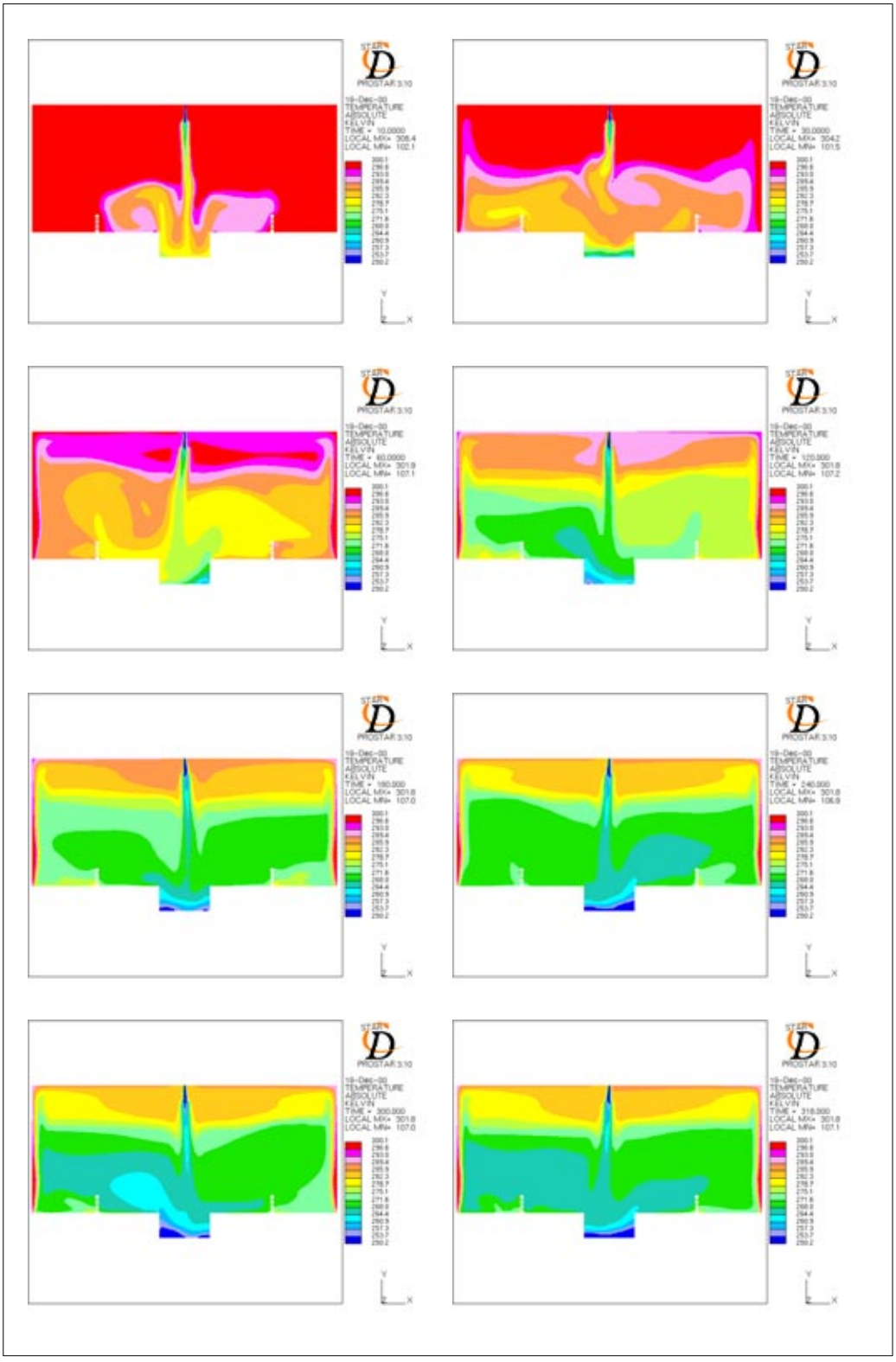

Figure B.56 Temperature distribution 10,30,60,120,180,240,300 and 318 s after the spill

TEST 10
Comparison

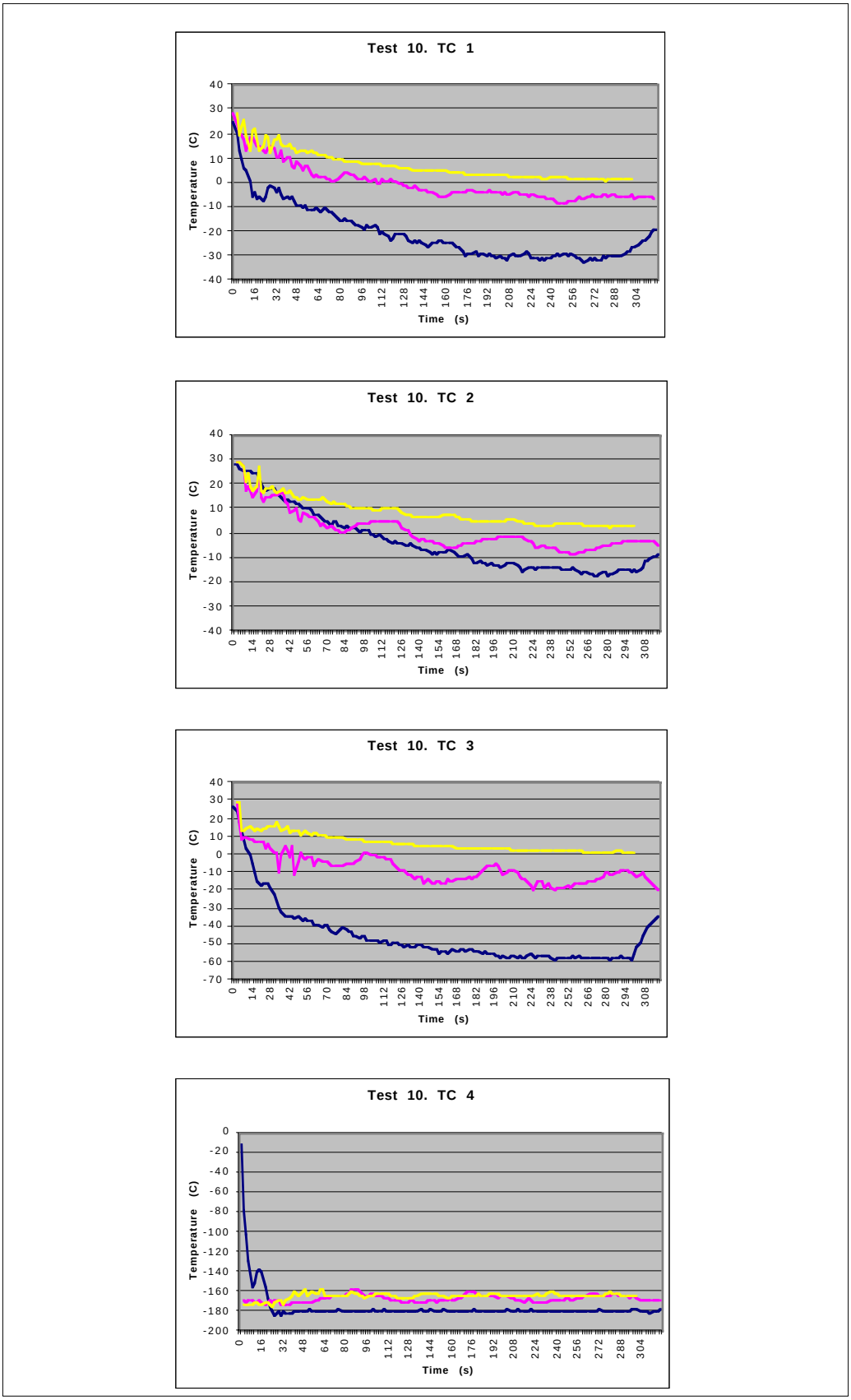

Figure B.57 Temperature comparison. Blue: Experiment, Pink: Energy Sinks; Yellow: One-Phase

TEST 10
Comparison

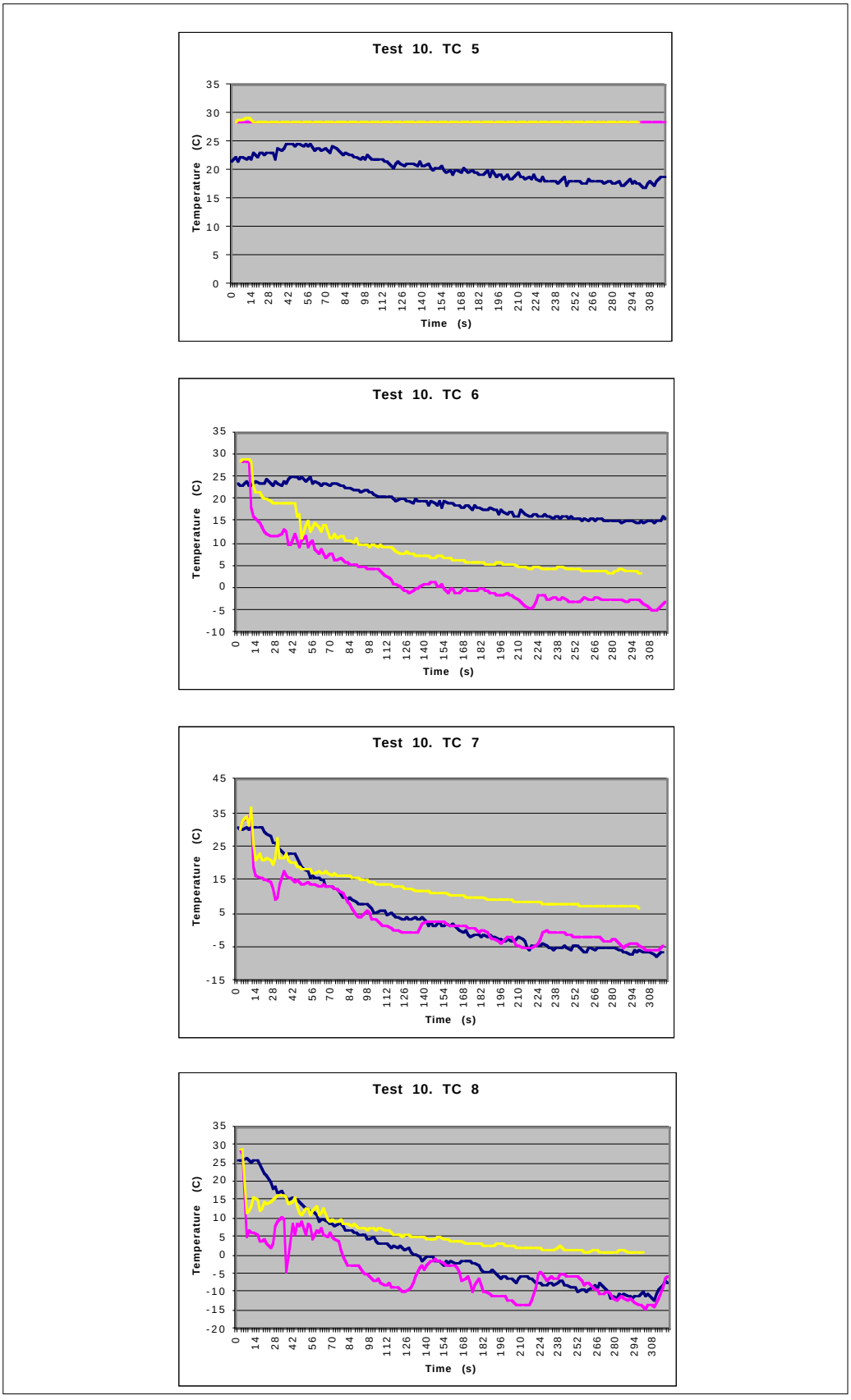

Figure B.58 Temperature comparison. Blue: Experiment, Pink: Energy-Sinks; Yellow: One-Phase

TEST 10
Comparison

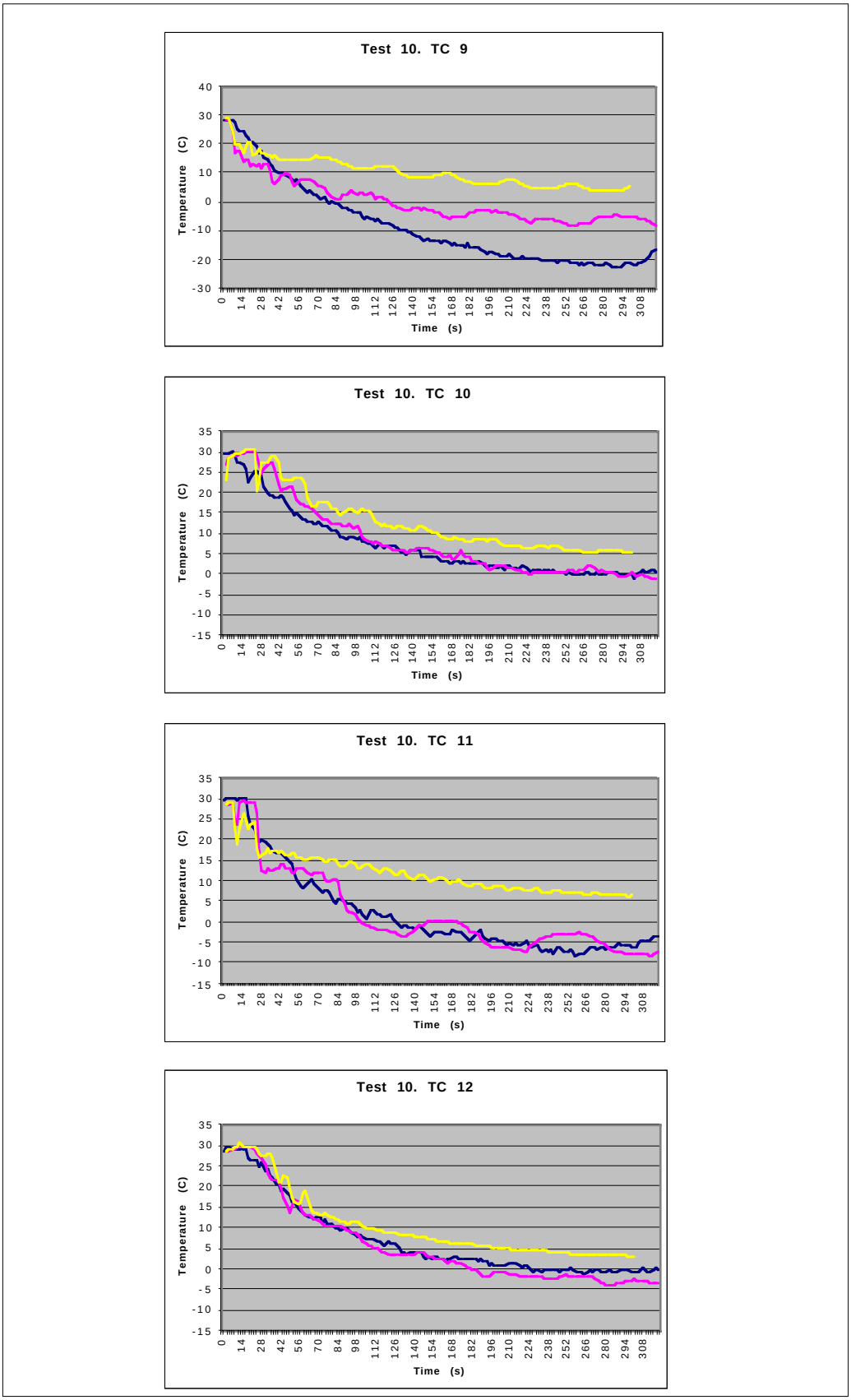

Figure B.59 Temperature comparison. Blue: Experiment, Pink: Energy-Sinks; Yellow: One-Phase

TEST 10
Comparison

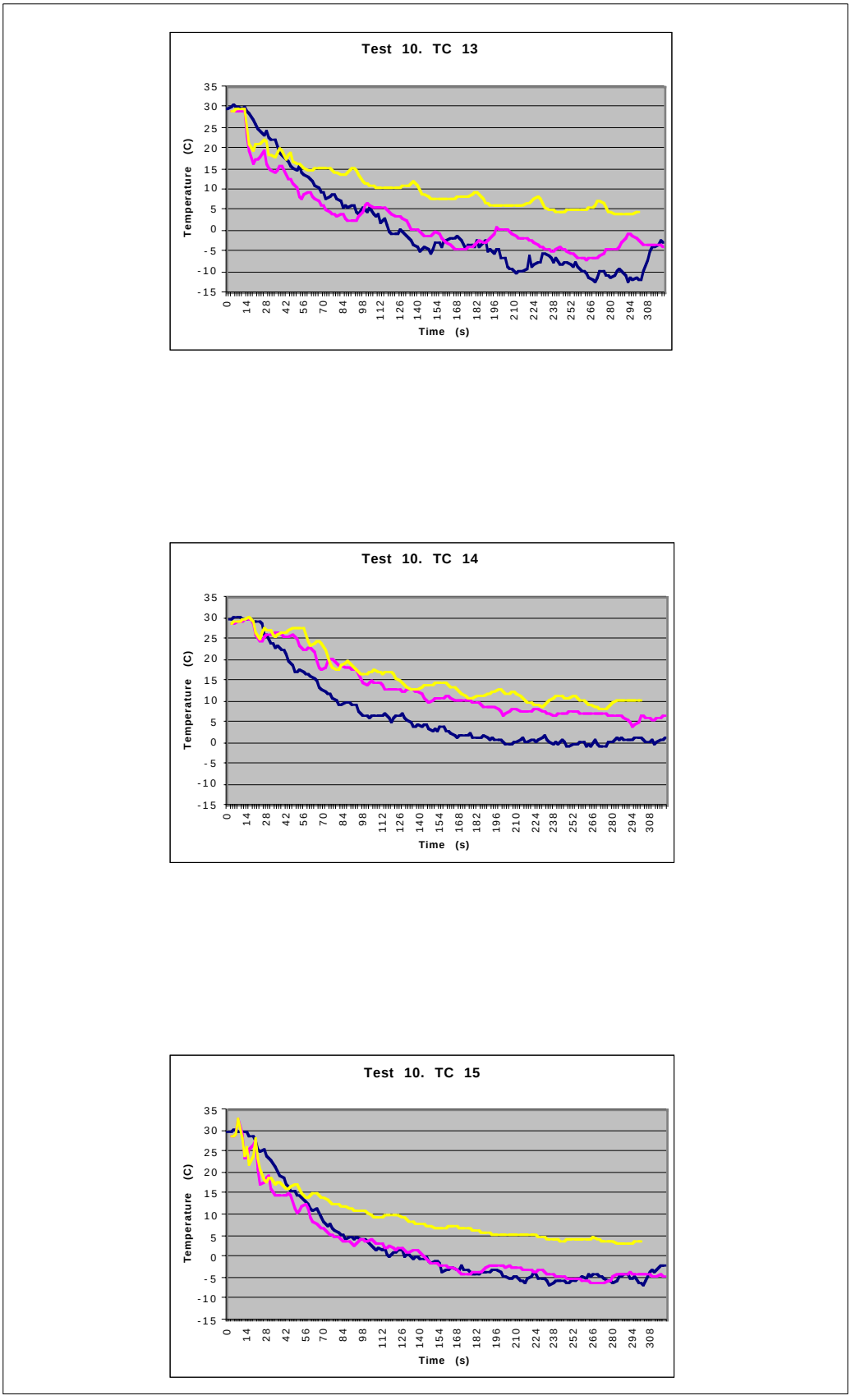

Figure B.60 Temperature comparison. Blue: Experiment, Pink: Energy-Sinks; Yellow: One-Phase

TEST 10
Comparison

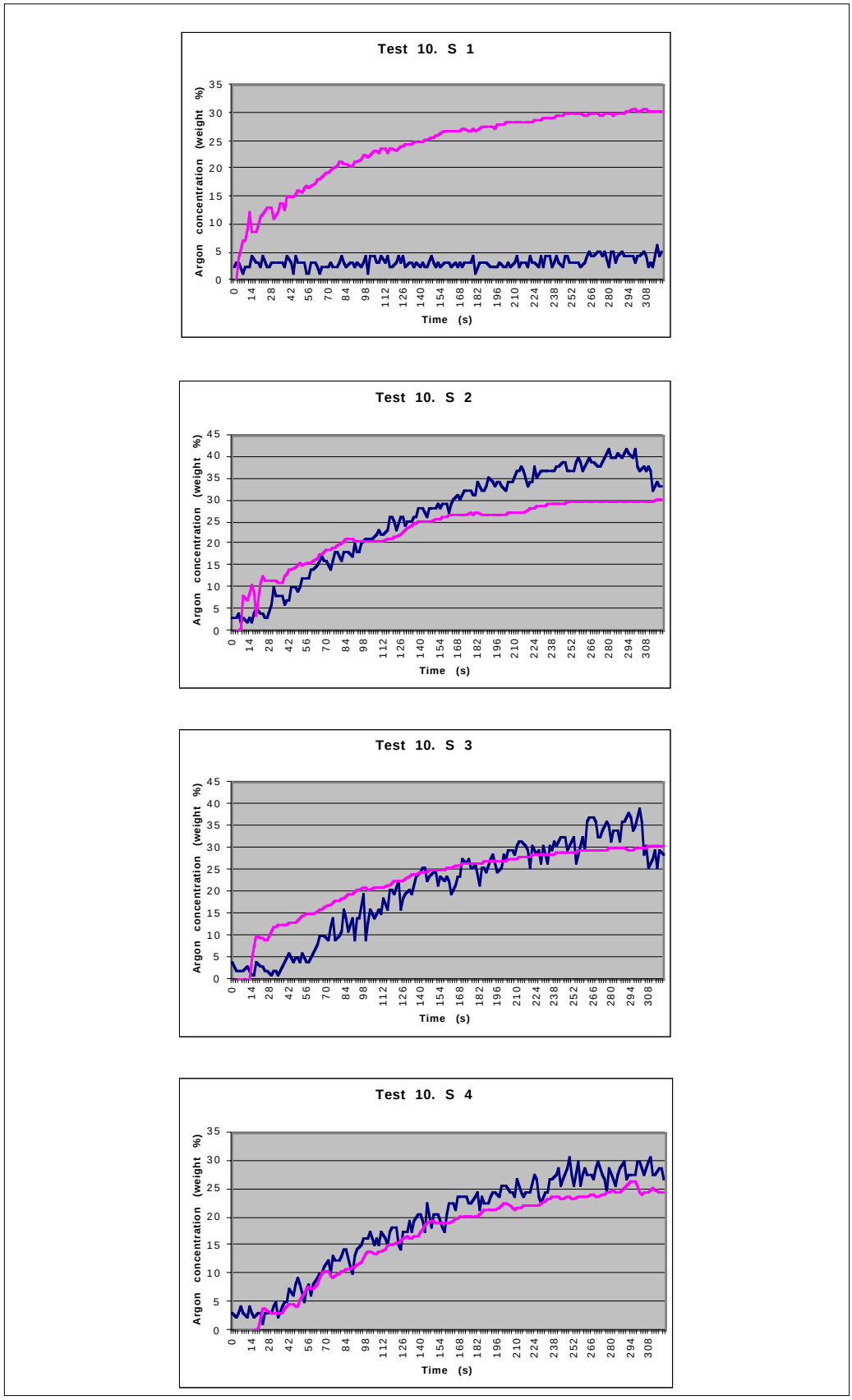

Figure B.61 Argon concentration comparison. Blue: Experiment, Pink: Energy-Sinks / One-Phase

TEST 10
Comparison

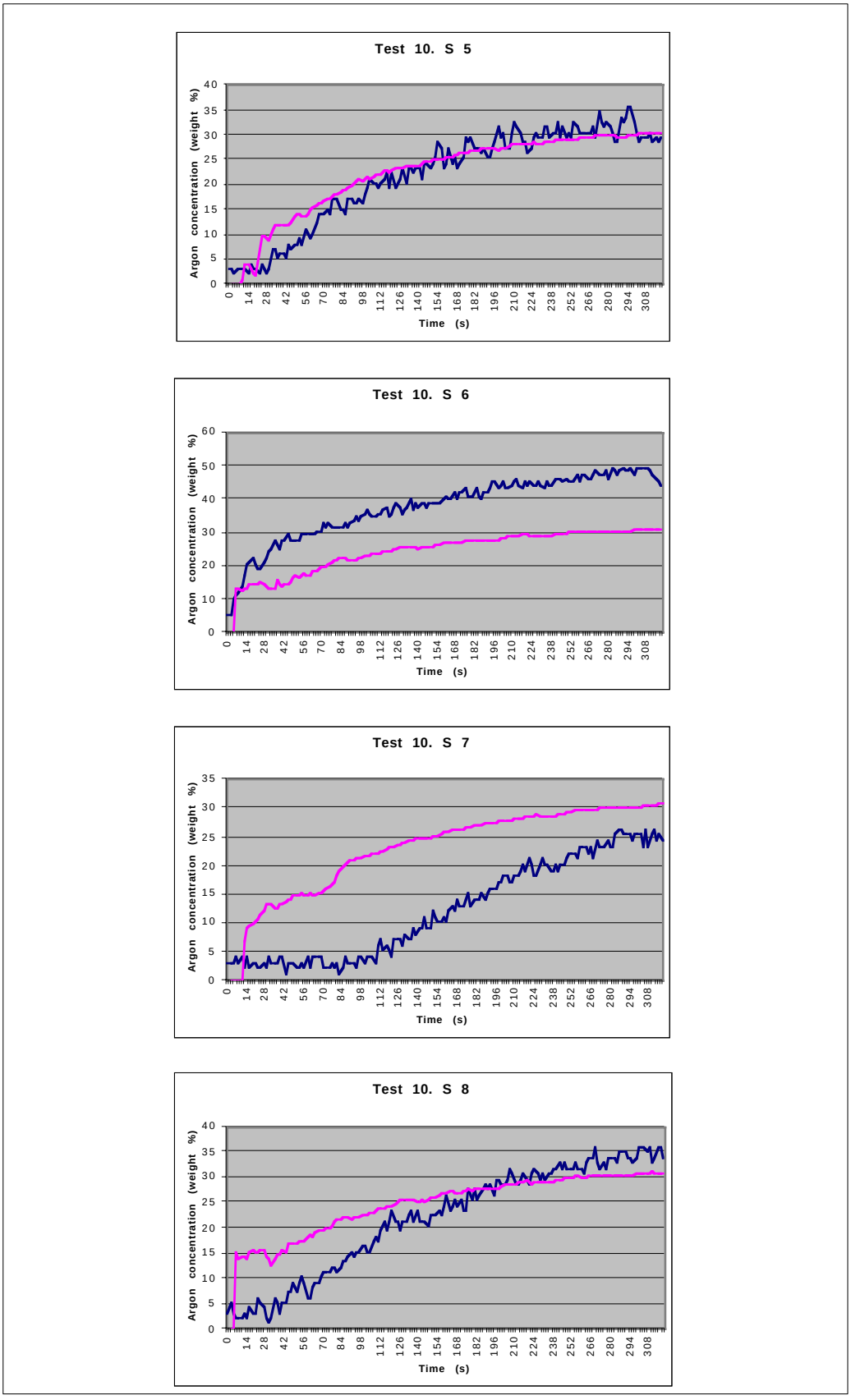

Figure B.62 Argon concentration comparison. Blue: Experiment, Pink: Energy-Sinks / One-Phase

TEST 10
Comparison

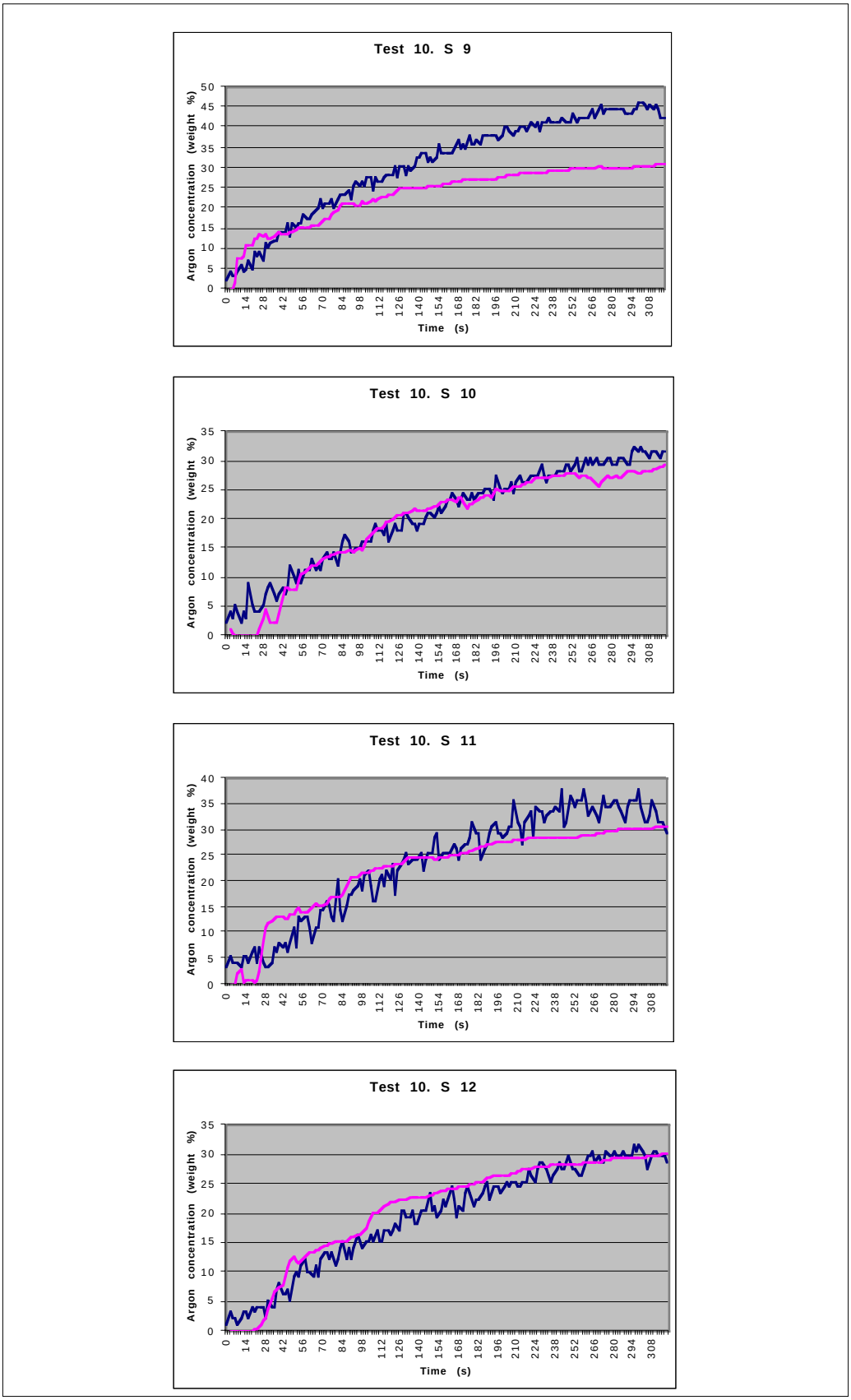

Figure B.63 Argon concentration comparison. Blue: Experiment, Pink:Energy-Sinks / One-Phase

B.2.8 TEST 11. 40,84 l LAr/min

TEST 11
One-Phase Flow

Q	**40,84 l LAr/min**				
Geometry	**Test scenario**				
Energy Sinks	**Non**				
Boundaries	*v (m/s)*	*k (m^2/s^2)*	*ε (m^2/s^3)*	*T (K)*	*ρ (kg/m^3)*
Argon Inlet	1,835	0,051	0,892	90	5,337
Exhaust fan	0,412	$2,55\ 10^{-3}$	$1,35\ 10^{-3}$	298	1,2
Ceiling extraction	0,197	$5,85\ 10^{-4}$	$1,40\ 10^{-5}$	299	1,2
Right and left diffusors	0,161	$3,91\ 10^{-4}$	$1,0\ 10^{-5}$	299	1,2
Walls	296,6 K Isothermal				
Heat Load	131,6 W / m^2 Constant heat flux				
Turbulence Model	K - E / R N G				
Differential schemes	*u,v*	*KE*	*ε*	*T*	*ρ*
Time	F u l l y I m p l i c i t				
Space	UD	UD	UD	UD	CD 0,8
Control					
Piso Correctors	3 to 4				
Max. COU number	0,5 to 2,7				
Mean COU number	0,02 to 0,2				
HDIFF	0,1 to 3,6 W				
Residual tolerance	0,01 for u,v,T,KE,ε,ρ / 0,001 for P				
Under-relaxation for P	0,8				
Relaxation factors	v-0,7 / KE-0,7 / P-1,0 / T-0,95 / ρ-0,5				
Precision	Double				
Simulated time	4 minutes and 10 seconds				
Folder	TEST 11 / Alpha				

TEST 11
One-phase flow

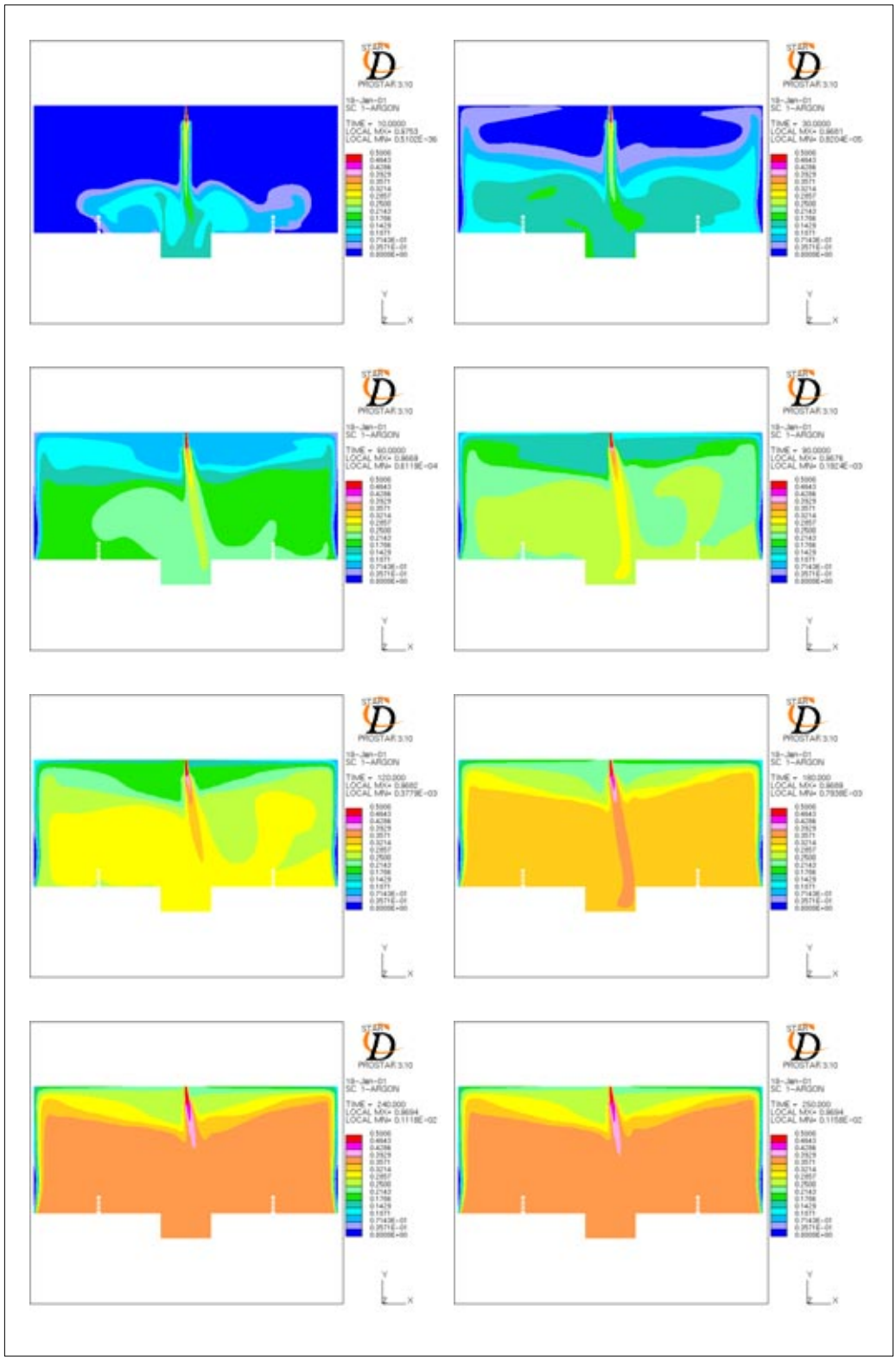

Figure B.64 Argon concentration distribution 10,30,60,90,120,180,240 and 250 s after the spill

TEST 11
One-phase flow

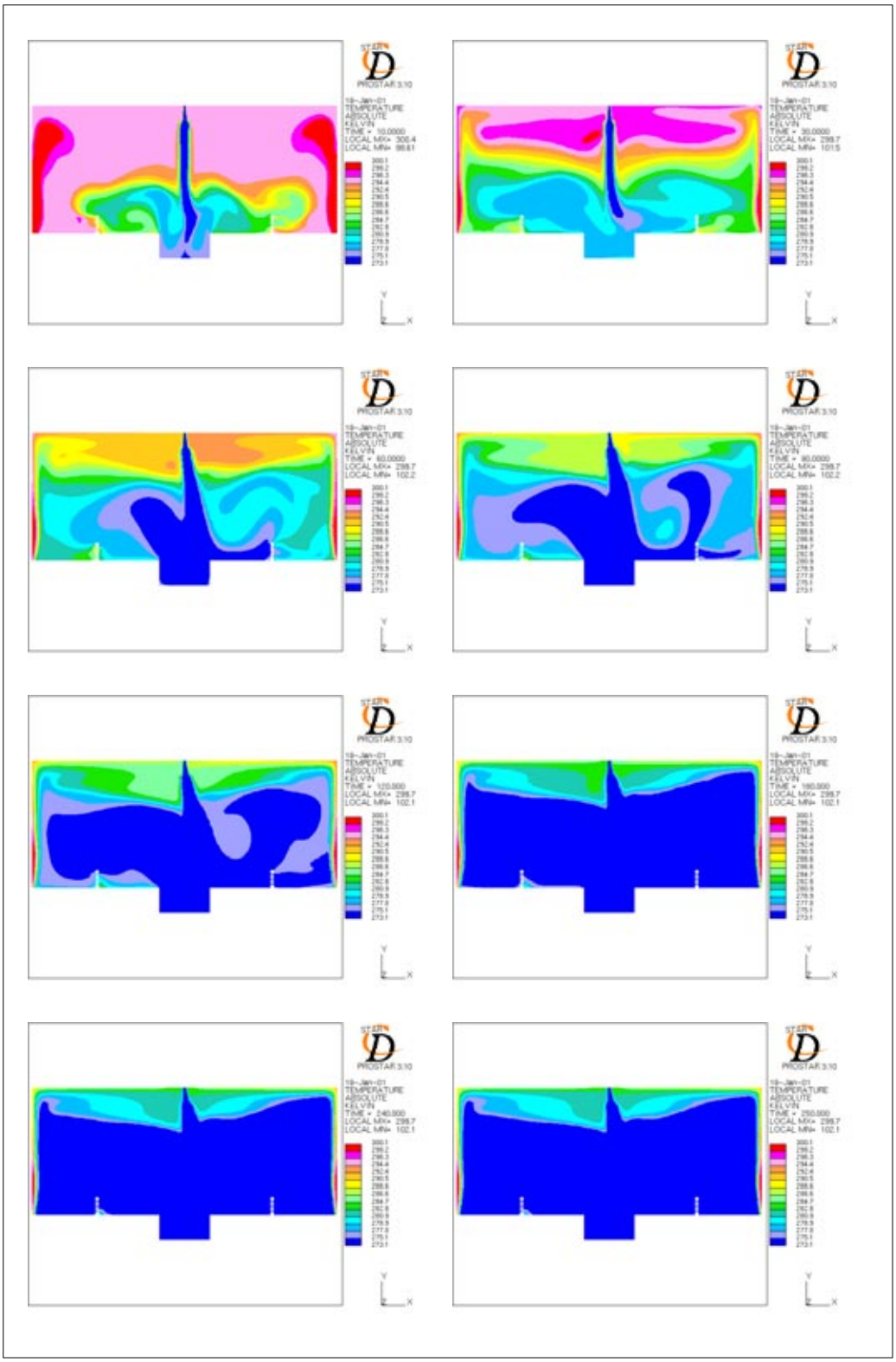

Figure B.65 Temperature distribution 10,30,60,90,120,180,240 and 250 s after the spill

TEST 11
Comparison

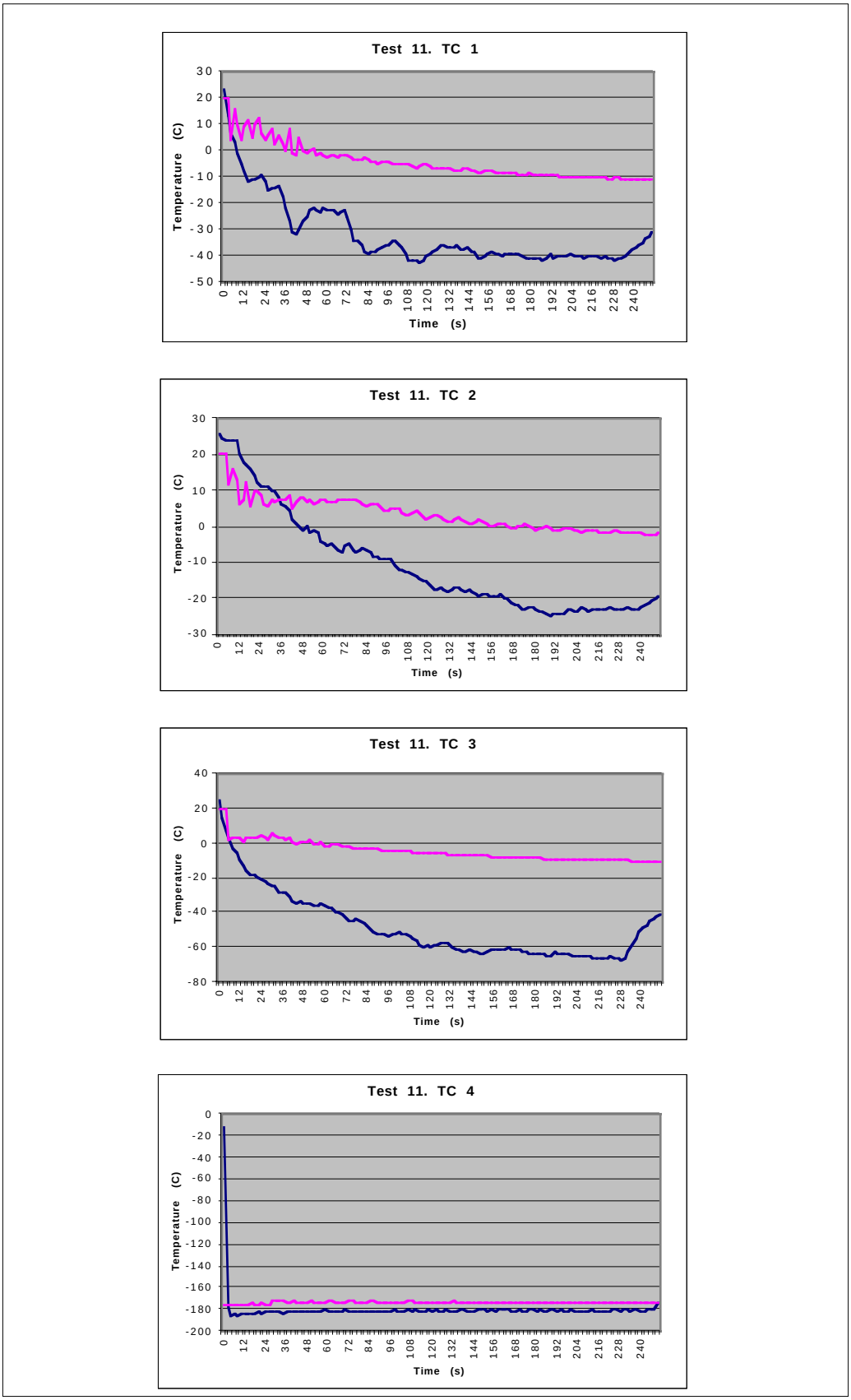

Figure B.66 Temperature comparison. Blue: Experiment, Pink: One-Phase

TEST 11
Comparison

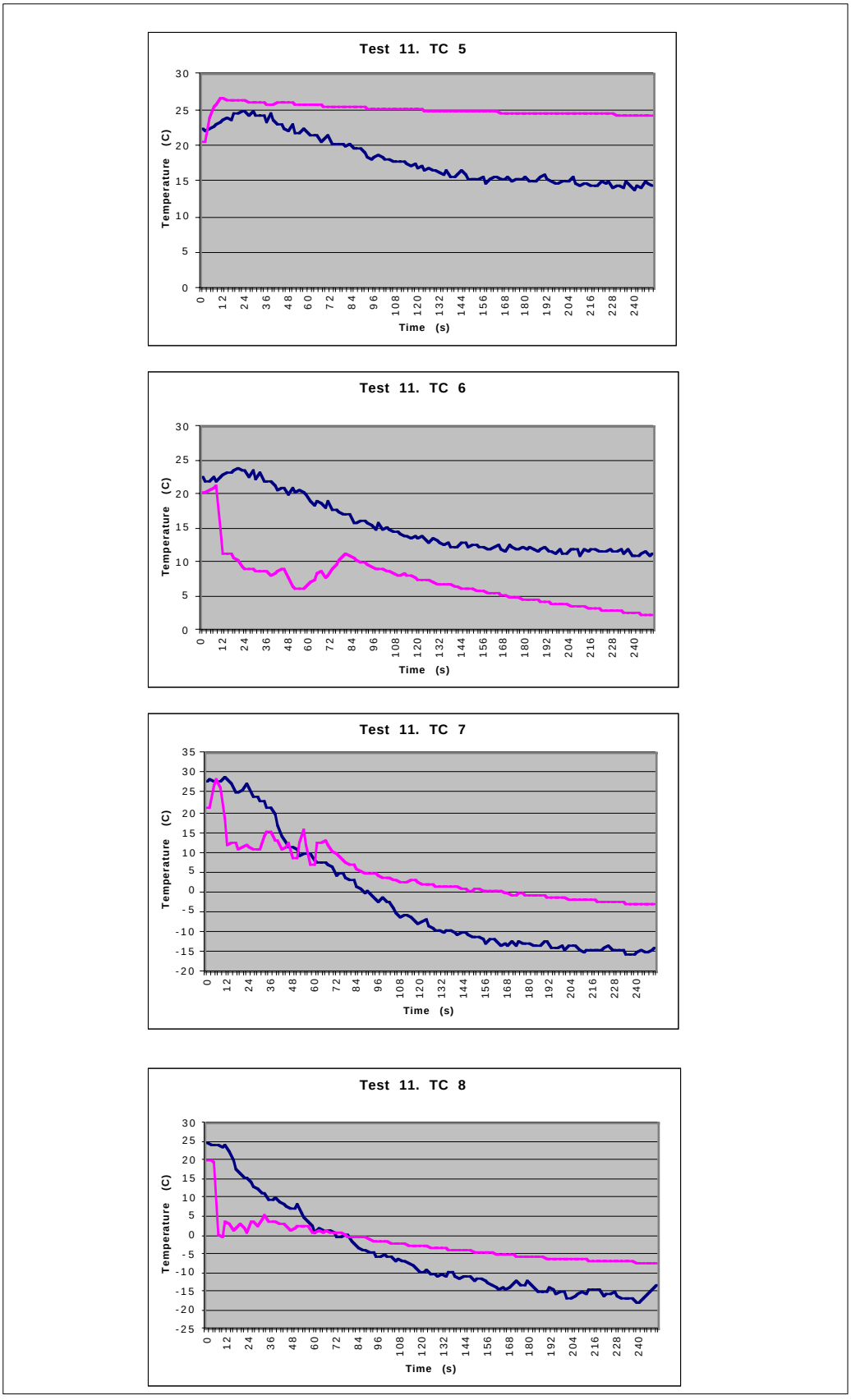

Figure B.67 Temperature comparison. Blue: Experiment, Pink: One-Phase

TEST 11
Comparison

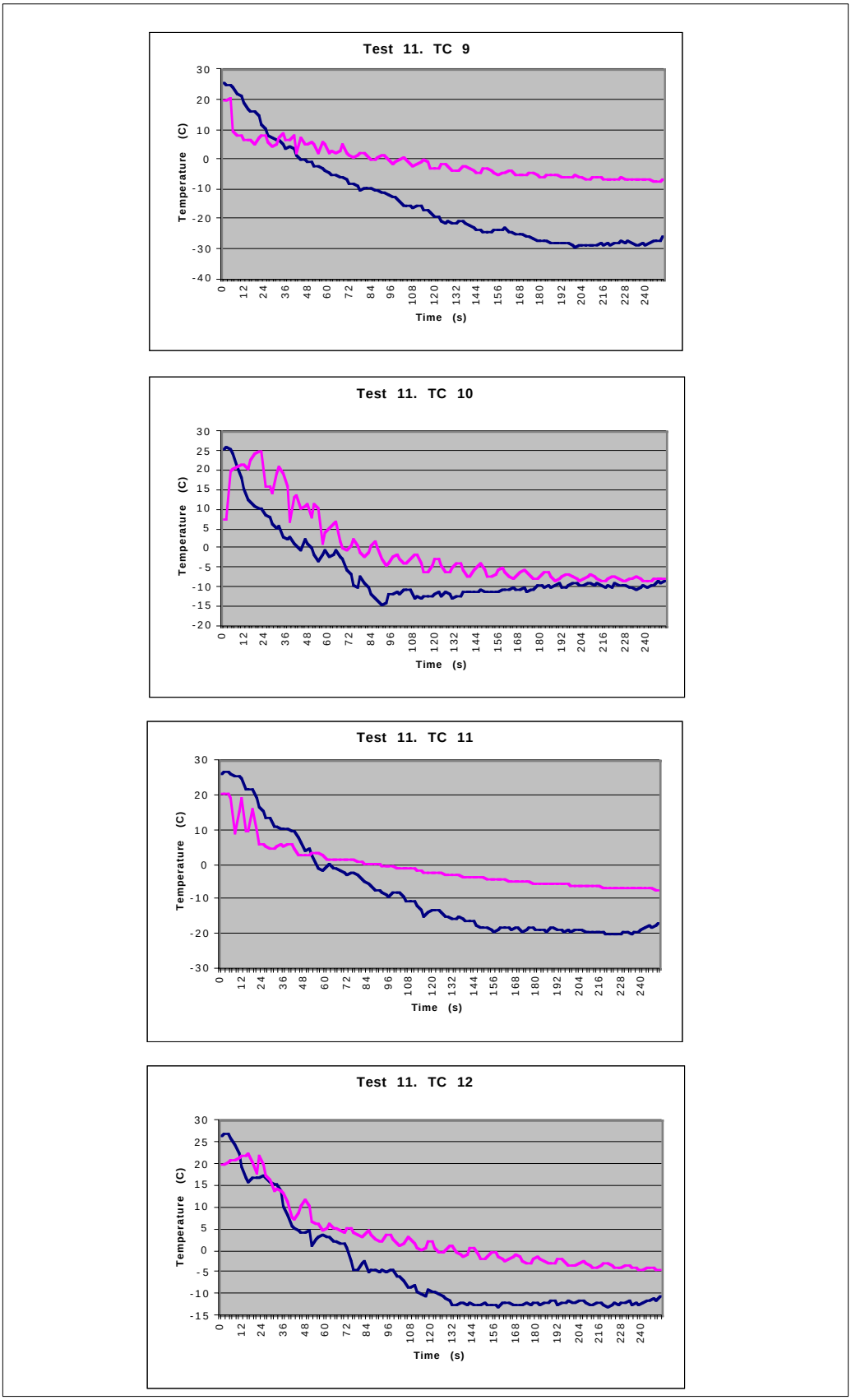

Figure B.68 Temperature comparison. Blue: Experiment, Pink: One-Phase

TEST 11
Comparison

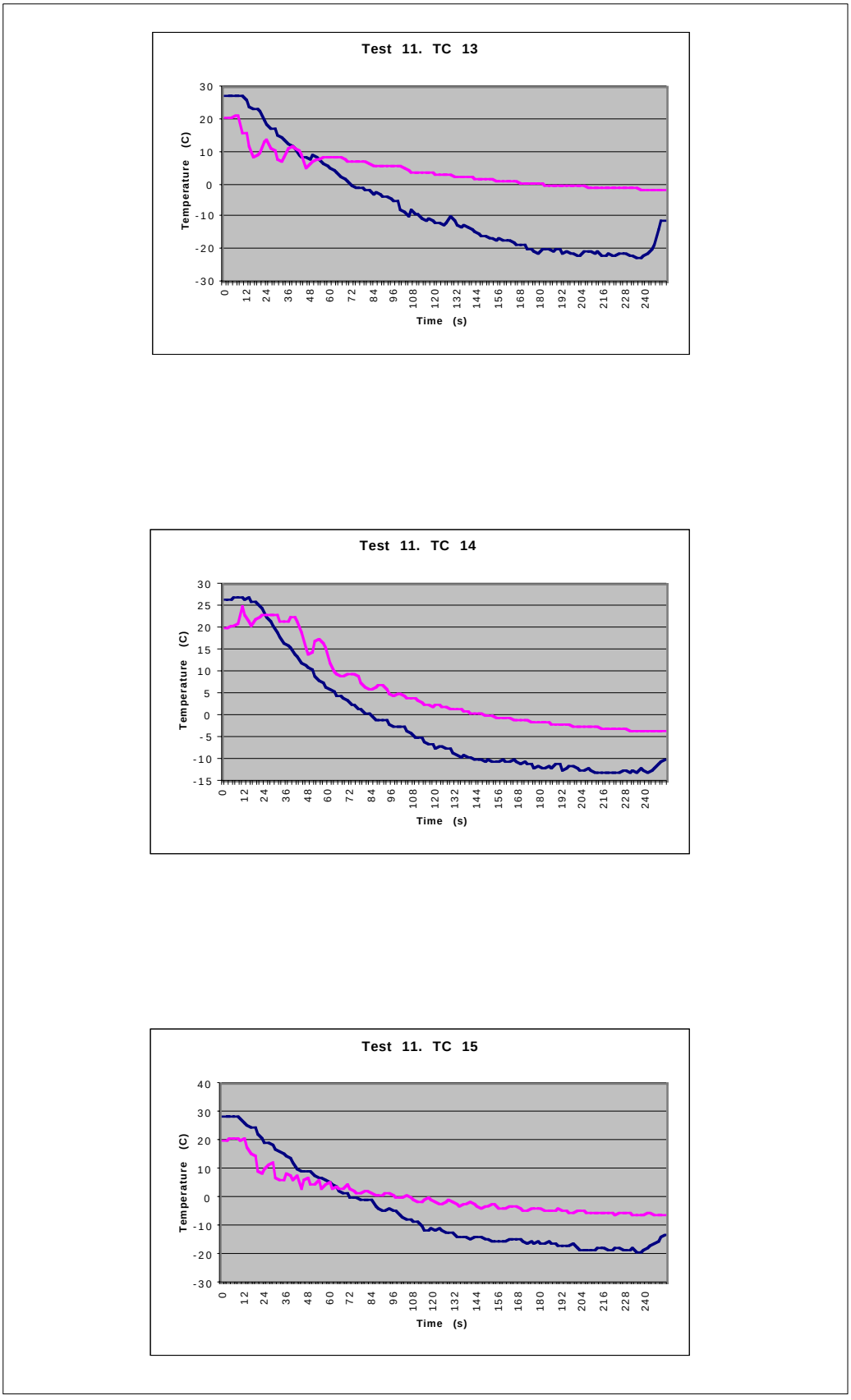

Figure B.69 Temperature comparison. Blue: Experiment, Pink: One-Phase

TEST 11
Comparison

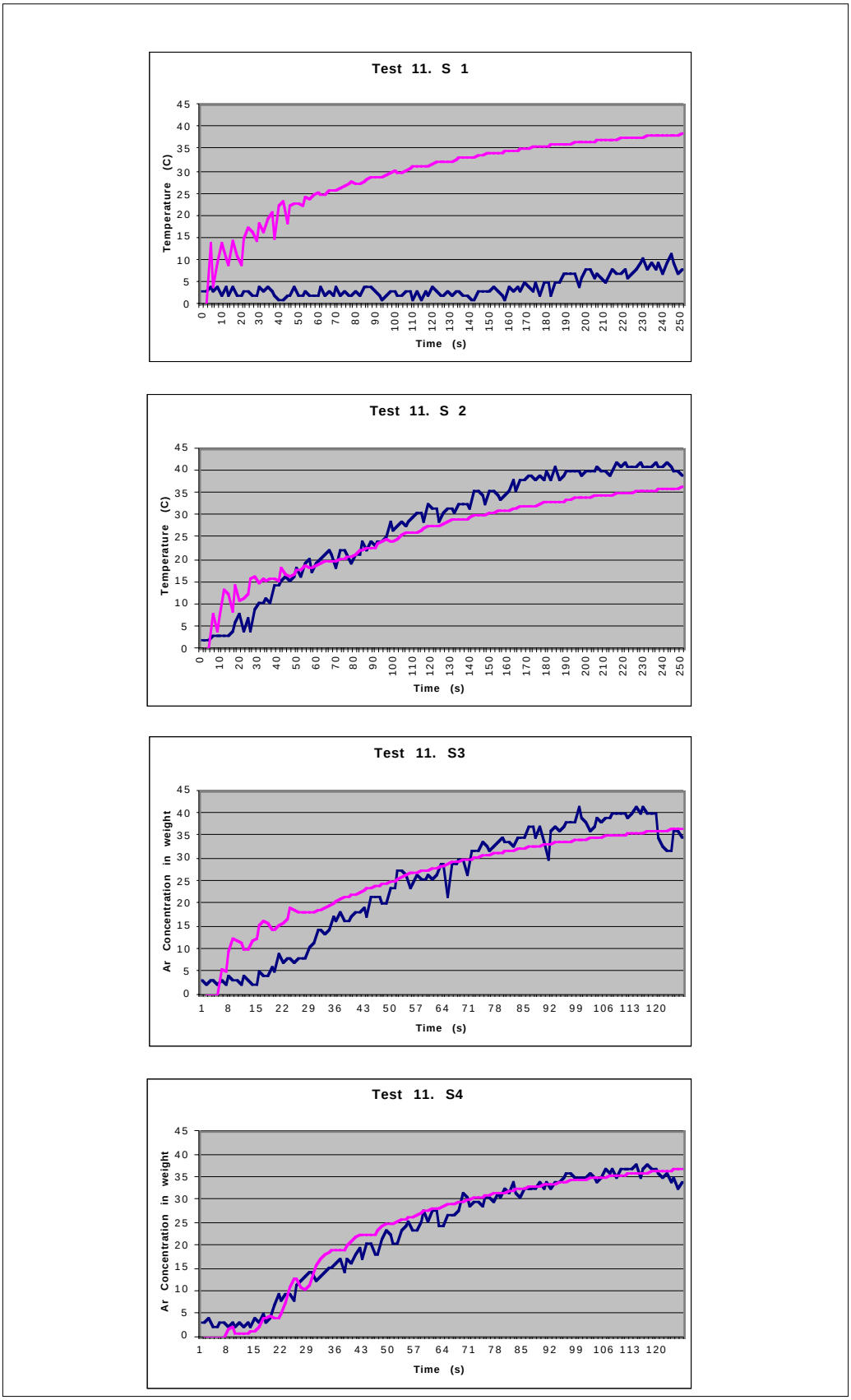

Figure B.70 Argon concentration comparison. Blue: Experiment, Pink: One-Phase

TEST 11
Comparison

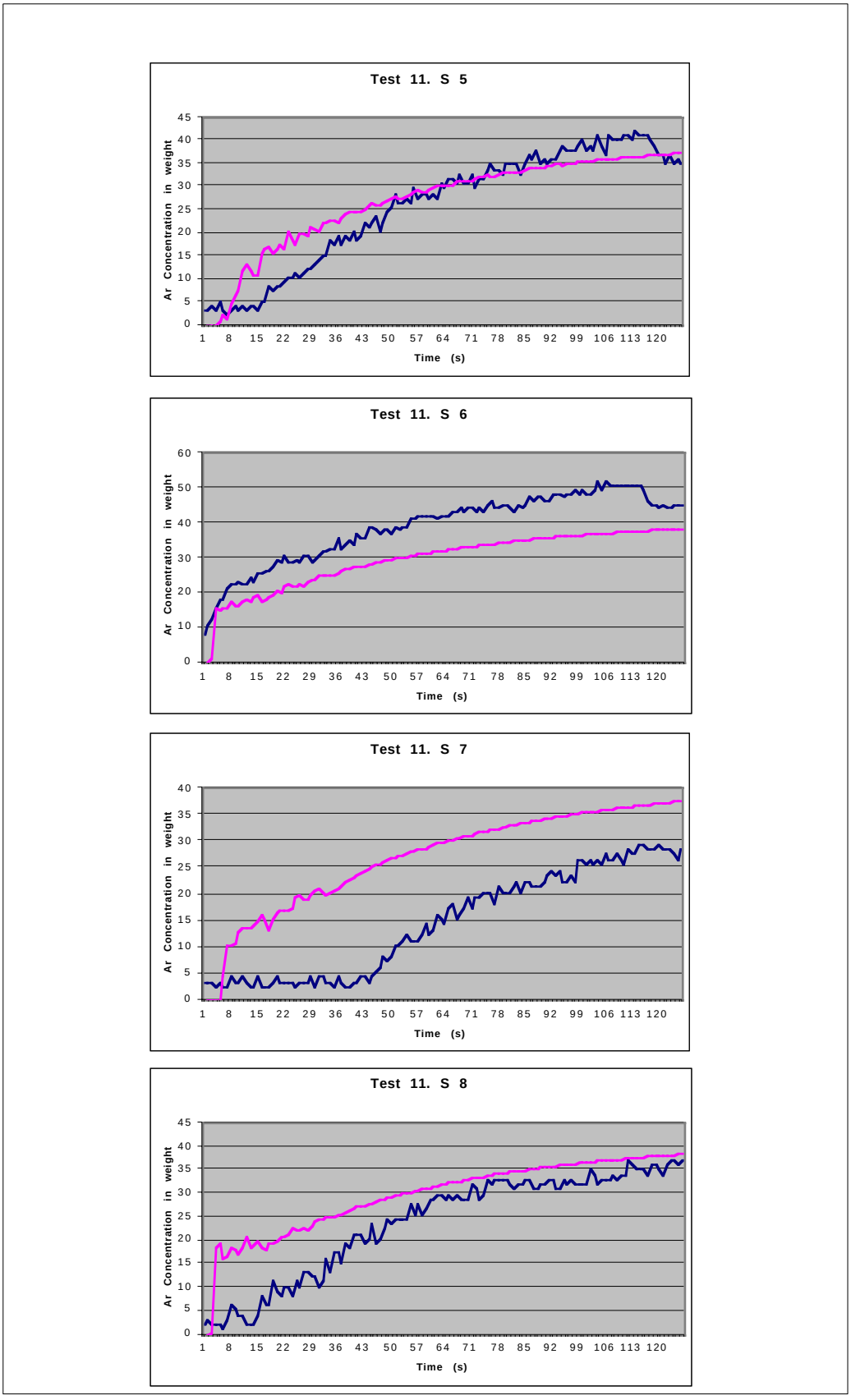

Figure B.71 Argon concentration comparison. Blue: Experiment, Pink: One-Phase

TEST 11
Comparison

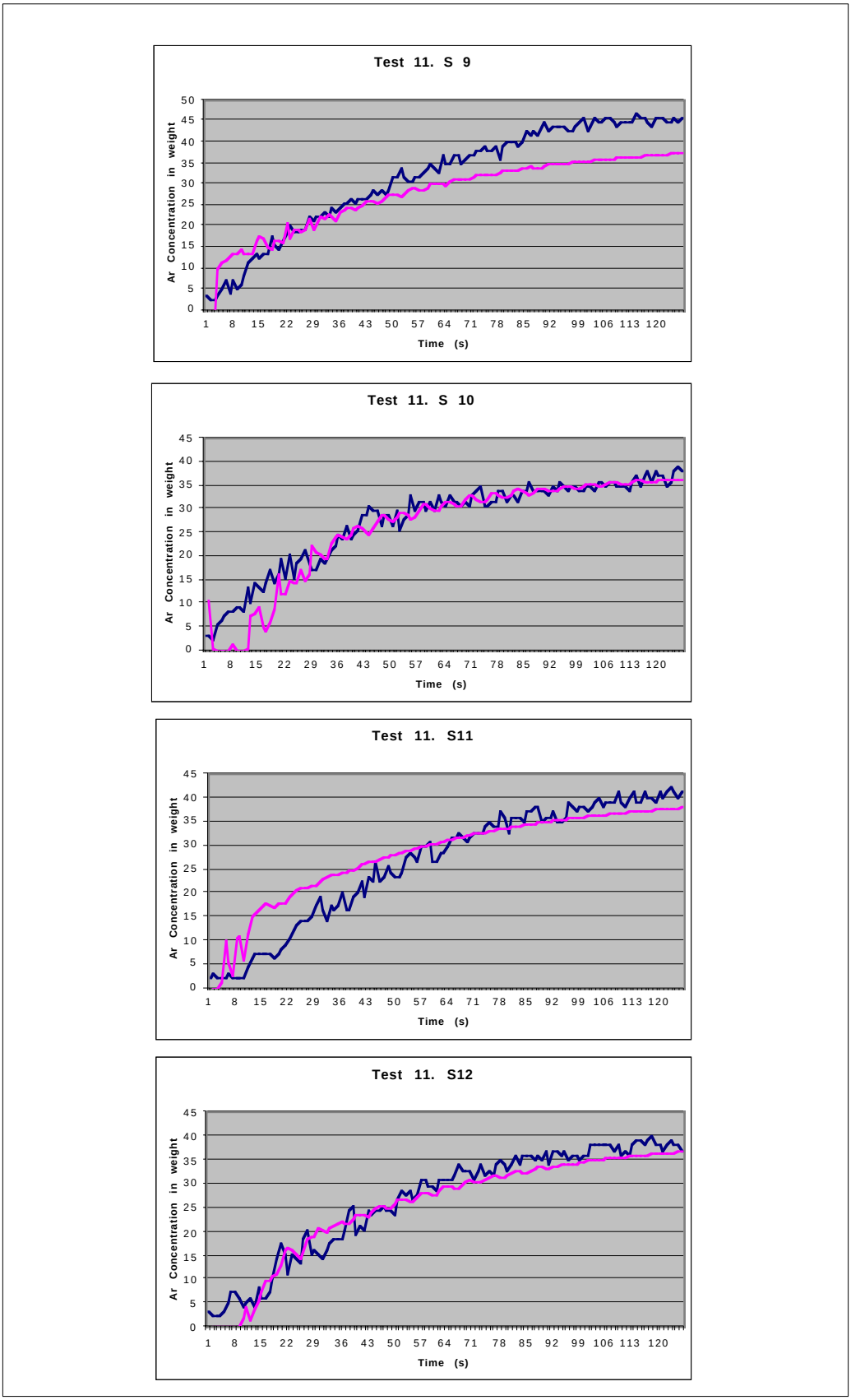

Figure B.72 Argon concentration comparison. Blue: Experiment, Pink: One-Phase

Appendix C

New ATLAS Models Figures

In this Appendix we collect all the evolution within time of temperature and argon concentrations for all the models described in Chapter 6.

C.1 69,34 l LAr/s

Q	**69,34 l LAr/s**				
Geometry	**Open detector scenario**				
Ventilation & Heat Load	**New Specifications**				
Energy Sinks	**Yes: 2795,5 kW / 56.598 W/m^3**				
Boundaries	*v (m/s)*	*k (m^2/s^2)*	*ε (m^2/s^3)*	*T (K)*	*ρ (kg/m^3)*
Argon Inlet	5,0	0,375	4,537	90	5,337
Exhaust fan	0,079	9,53 10^{-5}	1,57 10^{-7}	297	1,2
Left diffusor	0,185	5,14 10^{-4}	9,18 10^{-6}	290	1,2
Right top diffusor	0,082	1,01 10^{-4}	7,01 10^{-7}	290	1,2
Right bottom diffusor	0,185	5,14 10^{-4}	9,18 10^{-6}	290	1,2
Central pit extractor	0,167	4,21 10^{-4}	1,52 10^{-5}	297	1,2
Right pit extractor	0,046	3,18 10^{-5}	3,28 10^{-7}	297	1,2
Pit	293,6 K Isothermal				
Racks	6,34 W / m^2 Constant heat flux				
Muon chambers	29,78 W / m^2 Constant heat flux				
Walls	293,6 K Isothermal				
Turbulence Model	K - E / RNG				
Differential schemes	*u,v*	*KE*	*ε*	*T*	*ρ*
Time	Fully Implicit				
Space	UD	UD	UD	UD	CD 0,8
Control					
Piso Correctors	3 to 6				
Max. COU number	10 to 30				
Mean COU number	0,1 to 0,8				
HDIFF	1 to 20 W				
Residual tolerance	0,01 for u,v,T,KE,ε,ρ / 0,001 for P				
Under-relaxation for P	0,8				
Precision	Double				
Simulated time	5 minutes				
Folder	ATLAS PLUS 9 /Linux				

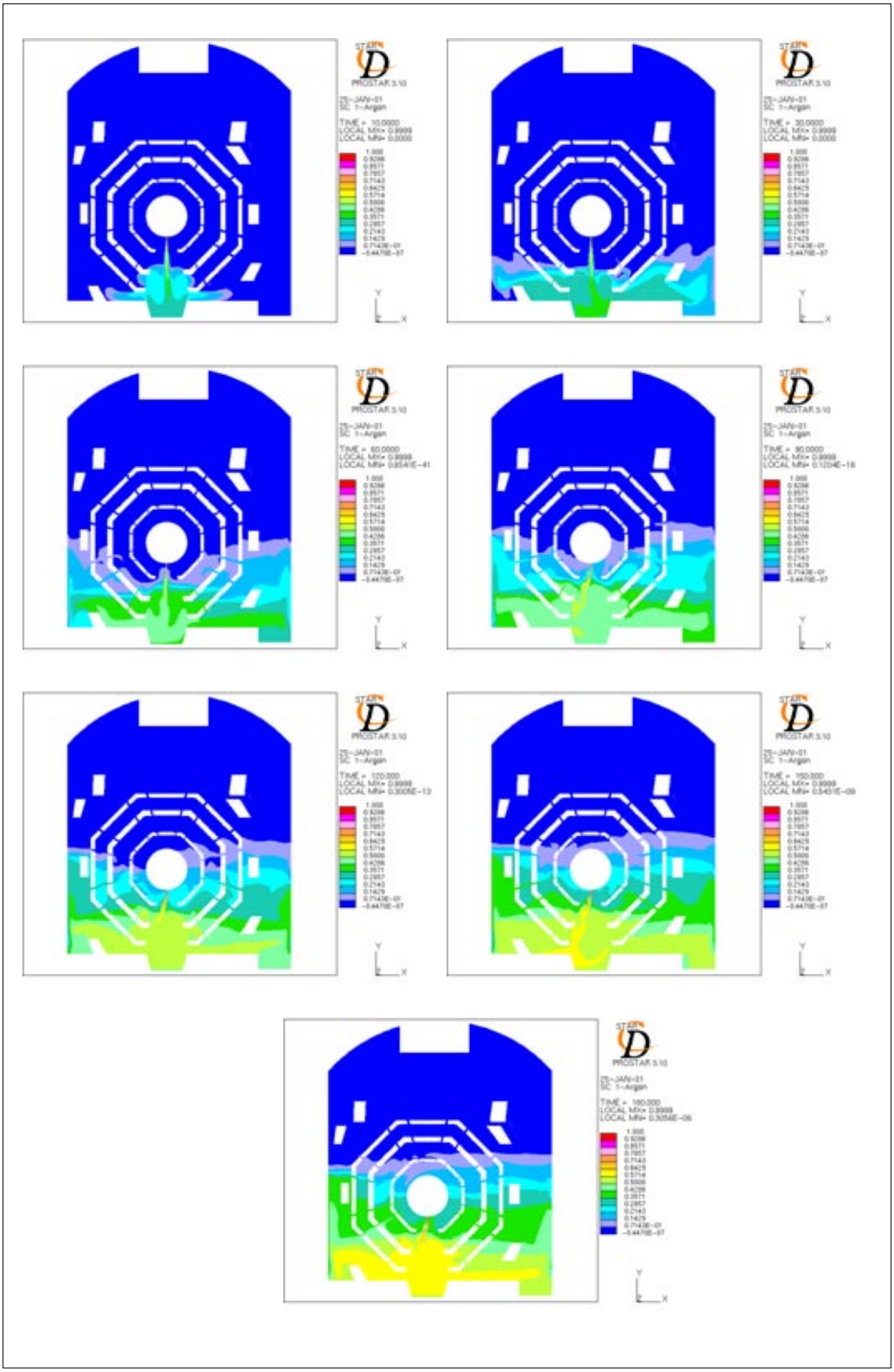

Figure C.1 Argon concentration distributions 10,30,60,90,120,150 and 180 s after the spill

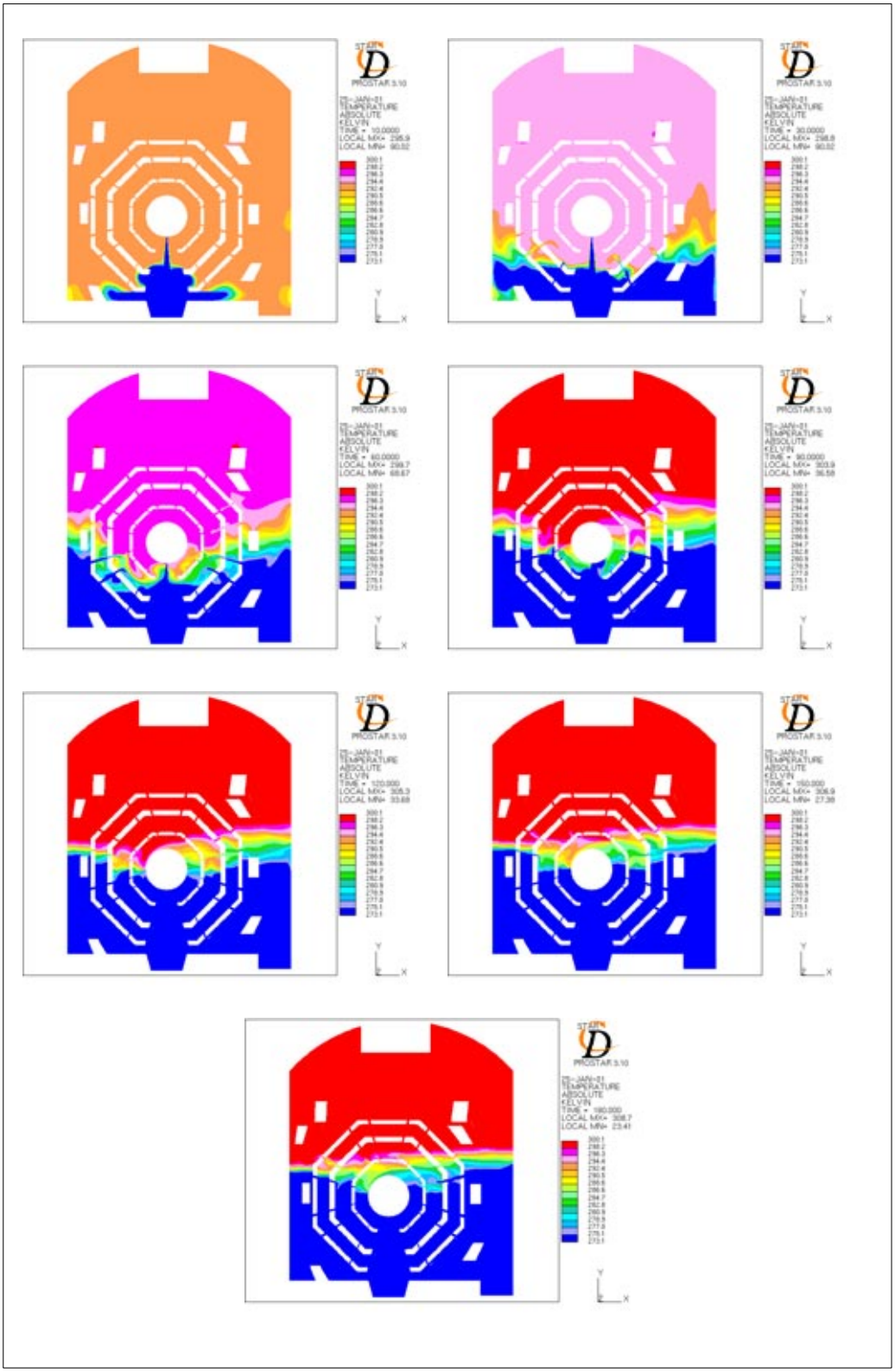

Figure C.2 Temperature distribution 10,30,60,90,120,150 and 180 s after the spill

C.2 17,46 l LAr/s.

Q	**17,46 l LAr/s**				
Geometry	**Open detector scenario**				
Ventilation & Heat Load	**New Specifications**				
Energy Sinks	**Yes: 703,92 kW / 14,25 W/m^3**				
Boundaries	*v (m/s)*	*k (m^2/s^2)*	*ε (m^2/s^3)*	*T (K)*	*ρ (kg/m^3)*
Argon Inlet	2,5	0,0937	1,129	90	5,337
Exhaust fan	0,079	$9{,}53\ 10^{-5}$	$1{,}57\ 10^{-7}$	297	1,2
Left diffusor	0,185	$5{,}14\ 10^{-4}$	$9{,}18\ 10^{-6}$	290	1,2
Right top diffusor	0,082	$1{,}01\ 10^{-4}$	$7{,}01\ 10^{-7}$	290	1,2
Right bottom diffusor	0,185	$5{,}14\ 10^{-4}$	$9{,}18\ 10^{-6}$	290	1,2
Central pit extractor	0,167	$4{,}21\ 10^{-4}$	$1{,}52\ 10^{-5}$	297	1,2
Right pit extractor	0,046	$3{,}18\ 10^{-5}$	$3{,}28\ 10^{-7}$	297	1,2
Pit	293,6 K Isothermal				
Racks	6,34 W / m^2 Constant heat flux				
Muon chambers	29,78 W / m^2 Constant heat flux				
Walls	293,6 K Isothermal				
Turbulence Model	K - E / R N G				
Differential schemes	*u,v*	*KE*	*ε*	*T*	*ρ*
Time	Fully Implicit				
Space	UD	UD	UD	UD	CD 0,8
Control					
Piso Correctors	4 to 5				
Max. COU number	9 to 24				
Mean COU number	0,1 to 0,5				
HDIFF	0,05 to 2 W				
Residual tolerance	0,01 for u,v,T,KE,ε,ρ / 0,001 for P				
Under-relaxation for P	0,8				
Precision	Double				
Simulated time	5 minutes				
Folder	ATLAS PLUS 12 / Linux				

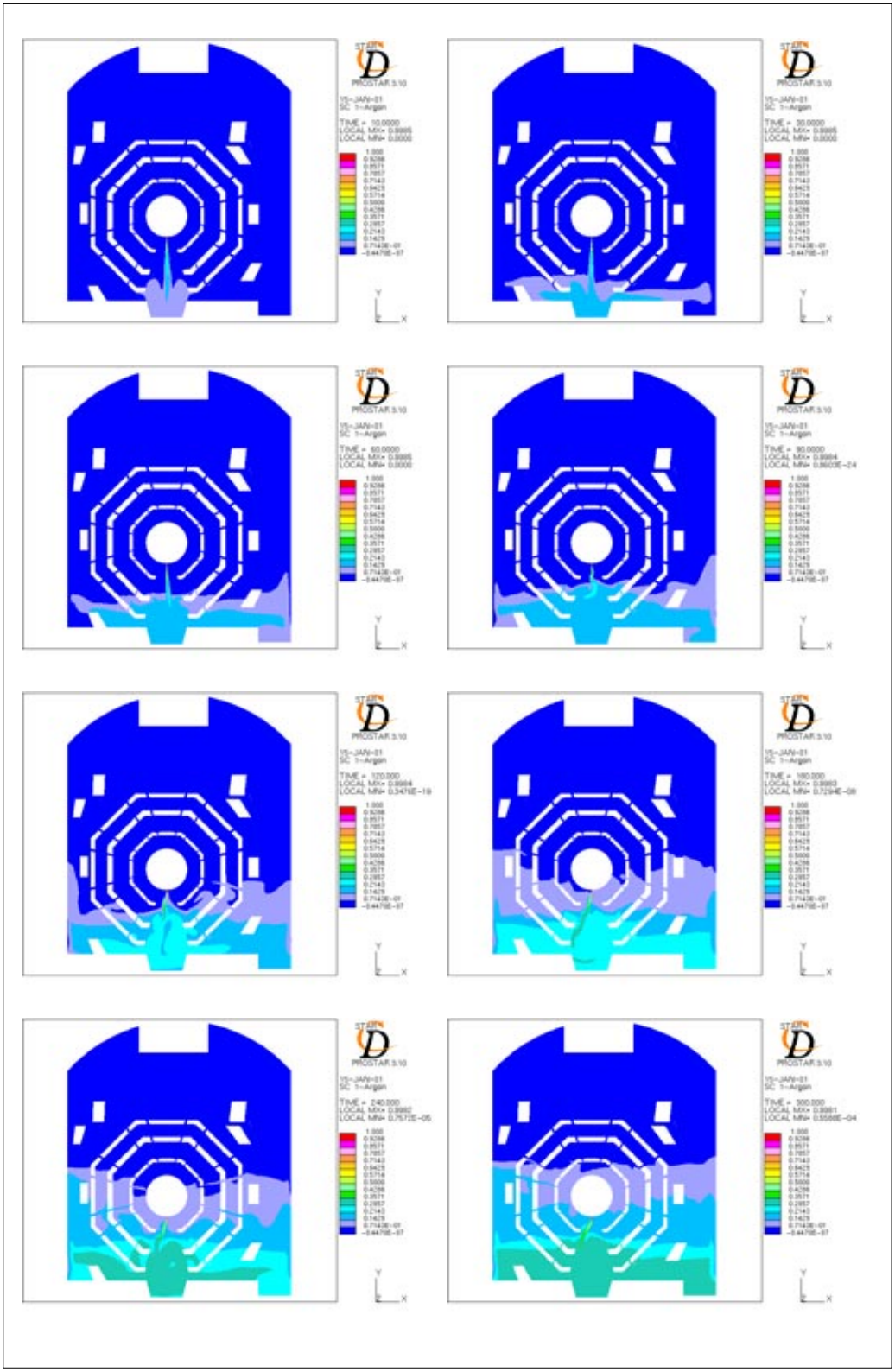

Figure C.3 Argon concentration distribution. 10,30,60,90,120,240 and 300 s after the spill.

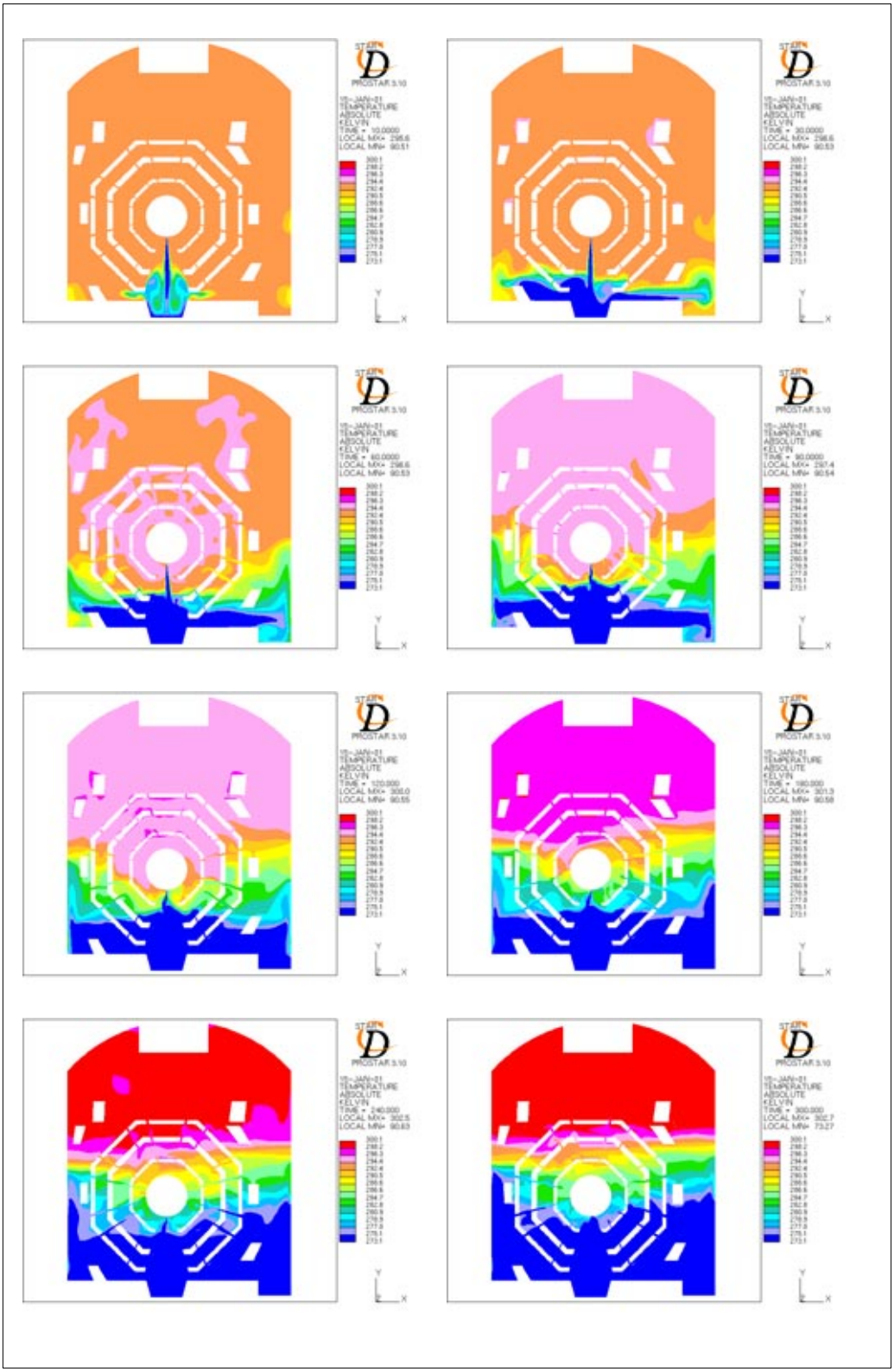

Figure C.4 Temperature distribution 10,30,60,90,120,180,240,300 s after the spill

C.3 12,39 l LAr/s

Q	**12,39 l LAr/s**				
Geometry	**Open detector scenario**				
Ventilation & Heat Load	**New Specifications**				
Energy Sinks	**Yes: 499,5 kW / 11.113 W/m^3**				
Boundaries	*v (m/s)*	*k (m^2/s^2)*	*ε (m^2/s^3)*	*T (K)*	*ρ (kg/m^3)*
Argon Inlet	4,0	0,24	10,398	90	5,3375
Exhaust fan	0,079	$9{,}53\ 10^{-5}$	$1{,}57\ 10^{-7}$	297	1,2
Left diffusor	0,185	$5{,}14\ 10^{-4}$	$9{,}18\ 10^{-6}$	290	1,2
Right top diffusor	0,082	$1{,}01\ 10^{-4}$	$7{,}01\ 10^{-7}$	290	1,2
Right bottom diffusor	0,185	$5{,}14\ 10^{-4}$	$9{,}18\ 10^{-6}$	290	1,2
Central pit extractor	0,167	$4{,}21\ 10^{-4}$	$1{,}52\ 10^{-5}$	297	1,2
Right pit extractor	0,046	$3{,}18\ 10^{-5}$	$3{,}28\ 10^{-7}$	297	1,2
Pit	293,6 K Isothermal				
Racks	6,34 W / m^2 Constant heat flux				
Muon chambers	29,78 W / m^2 Constant heat flux				
Walls	293,6 K Isothermal				
Turbulence Model	K - E / R N G				
Differential schemes	*u,v*	*KE*	*ε*	*T*	*ρ*
Time	Fully Implicit				
Space	UD	UD	UD	UD	CD 0,8
Control					
Piso Correctors	4 to 6				
Max. COU number	11 to 41				
Mean COU number	0,4 to 0,8				
HDIFF	0 to 5 W				
Residual tolerance	0,01 for u,v,T,KE,ε,ρ / 0,001 for P				
Under-relaxation for P	0,8				
Precision	Double				
Simulated time	5 minutes				
Folder	ATLASPLUS 71 / Linux				

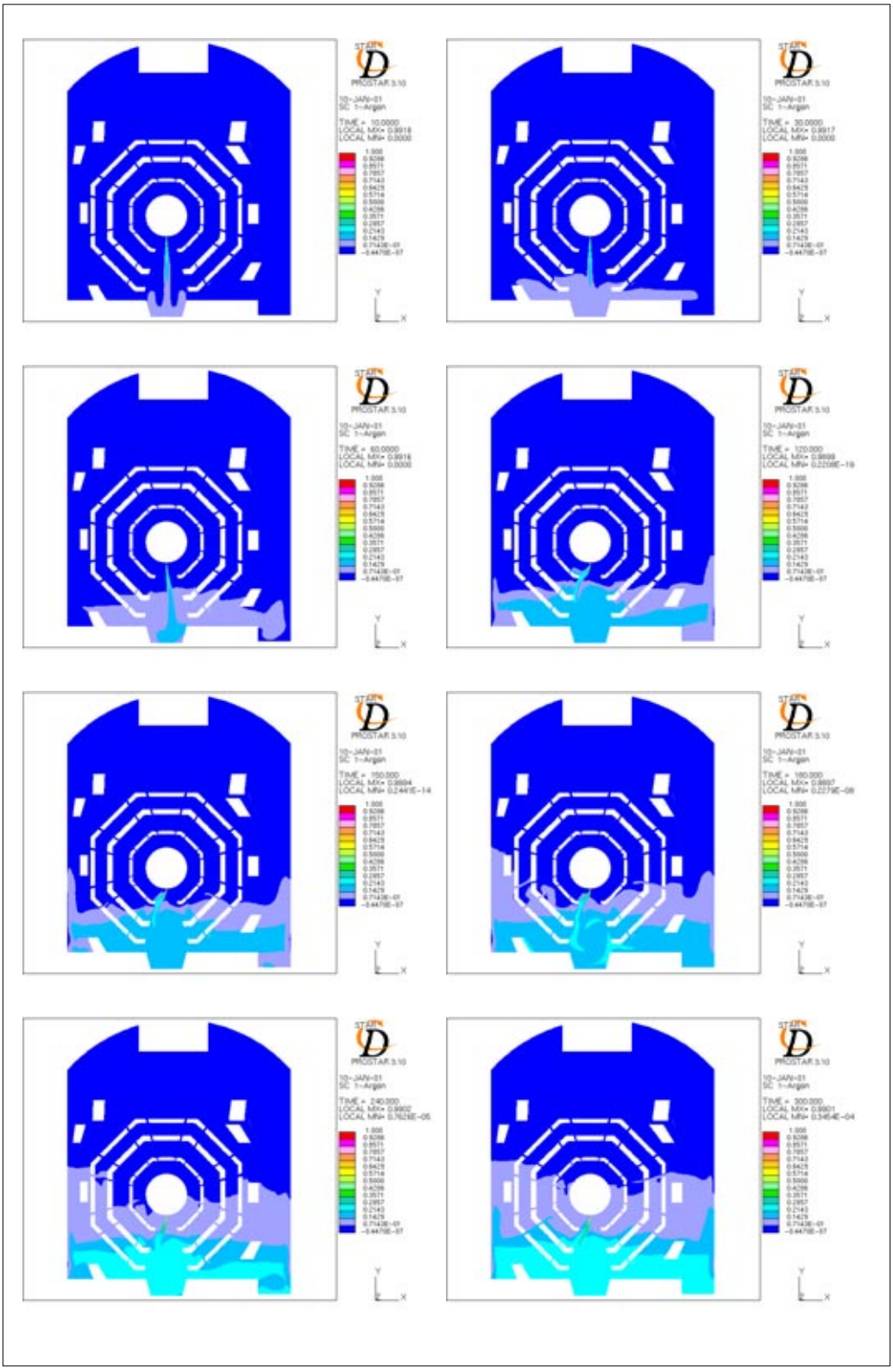

Figure C.5 Argon concentration 10,30,60,120,150,180,240 and 300 s after the spill

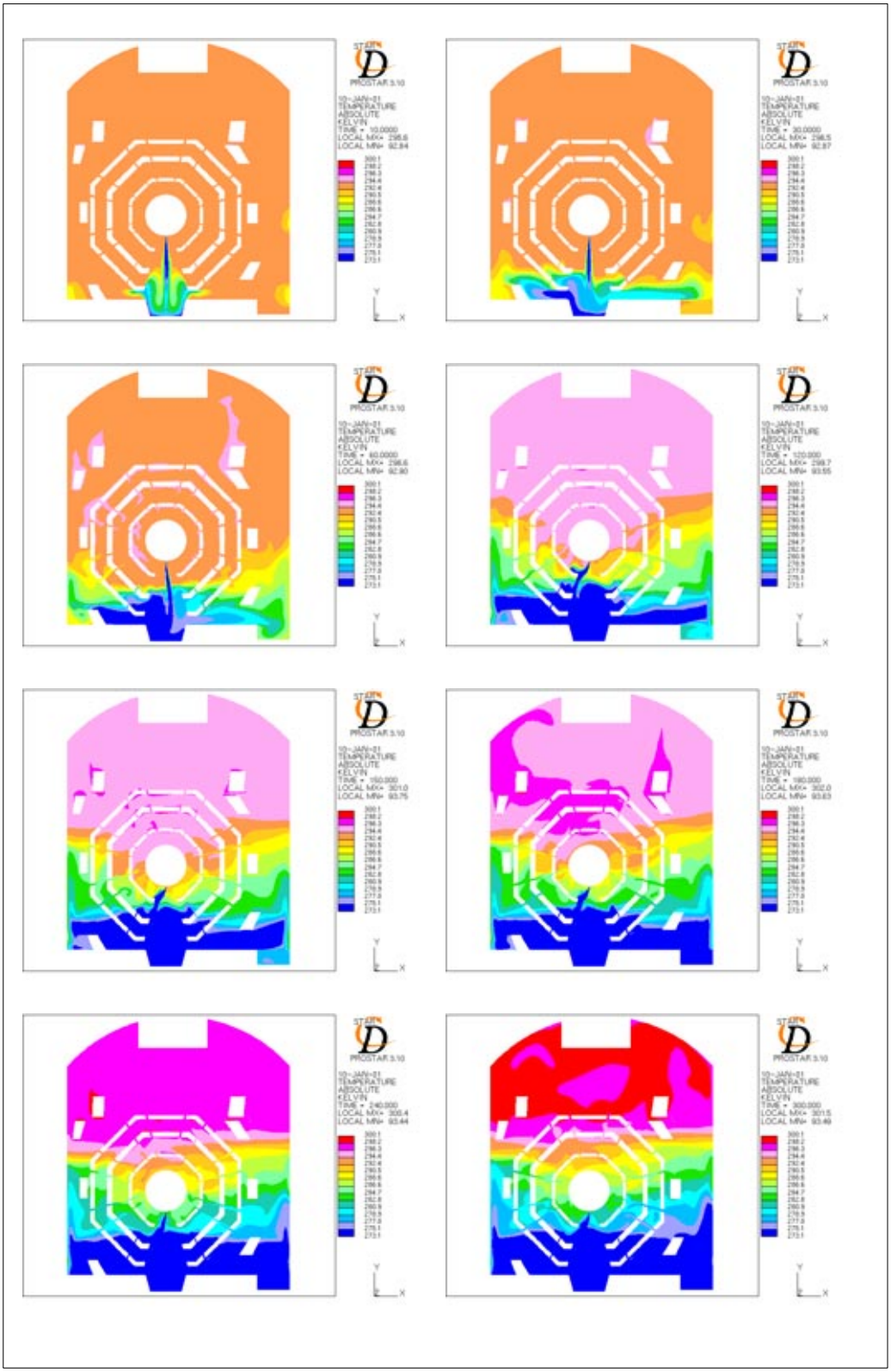

Figure C.6 Temperature distribution 10,30,60,120,150,180,240 and 300 s after the spill

C.4 9,3 l LAr/s

Q	**9,3 l LAr/s**				
Geometry	**Open detector scenario**				
Ventilation & Heat Load	**Old Specifications**				
Energy Sinks	**Yes: 374,93 kW / 7591,0 W/m^3**				
Boundaries	*v (m/s)*	*k (m^2/s^2)*	*ε (m^2/s^3)*	*T (K)*	*ρ (kg/m^3)*
Argon Inlet	3,0	0,135	1,583	90	5,507
Exhaust fan	0,059	5,364 10^{-5}	6,949 10^{-8}	295	1,2
Left diffusor	0,138	2,893 10^{-4}	4,044 10^{-6}	290	1,2
Right top diffusor	0,083	1,016 10-4	7,012 10-7	290	1,2
Right bottom diffusor	0,138	2,893 10^{-4}	4,044 10^{-6}	290	1,2
Central pit extractor	0,167	4,214 10^{-4}	1,527 10^{-5}	295	1,2
Right pit extractor	0,046	3,186 10^{-5}	3,284 10^{-7}	295	1,2
Pit	292,5 K Isothermal				
Racks	3,7134 W / m^2 Constant heat flux				
Muon chambers	16,56 W / m^2 Constant heat flux				
Walls	292,5 K Isothermal				
Turbulence Model	K - E / R N G				
Differential schemes	*u,v*	*KE*	*ε*	*T*	*ρ*
Time	F u l l y I m p l i c i t				
Space	UD	UD	UD	UD	CD 0,8
Control					
Piso Correctors	4 to 5				
Max. COU number	22 to 32				
Mean COU number	0,4 to 0,7				
HDIFF	0,5 to 12 W				
Residual tolerance	0,01 for u,v,T,KE,ε,ρ / 0,001 for P				
Under-relaxation for P	0,8				
Precision	Double				
Simulated time	5 minutes				
Folder	ATLAS PLUS 8 / Linux				

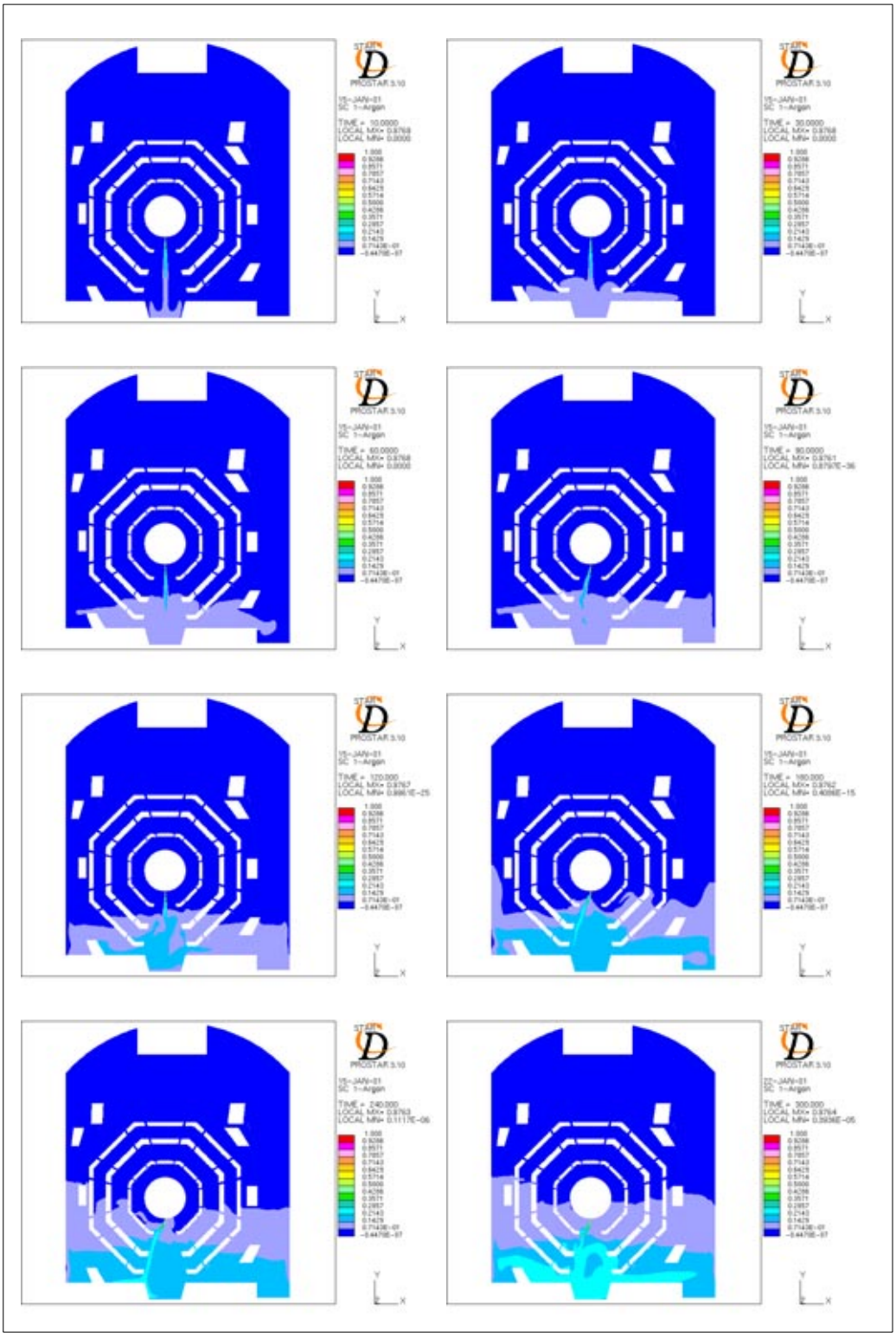

Figure C.7 Argon Concentration 10,30,60,90,120,180,240 and 300 s after the spill

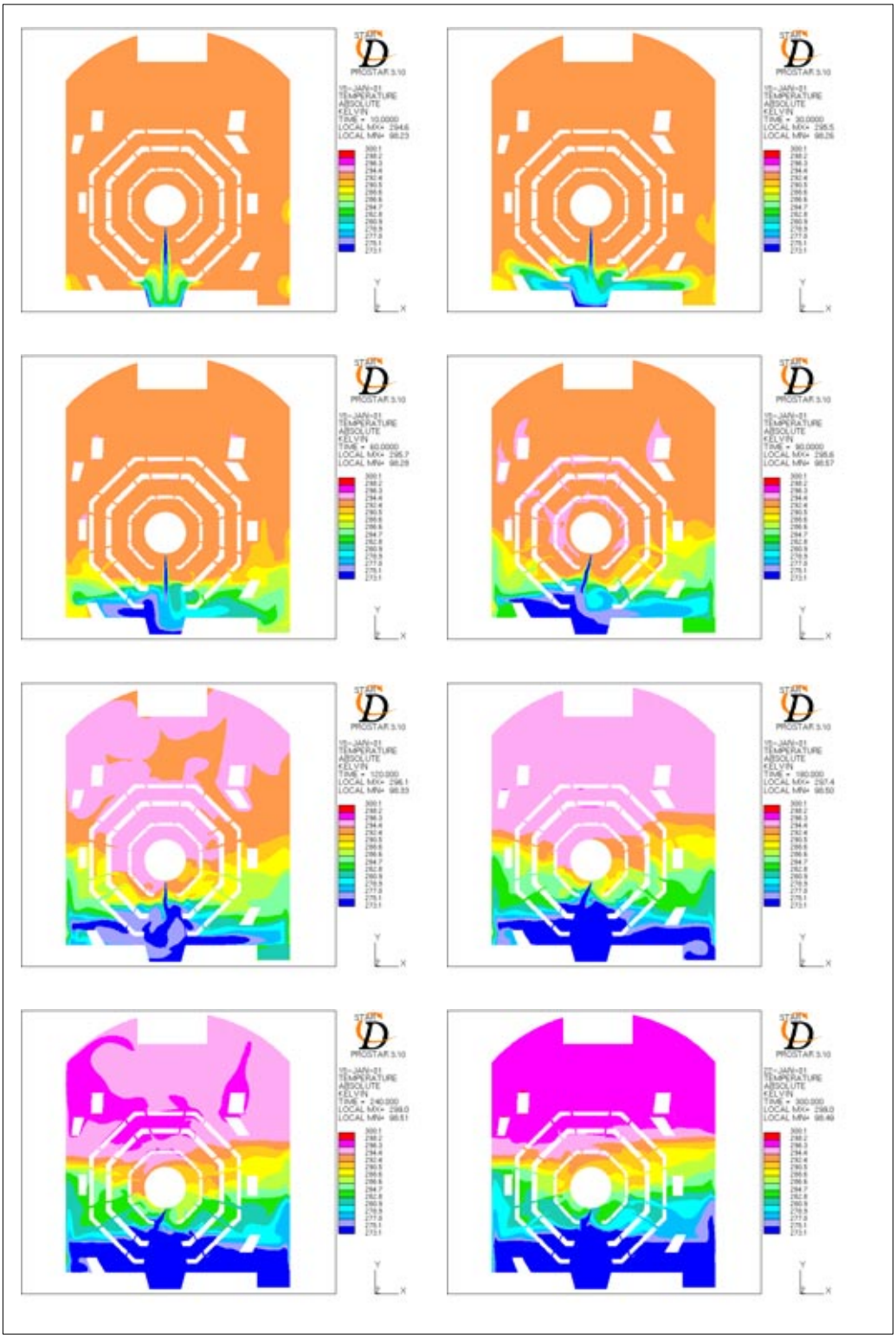

Figure C.8 Temperature distribution 10,30,60,90,120,180,240 and 300 s after the spill

C.5 50 l LAr/min. / 0,834 l LAr/s

Q	**0,834 l LAr/s**				
Geometry	**Open detector scenario**				
Ventilation & Heat Load	**New Specifications**				
Energy Sinks	**Yes: 33,62 kW / 680,74 W/m^3**				
Boundaries	*v (m/s)*	*k (m^2/s^2)*	*ε (m^2/s^3)*	*T (K)*	*ρ (kg/m^3)*
Argon Inlet	0,2783	0,00117	0,0036	90	5,3375
Exhaust fan	0,079	$9{,}53\ 10^{-5}$	$1{,}57\ 10^{-7}$	297	1,2
Left diffusor	0,185	$5{,}14\ 10^{-4}$	$9{,}18\ 10^{-6}$	290	1,2
Right top diffusor	0,082	$1{,}01\ 10^{-4}$	$7{,}01\ 10^{-7}$	290	1,2
Right bottom diffusor	0,185	$5{,}14\ 10^{-4}$	$9{,}18\ 10^{-6}$	290	1,2
Central pit extractor	0,167	$4{,}21\ 10^{-4}$	$1{,}52\ 10^{-5}$	297	1,2
Right pit extractor	0,046	$3{,}18\ 10^{-5}$	$3{,}28\ 10^{-7}$	297	1,2
Pit	293,6 K Isothermal				
Racks	6,34 W / m^2 Constant heat flux				
Muon chambers	29,78 W / m^2 Constant heat flux				
Walls	293,6 K Isothermal				
Turbulence Model	K - E / R N G				
Differential schemes	*u,v*	*KE*	*ε*	*T*	*ρ*
Time	F u l l y I m p l i c i t				
Space	UD	UD	UD	UD	CD 0,8
Control					
Piso Correctors	4				
Max. COU number	4,6 to 15				
Mean COU number	0,1 to 0,3				
HDIFF	0,2 to 0,5 W				
Residual tolerance	0,01 for u,v,T,KE,ε,ρ / 0,001 for P				
Under-relaxation for P	0,8				
Precision	Double				
Simulated time	5 minutes				
Folder	ATLAS PLUS 1 / Linux				

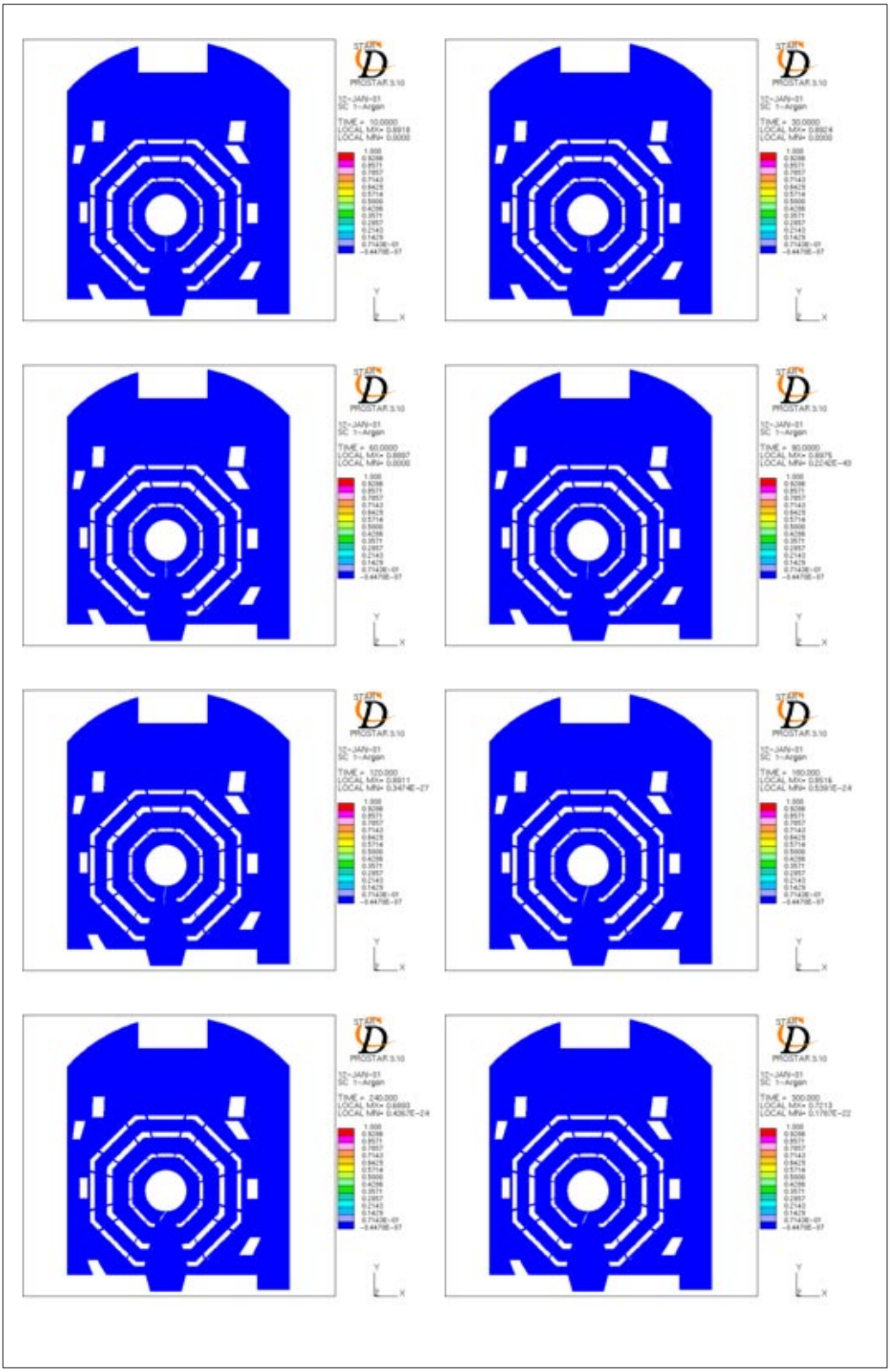

Figure C.9 Argon concentration distribution 10,30,60,90,120,180,240 and 300 s after the spill

Figure C.10 Argon concentration distribution 10,30,60,90,120,180,240 and 300 s after the spill

Figure C.11 Temperature distribution 10,30,60,90,120,180,240 and 300 s after the spill

Bibliography

1 **Star-CD. Methodology (version 3.1)**
Computational Dynamics, 1999

2 **Star-CD. User Guide (version 3.1)**
Computational Dynamics, 1999

3 **Star-CD Training Courses. Advanced Modelling isssues**
Computational Dynamics, 2000

4 **Encyclopedie des Gaz**
Elsevier / L'Air Liquide, 1976

5 **Simulations of Argon accident scenarios in the ATLAS experimental cavern - a safety analysis**
F.Balda, M.Vadon. CERN-TIS / 2000-009 / GS, June 2000

6 **Liquid Argon Spill Tests**
C.R.Gregory, J.Nebout; CERN AT-XA / 01N / CG / JN, May1994

7 **ATLAS - Liquid Argon Calorimeter Technical Design Report**
CERN / LHCC 96-41

8 **ATLAS - Technical proposal for a General-Pursose pp Experiment at the Large Hadron Collider at CERN**
CERN / LHCC / 94-43,1994

9 **Numerical Analysis of depressurisation of highly pressurised liquid propane**
M.A. Aamir, A.P.Watkins, Mechanical Engineering Department, UMIST, Manchester. International Journal of Heat and Fluid Flow 21 (2000)

10 **Two Phase discharge of liquefied gases through pipes. Fields Experiments with ammonia and theoretical model**
K.Nyren and S.Winter. National Research Institute, Umea, Sweden

11 **Discharges of Pressurised Liquefied Gases through apertures and pipes**
H.E.A. Van den Akker, H.Snoey and H.Spoelstra

12 **Methods for the calculations of physical effects**
CPR 14E- Committee for the Prevention of Disasters - The Netherlands Organization of Applied Scientific Research. Second edition, 1992

13 **Convection Heat Transfer**
Adrian Bejan. Wiley, second edition

14 **Modelling Axisymmetric Flows**
Stanley Middleman. Department of Applied Mechanics and Engineering Sciences. University of California, San Diego. Academic Press, 1995

15 **Two Phase Flow and Heat Transfer**
P.B. Whalley. Oxford Science Publications

16 **Transmissio de calor**
Bonals Muntada, Ruiz Mansilla. Edicions UPC,1996

17 **Fundamentos de Termodinamica Tecnica**
Moran and Shapiro. Editorial Reverte, S.A. 1994